Developing novel agents targeting the NF-κB pathway for the treatment of multiple myeloma

Melanie Varley

Supervisors: Dr. Paul Brennan

Prof. Chris Pepper

September 2017

This thesis is being submitted to Cardiff University in partial fulfillment of the requirements for the degree of Doctor of Philosophy

DECLARATION
This work has not been submitted in substance for any other degree or award at this or any other university or place of learning, nor is being submitted concurrently in candidature for any degree or other award.

Signed ……..……..…….……..…… (candidate) Date ……..…

STATEMENT 1
This thesis is being submitted in partial fulfillment of the requirements for the degree of PhD

Signed ……..……..…….……..…… (candidate) Date ……..…

STATEMENT 2
This thesis is the result of my own independent work/investigation, except where otherwise stated, and the thesis has not been edited by a third party beyond what is permitted by Cardiff University's Policy on the Use of Third Party Editors by Research Degree Students. Other sources are acknowledged by explicit references. The views expressed are my own.

Signed ……..……..…….……..…… (candidate) Date ……..…

STATEMENT 3
I hereby give consent for my thesis, if accepted, to be available online in the University's Open Access repository and for inter-library loan, and for the title and summary to be made available to outside organisations.

Signed ……..……..…….……..…… (candidate) Date ……..…

STATEMENT 4: PREVIOUSLY APPROVED BAR ON ACCESS
I hereby give consent for my thesis, if accepted, to be available online in the University's Open Access repository and for inter-library loans **after expiry of a bar on access previously approved by the Academic Standards & Quality Committee.**

Signed ……..……..…….……..…… (candidate) Date ……..…

Table of contents

Abstract

The key aim was to characterise Nuclear factor-κB (NF-κB) inhibitors in four multiple myeloma (MM) cell lines to evaluate their use as potential therapeutic agents in this incurable haematological malignancy. The NF-κB inhibitors were characterised in terms of their effects on cytotoxicity, nuclear NF-κB activity, global gene expression changes and the survival protein Mcl-1. Using this workflow, the following inhibitors were investigated: the commercial non-specific NF-κB inhibitor BAY 11-7082; a series of first-in-class putative IKKα inhibitors (SU compounds); and a novel putative NIK inhibitor (CW15337) in MM cell lines.

BAY 11-7082, CW15337 and most of the SU compounds induced dose-dependent cytotoxicity in the MM cell lines. For BAY 11-7082 and CW15337, cytotoxicity was associated with dose-dependent changes in NF-κB activity, although BAY 11-7082 inhibited both the canonical and the non-canonical NF-κB pathway, whereas CW15337 specifically inhibited the non-canonical NF-κB activity. In addition, the apoptosis induced by CW15337 was accompanied by a dose-dependent decrease in Mcl-1 expression in all tested MM cell lines.

In contrast, the cytotoxicity of the SU compounds did not correlate with the dose-dependent down-regulation of Mcl-1 expression or NF-κB activity, and could not be completely explained by the SU compounds IKKα, IKKβ and CDK9 inhibitory profiles. Microarray analysis indicated a large disparity between the numbers of genes differentially regulated by some of the SU compounds; the number altered and the magnitude of the changes was associated with their cytotoxicity. Therefore, it seems likely that the increased potency of some of the SU compounds was caused by off-target effects.

Overall, this work supports the concept of NF-κB as a molecular target in MM and suggests that NIK inhibition may present the most promising therapeutic option for specific non-canonical NF-κB targeting in MM. However, a more detailed investigation of CW15337 across the kinome is merited.

List of Figures

List of Tables

Abbreviations

APRIL	A proliferation-inducing ligand
ASCT	Autologous stem cell transplantation
BAFF	B-cell activating factor
BAFF-R	BAFF receptor
BCMA	B-cell maturation antigen
BCR	B-cell receptor
BM	Bone marrow
BMM	Bone marrow microenvironment
BMSC	Bone marrow stromal cells
BSA	Bovine serum albumin
CAM-DR	Cell adhesion mediated drug resistance
CAML	Calcium-modulator and cyclophilin ligand
CBS	Central Biotechnology Services
CD	Cluster of differentiation
cDNA	complementary DNA
CD40L	CD40 ligand
CI	Confidence intervals
cIAP	C inhibitors of apoptosis proteins
CO_2	Carbon dioxide
CR	Complete remission
CRAB	Hypercalcemia (C), renal failure (R), anemia (A), and/or bone disease (B)
CXCR	CXC chemokine receptor
DE	Differentially expressed
DMEM	Dulbecco's Modified Eagle's medium
DNA	Deoxyribonucleic acid
ELISA	Enzyme linked immunosorbent assay
EMSA	Electrophoretic mobility shift assay
FBS	Foetal bovine serum
FC	Fold change
FITC	Fluorescein isothiocyanate
FSC	Forward scatter
GM-CSF	Granulocyte-macrophage colony-stimulating factor
GO	Gene ontology

GRR	Glycine-rich region
H_2O	Dihydrogen monoxide - water
HTA	Human Transcriptome Array
IAP	Inhibitors of apoptosis protein
IBT-Tween	I-Block Tween
Ig	Immunoglobulin
IgH	Ig heavy-chain
IκB	Inhibitor of κB
IKK	IκB kinase
IKKK	IKK kinases
IL	Interleukin
IMiDs	Immunomodulatory agents
ISS	International staging system
K63-pUb	Lys63-linked polyubiquitination
LD_{50}	Median lethal dose
LDH	Lactate dehydrogenase
mAb	Monoclonal antibody
MCL	Myeloma cell line
MFI	Mena fluorescent intesity
MGUS	Monoclonal gammopathy of undetermined significance
mIg	Monoclonal immunoglobulin
MM	Multiple myeloma
NBD	NEMO-binding domain
H929	NCI-H929
NEMO	NF-κB essential modulator
NES	Nuclear export sequence
NF-κB	Nuclear factor-κB
NIK	NF-κB inducing kinase
NLS	Nuclear localisation signal
NTL	Non-transfected ligand
OD_{450}	Optical density at an absorbance of 450nm
PBS	Phosphate buffered saline
PCA	Principal component analysis
PI	Propidium iodide

PM	Perfect match
PS	Phosphatidylserine
pUb	Polyubiquitination
PVDF	Polyvinylidene difluoride
qRT-PCR	Real-time quantitative polymerase chain reaction
RANK	Receptor activator of NF-κB
RANKL	RANK ligand
RHD	Rel homology domain
RIN	RNA integrity number
R-ISS	Revised ISS
RNA	Ribonucleic acid
RPMI-1640	Roswell Park Memorial Institute-1640
SEM	Standard error of the mean
SD	Standard deviation
SDS-PAGE	Sodium dodecyl sulphate polyacrylamide gel electrophoresis
SSC	Side scatter
TACI	Transmembrane activator and CAML interactor
TAD	Transcription activation domain
TAK1	Transforming growth factor beta-activated kinase 1
TF	Transcription factor
TNF	Tumor necrosis factor
TNFR	TNF receptor
TRAF	TNF receptor-associated factor
UT	Untreated
VCAM-1	Vascular cell adhesion molecule 1
VEGF	Vascular endothelial growth factor
XIAP	X-linked IAP

Acknowledgements

Firstly, I would like to thank my supervisors, Dr Paul Brennan and Prof. Chris Pepper, for providing me with the opportunity to carry out this PhD and supporting me throughout the whole process. Thank you for never turning me away when I came to ask one question that ended up turning into ten, and teaching me to be more optimistic.

I would like to thank all the members of the Cardiff CLL research group, both past and present, for their support and guidance. In particular, I would like to thank Dr Elisabeth Walsby and Dr Liam Morgan, who have both been there from day 1, for their support and encouragement throughout the course of this PhD. I would also like to take this opportunity to thank the group for keeping a smile on my face when times got tough. In particular, a massive thank you to Dr Lauren Elston, Julia Grimstead and Marie Clarke for your friendship and support.

A special thank you also goes out to the Leukaemia Research Appeal for Wales for funding my PhD, and to Prof. Simon MacKay at the University of Strathclyde for kindly providing the novel NF-κB inhibitors used throughout this thesis.

Finally, I would like to thank my family; especially my Mam, Dad, brother Philip and husband Rob. Without your constant support, none of what I have achieved would have been possible. Mam and Dad, you have always supported me in everything I have ever done and you have never stopped believing in me. Thank you for being there in all the times I have needed you, and constantly telling me 'I can do anything that I put my mind to'. Rob, you are my best friend and a wonderful husband, thank you for sticking with me and caring for me during this PhD.

Chapter 1- Introduction

1.1. Multiple myeloma (MM)

Multiple myeloma (MM) accounts for approximately 10% of haematological malignancies and is predominantly a disease of the elderly, where two thirds of newly diagnosed individuals are 65 years or more (CRUK 2014; HMRN 2014). Overall, there are approximately 4,000 new cases of MM in the UK per year and the disease is more common in males relative to females, with a male:female ratio of 1.3:1 (CRUK 2014; HMRN 2014). Despite the recent advances in treatments for MM, the disease remains incurable, although patients are now predicted to live for approximately 5 years following diagnosis (Bergsagel et al. 2013).

1.1.1. MM biology

MM is a B-cell malignancy in which the accumulation and infiltration of malignant plasma cells in the bone marrow (BM) is the key characteristic (Kyle et al. 2003; Greipp et al. 2005). Plasma cells are terminally differentiated B-cells and these cells have a crucial role in the adaptive immune system because plasma cells are involved in the production of antibodies. B-cells are derived from haematopoietic stem cells and undergo immunoglobulin (Ig) rearrangement in their early stages to generate a large antigen recognition repertoire. B-cells differentiate to plasma cells in response to stimulation and activation by exogenous antigens through both T-cell independent and T-cell dependent pathways. The activation of B-cells triggers extensive somatic hypermutation of the variable region of immunoglobulin genes, which allows the production of antigen-specific antibodies.

The resulting plasma cells then localise to the BM where they can survive as long-lived plasma cells (Brieva et al. 1991; Slifka et al. 1995; Manz et al. 1997). The process of bone marrow homing is prompted by the reduced expression of the CXC chemokine receptor 5 (CXCR5) and the increased expression of CXCR4, CXCR3, CXCR6 and $\alpha_4\beta_1$-integrin on the surface of plasma cells (Hargreaves et al. 2001; Hauser et al. 2002; Kunkel a Butcher 2003; Odendahl et al. 2005). The BM microenvironment (BMM) then

provides a supportive environment to promote the survival of long-lived plasma cells through interleukin-6 (IL-6), B-cell-activating factor (BAFF), IL-5 and tumour-necrosis factor (TNF) secretion, and the expression of survival receptors such as CXCL12, CD44 ligand and CD40 ligand (Minges Wols et al. 2002; Cassese et al. 2003; O'Connor et al. 2004).

The malignant plasma cells in MM retain many similarities with their long-lived normal counterparts in the respect that the cells retain a strong BM dependence, are positive for the surface antigens CD38 and CD138, and usually possess extensive somatic hypermutation of immunoglobulin genes (Ruiz-Argüelles a San Miguel 1994; Wijdenes et al. 1996; Kuehl a Bergsagel 2012). However, unlike normal plasma cells, malignant plasma cells produce excess amounts of damaging proteins with no useful function in the place of normal monoclonal immunoglobulin (mIg), known as paraproteins. Furthermore, MM plasma cells retain the ability to proliferate at a low rate (Kuehl a Bergsagel 2012). Malignant plasma cells typically lack the expression of the B-cell associated antigen CD19, the CD27 antigen and CD45, and may also aberrantly express CD56 and CD28 (San Miguel et al. 2002; Bianchi a Anderson 2014). As a result, myeloma plasma cells can be differentiated from normal plasma cells through a variety of diagnostic techniques, such a multi-parametric flow cytometry, to allow the MM disease to be diagnosed and its progression monitored.

1.1.2. Symptoms

The majority of MM symptoms are a consequence of the accumulation of malignant plasma cells within the BM and the presence of excess paraproteins. MM patients frequently present with symptoms such as bone pain, hypercalcaemia, anaemia and recurrent infections. In addition, the presence of end-organ failure is one of the main symptoms that is required for MM diagnosis and the specific symptoms required can be abbreviated to the CRAB acronym. These specifically include hypercalcemia (C), renal failure (R), anemia (A), and/or bone disease (B) in the form of osteolytic lesions (IMWG 2003).

Hypercalcaemia, anaemia and recurrent infections arise due to osteolytic bone destruction and impaired haematopoiesis. This is a result of the localisation of the malignant plasma cells within the BM (Bommert et al. 2006). Normal BM structure is maintained due a balance of osteoblast and osteoclast cell activity. In MM, the abundance of malignant plasma cells within the BM leads to an imbalance in the regulation of these cells, which ultimately results in decreased bone construction and increased bone destruction (Xi et al. 2016). Increased osteoclast activity is caused as a result of increased levels of tumour-associated cytokines, such as IL-6 and TNFα, and the interaction of MM cells with the BMM through pathways such as receptor activator of nuclear factor-κB (RANK) and its ligand (RANKL) (Xi et al. 2016).

The excess paraprotein that is produced by malignant plasma cells in MM leads to symptoms such as kidney injury, which can then result in renal failure, and in some cases peripheral neuropathy and encephalopathy (Bianchi a Anderson 2014).

1.1.3. Diagnosis

Some patients present with a pre-malignant condition before they are diagnosed with symptomatic MM. Monoclonal gammopathy of undetermined significance (MGUS) is an asymptomatic condition that in most cases precedes the diagnosis of MM, although not all MGUS cases will progress to MM (Landgren et al. 2009; Weiss et al. 2009). Moreover, approximately 3-4% of the population over the age of 50 years have features of MGUS (Dispenzieri et al. 2010). MGUS is characterised by the presence of mIg in the serum (<30 g/L) but in the absence of the usual CRAB clinical signs of malignancy (Rajkumar et al. 2014). In addition, the percentage of clonal plasma cells within the BM is less than 10% (Rajkumar et al. 2014).

Before MGUS transforms to symptomatic MM, it often progresses to an intermediate clinical stage of the disease known as smoldering MM (or asymptomatic myeloma). Smoldering MM is diagnosed if there is a high level of paraprotein detected in serum (≥30 g/L) and/or the BM contains ≥ 10% plasma cells (Rajkumar et al. 2014). However, smoldering MM is not

classed as symptomatic MM because it is only diagnosed in the absence of the usual CRAB clinical symptoms of MM. As a result, many arguments exist as to whether treatment for MM should be initiated in the smoldering MM phase of the disease or to wait to see whether progression to symptomatic MM arises (Dispenzieri et al. 2013).

The next stage of disease progression is symptomatic MM and this is usually detected based on the appearance of a variety of clinical symptoms. The diagnosis of MM is achieved if three criteria are met:

1. There must be greater than 10% plasma cells found within the bone marrow aspirate. In addition, more than 90% of these plasma cells will present with a malignant phenotype.

2. There are excess levels of paraproteins (≥ 30 g/L) within the serum and/or urine.

3. There is evidence of all the CRAB symptoms of MM.

A more advanced stage of MM may be observed and this is known as plasma cell leukemia or extramedullary MM. In this stage of the disease, malignant plasma cells leave the BMM and enter the peripheral blood where they can account for more than 20% of cells present in this fraction (Rajkumar et al. 2014).

1.1.4. Prognosis

The prognosis of MM is determined based on a variety of prognostic factors, including tumour burden, the age and relative fitness of the patient, and cytogenetics (Bianchi a Anderson 2014). In addition, patients with a previous diagnosis of MGUS preceding MM have a better survival outcome, which may be consequence of increased follow-up leading to earlier treatment once MGUS eventually progresses to MM (Sigurdardottir et al. 2015).

The International Staging System (ISS) can be used to assess the level of tumour burden in MM patients and used to categorise patients into three

separate groups (Table 1.1) (Greipp et al. 2005). The measurements used for the three-stage ISS are serum β2-microglobulin and serum albumin, both of which are measured easily and inexpensively using simple laboratory tests. As a result, the ISS provides a highly accessible and significantly relevant prognostic indicator of tumour burden (Greipp et al. 2005).

Table 1.1 The International Staging System (ISS)
The table shows the criteria used in respect to β2 microglobulin and serum albumin measurements for stratifying patients into the three stages of the ISS. The overall survival in months that is predicted by ISS is also provided. In summary, the higher the ISS stage of tumour burden, the worse the predicted outcome is for the patient at diagnosis. Adapted from (Greipp et al. 2005; Bianchi a Anderson 2014).

Stage	ISS criteria	Overall survival according to ISS (months)
I	Serum β2-microglobulin <3.5 mg/dL AND serum albumin ≥3.5 g/dL	62
II	Meets criteria for neither stage I nor stage III	44
III	Serum β2-microglobulin ≥5.5 mg/dL	29

The use of a combination of prognosis factors, such as tumour burden and cytogenetics, are then used to place patients into different risk categories, such as standard-risk patients and high-risk patients, which can help to decide what treatment regime they should receive. Patients diagnosed with standard-risk MM can survive for 10 years or more, whereas the median survival for a patient who presents with high-risk MM is less than 2 years (Chng et al. 2014).

20% of cases of high-risk MM arise as a consequence of specific cytogenetic abnormalities (Egan et al. 2016). For this reason, a revised ISS (R-ISS) is now used to assess prognosis using a combination of the original ISS criteria, cytogenetic evaluation and the measurement of serum lactate dehydrogenase (LDH) to provided a more reliable assessment of risk stratification for MM patients (Palumbo et al. 2015). Serum LDH has been shown to be a relevant biomarker in MM and increased levels of serum LDH

indicate increased disease aggressiveness and MM cell proliferation (Terpos et al. 2010).

The chromosomal abnormalities that are frequently detected in MM can be separated into two main cytogenetic categories; translocations involving the Ig heavy-chain (IgH) locus and genomic imbalances (Bergsagel et al. 2013). Table 1.2 shows the most common cytogenetic abnormalities that are detected in MM along with whether they are associated with a high-risk prognosis. The majority of these primary genetic abnormalities lead to deregulation of cyclin D genes (chromosome 14), which results in uncontrolled MM plasma cell proliferation (Bergsagel et al. 2005). Interestingly, these genetic abnormalities have been found to arise before the MGUS stage of disease and increase in number throughout MM disease progression, indicating their importance in tumour progression (Walker et al. 2014).

Table 1.2 The most common cytogenetic abnormalities in MM and their association with MM prognosis.
The cytogenetic abnormalities can be separated into two main cytogenetic categories; IgH translocations and genomic imbalances. Those shown in red are associated with a worse prognosis and can stratify MM patients into the high-risk category. The most commonly observed high-risk genetic abnormalities in MM are the t(4;14) translocation and 17p deletion. Adapted from (Bergsagel et al. 2013).

IgH translocations	Genomic imbalances
t(4;14)	Hyperdiploid
t(14;16)	Non-hyperdiploid
t(14;20)	1q gains
t(11;14)	Monosomy 13
t(6;14)	17p deletions

The cytogenetic evaluation used in the R-ISS evaluates deletions of chromosome 13 and 17p deletion, and IGH translocations. Based on the new R-ISS criteria, cytogenetic detection of deletion of 17p, translocation t(4;14) and/or translocation t(14;16) are considered to stratify a patient as high-risk (Palumbo et al. 2015). The R-ISS criteria can be found in Table 1.3 and is now used to assess prognosis in newly diagnosed MM patients.

Table 1.3 The Revised International Staging System (R-ISS)
The table shows the criteria used in respect to original ISS criteria (see Table 1.1), cytogenetic evaluation and serum LDH measurement for stratifying patients into three stages of prognosis. Cytogenetic detection of deletion of 17p, translocation t(4;14) and/or translocation t(14;16) are considered to stratify a patient as high-risk. Adapted from (Palumbo et al. 2015).

Stage	R-ISS criteria
I	ISS stage I, standard-risk cytogenetics, and serum LDH < the upper limit of normal
II	Meets R-ISS criteria for neither stage I nor stage III
III	ISS stage III, high-risk cytogenetics, and serum LDH > the upper limit of normal

In addition, patients may accumulate new cytogenetic abnormalities over time due to genomic instability and these secondary genetic events usually relate to pathways that drive tumour progression, such as proliferation and survival (Brioli et al. 2014b). The acquirement of new mutations as the disease progresses is known as clonal evolution and leads to different tumour sub-clones arising and becoming dominant at any one time (Brioli et al. 2014a; Paíno et al. 2015). This creates an even more complex level of heterogeneity in MM because the change in tumour cytogenetic profile can impact on a patients prognosis and response to individual treatments. For example, a treatment that may have previously reduced the tumour burden previously, may not be successful a second time due to a different sub-clone gaining dominance.

1.1.5. Current therapies

As mentioned previously, MM remains an incurable disease. Therefore, the main aim of current MM treatment is to achieve and then maintain a complete remission (CR), which should result in an increase the disease free survival of the MM patient. The recent increase in our understanding of the biology of MM has led to an increase in the treatments available for this disease.

The treatment of MM involves three main therapy steps: induction, consolidation and maintenance (Moreau et al. 2015). The induction stage of treatment aims to reduce the main bulk of the tumour burden, whereas consolidation therapy aims to eliminate all remaining tumour cells, including sub-clones that may have risen through clonal evolution. Finally, maintenance therapy acts to pressure the tumour cell selection process so that less aggressive malignant plasma cells are selected, to prevent or delay relapse.

The current therapy for MM involves using pharmaceutical agents alongside autologous stem cell transplantation (ASCT). However, ASCT is limited to MM patients that have a good fitness score and are usually less than 65 years old due to the intensity of this treatment option. Therefore, for most MM patients, comparatively less intensive drug therapies may be the only available treatment option. The current therapies for MM include cytotoxic agents, immunomodulatory agents (IMiDs), proteasome inhibitors and corticosteroids, all of which may be used as a monotherapy or in combination. Over the last decade, a handful of novel frontline agents have been approved for use in MM treatment and these include the IMiDs thalidomide, lenalidomide and pomalidomide, and the proteasome inhibitors bortezomib and carfilzomib. These agents are regularly used for both transplant and non-transplant eligible MM patients. However, MM patients with high-risk disease often have a poor prognosis even with the conventional therapies and are frequently enrolled on clinical trials at diagnosis to improve their outcome (Naymagon a Abdul-Hay 2016).

1.1.5.1. Immunomodulatory agents

Thalidomide and its derivative lenalidomide are two of the IMiDs that are used as frontline therapy for the treatment of MM. These have been found to be highly effective against MM, especially when used in combination with bortezomib and dexamethasone, and their use has resulted in a 50% improvement in median MM survival (Kumar et al. 2008; Stewart et al. 2009). Preclinical studies suggest that these agents induce cell cycle arrest and apoptosis in MM cells as well as interrupting the

interaction of malignant plasma cells with the BMM (Davies a Baz 2010). The immunomodulatory action of these agents involves increasing tumour cell killing through activation of $CD8^+$ T cells and increasing the expression of death effector molecules on natural killer cells (Davies a Baz 2010). Despite this, the two agents possess some mechanistic differences, for example lenalidomide possesses greater immunomodulatory properties when compared to thalidomide (Davies a Baz 2010). For this reason, lenalidomide can be used as a second line treatment for MM regardless of prior response to thalidomide.

Pomalidomide, a next generation thalidomide derivative, was granted accelerated approval for use in MM in 2013 and this is currently used a third line treatment option after the MM disease becomes resistant to precursor IMiDs and bortezomib (McCurdy a Lacy 2013). Pomalidomide has been found the be the most potent of the IMiDs and is predicted to have 100 times and 10 times the potency of thalidomide and lenalidomide, respectively (Gertz 2013).

1.1.5.2. Proteasome inhibitors

Bortezomib was the first proteasome inhibitor used for the treatment of MM and today remains a crucial frontline agent in the treatment of MM. Bortezomib is mainly a reversible inhibitor of the 26S proteasome, which is responsible for the degradation of a wide range of proteins (Boccadoro et al. 2005). As a result, 26S proteasome inhibition can lead to apoptosis, an unfolded protein response, a heat-shock response and cell cycle arrest in MM cells due to the accumulation of misfolded, ubiquitinated and pro-apoptotic proteins (Hideshima et al. 2002; Obeng et al. 2006). Malignant cells on average display a higher level of proteasome activity so are more sensitive to the negative effects caused by proteasome inhibition (Dou a Li 1999). Moreover, bortezomib may also indirectly disrupt MM cell survival and drug resistance through inhibiting the interaction of MM cells with the BMM (Reddy a Czuczman 2010; Zangari et al. 2012). One of the main adverse events that are observed with bortezomib is the development of peripheral neuropathy in some patients

(Richardson et al. 2012). This is thought to be due to the lack of inhibitory specificity of bortezomib because this agent can reversibly inhibit a wide range of other serine proteases.

Carfilzomib is a second-generation proteasome inhibitor that is also approved for the treatment of MM, although at present only as a third-line therapy following the use bortezomib and IMiDs (Perel et al. 2016). It is approved for use either as a monotherapy or in combination with dexamethasone (a corticosteroid) and lenalidomide (Perel et al. 2016). Carfilzomib is an irreversible inhibitor of the 20S proteolytic core of the 26S proteasome and this activity has been shown to promote apoptosis, cell cycle arrest and inhibition of tumourigenesis in MM cells (Kortuem a Stewart 2013). In addition, this proteasome inhibitor provides a more specific alternative to bortezomib and less adverse events relating to neuropathy (Dimopoulos et al. 2016). As a result, carfilzomib can be used as a proteasome inhibitor alternative in those patients who cannot tolerate bortezomib due to the development of neuropathy. Moreover, the difference in the molecular targeting of carfilzomib also means that this agent may still successfully treat MM even after the development of bortezomib resistance (Siegel et al. 2012).

1.1.6. The future of MM treatment

Despite the recent increase in novel agents for the treatment of MM over the last decade, the disease still remains incurable and progression-free survival is limited, especially in the high-risk MM patient group (Kumar et al. 2008; Naymagon a Abdul-Hay 2016). A limiting factor is the emergence of treatment resistant sub-clonal populations in MM, which leads to patient relapse and refractory MM (Egan et al. 2012; Magrangeas et al. 2013). At this point, the treatment options are limited as the frontline therapies are exhausted.

As a result, targeted therapies have become an interesting alternative to the current therapies that exist for MM and may provide a more beneficial form of treatment that can remain effective even in refractory patients. Their clinical use in MM is further favoured due to advances in cytogenetic

screening and the understanding of the relevance of specific cytogenetic abnormalities in disease progression and risk stratification. In the future, this may encourage the use of more specific agents earlier in the treatment regime based on the outcome of patient cytogenetic screening. In addition, targeted therapies may also help to reduce the adverse effects of treatment, which would be particularly beneficial for MM patients due to their relatively high mean age at diagnosis and comorbidities associated with ageing.

Many novel agents are currently in development for MM and these are targeting a wide a range of tumour mitigating factors in MM (Table 1.4). These include, but are not limited to, CD138 and CD38 targeting mAbs, cyclin-dependent kinase inhibitors, Bcl-2 inhibitors, IL-6 inhibitors, and BAFF and APRIL inhibitors, which are all factors that have been shown to be essential for malignant plasma cells so are frequently dysregulated in MM (Naymagon a Abdul-Hay 2016). In addition, as proteasome inhibitors are still used as efficacious treatments in MM, substantial effort is going into producing the next generation of improved proteasome inhibitors that may overcome bortezomib resistance (Table 1.4).

Another example of a tumour-promoting genetic abnormality that is commonly expressed in MM patients involves deregulation of the nuclear factor-κB signalling pathways (Annunziata et al. 2007; Keats et al. 2007; Chapman et al. 2011). These pathways have been shown to be highly relevant in MM disease progression due to their role in supporting the growth, survival and proliferation of malignant plasma cells within the BMM (Hideshima et al. 2002). Moreover, there is much evidence that targeting this signalling pathway may provide a potential therapeutic option due to some of the existing MM treatments imparting some of their anti-tumour activity through inhibition of nuclear factor-κB signalling pathways.

Table 1.4 A list of some of the next generation novel agents that are currently in development for the treatment of MM.
Adapted from (Hengeveld a Kersten 2015; Naymagon a Abdul-Hay 2016).

Name	Type	Target	Progress
Ixazomib	PI	20S proteasome	Ixazomib is the first oral PI to enter clinical trials and is effective in BTZ resistant MM cells, induces a noticeable improvement in PFS in both standard and high risk patient groups, and shows a good toxicity profile with an acceptable incidence of neuropathies. Approved by the FDA in 2015 for use in combination with Len and Dex to treat MM patients that have received one previous therapeutic agent.
Marizomib	PI	20S proteasome	This investigational agent displays increased cytotoxicity and duration of action, even in BTZ resistant MM cells. Phase I studies show that AE's are limited and do not include neuropathies . In vitro synergy has been observed with IMiDs and marizomib could be used in combination with BTZ due to the difference in apoptosis related MOA.
Daratumumab	mAb	CD38	Due to the high CD38 expression on MM cells, this mAb has been shown to mediate the phagocytosis of MM cells by macrophages. Phase I/II trials showed high efficacy when used in combination with Len and subsequent trials also demonstrated an encouraging efficacy when used as a monotherapy in refractory MM patients who had received a median of five prior treatments. In 2015, the FDA approved its use as a MM therapy in patients that had received three prior treatments and it was approved by the EMA in 2016 for MM patients resistant to IMiDs and PI's.
Indatuximab	mAb	CD138	Indatuximab is a chimerised anti-CD138 mAb conjugated to DM4, which is a potent inhibitor of microtubule assembly. As CD138 is a plasma cell specific antigen, this allows specific targeting of this agent to MM cells and internalization of DM4 resulting in MM cell death. Preclinical results demonstrated synergy with Len and a phase I/IIa study has shown high efficacy when used in combination with Len and Dex in refractory MM patients, where even non-responders still achieved disease stabilisation.
ABT-199	SMI	Bcl-2	Bcl-2 is an important anti-apoptotic regulatory protein in a number of haematological malignancies and Bcl-2 SMI's have been shown to induce tumour cell apoptosis. ABT-199 is the first orally bioavailable Bcl-2 inhibitor and preliminarily investigations in MM show that it is highly effective at inducing cell death in cells that are dependent on Bcl-2 expression for survival. This indicates that this agent may be therapeutically relevant in certain MM patient groups as a targeted therapy and this is further supported by the effectiveness of ABT-199 in MM cell lines that possess the t(11;14) cytogenetic MM phenotype. ABT-199 has demonstrated ex vivo synergy with carfilzomib but so far the safety profile of this specific agent is flawed with TLS presenting as a common feature.

Table 1.4 continued

Dinaciclib	SMI	CDK	CDKs are protein kinases that are essentials in the regulation of the cell cycle. Dinaciclib is an inhibitor of CDK1, CDK2, CDK5 and CDK9. Its use as a single agent in relapsed/refractory MM in a phase I trial has indicated it has moderate efficacy. A trial investigating the use of Dinaciclib in combination with BTZ in MM is a future possibility due to evidence suggesting that CDK5 inhibition may enhance the activity of PI's.
Siltuximab	mAb	IL-6	Siltuximab is a chimeric mAb targeting IL-6, which is a major BMM factor that supports the survival of malignant MM cells. Phase II trials have so far failed to show increased efficacy or PFS when compared to the current regimes used to treat MM or even when the IL-6 inhibitor is used in combination with BTZ. However, it is presently being investigated for use in high-risk SMM due to the association of IL-6 concentration with MM disease stage.
Atacicept	RFP	BAFF & APRIL	Atacicept is a RFP consisting of the Fc region of human IgG and the binding domain of the TACI receptor. Therefore, it can bind both BAFF and APRIL, preventing their interaction with their receptors. BAFF and APRIL are two factors that have been shown to be highly relevant to MM disease progression and mediate some of this action through NF-κB signalling. In a human mouse model of MM and in myeloma cell lines, Atacicept was shown to promote anti-myeloma activity, especially in those cells that possessed high expression of TACI. A phase I study showed further clinical efficacy in MM through stabilisation or reduction in the number of BM plasma cells with 5/11 patients achieving PFS following 1 cycle. However, further progress has been stalled due to the immunosuppression arising.
Tabalumab	mAb	BAFF	Tabalumab is a human mAb that has neutralising activity against both soluble and receptor-bound BAFF. In murine xenograft models, the agent has shown promising anti-MM effects, including osteoclastogenesis. A phase I study showed that when Tabalumab is used in combination with BTZ, it is well tolerated and induced a PR or CR in ~50% of patients. Other phase I studies in refractory MM patients have shown that Tabalumab has an acceptable safety profile and can be used in combination with Dex and BTZ to improve response rates. However, a recent phase II trial failed to show an improvement in PFS when Tabalumab was used in combination with Dex and BTZ, compared to treatment with Dex and BTZ in relapsed or refractory MM.

AE = adverse event, **APRIL** = a proliferation-inducing ligand, **BAFF** = B-cell activating factor, **BTZ** = bortezomib, **CDK** = cyclin-dependent kinases, **CR** = complete response, **Dex** = Dexamethasone, **EMA** = European Medicines Agency, **Fc** = fragment crystallisable, **FDA** = the US Food and Drug Administration, **IMiDs** = immunomodulatory agents, **Len** = Lenalidomide, **mAb** = monoclonal antibody, **MM** = multiple myeloma, **MOA** = mechanism of action, **PFS** = progression-free survival, **PI** = proteasome inhibitor, **PR**= partial response, **RFP** = recombinant fusion protein, **SMI** = small molecule inhibitor, **SMM** = smoldering MM, **TACI** = transmembrane activator and CAML interactor, **TLS** =tumour lysis syndrome.

1.2. Nuclear factor-κB (NF-κB)

Nuclear factor-κB (NF-κB) was first discovered as a transcription factor that transcriptionally enhances the regulation of the immunoglobulin κ light chain gene by binding to a highly conserved DNA sequence known as the κB element (Sen a Baltimore 1986). NF-κB was at first thought to be a B-cell-specific nuclear protein but has since been found to be expressed in a number of cells due to its important regulatory role in a number of processes, including immunity and inflammation (Lawrence 2009; Hayden a Ghosh 2011). In normal B-cells, NF-κB is required for the regulation of genes relating to B-cell proliferation, differentiation, activation and survival (Gasparini et al. 2014).

1.2.1. NF-κB subunits

NF-κB exists as either homodimers or heterodimers of its five subunits; p65, p50, c-Rel, p52 and RelB. The structures of the five NF-κB subunits are shown in Figure 1.1. The subunits all contain the same highly conversed 300 amino acid region called the Rel homology domain (RHD) at their N-terminals and it is this region that allows subunit dimerisation, dimer nuclear localisation and DNA κB element binding (Zheng et al. 2011). The N-terminal of the RHD in NF-κB subunits interacts with DNA at the consensus sequence of NF-κB target genes corresponding to 5'-GGGRNYYYCC-3' (R = purine, Y = pyrimidine and N = any nucleotide) (Chen a Ghosh 1999). The nuclear localisation signals (NLS) in each NF-κB subunit is located at the C-terminal end of the RHD (Zheng et al. 2011).

Although all NF-κB subunit dimers bind to DNA κB sites to transcriptionally regulate target genes, the different dimer combinations can act as transcriptional activators or repressors. One reason for this is that the transcription activation domain (TAD), which is required for positive regulation of NF-κB target genes, is expressed in only the p65, c-Rel and RelB subunits (Ghosh et al. 2012). Therefore, NF-κB homodimers of p50 or p52 are thought to act as inhibitors or repressors of target genes due to the absence of a TAD (Figure 1.1), although they can become transcriptional

activators through interaction with nuclear IκB proteins (Ghosh et al. 2012; Hinz et al. 2012).

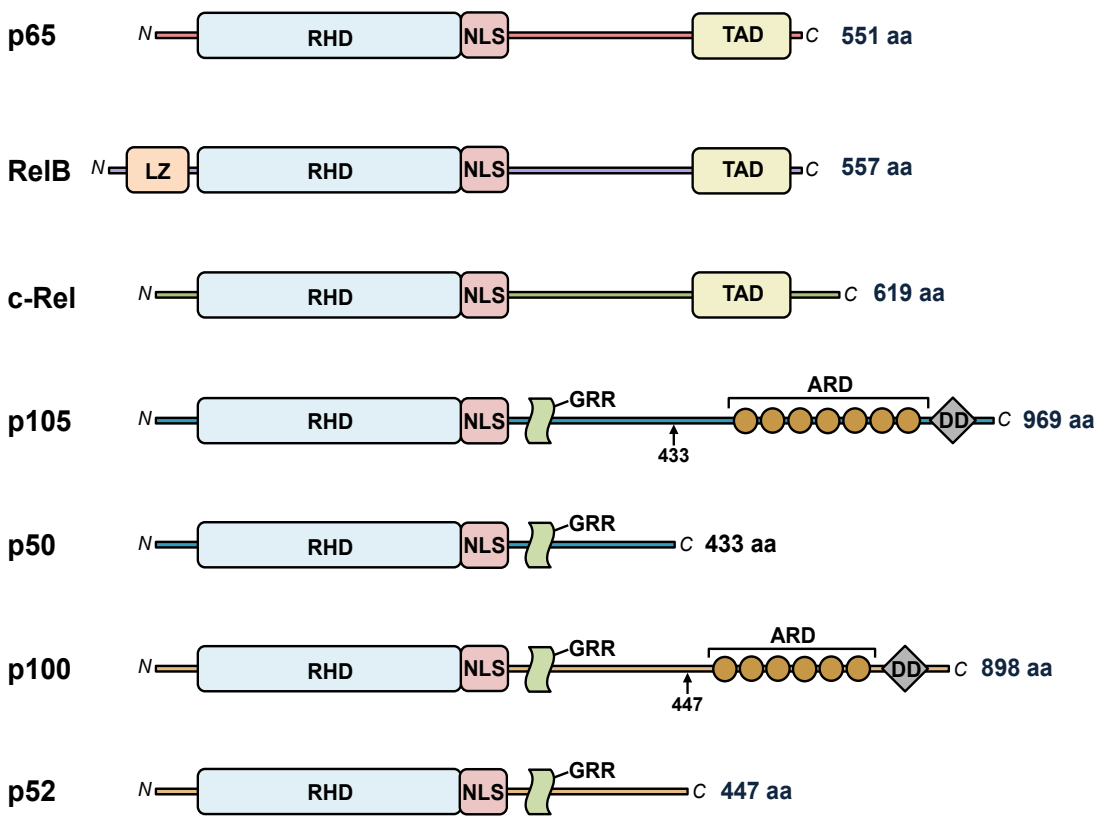

Figure 1.1 The structures of the NF-κB subunits p65, RelB, c-Rel, p105/p50 and p100/p52.
The structures of the five NF-κB subunits p65, RelB, c-Rel, p50 and p52 are shown alongside the precursor subunits p105 and p100. The N- and C-terminals of each subunit protein are indicated using *N* and *C*, respectively, and the length of each subunit protein in amino acids (aa) is provided. On the p105 and p100 precursor subunits, the arrow indicates the position of cleavage to the active NF-κB subunits p50 and p52, respectively. Adapted from (Chen a Greene 2004; Hayden a Ghosh 2012). ARD = ankyrin repeat domain, DD = death domain, GRR = glycine rich region, NLS = nuclear localisation signal, LZ = leucine zipper, RHD = Rel homology domain and TAD = transcription activation domain.

The NF-κB subunits can be divided into two categories; subunits that are synthesised in their mature form and those subunits that are synthesised in a precursor form and require further processing. The p65, c-Rel and RelB subunits are synthesised in their mature forms whereas the p50 and p52 NF-κB subunits are synthesised as precursor molecules p105 and p100, respectively (Hayden a Ghosh 2008; Zheng et al. 2011).

Each NF-κB subunit is expressed to varying extents in different cell types, although all five subunits are expressed in B-cells where they have been found to be highly relevant in modulating the differentiation, proliferation, survival and activation of B-cells (Gasparini et al. 2014).

1.2.2. Inhibitory protein of NF-κB (IκB proteins)

In unstimulated cells, NF-κB is held inactive in the cytoplasm as a result of interaction with inhibitory proteins of NF-κB (IκB proteins). The IκB proteins include the classical IκB proteins IκBα, IκBβ and IκBε, the nuclear IκB proteins, Bcl-3 and IκBζ, and the precursor proteins p100 and p105 (Hinz et al. 2012). The structures of the classical and nuclear IκB proteins are shown in Figure 1.2. The IκB proteins characteristically contain six to seven ankyrin-repeat motifs that interact with the RHD on the NF-κB subunits to mask the NLS and help regulate NF-κB activity by restricting it to the cytoplasm of the cell (Chen a Greene 2004; Zheng et al. 2011).

For NF-κB to become activated, the IκB proteins must undergo phosphorylation at specific serine residues (see Figure 1.2), which subsequently leads to ubiquitin-dependent proteasomal degradation (Kanarek et al. 2010; Hinz a Scheidereit 2014). The IκB proteins are polyubiquitinated at specific lysine residues (see Figure 1.2) that are located in their N-terminal regulatory domains and the polyubiquitinated IκB proteins are selectively degraded by the 26S proteasome (Chen et al. 1995; Karin et al. 2002).

In the case of the precursor proteins p100 and p105, the C-terminal protein domains are post-translationally cleaved to the smaller p52 and p50 subunits to remove the ankyrin-repeat regions that mask the NLS (Henkel et al. 1992). The structure of the p105 and p100 precursor subunits also contains a glycine-rich domain that follows the conventional RHD (see Figure 1.1). The glycine-rich region (GRR) in both the p105 and p100 subunit prevents complete protein degradation to allow the release of the active p50 and p52 subunits, respectively (Lin a Ghosh 1996; Heusch et al. 1999; Orian et al. 1999). The p105 protein is constitutively processed to the p50 subunit whereas p100 processing is a more closely regulated process in unstimulated

cells (Xiao et al. 2001). Constitutive processing of p105 and p100 is prevented by a C-terminal death domain downstream of the ankyrin repeat domain, which acts as a processing inhibitory domain (Xiao et al. 2001).

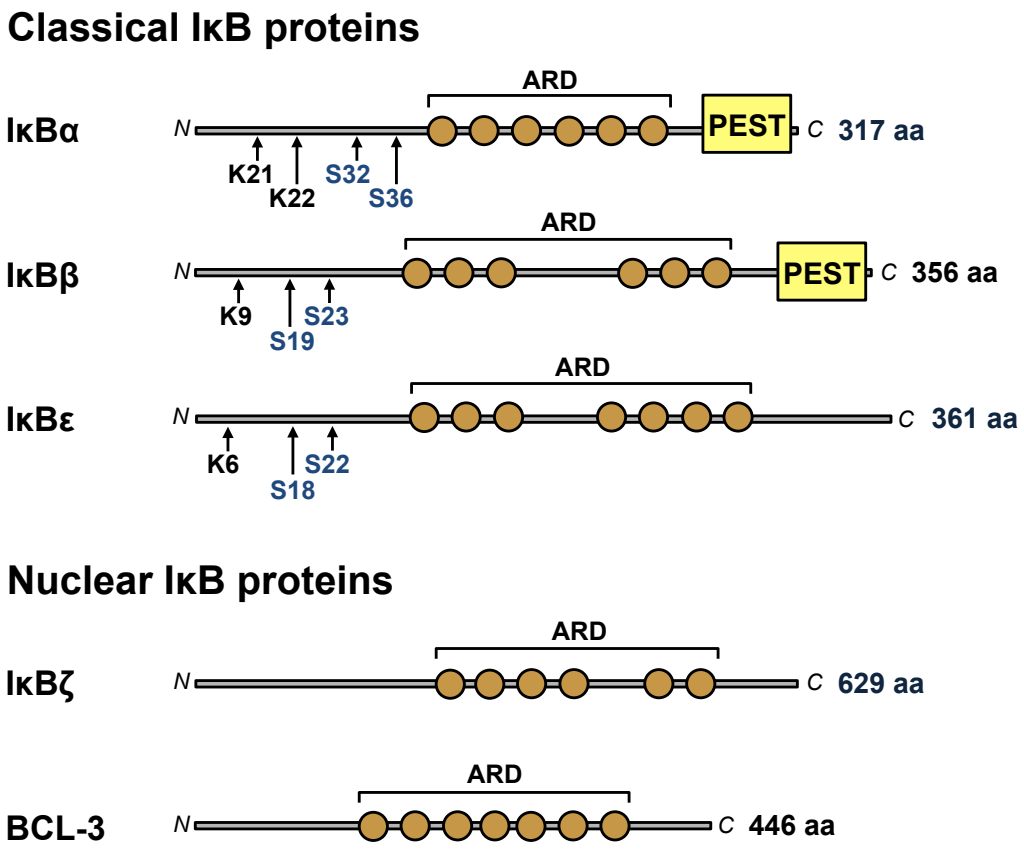

Figure 1.2 The structures of the IκB proteins IκBα, IκBβ, IκBε, IκBζ, and BCL-3. The structures of the three classical IκB proteins, IκBα, IκBβ and IκBε, are shown alongside the atypical, nuclear IκB proteins, IκBζ, and BCL-3. The N- and C-terminals of each subunit protein are indicated using *N* and *C*, respectively, and the length of each subunit protein in amino acids (aa) is provided. The specific serine residues that are required for IKK phosphorylation and specific lysine residue(s) that are essential for ubiquitination are indicated for each classical IκB protein. The PEST regions on the C-terminal of IκBα and IκBβ are also indicated. The nuclear IκB protein BCL-3 can interact with nuclear p50 and p52 proteins to function as a transcriptional co-activator. Adapted from (Huxford a Ghosh 2009; Vallabhapurapu a Karin 2009; Hayden a Ghosh 2012). ARD = ankyrin repeat domain, K = lysine residue, S = serine residue, PEST = proline (P), glutamic acid (E), serine (S), and threonine (T) domains are indicated as PEST.

Each IκB protein displays a selective binding preference towards the NF-κB subunits. For example, IκBα favours interactions with heterodimers that contain the p50, p65 and c-Rel subunits whereas the IκBβ and IκBε proteins preferentially sequester p65 and c-Rel heterodimers within the

cytoplasm (Hinz et al. 2012). Interestingly, the classical IκB proteins do not interact with the RelB subunit and it is the precursor protein, p100, that displays the highest affinity for RelB (Dobrzanski et al. 1994).

The IκB proteins Bcl-3 and IκBζ migrate to the nucleus when they become overexpressed and, once localised in the nucleus, they possess binding specificity towards p52 and p50 homodimers (Hinz et al. 2012). Through interaction with the p50 and p52 homodimers, the nuclear proteins Bcl-3 and IκBζ can function as transcriptional co-activators (Ghosh et al. 2012).

1.2.3. The IκB kinase (IKK) complex

Upon activation of NF-κB signalling, the IκBα, IκBβ or IκBε proteins undergo phosphorylation by the IκB kinase (IKK) complex. This is a complex that is composed of three proteins called IKKα, IKKβ and NF-κB essential modulator (NEMO), which is also known as IKKγ (Liu et al. 2012). Figure 1.3 shows the structures of the three IKK proteins.

The IKKα and IKKβ proteins share approximately 51% sequence homology, which includes an N-terminal kinase domain consisting of two serine residues and a NEMO-binding domain (NBD) at the C-terminals. On the other hand, NEMO is structurally different from the IKKα and IKKβ proteins (Figure 1.3) and does not include the kinase domain that is found in the other IKK proteins (Liu et al. 2012; Hinz a Scheidereit 2014). For this reason, the NEMO protein acts as a regulatory subunit within the IKK complex and allows the IKK complex to interact with upstream activators through its C-terminal zinc finger motif (Ghosh a Karin 2002). Moreover, in the absence of NEMO, the IKKα and IKKβ cannot become activated through normal NF-κB stimulation, which indicates that NEMO is essential in NF-κB regulation (Yamaoka et al. 1998).

The IKK complex is suggested to comprise of an IKKα and IKKβ heterodimer that binds to dimers of NEMO using the NBDs on each respective IKK (Rothwarf a Karin 1999; Miller a Zandi 2001). The IKKα and

IKKβ proteins dimerise using their leucine zipper domains and helix-loop-helix regions (Jost a Ruland 2007; Huxford a Ghosh 2009).

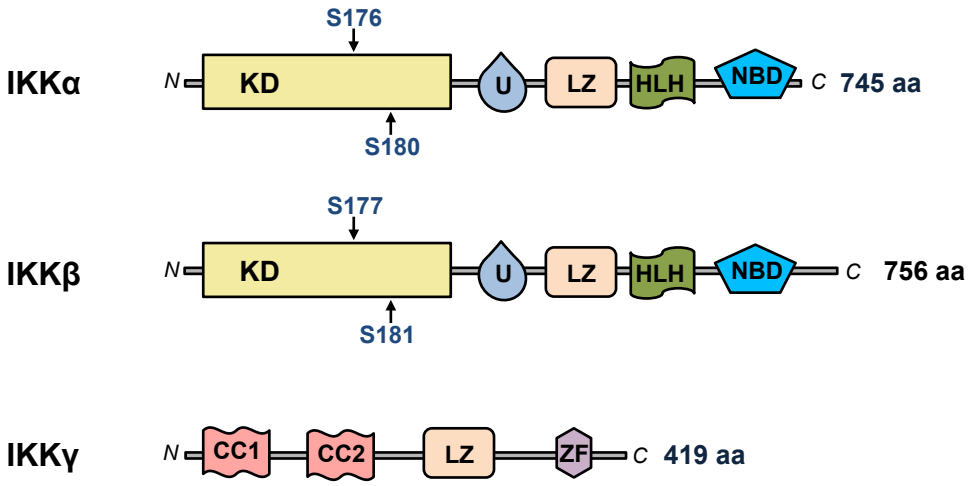

Figure 1.3 The structures of the IKK complex proteins IKKα, IKKβ and IKKγ (NEMO).
The structures of the three IKK proteins, IKKα, IKKβ and IKKγ, also known as NEMO, are shown. The N- and C-terminals of each subunit protein are indicated using *N* and *C*, respectively, and the length of each subunit protein in amino acids (aa) is provided. The specific serine residues within the kinase domain are indicated for IKKα and IKKβ, along with the position of the leucine zipper domains and helix-loop-helix regions that are required for subunit dimerisation. The location of other structural domains such as the NBD, ubiquitin-like domain, zinc-finger domain and predicted coiled-coil motifs are also shown on the schematic above. Adapted from (Hayden a Ghosh 2004; Huxford a Ghosh 2009).
CC1/2 = coiled-coil motifs, KD = kinase domain, HLH = helix-loop-helix, LZ = leucine zipper, NBD = NEMO binding domain, S =serine residue, U = ubiquitin-like domain and ZF = zinc-finger domain.

The IKK complex is activated through phosphorylation of the IKKα and IKKβ proteins at two specific serine residues, which induces a conformational change that activates the catalytic kinase domain (Mercurio et al. 1997; Ling et al. 1998; Delhase et al. 1999). However, the mechanism through which the IKK complex is phosphorylated remains unconfirmed, although two general mechanisms have been suggested; transauto-phosphorylation or specific IKK kinases (IKKK) (Liu et al. 2012; Hinz a Scheidereit 2014). The IKKKs recruited may differ based on the specific stimuli that initially induces the NF-κB activity.

1.2.4. NF-κB signalling

Bringing together the above information, the activation of NF-κB is generally described as occurring through two pathways; the canonical and non-canonical NF-κB signalling pathways.

1.2.4.1. The canonical signalling pathway

Examples of cellular stimuli that can directly activate the canonical pathway include the pro-inflammatory cytokines TNFα and IL-1, the B-cell agonists, RANKL and CD40; and the danger signals provided by toll-like receptors and lipopolysaccharide. The antigen receptors such as the B-cell receptor can also activate NF-κB (Siebenlist et al. 2005; Vallabhapurapu a Karin 2009).

The p65, p50 and c-Rel NF-κB subunits are typically associated with canonical NF-κB signalling. The IκB proteins act to sequester the canonical subunits in the cytoplasm and each IκB protein displays specific binding preferences towards the individual subunits.

In the canonical signalling pathway, the IKK complex is predicted to be phosphorylated by IKKKs, such as Transforming growth factor beta-activated kinase 1 (TAK1) (Wang et al. 2001). Activation of the IL-1 receptor is followed by the activation of the E3 ligase TNF receptor-associated factor 6 (TRAF6), which then facilitates the formation of Lys^{63}-linked polyubiquitination (K63-pUb) chains in the presence of the dimeric ubiquitin-conjugating Ubc13-Uev1A (Deng et al. 2000; Wang et al. 2001). Similarly, TNFα stimulation induces the polyubiquitination of RIP1 by activated cIAPs or TRAF2, allowing RIP1 to act as a scaffold for the recruitment of TAK1 and the IKK complex to the TNF receptor (Ea et al. 2006; Newton et al. 2008). In both scenarios, TAK1 is then activated through interaction with either TRAF6 formed K63-pUb chains or K63-pUb chains on RIP1, which induces autophosphorylation of TAK1 (Wang et al. 2001; Xia et al. 2009). The binding of K63-pUb chains to the NEMO domain of the IKK complex facilitates the activation of the IKKβ components by TAK1 phosphorylation (Ea et al. 2006; Wu et al. 2006). On the other hand, it has also been demonstrated that K63-pUb chains and linear pUb chains are

capable of directly activating the IKK complex through interaction with NEMO (Xia et al. 2009; Walczak et al. 2012).

In the canonical NF-κB pathway, the classical IκBs are mainly phosphorylated by activated IKKβ, although it has also been suggested that IKKα may also be capable of carrying out this phosphorylation, although less efficiently (Adli et al. 2010). IKKβ phosphorylates IκBα at serines 32 and 36; IκBβ at serines 19 and 23, and IκBε at serines 18 and 22 (Vallabhapurapu a Karin 2009). The phosphorylated IκB then undergoes polyubiquitination by a ubiquitin ligase related to SCF and is consequently degraded by the proteasome (Kanarek a Ben-Neriah 2012).

Following the degradation of IκB, the NLS is exposed on the NF-κB subunits and so they are no longer sequestered in the cytoplasm. However, IκBα is not fully effective at masking the NLS on NF-κB dimers so NF-κB-IκBα complexes can translocate to the nucleus in the absence of canonical pathway stimuli (Carlotti et al. 2000; Malek et al. 2001). The existence of a nuclear export sequence (NES) on IκBα results in the oscillation of these complexes between the nucleus and cytoplasm, with nuclear export being dominant so as to localise the complexes mainly in the cytoplasm (Johnson et al. 1999; Huang et al. 2000). As a result, the degradation of IκBα shifts this balance to favour the nuclear localistaion of NF-κB dimers (Hayden a Ghosh 2008).

In the nucleus, NF-κB subunits bind to DNA κB elements to transcriptionally regulate genes. During nuclear translocation, the canonical NF-κB subunit p65 can undergo phosphorylation by cyclic AMP-dependent protein kinase or casein kinase II. The purpose of phosphorylation of p65 appears to allow the NF-κB subunit to bind DNA with a greater affinity than its unphosphorylated form (Ghosh a Karin 2002).

Figure 1.4 provides a schematic overview of the canonical NF-κB signalling pathway.

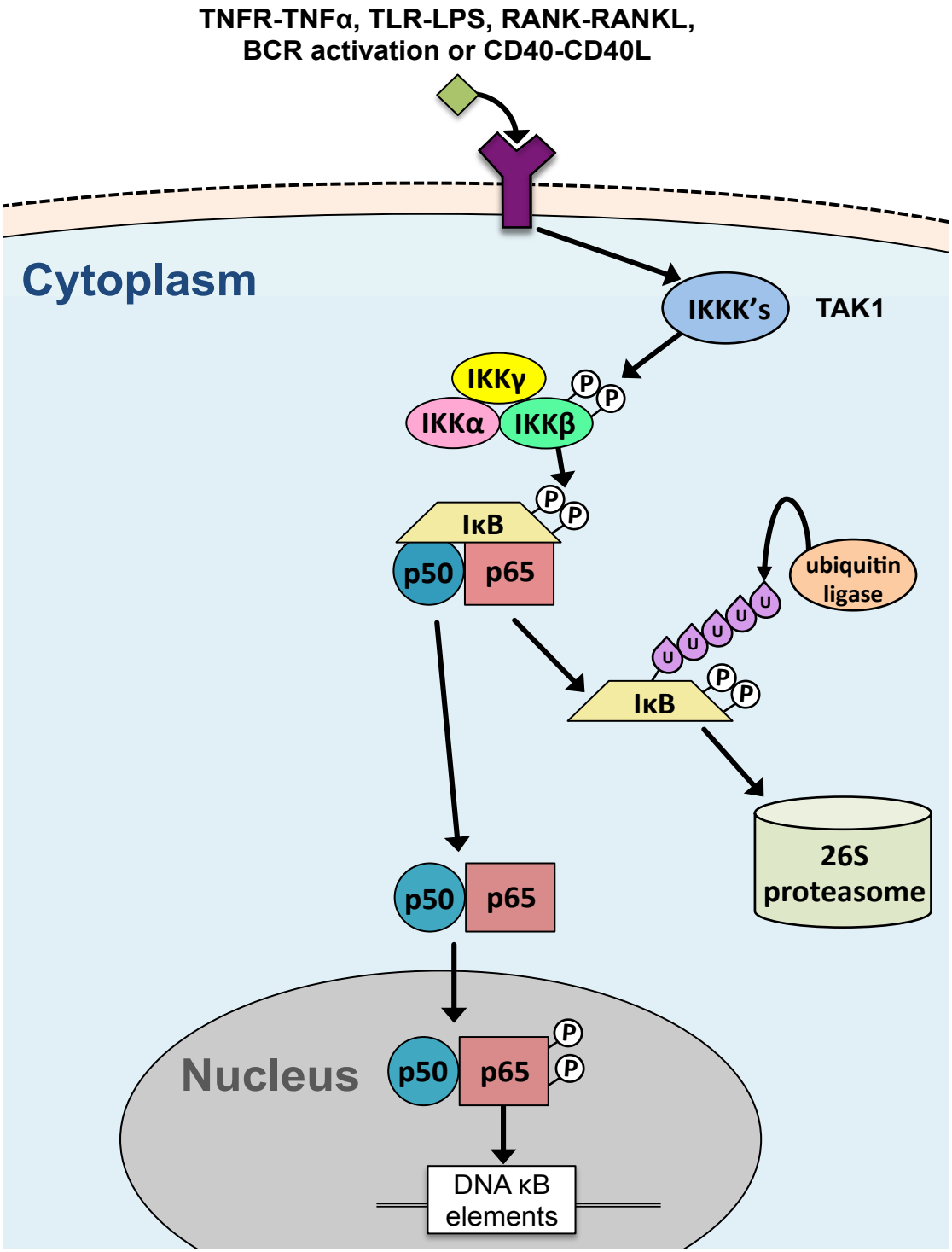

Figure 1.4 The canonical NF-κB signalling pathway.
The canonical signalling pathway is activated through a variety of stimuli, which activates IKKK's, such as TAK1. IKKK's phosphorylate and activate IKKβ and IKKβ phosphorylates the IκB protein at the residues 18 and 22. The IκB protein is subsequently ubiquitinated by a SCF-family ubiquitin ligase and undergoes degradation by the 26S proteasome. The free NF-κB dimers translocate to the nucleus where they bind to DNA κB elements to regulate gene transcription. Adapted from (Jost a Ruland 2007; Hayden a Ghosh 2012).
BCR = B-cell receptor, IκB = Inhibitor of κB, IKK = IκB kinase, IKKK's = IKK kinases, LPS = lipopolysaccharide, P = phosphorylate, RANK = receptor activator of NF-κB, RANKL = RANK ligand, TLR = toll-like receptor, TNFα = Tumour necrosis factor α, TNFR = TNF receptor, U = ubiquitin.

1.2.4.2. Non-canonical signalling pathway

The non-canonical pathway can be activated by some of the same and some different cell stimuli, including BAFF, lymphotoxin β, RANK and CD40 ligand (Vallabhapurapu a Karin 2009; Kaileh a Sen 2012).

Before it is processed to p52, the IκB-like protein p100 can inhibit the nuclear translocation of the RelB subunit through interaction with the RHD of RelB (Solan et al. 2002). Therefore, the conversion of p100 activates non-canonical NF-κB signalling by allowing the nuclear translocation of p52 and RelB dimers. However, under normal cellular conditions the generation of p52 is tightly regulated and can only occur following stimulation of the non-canonical pathway (Heusch et al. 1999).

NF-κB inducing kinase (NIK) is a MAP3K-related protein kinase that activates NF-κB mainly through the phosphorylation of IKKα, which predominantly results in non-canonical NF-κB pathway signalling (Malinin et al. 1997; Ling et al. 1998). NIK is also capable of phosphorylating IKKβ to activate the canonical pathway but NIK has less affinity for this IKK so IKKα is the preferred substrate (Ling et al. 1998; Senftleben et al. 2001).

In unstimulated cells, NIK undergoes constant proteasomal degradation due to interaction with TRAF3. Upon cellular stimulation of the non-canonical NF-κB pathway, the ubiquitin ligase complex TRAF2-cIAP1/2 is recruited to TRAF3 and TRAF2 becomes activated (Vallabhapurapu et al. 2008). TRAF2 then carries out the ubiquitination of cIAP1/2, which enhances its ubiquitin ligase activity and TRAF3 in turn become ubiquitinated. The ubiquitinated TRAF3 dissociates from NIK and undergoes proteasomal degradation. Once dissociated, NIK is stabilised and can undergo activation through autophosphorylation (Vallabhapurapu et al. 2008).

Once activated, IKKα phosphorylates the p100 precursor subunit to the active p52 subunit. The processing of p100 to the active p52 subunit has been shown to be dependent on IKKα phosphorylation and can occur in the absence of IKKβ and IKKγ (NEMO) (Senftleben et al. 2001).

Phosphorylation of p100 promotes β-TrCP binding to the IκB phosphopeptide region, which in turn allows polyubiquitination and subsequent proteasomal degradation of the multiple ankyrin repeats (Yaron et al. 1998; Fong a Sun 2002).

RelB does not associate with any other IκB proteins other than the p100 precursor protein (Solan et al. 2002). Therefore, proteasomal degradation of the ankyrin-repeat domain of p100 exposes the NLS on the RelB and p52 subunits. RelB cannot homodimerise and commonly forms a heterodimer with the p52 subunit, although it may also heterodimerise with the p50 subunit (Ryseck et al. 1992; Dobrzanski et al. 1994). Exposure of the NLS allows the RelB-p52 dimer to translocate to the nucleus to bind to DNA κB elements and regulate gene expression. Please refer to Figure 1.5 for a schematic summary of the non-canonical NF-κB signalling pathway.

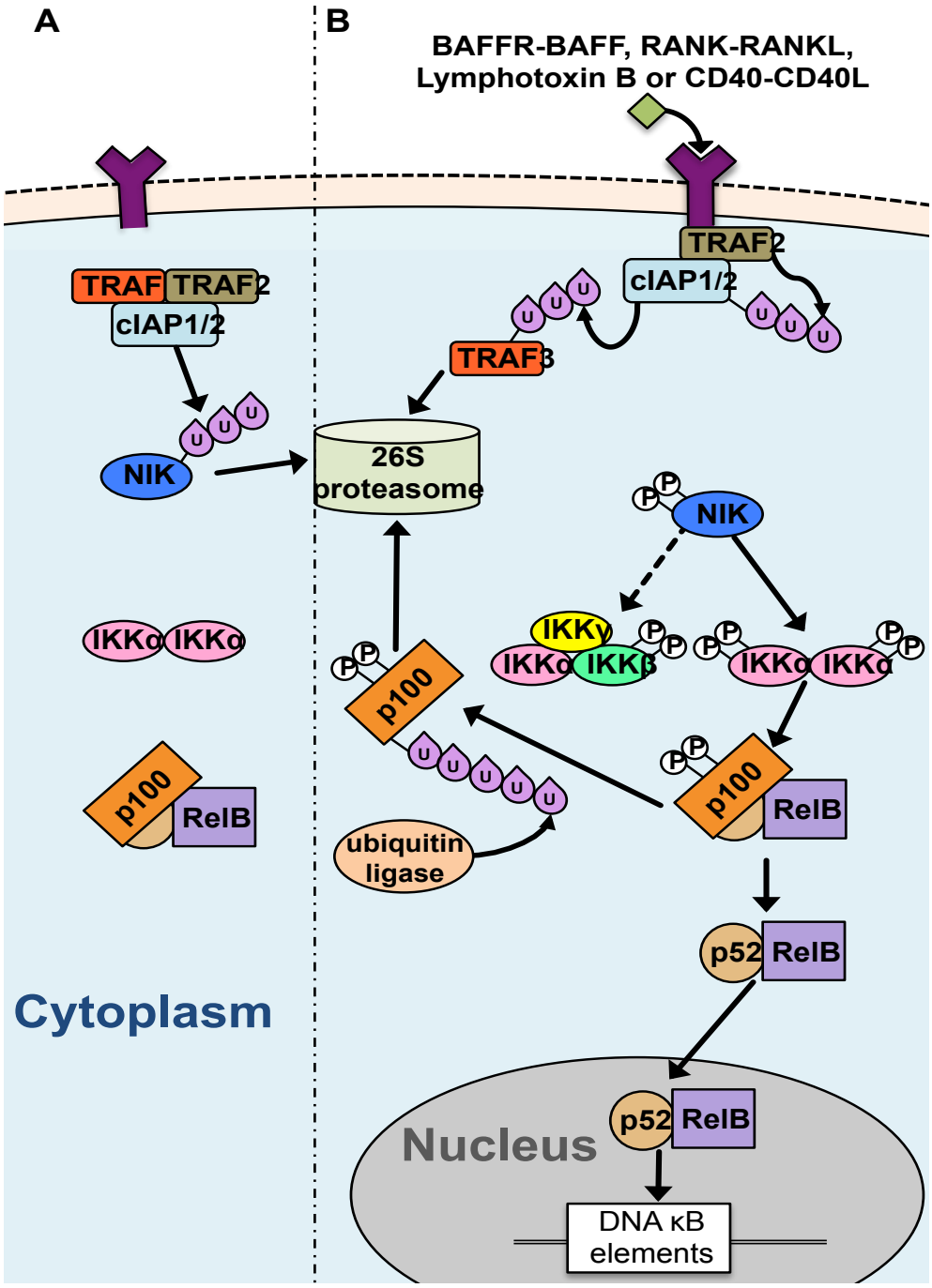

Figure 1.5 The non-canonical NF-κB signalling pathway.
(**A**) In unstimulated cells, NIK undergoes constant proteasomal degradation through interaction with TRAF3. (**B**) Following cellular stimuli, TRAF2/cIAP1/2 is recruited to the receptor and this induces TRAF2 dependent ubiquitination of cIAP1/2. cIAP1/2 then ubiquitinates TRAF3 and TRAF3 undergoes proteasomal degradation. Activated NIK mainly phosphorylates IKKα but to a lesser extent can phosphorylate IKKβ to activate the canonical signalling pathway. Activated IKKα phosphorylates p100 to promote ubiquitination and degradation of the IκB region to free activated p52. The p52/RelB dimers then translocate to the nucleus where they bind DNA κB elements. Adapted from (Jost a Ruland 2007; Hayden a Ghosh 2012).
BAFF = B-cell activating factor, BAFF-R = BAFF receptor, cIAP1/2 = c inhibitors of apoptosis proteins 1/2, IKK = IκB kinase, NIK = NF-κB inducing kinase, P = phosphorylate, RANK = receptor activator of NF-κB, RANKL = RANK ligand, TRAF = TNF receptor-associated factor, U = ubiquitin.

1.2.5 Downstream NF-κB gene regulation

Many genomic studies have identified DNA binding κB sites within a huge number of genes, which indicates that NF-κB is capable of regulating a large number of biological processes (Wang et al. 2012). In addition, changes in the base pairs that construct a target gene's individual DNA κB site can alter the binding preferences of specific NF-κB subunit dimers and define whether the target gene is up- or down-regulated (Leung et al. 2004). As a result, activation of the canonical or non-canonical signalling pathways can regulate different target genes. Two of the main cellular processes that NF-κB signalling is responsible for governing are cell proliferation and apoptosis.

1.2.5.1. Cell proliferation

In B-cells deletion of either the c-Rel, p65 or p105 subunit all result in proliferative defects (Joyce et al. 2001). This indicates that NF-κB signalling is important in cell proliferation and growth and in B-cells this is likely a consequence of activation of the canonical signalling pathway.

More specifically, NF-κB can directly up-regulate the transcription of cyclin D_1, which is associated with the progression into the S phase of the cell cycle, due to the existence of a DNA κB binding site that is present within the cyclin D_1 promoter (Guttridge et al. 1999; Hinz et al. 1999). In addition, NF-κB can regulate the expression of a number of cytokines that can support cell growth and proliferation, including IL-6, Granulocyte-macrophage colony-stimulating factor (GM-CSF) and BAFF (Hideshima et al. 2002; Fuchs 2013). In MM, IL-6 has been shown to be an essential growth factor and most MM cells cannot survive in its absence (Kawano et al. 1988; Hirata et al. 2003). Moreover, the cytokine GM-CSF can synergistically increase MM cell growth with IL-6 (Zhang et al. 1990; Villunger et al. 1998). BAFF is also important in MM cell proliferation, survival and BMM cell adhesion (Novak et al. 2004; Fuchs 2013).

1.2.5.2. Cell survival and anti-apoptotic proteins

The importance of NF-κB in the regulation of apoptosis was shown through several knockout experiments. For example, B-cells that lack

expression of the NF-κB subunits c-Rel, p65 or p50, or the protein IKKβ experience increased cell death (Grossmann et al. 2000; Pasparakis et al. 2002). Moreover, *in vivo* mouse models show that when the canonical-related NF-κB proteins, such as p65, IκBα and IKKβ, are deleted, cells undergo rapid apoptosis (Gasparini et al. 2014). In addition, constitutive RelB activation is observed in approximately 40% of MM cases and the phenotypic advantage of this is to promote MM cell survival by increasing the expression of anti-apoptotic NF-κB target genes such as cIAP2 (Cormier et al. 2013). Overall, this indicates that both the canonical and non-canonical NF-κB pathways are critically involved in cell survival and anti-apoptosis in MM.

Apoptosis can be induced through two main pathways; the extrinsic and intrinsic pathways (Millimouno et al. 2014). The extrinsic pathway involves the activation of death receptors, while molecules that are released from the mitochondria mediate the intrinsic pathway (Ichim a Tait 2016). Both pathways activate caspases, which are cysteine proteases that initiate apoptosis or programmed cell death through the cleavage of cellular proteins. NF-κB can directly increase cell survival by protecting cells from apoptosis induced by TNF activation of the extrinsic pathway. For example, NF-κB induces transcriptional activation of TRAF1/2 and inhibitors of apoptosis proteins (IAPs) such as c-IAP1, cIAP2 and XIAP, all of which block caspase activation and apoptosis (Wang et al. 1998). Other anti-apoptotic NF-κB target genes include X-linked IAP (XIAP) and Bcl-2 and its homologues, such as Bcl-X_L and Mcl-1 (Grossmann et al. 2000; Li et al. 2008).

1.2.5.3. The role of NF-κB in the progression of malignancies

As outlined previously, NF-κB is responsible for regulating increased proliferation and increased cell survival. Further to this, NF-κB can be intrinsic to other tumourgenic processes such as metastasis, replicative immortality and the development of drug resistance. For example, tumours that possess constitutive NF-κB activity usually display more resistance to chemotherapy so it has been suggested that NF-κB

pathway activation may induce multidrug resistance through the increased expression of P-glycoprotein (Dolcet et al. 2005). In addition, increased NF-κB activity in MM cells has been shown to contribute to cell adhesion mediated drug resistance (CAM-DR) following adhesion of MM cells with fibronectin within the BMM (Landowski et al. 2003). Immortality of malignant plasma cells may arise through increased NF-κB activation because NF-κB is a regulator of telomerase, which is the enzyme responsible for maintaining telomere length (Yin et al. 2000).

Therefore, NF-κB is responsible for regulating several of the established hallmarks of cancer (Hanahan a Weinberg 2000, 2011). For this reason, this transcription factor is frequently dysregulated in a number of human cancers.

1.3. Activation of NF-κB in MM

The name of the transcription factor, NF-κB, is related to its discovery in B-cells and its role in enhancing immunoglobulin-κ light chain (Matthews et al. 2016). Therefore, NF-κB also possesses important roles in non-malignant plasma cells, which are fully differentiated B-cells, in terms of the production of antibodies. Moreover, malignant MM plasma cells express relatively high levels of NF-κB, which contributes to the progression and pathophysiology of this haematological malignancy (Annunziata et al. 2007; Keats et al. 2007; Demchenko et al. 2010; Chapman et al. 2011).

1.3.1 Mutation based activation

Deregulation of NF-κB signalling can arise as a consequence of overexpression or gain-of-function mutations in positive regulators of NF-κB and loss-of-function mutations in negative regulators (Annunziata et al. 2007; Keats et al. 2007). Overall, genetic abnormalities leading to constitutive NF-κB activity have been found in approximately 20% of MM patients and 40% of MM cell lines (Annunziata et al. 2007; Keats et al. 2007; Demchenko et al. 2010).

Frequent genetic abnormalities relating to NF-κB pathway deregulation in MM include aberrant expression of NIK, CD40, TRAF2, TRAF3, transmembrane activator and CAML interactor (TACI) and cIAP1/2 (Annunziata et al. 2007; Keats et al. 2007). In these studies, the majority of MM cases possessed overexpression of the positive NF-κB regulators NIK, TACI and CD40, or reduced or silenced activity of the negative NF-κB regulators TRAF2, TRAF3 and cIAP1/2. All of these phenotypes contribute to increased NF-κB signalling, with a preference towards non-canonical NF-κB signalling (Keats et al. 2007; Demchenko et al. 2010). In addition, other less common genetic abnormalities that also lead to constitutive NF-κB signalling in MM were identified. These included high expression of the *NFKB1* gene (p105) and abnormalities within the *NFKB2* gene (p100), which results in increased canonical and non-canonical NF-κB signalling, respectively (Annunziata et al. 2007; Keats et al. 2007; Demchenko et al. 2010).

1.3.2 Bone marrow microenvironmental activation

Although a large number of genetic abnormalities have been described that explain the high NF-κB activity in some MM cell lines and patient samples, it is likely that a substantial portion of the NF-κB signalling in MM cells arises as a consequence of the BM microenvironment (BMM) (Li et al. 2008; Demchenko et al. 2010).

One mechanism by which NF-κB can be activated in the BMM in MM is through CD40-CD40L interactions (Coope et al. 2002; Tai et al. 2003; Hauer et al. 2005). CD40 is a cell surface marker that is not usually expressed on normal plasma cells but has been shown to be present in the early stages of MM (Tong et al. 2000; Perez-Andres et al. 2009). CD40 is abundant in the BMM and is involved in the cell homing of MM cells to the BM. Moreover, CD40 expression is frequently increased on MM cells and blocking the interaction of CD40 with CD40L decreases NF-κB activation (Richardson et al. 2004; Annunziata et al. 2007). This results in the inhibition of IL-6 and vascular endothelial growth factor (VEGF) secretion, which leads to growth arrest and cell death of MM cells (Richardson et al. 2004). In addition,

inhibition of canonical and non-canonical NF-κB signalling can abolish CD40-induced MM cell migration (Fuchs 2013). This indicates the importance of the CD40-CD40L pathway in both NF-κB activation and subsequent MM pathogenesis.

Furthermore, the bone marrow stromal cells (BMSC) found in the MM tumour microenvironment have also been found to possess high levels of NF-κB activation that helps to support the proliferation, survival and drug resistance of malignant plasma cells within the BMM (Chauhan et al. 1995; Chauhan et al. 1996; McMillin et al. 2013). Adherence of MM cells to BMSCs induces NF-κB-dependent cytokine transcription and secretion of TNFα, IL-6, VEGF, RANKL and BAFF, to promote MM cell survival and growth through MM cell NF-κB activation (Chauhan et al. 1996; Landowski et al. 2003; Bommert et al. 2006). The production of IL-6 is one of the main NF-κB regulated factors that induces these effects to help to produce and support the malignant plasma cell population in MM (Chauhan et al. 1996).

RANKL binds to RANK, which is usually expressed on osteoclasts. Although normal plasma cells do not usually express RANKL, in MM malignant plasma cells can gain the expression of RANKL (Sezer et al. 2002). Activation of, RANKL-RANK signalling in osteoclasts through interaction with MM cells, mediates cell differentiation and activation through activation of NF-κB (Xi et al. 2016). Inhibition of NF-κB signalling blocks osteoclastogenesis, which indicates the role of NF-κB in the RANKL-RANK signalling pathway and consequently the role that this transcription factor plays in establishing the BMM and the bone destruction that occurs in MM (Dai et al. 2004a; Feng et al. 2007).

NF-κB activation in plasma cells within the BMM can also result from BAFF and a proliferation-inducing ligand (APRIL). For example, interference with BAFF signalling significantly reduces plasma cell numbers, which suggests that activation of NF-κB by BAFF contributes to the survival of plasma cells found in the BMM (O'Connor et al. 2004). The expression of BAFF and its receptor, BAFF-R, are essential for mature B-cell survival and

this is partially due to both canonical and non-canonical NF-κB activation (Mackay a Schneider 2008; Sasaki a Iwai 2016). In addition, BAFF, itself, is a target gene of NF-κB, which creates a positive feedback loop to further increase the activation of both molecules in MM to promote tumour cell survival (Novak et al. 2004).

Normal plasma cells and MM cells highly express two receptors to both BAFF and APRIL, which are B-cell maturation antigen (BCMA) and TACI (Moreaux et al. 2005). BCMA and TACI are both overexpressed in MM, which indicates their importance in the pathogenesis of the disease and in tumour cell survival (Claudio et al. 2002b; Tarte et al. 2002; Keats et al. 2007). However, low TACI expression on malignant plasma cells produces a more aggressive phenotype that leads to a worse overall prognosis in MM (Moreaux et al. 2005). This is predicted to indicate that MM tumour cells that lose expression of BAFF and APRIL receptors become independent of BMM activation perhaps as a result of acquiring NF-κB genetic abnormalities.

In conclusion, the NF-κB signalling pathway plays a highly relevant role in many aspects of MM pathogenesis, both as a consequence of MM cell mediated NF-κB activity through genetic abnormalities and through NF-κB activation within the BMM and as a consequence of the BMM.

1.4. NF-κB as a therapeutic target in MM

Over more than two decades there has been increased interest in designing therapeutic agents that target specific signalling pathways. Targeting NF-κB may provide a promising therapeutic strategy for the treatment of MM due to the important reliance the disease has on NF-κB activation, as outlined above. Moreover, inhibiting NF-κB signalling through targeting specific proteins within the NF-κB signalling pathway would likely reduce overall NF-κB activity regardless of whether it was generated as a consequence of NF-κB genetic abnormalities or BMM activation.

Inhibiting both canonical and non-canonical NF-κB signalling has been shown to reduce MM cell growth, induce cell cycle arrest and promote apoptosis (Ni et al. 2001; Hideshima et al. 2002; Mitsiades et al. 2002b; Bharti

et al. 2003). Moreover, several of the current treatments for MM impart some of their therapeutic activity through the inhibition of NF-κB signalling pathways.

Bortezomib has been shown to induce some of its therapeutic activity in MM through the inhibition of the canonical NF-κB signalling pathway due to preventing the 26S proteasomal degradation of the IκB protein (Hideshima et al. 2001; Hideshima et al. 2002). NF-κB inhibition by bortezomib has been shown to induce cell cycle arrest and apoptosis, and reduce the expression of the NF-κB target genes such as IL-6 and vascular cell adhesion protein 1 (VCAM-1) (Palombella et al. 1998; Hideshima et al. 2001; Hideshima et al. 2002). The reduction in VCAM-1 expression interferes with the MM cell interaction with the BMM, which acts to further reduce overall NF-κB activation (Hideshima et al. 2001).

Additionally, the success of IMiDs in MM may also be partially a consequence of these agents targeting NF-κB. Thalidomide has been shown to inhibit the DNA-binding activity of NF-κB by reducing the activity of IKK (Keifer et al. 2001; Mitsiades et al. 2002c). As a result, thalidomide can reduce the expression of NF-κB-regulated genes such as TRAF1, TRAF2 and c-IAP2, which likely contributes to the overall cell apoptosis that this agent induces. Furthermore, dexamethasone, a corticosteroid that is frequently used in combination with proteasome inhibitors and IMiDs in MM, also reduces NF-κB activity (Mitsiades et al. 2002c).

Moreover, it has been speculated that combining a specific NF-κB inhibitor with current therapies used for MM, such as dexamethasone or bortezomib, may act synergistically to induce anti-cancer effects (Mitsiades et al. 2002a). This may be a consequence of the overcoming the drug resistance that constitutive NF-κB activation often imparts in MM cells.

In summary, NF-κB represents a prominent transcription factor that is critical in MM disease progression and pathogenesis. Therefore, specific inhibitors targeting the NF-κB signalling pathway may be of benefit as a future treatment for this haematological malignancy. However, as NF-κB is

involved in the regulation of a number of biological processes including inflammation, immunity, survival and proliferation, global inhibition of NF-κB signalling gives rise to a number of toxicities related to immune suppression and inflammation (DiDonato et al. 2012). Therefore, the development NF-κB inhibitors that selectively target specific components of the NF-κB pathway should minimise the serious toxicities that are associated with global inhibition.

1.5. Aims and objectives

The NF-κB pathway can be specifically inhibited at several points; prevention of IκB protein degradation, inhibition of IKK activation and blockage of NF-κB DNA-binding (Godwin et al. 2013). Due to the crucial roles that IKK plays in the regulation of NF-κB activity, both through canonical and non-canonical pathway activation, inhibition of IKK activation may be a promising therapeutic strategy.

Multiple IKKβ inhibitors have been evaluated in MM, but concerns over the their safety profiles has prevented further development. For example, complete ablation of the canonical pathway activity through IKKβ inhibition is likely to impair the function of the adaptive and innate immune system, lead to IL-1β induced neutrophilia and inflammation and may also lead to hepatic toxicity (Li et al. 1999a; Li et al. 1999b; Tanaka et al. 1999; Greten et al. 2007; Vallabhapurapu a Karin 2009; Hsu et al. 2011).

This thesis investigates the use of a series of first-in-class IKKα inhibitors and a novel NIK inhibitor as therapeutic agents in four MM cell lines. The main hypothesis of this work was that specific inhibitors of IKK activation would induce apoptotic responses in MM cells and this would be a consequence of inhibition of NF-κB activation.

The aims of this study were as follows;

1. Characterisation of the four MM cell lines in terms of growth characteristics, cell surface phenotype, and overall NF-κB activity at baseline and in response to NF-κB stimulation or inhibition.

2. Characterisation of a selection of novel putative IKKα inhibitors in the MM cell lines by investigating cytotoxicity and effects on NF-κB activity and gene expression.

3. Characterisation of the use of a novel putative NIK inhibitor in the MM cell lines by investigating cytotoxicity and effects on NF-κB activity and gene expression.

Chapter 2 - **Materials and methods**

2.1. Cell culture

2.1.1. Cell viability analysis and cell counting

A Vi-CELL XR Cell Viability Analyser (Beckman-Coulter) was used to assess cell viability and count cells to ensure cell lines were maintained at a suitable cell density and viability. 500µL of each multiple myeloma (MM) cell line was as counted twice weekly in a Vi-CELL sample cup. In some scenarios, cells were counted at a 1:10 dilution in which 50µL of each cell line was diluted in 450µL phosphate buffered saline (PBS) in a Vi-CELL sample cup. Viability analysis was assessed using the trypan blue dye exclusion method.

2.1.2. Culture of MM cell lines

NCI-H929 (H929), U266B1 and RPMI8226 cell lines were cultured in Roswell Park Memorial Institute (RPMI-1640) culture medium supplemented with 10% foetal bovine serum (FBS), 1% L-glutamine and 2% penicillin/streptomycin while the JJN3 cell line was cultured in Dulbecco's Modified Eagle's medium (DMEM) supplemented with 20% FBS, 1% pyruvate, 1% non-essential amino acids and 2% penicillin/ streptomycin. All cells were cultured at 37^{o}C with 5% CO_2 and were maintained at cell densities between 3×10^5 and 1×10^6 cells/mL and at a viability exceeding 85%.

The MM cell lines used were chosen because they each represent different clinical features of MM (Drexler a Matsuo 2000; Annunziata et al. 2007; Keats et al. 2007). For example, H929 was chosen because it possesses no known genetic abnormalities in the NF-κB pathway. On the other hand, U266B1, RPMI8226 and JJN3 possess activating mutations affecting the NF-κB pathway (Annunziata et al. 2007; Keats et al. 2007). U266B1 and RPMI8226 possess inactivating TRAF3 mutations while JJN3 possesses an activating mutation in NIK.

2.1.3. Culture of CD40 ligand (CD40L) transfected and non-transfected ligand (NTL) fibroblast cell lines

CD40L and NTL transfected fibroblast cell lines were cultured in DMEM culture medium supplemented with 10% FBS, 1% pyruvate and 2% penicillin/ streptomycin. Fibroblast cells were sustained at 37°C with 5% CO_2 in 15mL of culture medium within T75 culture flasks. When the adherent fibroblast cell layer became confluent, cell lines were passaged. This involved discarding used culture medium and then washing the adherent fibroblast cells with 8mL PBS. PBS was used to wash the cell layer before addition of trypsin because the FBS in the media can affect the enzyme reaction. Adherent cells were removed from flasks by incubation with 5mL of trypsin at 37°C with 5% CO_2 for 8-10 minutes. Once adherent cells were in suspension, the 5mL of trypsin was removed (containing suspended fibroblast cells) and diluted in 5mL culture medium in a 15mL falcon tube to stop the enzyme reaction. Cells were subsequently centrifuged at 300 × *g* for 5 minutes and the remaining pellet resuspended in 1mL of culture medium. 200μL fibroblasts were reseeded into new T75 flasks with 15mL of fresh culture media. If required for experiments, the remaining fibroblasts were prepared for co-culture with the MM cell lines.

2.1.4. Co-culture of MM cell lines with CD40L and NTL transfected fibroblasts

The MM cell lines were co-cultured with CD40L transfected and non-transfected fibroblast cell lines to investigate the impact of CD40L on MM cell line phenotype, growth, survival and NF-κB activation. Prior to co-culture with MM cell lines, the CD40L and NTL transfected cells were irradiated at 75 Grays (30 minutes in the presence of Caesium-137). Irradiation prevents the fibroblasts from replicating but does not affect their viability or biological activity, including the expression of the transfected CD40L. Post-irradiated fibroblasts were counted and 2.5×10^5 cells were plated into each well of a 12-well plate with 2mL of culture medium. The cells were left to adhere to the plate overnight at 37°C with 5% CO_2.

The next day, the old fibroblast media was discarded, along with any cells that had not adhered, and replaced with 3mL of fresh MM cell line

culture medium. 1×10^6 MM cells were added to each well of the 12-well plate to give an optimal ratio of 1 fibroblast cell to every 4 MM cells. MM cells were then co-cultured with transfected and non-transfected fibroblasts for 24h.

Subsequently, the media containing the non-adhering MM cells was carefully removed from the 12-well plates and used as appropriate in experiments. The adherent fibroblast cells remaining in the 12-well plates were then discarded. Where more than 1×10^6 cells were required for experiments, plate wells for the same co-culture condition were combined to produce the correct number of cells.

2.2. Flow cytometry

All flow cytometric analysis was carried out using an Accuri C6 flow cytometer (BD Biosciences). The flow cytometer was maintained as per manufacturer's recommendations to keep the flow cytometer free of debris and the fluidics system free from air bubbles. The majority of flow cytometric data was analysed using Cflow Plus software and the Prism 6.0 statistical package (Graphpad Software), unless otherwise specified.

2.2.1. Cell cycle analysis using propidium iodide (PI)

PI is a fluorescent dye that is commonly used for cell cycle analysis. PI intercalates to the major groove of double stranded DNA in a stoichiometric manner facilitating the identification of the proportion of cells in each stage of the cell cycle and allowing assessment of the replicative capability of cell populations.

MM cells were harvested and washed twice in PBS. The resulting cell pellet was resuspended in cold 70% ethanol at a cell density of 1×10^5 cells/mL. To avoid clumping and cell loss due to incomplete fixation, the ethanol was added forcefully by dispelling from a pipette and then vortexing. Cells were fixed in ethanol for at least 1 hour at −20°C. Following this, cells were washed twice in an equal volume of PBS. At this stage of

ethanol fixation the cells can become more buoyant so a higher centrifuge speed of 700 × *g* for 5 minutes was used. Cells were treated with 50µL of 10µg/mL ribonuclease A solution at 37°C for 45 minutes. This is necessary because PI is also capable of binding to ribonucleic acid (RNA) so digesting the RNA present in the samples means that specific labelling of DNA can be achieved. Cells were stained immediately with 500µL PI solution for 10 minutes at 37°C before flow cytometric analysis on 20,000 events.

2.2.1.1. Interpreting PI cell cycle analysis flow cytometric data

For this flow cytometric measurement FlowJo V.10.1 software was used to analyse the data. This software will plot a computer based model of the cell cycle profile that relates to the collected data. Analysis of PI cell cycle data was carried out after first gating cells to exclude debris based on FSC-A and SSC-A profiles (Figure 2.1). Cells gated in P1 were used to create a scatter plot of FSC-H against FSC-A profile to allow a second level of gating to include only singlet cells (Figure 2.2). This allows exclusion of doublets and clumped cells that if included in analysis would give false results for the proportion of cells in certain regions of the cell cycle. For example, if a doublet occurs between two cells that are both in the G_0/G_1 phase of cell cycle, then this will produce the same readout as a single cell that is in G_2/M phase. This is a consequence of the PI binding the same amount of DNA in both scenarios because in the G_0/G_1 phase only one copy of DNA is present within the nucleus while at G_2/M phase the DNA has been duplicated in preparation for cell division.

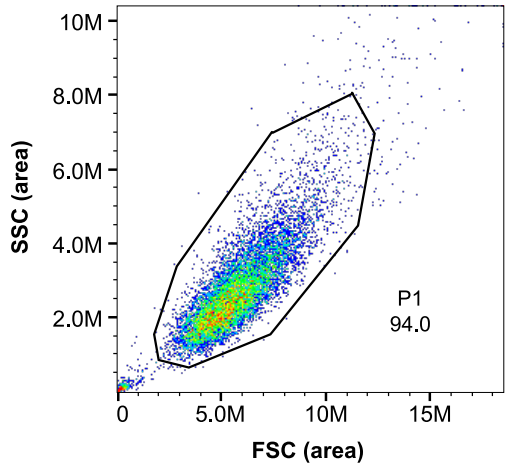

Figure 2.1 The gating (P1) used to exclude debris and select cells based on their forward scatter-area (FSC-A) and side scatter-area (SSC-A) profiles for PI cell cycle flow cytometric data.

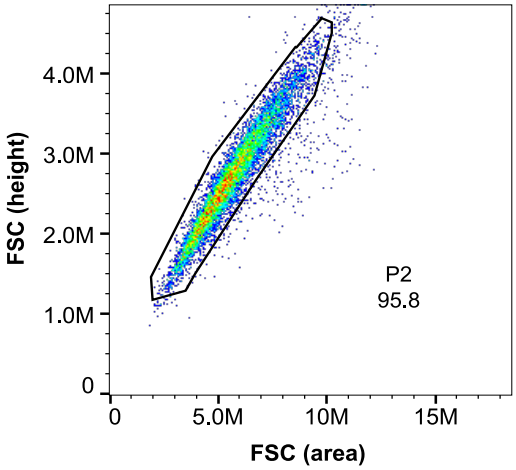

Figure 2.2 The gating (P2) used to exclude doublets and clumps based on their FSC-A profile and forward scatter-height (FSC-H) parameter for PI cell cycle flow cytometric data.

A histogram of the amount of PI staining in cells gated by P2 (P1 in all) was plotted and a gate was applied to this graph to exclude the sub G_0 phase (Figure 2.3A) to result in the final profile that the FlowJo software could then fit a cell cycle model to (Figure 2.3B). An example of the final plot produced is shown in Figure 2.4. The first peak in the histogram represents the cells in G_0/G_1 phase of the cell cycle because these cells possess diploid chromosome content. The last peak represents cells in G_2/M phase because PI staining reveals that these cells have double diploid chromosome content. Cells in between the two prominent peaks are in S phase because these cells are in the transition of single to double

diploid chromosome content. The FlowJo software will give an output of the percentages of cells in each phase of the cell cycle, which can then be input into Graphpad Prism 6.0 software for statistical analysis.

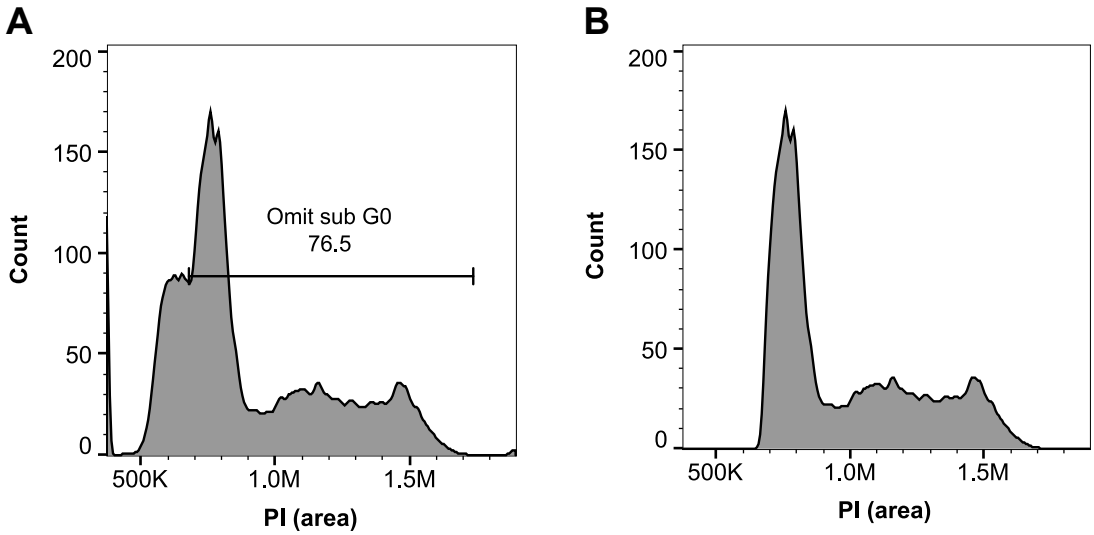

Figure 2.3 An example of a histogram plot used to apply the cell cycle profile model to in FlowJo after gating cells using P2 (P1 in all).
(**A**) A historgam of PI (area) was plotted for the cells gated by P2 (P1 in all) and a gate was applied to this graph to exclude the sub G_0 phase. (**B**) The resultant PI cell cycle profile for the FlowJo software to fit a cell cycle model.

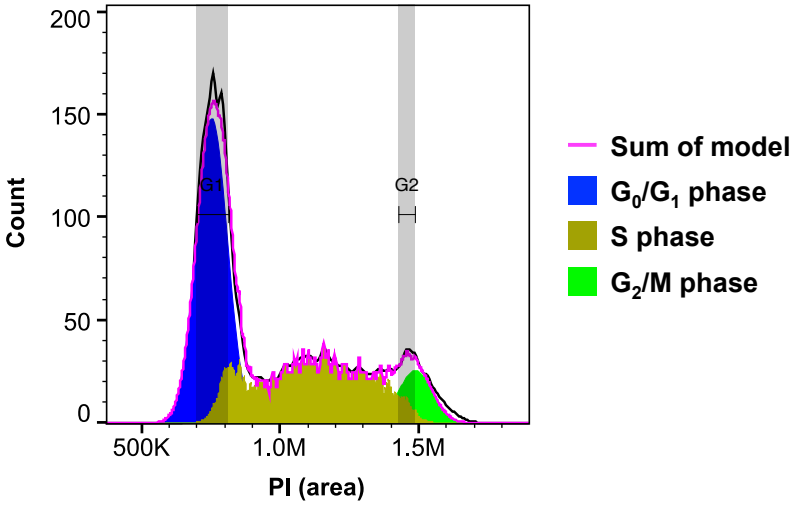

Figure 2.4 The final PI cell cycle profile after FlowJo has fitted a model to calculate the percentage of cells in each phase of the cell cycle.
The FlowJo software uses the Watson pragmatic model to create the Gaussian distributions that result in final fitted cell cycle model. The gates G1 and G2 are manually applied to suggest to the software the areas in which it should begin to base its model. The cell cycle model is then plotted for the data as shown and the software calculate the percentage of cells in each phase of the cell cycle. The complete model is the sum of the three phases.

2.2.2. Annexin V/ propidium iodide apoptosis assay

Apoptosis was assessed in MM cells by dual staining with fluorescein isothiocyanate (FITC)-labelled Annexin V and propidium iodide (PI) (BD Biosciences). Briefly, 2.5×10^5 cells were washed in 1mL of PBS. After removing supernatant, cells were incubated in darkness for 10 minutes with 190µL a 1:4 dilution of binding buffer diluted in autoclaved deionized H_2O containing 4µL of Annexin V-FITC. Before flow cytometric analysis, 10µg/mL of PI was added and then flow cytometric data on 25,000 events was collected.

2.2.2.1. Interpreting Annexin V/PI flow cytometric data

Annexin V/PI flow cytometric data was analysed after first gating cell populations to exclude debris and select cells based on forward scatter (FSC-A) and side scatter (SSC-A) profiles (Figure 2.5). The cells gated in P1 were used to generate a scatter plot of Annexin V-FITC area (-A) against PI-A positivity and the plot was split into quadrants. Figure 2.6 illustrates one of the scatter plots used to calculate Annexin V/PI positivity.

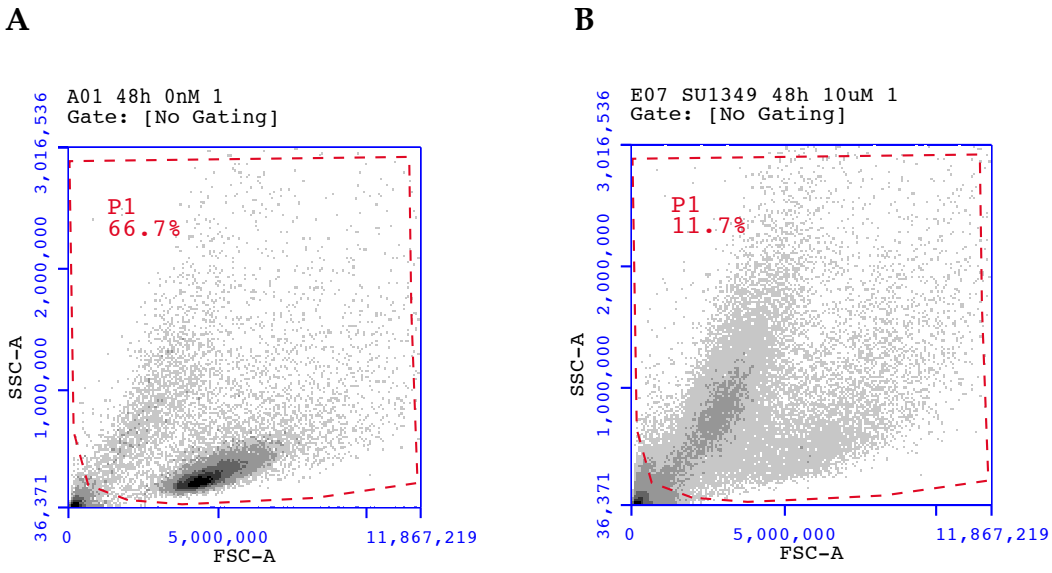

Figure 2.5 The gating (P1) used to exclude debris and select cells based on their forward scatter (FSC-A) and side scatter (SSC-A) profiles for Annexin V/PI flow cytometric data.
(A) Untreated MM cells that have a high percentage of viabilty. (B) MM cells treated for 48h with a high concentration of a cytotoxic agent.

Annexin V binds to phosphatidylserine (PS), a phospholipid present on the cytosolic side of the plasma membrane in non-apoptotic cells. Upon initiation of apoptosis, PS translocates to the extracellular side of the plasma membrane allowing Annexin V-FITC to identify apoptotic cells (Andree et al. 1990; Fadok et al. 1992). PI is used in conjunction with Annexin V-FITC to differentiate late stage apoptotic cells from early stage apoptotic cells. PI is an indicator of late stage apoptotic cells because the cell membranes of apoptotic cells become damaged allowing PI to permeate cells (Vermes et al. 1995).

Using this principle, the percentage of viable cells was calculated as the percentage of cells that were Annexin V- negative/ PI- negative (viable cell quadrant). For the example shown in Figure 2.6A, this equals 77.1%. In contrast, the percentage of apoptotic cells was quantified from the summation of the percentage of Annexin V- positive /PI- negative (early stage apoptotic cell quadrant) and Annexin V- positive/PI - positive (late stage apoptotic cell quadrant). For example, for the plot shown in Figure 2.6B the total percentage of apoptotic cells in this population is 85.8% (65.3% + 20.5%). Scatter plots similar to that shown in Figure 2.6 were generated for each sample and the percentage of apoptotic and viable cells was calculated.

A

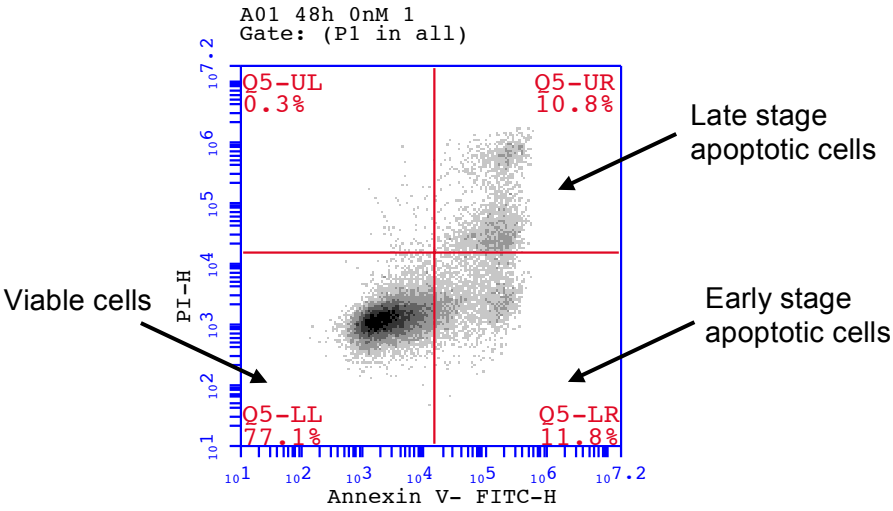

B

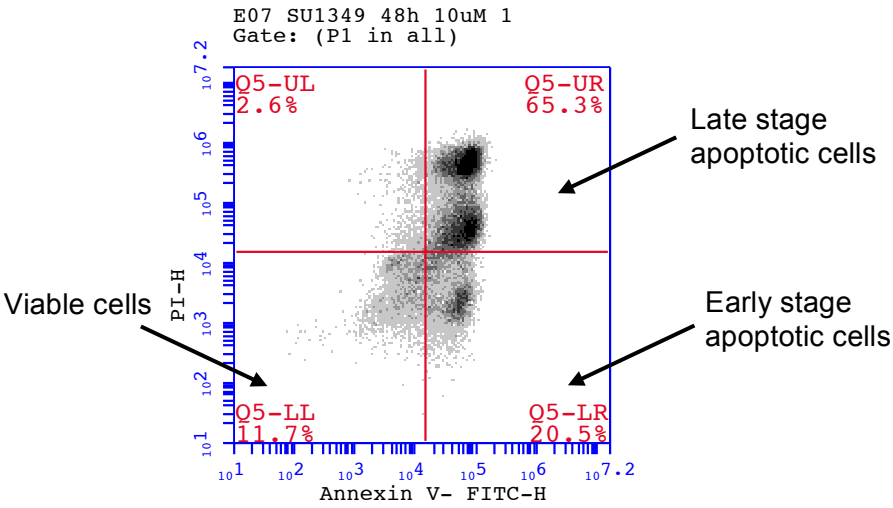

Figure 2.6 An example of the scatter plots used to calculate Annexin V/PI positivity with the quadrants labelled.

Cells gated in P1 were then used to generate a scatter plot of Annexin V-FITC-H against propidium iodide–A (PI-H) positivity and the plot was split into quadrants to represent the differents stages of apoptosis that the staining identifies. (A) Untreated MM cells that have a higher percentage of viabilty. (B) MM cells treated for 48h with a high concentration of a cytotoxic agent. In this scatter plot, it is clear to see that more cells are appearing in the apoptotic regions.

2.2.3. Cell surface analysis

2.2.3.1. CD38, CD138 and CD40 expression

The expression of the cell surface markers CD38, CD138 and CD40 was measured by labelling MM cells with monoclonal antibodies (mAb) raised against each specific antigen and conjugated to different fluorochromes to facilitate simultaneous analysis of multiple parameters. The mAbs used included CD38 mouse anti-human R-phycoerythrin (PE) conjugate (MHCD3804, Invitrogen), CD138 mouse anti-human allophycocyanin (APC) conjugate (356506, BioLegend UK Ltd) and CD40 mouse anti-human mAb FITC conjugate (CD4001, Life Technologies), respectively.

Duplicate samples of 2.5×10^5 MM cells were harvested and washed in 1mL of PBS by centrifuging at 300 × *g* for 5 minutes. After removing supernatant, one of the duplicates was incubated in darkness for 10 minutes with 5µL of the desired mAbs while the other sample was left unstained to act as the negative control. 1mL of PBS was added to the samples and the cells were washed again to remove any unbound mAb that may interfere with flow cytometric measurements. The supernatant was aspirated and the cell pellet was re-suspended in 200µL of PBS. Flow cytometric analysis was then carried out and 20,000 events were collected for each sample after carrying out the gating shown in Figure 2.7. Representative histograms for a CD138-APC stained sample verses an unstained sample are also shown in Figure 2.7.

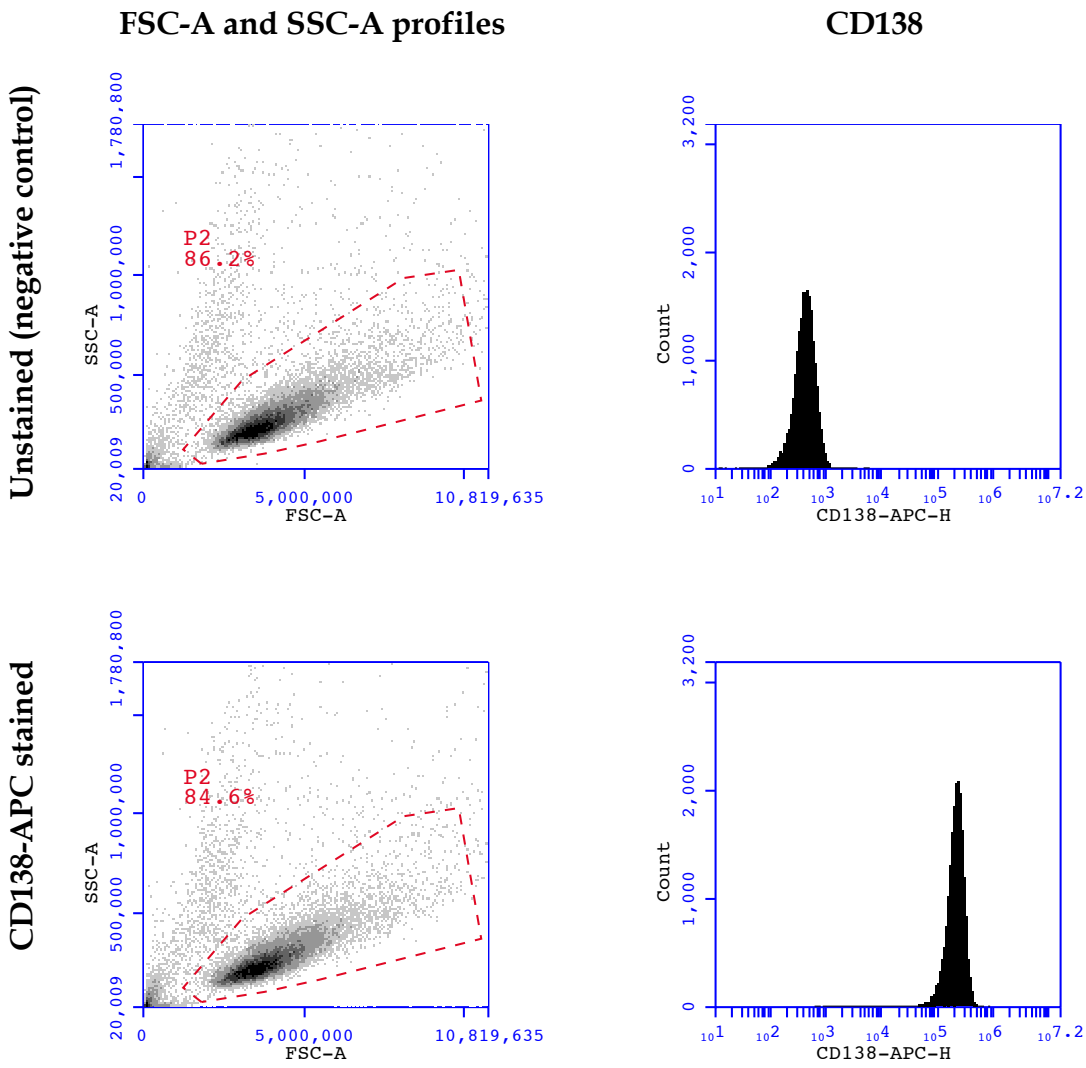

Figure 2.7 FSC-A and SSC-A scatter plots with their respective histograms to provide a representative demonstration of the gating strategy used for cell surface analysis.

In this particular example, the top panel of graphs show an unstained sample whereas the bottom panel shows a sample that has been stained for cell surface analysis of CD138 using the CD138-APC mAb. The FSC-A and SSC-A scatter plots show the gating (P2) used to select a population of viable cells. 20,000 events are then recorded in the P2 viable cell gate and the results for CD138 expression are shown in the histograms that plot the level of CD138-APC-H staining against count. As can be seen, the unstained MM cells show minimal CD138 expression compared to MM cells stained with the CD138-APC mAb. An identical strategy is used for CD38 and CD40 cell surface analysis, when cells are stained with the respective mAb.

2.2.4. Intracellular analysis

2.2.4.1. Mcl-1 expression

Mcl-1 is an intracellular protein that is a member of the Bcl-2 protein family and is essential for MM cell survival (Derenne et al. 2002; Zhang et al. 2002). As it is an intracellular protein, a FIX & PERM® Cell Permeabilization Kit (Invitrogen) was used to allow the anti-Mcl-1 mAb to access its intended target. The staining process outlined below is shown in Figure 2.4.

Duplicate samples of 3×10^5 MM cells were harvested and washed in 1mL of PBS by centrifuging at 300 × *g* for 5 minutes. After removing supernatant, samples were incubated for 10 minutes at room temperature in darkness with 60µL Reagent A. This is provided within the FIX & PERM® Cell Permeabilization Kit. Cells were then washed in 1mL PBS and the supernatant again aspirated. The cell pellets were re-suspended in 60µL Reagent B. Reagent B is also part of the FIX & PERM® Cell Permeabilization Kit. Additionally, 4µL of Mcl-1 mouse anti-human monoclonal IgG_1 antibody (sc-12756, Santa Cruz Biotechnology) was added to one of the duplicate samples and the other was left unstained to act as the negative control. Samples were incubated in darkness for 10 minutes at room temperate after mixing with a vortex.

Samples were again washed in 1mL PBS then incubated with 4µL goat anti-mouse IgG_1 FITC-conjugated antibody (SC-2078, Insight Biotechnology) at room temperate for 5 minutes. The secondary antibody was conjugated to the fluorchrome thereby allowing fluorescence detection of Mcl-1 (Figure 2.8).

Samples were washed a final time in 1mL PBS and finally re-suspended in 200µL PBS. Flow cytometric analysis was then carried out on 20,000 events after carrying out gating similar to that shown in Figure 2.5.

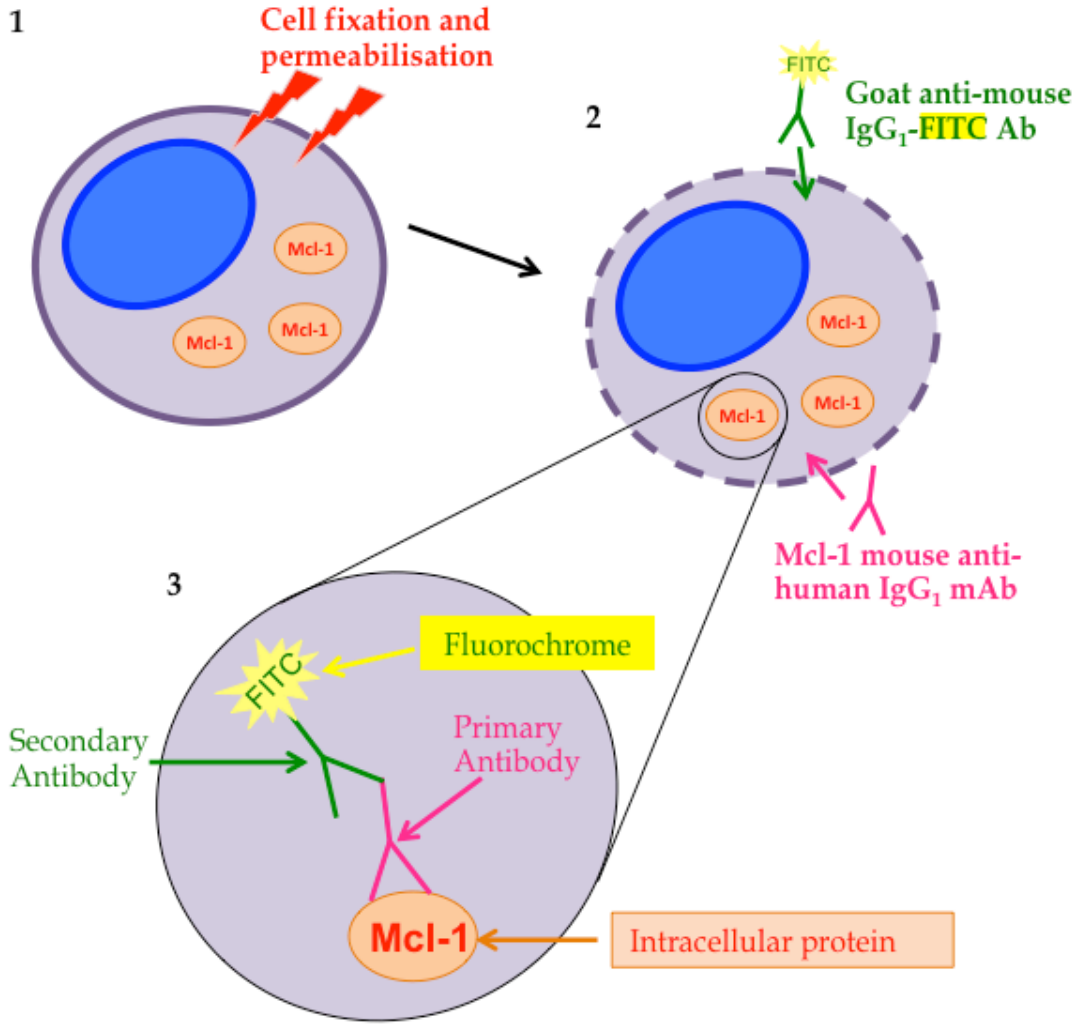

Figure 2.8 Intracellular analysis of Mcl-1 expression.
(**1**) Cells are fixated and permeabilised using a FIX & PERM® Cell Permeabilization Kit. Fixation preserves cellular antigens and maintains natural cell configuration while permeabilisation allows the antibodies access to the intracellular proteins they are targeted to. (**2-3**) Once cells are fixed and permeabilised, the antibodies can be added. Mcl-1 mouse anti-human IgG_1 mAb is added first and acts as the primary antibody in the reaction because it binds to human Mcl-1 intracellular protein in the MM cell lines. The secondary antibody, goat anti-mouse IgG_1 antibody conjugated to FITC is then added. This is an isotype-specific antibody, meaning that it is targeted to the IgG_1 mouse region of the primary antibody. The FITC-conjugated secondary antibody then allows detection of the protein complex formed by flow cytometric analysis.

2.3. Analysis of NF-κB activity

2.3.1. Preparation of nuclear extracts

5-10×10^6 cells were washed in 1mL PBS and centrifuged at 16,000 × *g* for 1 minute. The supernatant was discarded to create a semi-dry pellet. Pellets were re-suspended in 100µL of lysis buffer (Table 2.1) for 10 minutes on ice after vortexing to ensure that they were completely re-suspended in the lysis buffer. The lysis buffer contains a detergent (NP-40) that is capable of breaking down the cytoplasmic membrane. The lysed samples were centrifuged for 5 minutes at 16,600 × *g* at 4°C (Heraeus Biofuge) and the supernatant (cytoplasmic extract) was removed. The remaining pellets, mainly consisting of cell nuclei, were then re-suspended in 50µL of high salt buffer (Table 2.1) for 25 minutes on ice after vortexing. The high salt buffer breaks down the nuclear membrane and also releases the transcription factors bound to the DNA by disrupting their electrostatic interactions. Samples were centrifuged at 16,600 × *g* for 5 minutes at 4°C and the supernatant (nuclear extract) was removed to be stored at -20°C in a fresh tube.

Table 2.1 Components of the nuclear extraction buffers.
*These reagents were added to the buffers immediately before use. PMSF has a short half-life of 30 minutes in water. PMSF= phenylmethanesulfonylfluoride.

Lysis buffer	**High salt buffer**
10mM Hepes pH 7.9	25% Glycerol
1.5mM $MgCl_2$	20mM Hepes pH 7.9
10mM KCl	420mM NaCl
*0.1% PMSF	1.5mM $MgCl_2$
*0.1% NP40	0.2mM EDTA
	**0.1% PMSF

2.3.2. Nuclear extract protein quantification

Protein concentration of all nuclear extracts was determined using a Bio-Rad Protein Assay (5000006, Bio-Rad), which quantifies protein using the Bradford method.

Unknown nuclear extract protein was quantified using known protein concentrations of bovine serum albumin (BSA) solution at concentrations varying from 0–3.2µg/µL. 3µL of each BSA solution concentration was pipetted into triplicate wells of a 96-well microplate alongside 2.5µL/well of each nuclear extract sample. 200µL of the Bio-Rad protein assay dye reagent (prepared at a 1:5 dilution in H_2O) was added to each well. This was left for approximately 5 minutes to develop at room temperature and then the absorbance was read at 595nm on a spectrophotometer.

The absorbance readings for known concentrations of BSA solution was then used to plot a standard curve and the polynomial equation of the line was used to calculate the unknown protein concentrations of the nuclear extract samples (Figure 2.9).

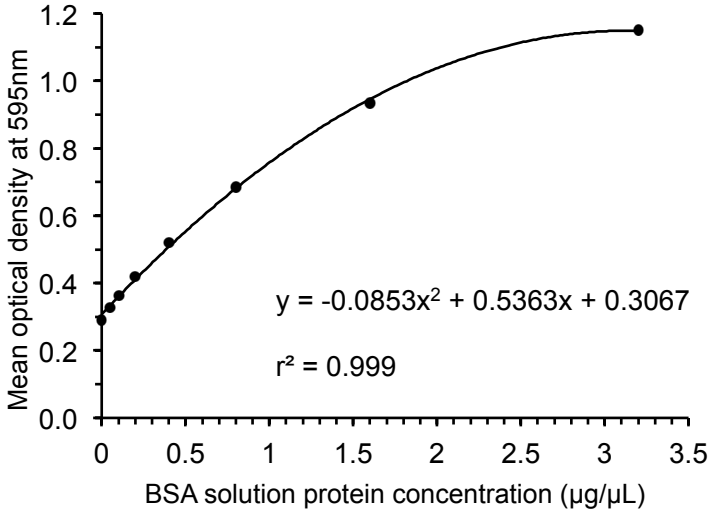

Figure 2.9 Standard curve created with BSA solution standards for quantification of nuclear extracts using a Bio-Rad Protein Assay.
A polynomial trendline was plotted which produced an equation of the line and an R^2 value using Microsoft Excel. The R^2 value was used to assess linearity while the polynomial equation was used to calculate unknown nuclear extract protein concentrations.

2.3.3. Electrophoretic mobility shift assay (EMSA)

EMSA is a semi-quantitative technique that can be used to investigate protein-DNA interactions. For the purpose of this thesis, EMSA was specifically used to characterise active NF-κB binding activity within cells. The technique relies on the principle that if a specific DNA-binding protein is present in the nucleus of cells, it will bind a corresponding radiolabelled DNA sequence. This DNA-protein complexes can then be electrophoretically separated because their electrophoretic mobility will be less than that of free radiolabelled DNA.

2.3.3.1. Labelling NF-κB consensus oligonucleotides with ^{32}P

NF-κB consensus oligonucleotides were first radiolabelled with ^{32}P. 20μL of reaction mix was prepared as outlined in Table 2.2 and incubated for 30 minutes at 37°C. Subsequently, 1μL of 0.5M EDTA and 20μL of Phenol:Chloroform:Isoamyl Alcohol (25:24:1) was added to the reaction mix followed by vortexing and centrifugation for 2 minutes at 1390 × *g* in a microcentrifuge. This resulted in an aqueous top layer that was transferred to a fresh tube and 1μL of 5M NaCl followed by 40μL of ice cold ethanol was added. The mix was then placed at -20°C for 30 minutes before centrifugation for 5 minutes at 1390 × *g*. This separated the ^{32}P labelled NF-κB consensus oligonucleotides from the ethanol so that the ethanol could consequently be discarded. Any remaining ethanol was eliminated by evaporation when the tube containing the resulting pellet was left at room temperature with the lid open for 10 minutes. The ^{32}P labelled NF-κB consensus oligonucleotide pellet was then resuspended in 50μL Tris-EDTA and stored at 20°C.

Table 2.2 The components of 20µL of reaction mix.
This was used for the preparation of the ^{32}P labelled NF-κB consensus oligonucleotides.

Component	Source	Volume
dH_2O		10µL
10 × kinase buffer	M4101, Promega	2µL
NF-κB consensus oligonucleotides	E3292, Promega	2µL
T4 Polynucleotide kinase	M4101, Promega	1µL
ATP [γ-^{32}P]	NEG002A250UC, Perkin Elmer	5µL
	Total:	**20µL**

2.3.3.2. EMSA

2µg of nuclear extract protein was incubated at room temperature for 30 minutes with 1µL 10× DNA binding buffer (Table 2.3), 2µL of 2µg/µL poly deoxyinosinic-deoxycytidylic acid (P4929, Sigma) and 1µL NF-κB consensus oligonucleotides labelled with ^{32}P to allow the DNA-protein complexes to form. 2µL of Bromophenol Blue (B3269, Sigma) was then added to the reaction mix containing the DNA-protein complexes and the reaction mix was loaded onto a 6% DNA retardation gel (EC6365BOX, Life Technologies). The NF-κB DNA binding complexes within samples were then electrophoretically separated at 75V for 1h and 30 minutes. Once electrophoretically separated, the gel was transferred to filter paper and dried for approximately 30 minutes using a gel drier (165-1746, Bio-Rad). Once the gel was dried, it was placed into a cassette with a phosphor screen and left to develop for a minimum of 3 days. The protein DNA binding present on the phosphor screen was visualised by autoradiography using a Typhoon Biomolecular Imager (Amersham).

Table 2.3 The components of 870µL of 10× DNA binding buffer.
This was prepared and then aliquoted to allow storage at -20°C. DTT= Dithiothreitol

Component	Source	Volume
40% Glycerol		400µL
10mg/mL Nuclease free BSA	B2518, Sigma	100µL
0.5M EDTA		20µL
1M DTT	43816, Sigma	50µL
5M NaCl		200µL
1M Tris pH 7.5		100µL
Total:		**870µL**

2.3.4. NF-κB family enzyme linked immunosorbent assay (ELISA)

The quantity of subunit in 1µg of MM cell line nuclear extract was quantified with an NF-κB family ELISA kit (Active Motif) according to the manufacturer's instructions. The kit contains 96-well plates to which an oligonucleotide containing the NF-κB consensus site (5'-GGGACTTTCC-3') has been immobilised. This allows the active NF-κB dimers to bind to the immobilised oligonucleotide. The optical density reading of samples was performed at an absorbance of 450nm (OD_{450}) on a spectrophotometer.

Standard curves were generated using known quantities of recombinant p65 protein (R^2 >0.99) so that the level of p65 subunit could be accurately quantified in the units of ng of subunit protein in 1µg of nuclear extract protein (Figure 2.10). Similarly, standard curves were generated using known quantities of recombinant p50 protein (R^2 >0.96) so were used to accurately quantify p50 from OD_{450} values. Both recombinant p65 and p50 proteins were used in duplicate at concentrations varying from 0.039-2.5ng. It was also necessary to use the recombinant p65 standard curves to approximate the quantities of the p52, RelB and c-Rel subunit proteins from mean OD_{450} values because recombinant protein for each of these proteins was not available.

Plotting a standard curve created an equation of the line ($y = 1.512x + 0.036$, in Figure 2.10), which was rearranged and used to quantify subunit

protein (the *x* value) based on the recorded absorbance (the *y* value). The plotted line also produced an R^2 value, which was used to assess linearity. If R^2 was calculated as >0.95 then the p65 or p50 standard lines were considered adequate to accurately quantify the respective subunit protein levels.

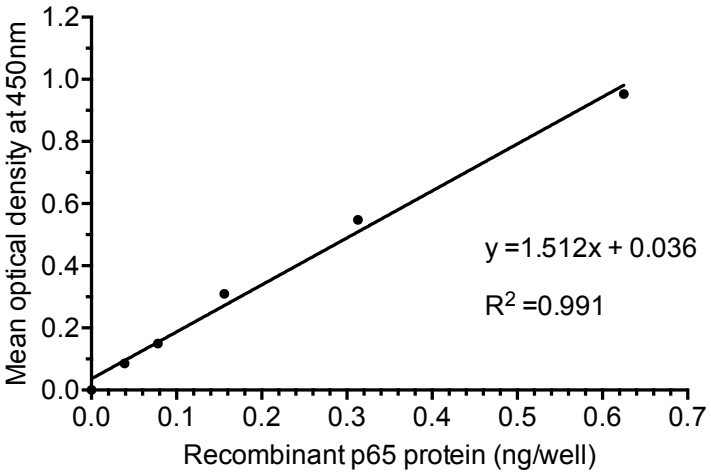

Figure 2.10 Standard curves were generated using known quantities of recombinant p65 or p50 protein and these were used to quantify NF-κB subunit expression in MM cell lines from OD_{450} values.

The example above shows a standard curve that was generated by assaying known quantities of recombinant p65 protein (ng/well) in duplicate using a p65 protein monoclonal antibody. The plotted line, equation and R^2 value were generated using Microsoft Excel.

2.3.5 Preparation of whole cell lysates

3×10^6 cells were harvested and washed in 1mL ice cold PBS by centrifuging at 300 × *g* for 5 minutes at 4°C. The supernatant was discarded and samples were lysed by the addition of 200µL ice cold lysis buffer containing phosphatase and protease inhibitors. The lysis buffer was made fresh immediately before use (Table 2.4). After centrifugation at 16,000 × g at 4°C for 20 minutes, the supernatants (whole cell lysates) were transferred to a fresh 500µL centrifuge tube to be stored at -20°C short term or -80°C long term.

Table 2.4 Components required to produce 10mL phospho-protein lysis buffer.
This lysis buffer was made immediately before use because some of the reagents within the buffer are not stable in aqueous solution for more than 30 minutes. Phosphatase Inhibitor Cocktail 2 is optimised to inhibit tyrosine protein phosphatases while Phosphatase Inhibitor Cocktail 3 is designed to specifically inhibit alkaline and serine-threonine protein phosphatases. Similarly, the Protease Inhibitor Cocktail inhibits enzymes that break down proteins. All three of these reagents improve the yield of intact proteins from the whole cell lysates.

Component	Quantity
HEPES	500µL
NaF	2.1mg
Iodoacetamide	9.25mg
NaCl	43.83mg
10% NP40	1mL
Protease Inhibitor Cocktail	100µL
Phosphatase Inhibitor Cocktail 2 (P5726, Sigma-Aldrich)	100µL
Phosphatase Inhibitor Cocktail 3 (P0044, Sigma-Aldrich)	100µL
Na_3VO_4	100µL
PMSF	100µL
H_2O	Make volume up to 10mL

2.3.5.1 Whole cell lysate protein quantification

The protein concentration of all whole cell lysates was measured using a BioRad DC protein assay kit (500-0116, Bio-Rad), which quantifies protein using the Lowry method. This is a different method to that used for the quantification of nuclear extracts because the whole cell lysate solution contains a detergent (10% NP40), which can interfere with the Bradford method of protein assay.

The BioRad DC protein assay kit was used according to the manufacturer's instructions. The kit contains three reagents; Reagent A (an alkaline copper tartrate solution), Reagent B (dilute Folin Reagent) and Reagent S (surfactant solution). For every 1mL of Reagent A used, 20µL of Reagent S must be added beforehand to created the Working Reagent A.

BSA solution was used as a protein standard at concentrations varying from 0–5µg/µL. 5µL of each BSA solution concentration was pipette into triplicate wells of a 96-well microplate alongside 5µL/well of each whole cell lysate sample. 25µL of Working Reagent A followed by 200µL Reagent B to

each used well of the 96-well microplate. This was left to develop for 15 minutes at room temperature before absorbance was read at 750nm on a spectrophotometer.

The absorbance readings for known concentrations of BSA solution were then used to plot a standard curve and the polynomial equation of the line was used to calculate the unknown protein quantities of the whole cell lysate samples (Figure 2.11).

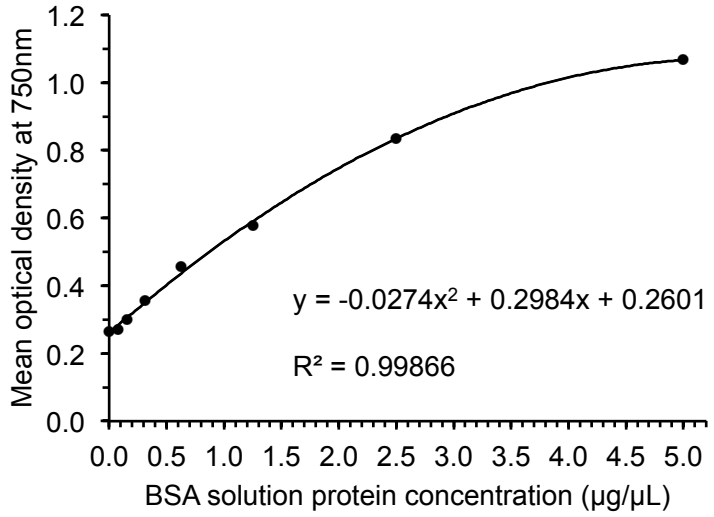

Figure 2.11 Standard curve created with BSA solution standards for quantification of whole cell lysate using a Bio-Rad DC Protein Assay Kit.
A polynomial trendline was plotted which produced an equation of the line and an R^2 vlaue in Microsoft Excel. The R^2 value was used to assess linearity while the polynomial equation was used to calculate unknown whole cell lysate protein concentrations. Absorbance was carried out at 750nm

2.3.6 Sodium dodecyl sulphate polyacrylamide gel electrophoresis (SDS-PAGE)

Sodium dodecyl sulphate polyacrylamide gel electrophoresis (SDS-PAGE) is a technique that is used to separate charged proteins based on their molecular weight. The first step involves denaturing proteins using SDS. SDS is an anionic detergent that can be used to remove secondary and tertiary protein structures, which reduces a complex protein to a negatively charged polypeptide chain.

Four micrograms of whole cell lysate were denatured by addition of 7.5µL NuPAGE lithium dodecyl sulphate (LDS) Sample Buffer (Invitrogen) and 3µL NuPAGE Reducing Agent (Invitrogen), while ensuring that

samples were kept on ice. The Sample Buffer contained Coomassie G250 and Phenol Red tracking dyes that can be used to track the movement of polypeptides during electrophoresis. The tubes containing the whole cell lysates, Sample Buffer and Reducing Agent were then heated at 80°C for 10 minutes on a pre-heated heating block before loading into pre-cast 12-well NuPage® Novex® 4-12% gel (Invitrogen).

The 12-well NuPage® Novex® 4-12% gel was previously prepared by removing from packaging, and removing the insulating tape and the well comb carefully to avoid damaging the loading wells. The gel was then rinsed in deionised H_2O before placing into the XCell SureLock Mini-Cell apparatus (Invitrogen). The electrophoresis running buffer was prepared by diluting 50mL NuPAGE MOPS SDS Running Buffer (Invitrogen) in 950mL-deionised H_2O and used to fill the central chamber of the electrophoresis apparatus, ensuring that the loading wells were completing submerged with no leaks. The first loading well was used to load 5µL of Novex SeeBlue Plus2 Pre-stained Protein Standard (Invitrogen) to ascertain the molecular weight of the resolved proteins detected by western blotting. Following this, the previously prepared denatured whole cell lysate samples were loaded.

The remaining running buffer was used to fill the external chamber of the electrophoresis apparatus and the denatured proteins within the samples were then electrophoretically separated at 200V for approximately 55 minutes, or until the dye front had reached the ridge at the bottom of the gel.

2.3.7 Western blotting

While the SDS-PAGE was running, the reagents and materials for the western blotting were prepared. One litre of non-reduced transfer buffer was prepared by diluting 50mL NuPAGE Transfer Buffer (Invitrogen) in 850mL deionised H_2O and 100mL methanol. The prepared transfer buffer was then used to soak two pieces of filter paper and six blotting pads. The polyvinylidene difluoride (PVDF) membrane was pre-soaked in methanol to prevent unspecific binding and then also soaked in the non-reduced transfer buffer.

Following electrophoresis, the polyacrylamide gels were removed from cassettes and placed on top of the pre-soaked PVDF membrane. The gel and transfer membrane were then sandwiched between two pieces of pre-soaked filter paper while ensuring any air bubbles were removed. The assembly was then sandwiched between six pre-soaked blotting pads (three on either side) before being placed into an XCell II Blot Module apparatus (Invitrogen) with the gel layer closest to the cathode core. The blot module was inserted into an XCell SureLock Mini-Cell apparatus (Invitrogen) and the central chamber filled with transfer buffer until the gel/membrane assembly was completely submerged. The external buffer chambers were filled with deionised H_2O to dissipate heat during transfer. The protein transfer was carried out at 30V for 1h and 30 minutes.

2.3.8 Immunodetection

Following transfer, the PVDF membrane was removed from the blot module and washed three times in PBS-Tween buffer. The membrane was blocked with 30mL I-Block Tween (IBT-Tween) solution (Table 2.5) for 1h at room temperature. The blocking agent prevents non-specific binding of primary and/or secondary antibodies to the membrane.

Table 2.5 Components and method required to produce I-Block Tween (IBT-Tween) solution.
The solution was prepared by placing PBS tablets into H_2O with Tween-20. The PBS-Tween was pre-heated to 80°C and then I-Block was added. The I-Block was dissolved in the heated PBS-Tween on a magnetic stirrer. The solution was cooled to room temperature and then sodium azide was added as a preservative. The IBT-Tween solution was stored at 4°C for up to 1 month.

Component	Quantity
Phosphate buffered saline (PBS) tablets (Fisher Scientific)	10 tablets
Distilled H_2O	950mL
Tween-20 (Sigma-Aldrich)	1mL
I-Block solution (Invitrogen)	2g
Sodium azide	4g

Following blocking, the PVDF membrane was probed overnight at 4°C on a roller with 10µL of primary antibodies (Table 2.6) diluted in 10mL of IBT-Tween blocking solution (1/1000). The blot was then removed from primary antibody solution and washed four times in PBS-Tween buffer, each

time for a period of 15 minutes on a rocking platform. This ensured that any unbound antibody was removed to decrease the likelihood of background staining. The blot was subsequently probed for 1h at room temperature on a roller with 1μL of the appropriate secondary antibody diluted in 10mL of IBT-Tween blocking solution (1/10,000). The blot was then removed from secondary antibody solution and washed four times in PBS-Tween buffer, each time for a period of 15 minutes on a rocking platform.

Table 2.6 Primary antibodies used for immunodetection.
For all western blots, anti-β-actin antibody was used as the control primary antibody.

Target protein	Source	Product number
Phospho-NF-κB2 p100 (Ser866/870)	Cell Signalling Technology	4810S
IκBα	Cell Signalling Technology	9242S
Phospho-NF-κB p65 (Ser536)	Cell Signalling Technology	3031S
NF-κB p100/p52	Merick Millipore	05-361
β-Actin	Cell Signalling Technology	3700S

The PVDF membrane was washed with 10mL alkaline phosphatase buffer for 5 minutes before removing excess buffer and transferring the blot to a plastic sheet. The blot was incubated with 600μL of the substrate CDP-Star (Invitrogen) for 5 minutes to enable detection of the protein bands probed for. Excess detection reagent was removed from plastic sheet and the plastic sheet was inserted into a film cassette case. In a darkroom, photographic film was exposed to the membranes for 15 minutes up to 2h. depending on the intensity of the bands obtained.

2.4. Gene expression analysis

2.4.1. Sample collection

RPMI8226 cells were incubated with increasing concentrations of the NF-κB inhibiting agents at a density of 1×10^6 cells/mL of cell culture media/ well of a 24-well cell culture plate. At 4h, $2\text{-}4\times10^6$ cells were harvested on ice from untreated and 2.5μM wells only. To reach the required cell number, wells containing 1×10^6 cells were combined as appropriate. The cells were washed in 1mL ice cold PBS and centrifuged at 300 × *g* for 5 minutes. The

supernatant was discarded to leave a cell pellet that was thoroughly re-suspended in 1mL of TRIzol® reagent (Invitrogen) to isolate total RNA. The TRIzol® lysates were stored at -80^{o}C.

At 48h, cytotoxicity was assessed in the 24-well cell culture plates where TRIzol® lysate samples had been generated using Annexin V/PI positivity. This provided a way of ensuring that the NF-κB inhibiting agents used on RPMI8226 cells were having the desired cytotoxic effect thereby allowing me to assess the suitability of the collected samples. This helped to avoid processing inadequate samples especially when the gene expression analysis techniques used were time consuming and expensive.

2.4.2. GeneChip® Human Transcriptome Array 2.0

TRIzol® lysate samples were analysed using GeneChip® Human Transcriptome Array (HTA) 2.0 following RNA extraction. RNA extraction and GeneChip® Human Transcriptome Array (HTA) 2.0 procedures were both performed by Central Biotechnology Services (CBS) at Cardiff University.

Briefly, the RNA was extracted from the samples and the quantity and quality was checked using an Agilent 2100 Bioanalyzer System (Agilent Technologies, Inc). 50-500ng of the resulting RNA samples was then analysed by GeneChip® Human Transcriptome Array 2.0 (Affymetrix, Santa Clara, CA) as per the manufacturers instructions. This Affymetrix GeneChip® is a high-resolution microarray that contains more than six million probes, 70% of which cover exons for coding transcripts whilst the remaining probes cover exon-exon splice junctions and non-coding transcripts. This allows complete coverage of all transcript isoforms to provide accurate and comprehensive gene expression profiling.

2.4.3. Microarray data analysis

The data from the Affymetrix GeneChip® HTA 2.0 analysis was returned by CBS in the form of a series of very large CEL files so all data analysis, calculations and statistics were carried out using the statistical software environment, R (R-Core-Team 2014). R is a highly versatile piece of

software that provides a variety of statistical and graphical techniques. The full R script for all of the data analysis performed throughout this thesis is available on request. The CEL files were imported into the R environment and opened using the 'oligo' package (Carvalho a Irizarry 2010). This produced a table of raw intensities of the perfect match (PM) probes.

2.4.3.1. RMA normalisation

The RMA normalisation, which is part of the 'oligo' package (Carvalho a Irizarry 2010), is a method that preforms three functions on the raw intensities PM probes: background correction, Log_2 transformation and normalisation. The background correction eliminates 'noise' that has arisen in each microarray sample by correcting for spatial variation within the individual sample arrays. The Log_2 transformation makes it easier to view the distribution and reduces skewing when visualising the data. The result of RMA normalisation should remove any 'noise' and improve the clarity of true biological variability between the individual sample arrays to allow meaningful conclusions to be drawn.

2.4.3.2. Visualisation of differentially expressed probesets

The individual array replicates were grouped into their respective treatment condition groups. The 'limma' package (Ritchie et al. 2015) was used in R Studio to fit linear models to the data to condense the Affymetrix HTA 2.0 probes to their corresponding probesets and calculate each probesets mean expression. The 'limma' package was then used to perform separate contrasts between the untreated (UT) group of arrays and each treatment condition group of arrays, which produced the Log_2 (fold change (FC)) of each probeset for each contrast. Then, an empirical Bayes moderated t-statistics test was performed on each UT vs. treated group contrast to generate p values for each probeset in each UT vs. treated contrast.

The results of the empirical Bayes moderated t-statistic test were sorted for each UT vs. treated contrast to only include only those probesets that experienced a significant ($p \leq 0.05$) Log_2 (FC) ≤ -1 or Log_2 (FC) ≥ 1. This then became the definition for a differentially expressed (DE) probeset.

This was achieved using global multiple testing procedures followed by a Benjamini and Hochberg correction to adjust the *p* values generated using a function within the 'limma' package (Ritchie et al. 2015) in R Studio. This revealed a list of DE probesets for each of the UT vs. treated contrasts.

2.4.3.3. Annotation of DE genes relating to DE probesets

The identified DE probesets were converted to their respective genes and annotated. For this analysis, only the probesets matching human genes were used. The DE probesets of the UT vs. treated contrasts were annotated with the gene level information using the file 'A-GEOD-17586_comments.txt' (Available from: https://www.ebi.ac.ukarrayexpress/files/A-GEOD-17586/A-GEOD-17586_comments.txt) (Hubbard 2014), which was imported into R Studio using the 'RCurl' package (Lang a the.CRAN.team 2016). This .txt file contained the gene level information corresponding to all the probesets of the Affymetrix GeneChip® HTA 2.0 and allowed the annotation of the probesets based on their likelihood of an identified transcript cluster corresponding to a gene.

Once the probesets were annotated with the transcript identity, the 'limma' package (Ritchie et al. 2015) was then used again to locate only those transcripts that were DE (Log_2 (FC) ≥ 1 in either direction and $p \leq 0.05$) in at least one of the UT vs. SU compound contrasts. This produced a list consisting of 1334 labelled DE transcripts. The majority of the transcripts within this list did not have a gene symbol and were either listed as '---', likely to be RNA transcripts, or 'NA' so were excluded from the study as it would be difficult to identify them.

2.4.3.4. Selection of DE genes to be used for validation in qRT-PCR

DE gene lists were generated for each UT vs. treatment condition group based on Log_2 (FC) thresholds. The respective gene lists were then analysed to assess the Gene Ontology (GO) and pathway terms using the online tool Enrichr (http://amp.pharm.mssm.edu/Enrichr/) (Chen et al. 2013; Kuleshov et al. 2016). Enrichr is an online tool that computes an enrichment analysis of a manually selected DE gene list and then provides

information on the gene lists based on accumulated knowledge of the 102 gene-set libraries in the database based on the function of the DE genes. The enrichment analysis is carried out using three approaches; a Fisher exact test and a z-score that is computed based on rank and standard deviation, followed finally by a combined score which is formulated by the first two approaches. Unlike the majority of other enrichment analysis tools available, Enrichr provides enrichment analysis information on areas such as gene ontologies, transcription, signalling pathways and biological and pharmacological processes. This allows Enrichr to provide an in depth insight into the function of a selected list of DE genes.

2.4.3.4.1. Enrichment analysis of biological Gene Ontology terms

The enrichment analysis produced a list of biological GO terms for each treatment conditions DE gene list. The lists of GO terms were sorted into a selection of GO categories so that the lists of processes generated could be more readily assessed for each UT vs. treatment condition contrast. This was achieved using a manually designed code in R Studio that sorted the terms based on key words that were likely to be associated with a certain GO category.

The six main GO categories used consisted of cell cycle, metabolic processes, development, regulation and detection/response to stimuli. Three additional GO sub-categories were also included (transcription, signalling and apoptosis) because these were areas that could be of particular interest in determining the mechanistic action of the SU compounds due to the ontologies association with NF-κB signalling. The designed method was thorough and successfully sorted >95% of the GO terms into the specified GO categories. Moreover, the small number of GO terms that remained unsorted belonged to GO categories not included in the analysis, such as sensory perception.

2.4.3.4.2. Enrichment analysis of Pathway terms

The enrichment analysis also produced pathway lists that each DE gene was responsible for regulating. The pathway information used was taken from a mixture of feedback from the WikiPathways 2015, BioCarta

2015 and Reactome 2015 gene-set libraries (Chen et al. 2013; Kuleshov et al. 2016) because each one produced a slightly different list of pathway terms that when combined gave much more detail about the DE genes pathway regulation. The *mus muculus* pathway terms were excluded so that only the *homo sapien* terms were included in the final analysis.

2.4.3.4.3. Expression levels of the SU1438, SU1411 and SU1349 DE gene lists

The list of selected DE genes was narrowed down further by investigating the specific Log_2 expressions, Log_2(FCs) and *p* values for each DE gene for its relevant treatment condition. If a DE gene was to be used in the qRT-PCR experiments to validate the microarray data, the DE gene must be expressed at a relatively high level in the RPMI8226 myeloma cells and experience a substantially large and significant FC in response to the SU compound relative to UT. By adhering to these criteria, the qRT-PCR experiments would be more likely to successfully detect the DE gene and allow validation of the microarray.

Therefore, DE genes were only selected if the Log_2 expressions of the gene in UT RPMI8226 cells was relatively high and the respective DE genes experience a relatively large and highly significant down regulation in response to the relevant treatment condition. In addition, specific patterns of expression for each SU compounds regulatory profiles were considered. Ideally, the selected DE genes would reflect the patterns observed in unique DE genes and shared DE genes between the individual .

2.4.4. Real-time quantitative polymerase chain reaction (qRT-PCR)

The microarray analysis revealed a number of differentially expressed genes that were associated with NF-κB activity and downstream gene regulation. A selection of these genes were analysed using qRT-PCR to validate the results obtained through microarray analysis.

2.4.4.1. RNA extraction and quantification

TRIzol® lysates were thawed at room temperature for approximately 5 minutes before the addition of 0.2 volume of chloroform. As samples were re-suspended in 1mL TRIzol® reagent, this equated to 200µL chloroform. To ensure chloroform was thoroughly combined, samples were vortexed for approximately 15 seconds prior to centrifugation at 11,330 × *g* for 15 minutes at 4ºC. After centrifugation, 500µL of the aqueous phase was transferred to a fresh tube, taking care not to touch the inter-phase layer so as to avoid RNA contamination. 500µL of 70% ethanol was mixed well with the aqueous layer.

The remainder of the protocol was carried out using an RNeasy mini kit (Qiagen), according the manufacturers instruction. Briefly, the samples were transferred to an RNeasy spin column suspended in a 2mL collection tube and centrifuged at 11,330 × *g* for 15 seconds at 4ºC to allow the RNA to bind to the RNeasy membrane. The flow-through was discarded and the RNA spin column membrane was washed with the two provided buffers, RW1 buffer and RPE buffer respectively, which efficiently removes any contaminants. After centrifugation at 11,330× *g* for 15 seconds at 4ºC, the flow-through was discarded between washes. Finally, 50µL of RNase-free water was added to the spin column and the RNA was eluted after centrifugation at 11,330 × *g* for 1 minute at 4ºC. To achieve the highest concentration of RNA eluted from the RNeasy spin column membrane, the final step was repeated using the same 50µL of eluted RNA. The eluted RNA was stored at -80ºC.

Before the RNA extracts were further processed, their quantities and qualities was assessed to ensure that the RNA extracted was of the highest quality and showed no genomic DNA contamination at this stage. This procedure was performed by CBS at Cardiff University on RNA at concentrations between 50-500ng/µg using an Agilent 2100 Bioanalyzer System. Briefly, RNA samples are first separated electrophoretically and then detected via laser induced fluorescence detection which generates a ratio of 18S to 28S ribosomal subunits. The resultant figures generated by

the Bioanalyzer software are a gel-like image of the electrophoretic separation and an electropherogram for visualisation of the ribosomal subunit ratio. Both pieces of information are standardised and an algorithym within the software is used to calculate an RNA integrity number (RIN) for each RNA sample. RNA was only used for subsequent qRT-PCR if the RIN was above a threshold of 6 because this indicates that the RNA is of an adequate quality for qPCR.

2.4.4.2. Reverse transcription reaction

1µg of eluted RNA was converted to single-stranded complementary DNA (cDNA) on ice using a high capacity cDNA reverse transcription kit (4368814, Applied BioSystems), according to the manufacturer's protocol. The 1µg RNA was made up to a volume of 10µL using nuclease-free H_2O. 10µL of 2× Reverse Transcription Master Mix (Table 2.7) was added to each sample and then placed in the thermal cycler under the conditions shown in Table 2.8, as specified by the manufacturer's instructions for this kit. The reaction produced 20µL of single-stranded cDNA and this is stored at -20°C.

Table 2.7 The components of 10µL 2× Reverse Transcription Master Mix. Excluding, nuclease-free H_2O, all components were included in the high capacity cDNA reverse transcription kit (Applied BioSystems).

Component	Volume
10× RT Buffer	2.0µL
25× dNTP Mix (100mM)	0.8µL
10× RT Random Primers	2.0µL
Multiscribe™ Reverse Transcriptase	1.0µL
Nuclease-free H_2O	4.2µL
Total:	**10µL**

Table 2.8 The optimal thermal cycler conditions for the high capacity cDNA reverse transcription kit (Applied BioSystems).
The reaction volume was set at 20µL.

	Step 1	Step 2	Step 3	Step 4
Temperature (°C)	25	37	85	4
Time	10 min	120 min	5 sec	∞

2.4.4.3. qRT-PCR primer design

The primers specific for target genes were designed using NCBI/Primer-BLAST (Ye et al. 2012). This software provides a tool that is capable of finding primers specific to a gene of interest by creating the PCR primer in Primer3 and then using BLAST to screen the primer in a user-selected databases to avoid issues such as primer dimers and non-specific binding.

The target genes reference sequence was inserted into the Primer-BLAST website and amplicon length was set to 70-200 base pairs to ensure that all qPCR products amplified at the highest efficiency. Additionally, the option of the designed primer to span an exon/exon boundary of the target gene mRNA was selected to ensure that the primer could distinguish between cDNA and potential contamination of genomic DNA. A list of primers is usually suggested and for each target gene the most suitable primer pair was selected based on properties such as compatible melting temperatures between the forward and reverse primers, GC content and complementarity between primer pairs. The primers selected and used for qRT-PCR are shown in Table 2.9

Table 2.9 The sequence of primer pairs for the endogenous control and target genes that were analysed using qRT-PCR.
All primers for target genes were designed using Primer-BLAST and produced by Eurofins Genomics. These were supplied lyophilised and were resuspended in nuclease-free H_2O to a concentration of 100μM. The primer for the endogenous control was provided by Eurogentec S.A, Belgium.

Primer for endogenous control		
RSP14	**Forward**	5'-GGC AGA CCG AGA TGA ACT CT-3'
	Reverse	5'-CCA GGT CCA GGG GTC TTG GT-3'
Primers for target genes		
TRAF6	**Forward**	5'-TGA AGG AGA GAA TCA GAG CAA GT-3'
	Reverse	5'-GGC AGT TCC ACC CAC ACT AT-3'
RIPK1	**Forward**	5'-GTG CTG AAA GCC GAG ATG AG-3'
	Reverse	5'-TTG AGC TGT AGC CTG AAC CTT-3'
POLA2	**Forward**	5'-TGA AGG CAC AAG AAG CTC CG-3'
	Reverse	5'-GGG CTC GGA CAC AAA CTG TA-3'
SRSF7	**Forward**	5'-CGA CCA AGA AGC AGT CGT-3'
	Reverse	5'-CAC TTT ACA GAC ATC ACA AAT CCC-3'
POLR2A	**Forward**	5'-ACC GAC ACT TGG CTC TCT TG-3'
	Reverse	5'-CAC GTC CAC CGT TTC CTC AA-3'
SRSF6	**Forward**	5'-TAG GAC GCC TGA GCT ACA AC-3'
	Reverse	5'-CCA CGA AGC CGT ACC CAT TT-3'
OFD1	**Forward**	5'-TGC CTT CAG TCC CTA GTG TC-3'
	Reverse	5'-GGA ACA AAG GTG CTG AAC GT-3'
PRKCI	**Forward**	5'-ACG GCA TGT GTA AGG AAG GAT-3'
	Reverse	5'-CAA GAG CCC ACC AGT CAA CA-3'
UBA2	**Forward**	5'-TTC TCC CAC ATC GAC CTG ATT G-3'
	Reverse	5'-AAC CTG TGC CTT TGA TCT TCC A-3'
NSUN2	**Forward**	5'-ACA AAA GCC ACG CAA AAG AGA T-3'
	Reverse	5'-CAG GCA AGT TCT TCA GGA TAC C-3'

2.4.4.4. Real-time quantitative polymerase chain reaction (qRT-PCR)

Single-stranded cDNA was diluted 1:5 in nuclease-free H_2O on ice and primer pairs were each diluted to a working stock of 10μM. A qRT-PCR master mix was prepared for each individual primer pair (Table 2.10). The fluorescent qPCR chemistry used for these experiment was the SYBR® Green dye-based assay. SYBR® Green I dye is a fluorescent DNA-binding dye that binds to the minor groove of double-stranded DNA to emit a much higher fluorescent signal than that of unbound SYBR® Green I dye.

Table 2.10 The components of 15μL of qRT-PCR master mix.
This could be scaled depending on how many wells were required.

Component	Source	Volume
Power SYBR® Green PCR Master Mix	4368706, Applied BioSystems	10μL
Forward primer (10μM working stock)		1μL
Reverse primer (10μM working stock)		1μL
DNase-free H_2O		3μL
Total:		**15μL**

15μL of the correct qRT-PCR master mix was then loaded into the appropriate wells of a MicroAmp Fast Optical 96-well reaction plate (4346906, Applied BioSystems) whilst taking care to avoid air bubbles in the wells as this can disrupt the fluorescent signal. 5μL of cDNA was then added to the appropriate wells of the 96-well reaction plate and the plate was then sealed using a MicroAmp Optical Adhesive Film (4311971, Applied BioSystems). The plate was briefly centrifuged at 300 × *g* for 2 minutes to remove any air bubbles that may be present and to concentrate all qRT-PCR reagents in each well. The sealed 96-well reaction plate was then placed in the ViiA™ 7 Real-Time PCR System (Applied BioSystems) and analysed under the conditions listed in Table 2.11.

Table 2.11 The thermal cycler conditions for qRT-PCR using the ViiA™ 7 Real-Time PCR System.

	Hold Stage	PCR Stage		Melt Curve Stage		
	Step 1	**Step 1**	**Step 2**	**Step 1**	**Step 2**	**Step 3**
Cycle number	**1**	**40**		**1**		
Temperature (°C)	95	95	60	95	60	95
Time	10 min	15 secs	1 min	15 secs	1 min	15 secs

2.4.4.5. Analysis of qRT-PCR results

The qRT-PCR results were analysed using ExpressionSuite Software v1.1 (ThermoFisher Scientific) and the melt curves, amplification plots and threshold cycles (C_t) were calculated. The fold changes were then manually calculated by the comparative C_t method ($2^{-\Delta\Delta Ct}$) using Equation 1 (Livak a Schmittgen 2001). The $2^{-\Delta\Delta Ct}$ method compares the gene expression of the DE gene of interest between the UT and SU compound treated samples relative to an endogenous control gene, which in this scenario was RSP14.

$$2^{-\Delta\Delta C_t} = [((C_t\ DE\ gene - C_t\ RSP14)treated\ sample - (C_t\ DE\ gene - C_t\ RSP14)UT\ sample)] \quad \textbf{Equation 1}$$

2.5. Statistical analysis

Unless otherwise stated, the majority of statistical analyses were produced using GraphPad Prism 6 software (Graphpad Software Inc., CA, USA). The analysis of the microarray and qRT-PCR data are the exceptions. In these scenarios R software and ExpressionSuite Software v1.1. (ThermoFisher Scientific) were used. The ExpressionSuite Software v1.1. was used to analyse amplification and melt curve plots produced through qRT-PCR.

Chapter 3 - Characterisation of the MM cell lines at baseline and in response to NF-κB stimulation or inhibition.

3.1. Characterisation of four multiple myeloma cell lines

This was the first project within our research group to use the multiple myeloma cell lines H929, U266B1, RPMI8226 and JJN3. Therefore, the first step of this project was to successfully grow and characterise the new MM cell lines. The main factors that were of interest to the project were the growth characteristics, cell surface phenotype and basal NF-κB activity of each MM cell line.

3.1.1. Growth characteristics of myeloma cell lines

3.1.1.1. Growth kinetics and cell cycle

Optimal growth conditions were established by altering the seeding density, passage frequency and media formulation for each MM cell line to ensure that the cell viability of each cell line was maintained at a level exceeding 85%. Whilst culturing the individual cell lines, it became apparent that the growth rates among the MM cell lines were not the same. The JJN3 cell line had the fastest doubling time of approximately 24h, the RPMI8226 cell line had an approximate doubling time of 48h and the H929 and U266B1 cell lines comparatively had the slowest doubling times of approximately 72h.

For this reason, the cell cycle distribution of the four cell lines was investigated. Cells were harvested from each MM cell line under optimal growth conditions and then fixed with ice cold 70% ethanol. The passage number used for the harvested cells was similarly low between the MM cell lines and was between the range of 15-25 passages. The fixed cells were then incubated with propidium iodide (PI) and the cell cycle distribution was measured by flow cytometry. PI is a fluorescent dye that binds in a stoichiometric manner to double stranded DNA. Therefore, it can be used to identify cells in different stages of the cell cycle i.e. cells with different DNA content. FlowJo V.10.1 software was used to analyse PI cell cycle in each cell line. Briefly, cells were gated to exclude debris,

doublets and the sub G_0/G_1 cell cycle phase so that the software could fit a cell cycle model. This allowed the calculation of the percentage of cells in each phase of cell cycle to be quantified.

Figure 3.1A shows representative cell cycle profiles for each of the four MM cell lines used throughout this thesis and Figure 3.1B presents a stacked bar chart showing the collated data from three independent experiments. Figure 3.1A shows that the cell cycle profiles differ between the cell lines based on the size and shape of peaks representing each cell cycle phase, and the scale on which the individual profiles are plotted.

The data in Figure 3.1B shows that overall H929 has the most cells in the G_0/G_1 phase (53.8% ± 1.0%) and a two-way ANOVA showed that this was significantly higher than the U266B1, RPMI8226 and JJN3 cell lines ($p = 0.004$, $p < 0.001$ and $p < 0.001$, respectively). In addition, the H929 cell line had the least cells in S phase (41.2% ± 3.5%) when compared to the other cell lines and this was also calculated to be significantly lower than the U266B1, RPMI8226 and JJN3 cell lines ($p = 0.004$, $p < 0.001$ and $p < 0.001$, respectively).

The JJN3 cell line has the least cells in the G_0/G_1 cell phase (40.8% ± 0.6%) relative to the H929 (53.8% ± 1.0%), U266B1 (48.3 ± 1.4%) and RPMI8226 (43.9 ± 2.3%) cell lines demonstrating that more JJN3 cells were actively cycling. Moreover, the JJN3 cell line showed the highest percentage of cells in G_2/M cell phase (11.0 ± 1.0%), although H929 also had a similarly high level of cells in the G_2/M phase (10.6 ± 1.4%) and this was not found to be significantly different ($p = 0.99$).

The cell lines RPMI8226 and JJN3 showed the highest percentage of cells in the S and G_2/M cell cycle phases (total of 58.4% and 60.5%, respectively), suggesting that these cell lines were growing more rapidly. Moreover, the percentages of cells in the G_0/G_1, S and G_2/M phases were

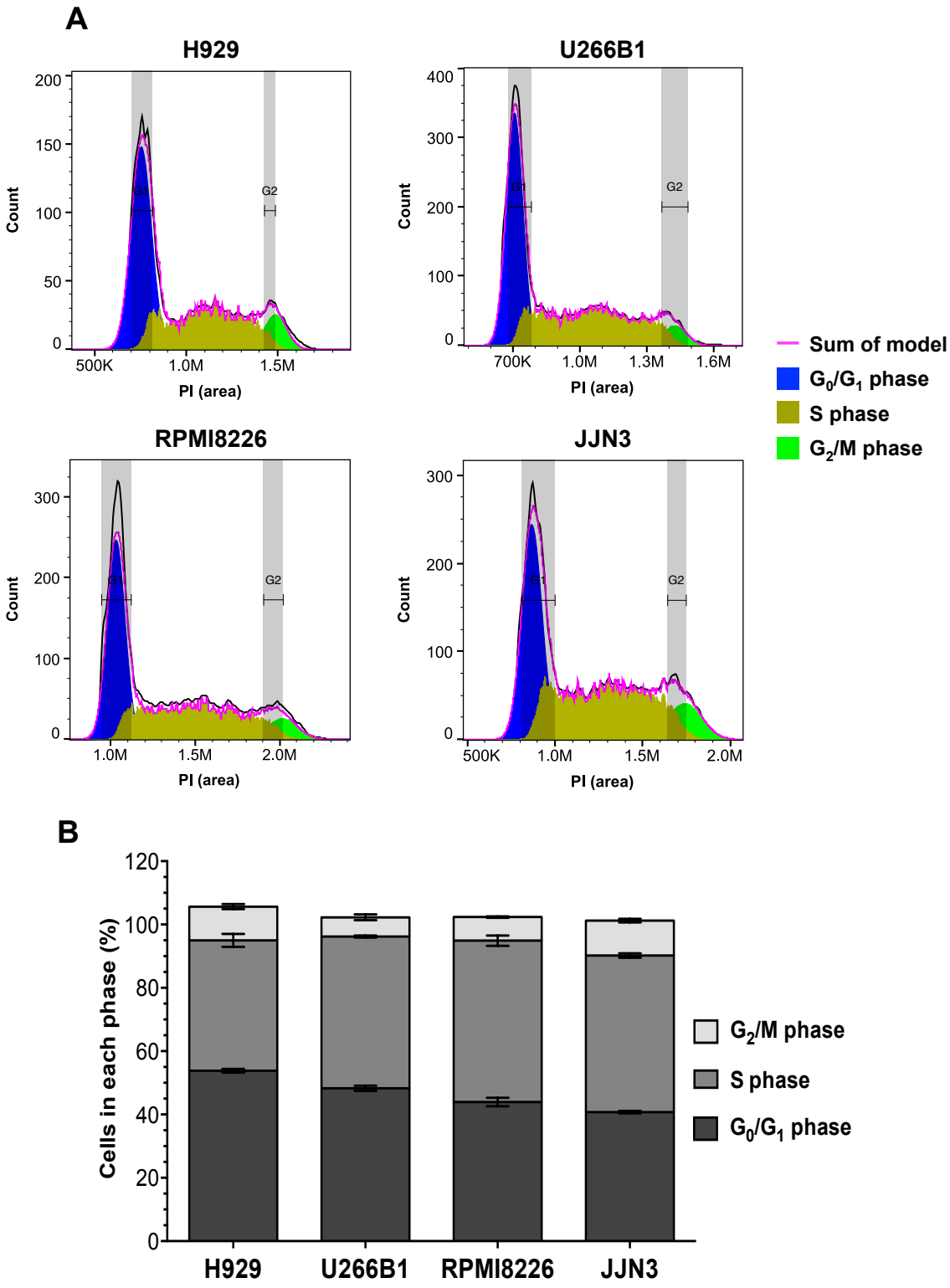

Figure 3.1 The PI cell cycle profiles for each of the MM cell lines H929, U266B1, RPMI8226 and JJN3.

Flow cytometric analysis was used to investigate the cell cycle profiles of each MM cell line. (**A**) Representative examples of the cell cycle profiles for each of the MM cell lines produced in FlowJo V.10.1. (**B**) The percentage of cells in each phase of cell cycle was input into Graphpad Prism 6.0 software and used to plot a stacked bar chart. Values reported represent mean ± SD where n = 3.

not significantly different between RPMI8226 and JJN3 cell lines (p = 0.14, p = 0.71 and p = 0.08, respectively) suggesting that the growth rates of these two cell lines were similar.

The U266B1 cell line showed a growth rate more similar to that of the H929 cell line. This was supported by the cell cycle profile in Figure 3.1, which showed that both the U266B1 and H929 cell lines had a more similar percentage of cells in G_0/G_1 (48.3 ± 1.4% and 53.8% ± 1.0%, respectively), although this was still significantly different (p = 0.004, two-way ANOVA).

Altogether, this suggests that comparatively the H929 cell line possesses the slowest growth rate whereas the JJN3 cell line possesses the fastest growth rate. Moreover, the growth rate of RPMI8226 is more similar to that of the JJN3 cell line suggesting that this cell line also has a fast doubling time. Finally, Figure 3.1 suggests that the U266B1 cell line has a growth rate that is more similar to that of the H929 cell line compared to the RPMI8226 cell line.

3.1.1.2. Baseline cell death

Another characteristic that was observed whilst culturing the individual cell lines was the variation in baseline cell viability among the MM cell lines. To investigate this further, the cell death occurring at optimal growth conditions was analysed. Cells were harvested from each MM cell line and the forward scatter area (FSC-A) and side scatter area (SSC-A) was measured using an Accuri C6 flow cytometer after any cell debris was excluded. Based on the FSC-A and SSC-A profiles, cells were gated to allow the calculation of the percentage of viable and apoptotic cells in normal growth cultures for each MM cell line (Figure 3.2A).

Figure 3.2B shows a stacked bar chart showing the collated data from three independent experiments. At optimal growth conditions, U266B1 and JJN3 cells demonstrated high levels of viability (93.7% ± 1.6% and 91.1% ± 1.9%, respectively). In contrast, RPMI8226 cell cultures showed the highest level of baseline cell death under optimal growth

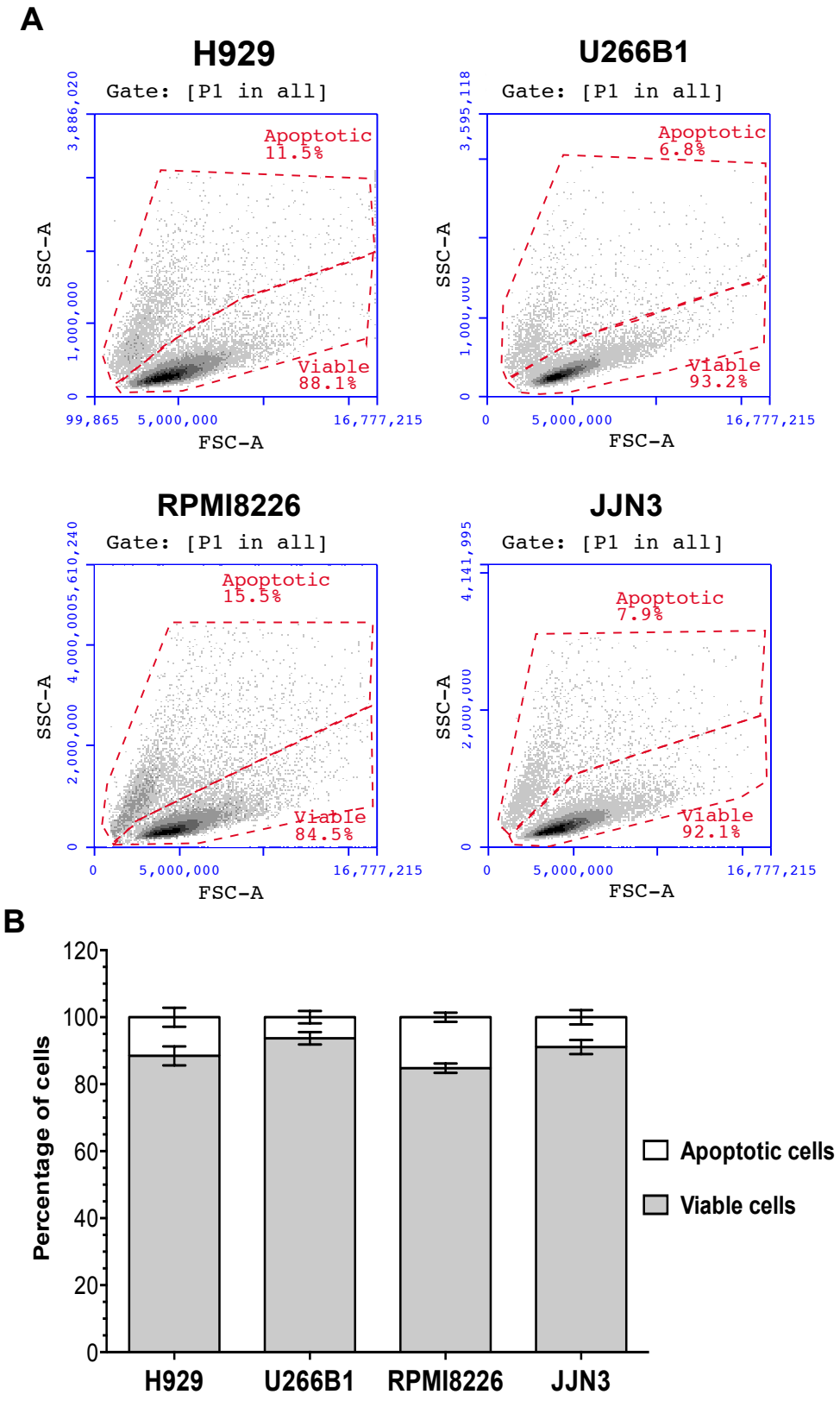

Figure 3.2 Baseline viability for each of the MM cell lines H929, U266B1, RPMI8226 and JJN3.

Myeloma cells were analysed on an Accuri C6 flow cytometer. (**A**) Representative examples of the forward scatter (FSC-A) and side scatter (SSC-A) profiles after cell debris has been excluded. The gates applied represent the populations of apoptotic and viable cells. (**B**) The percentage of viable and apoptotic cells was input into Graphpad Prism 6.0 software and used to plot a stacked bar chart. Values reported represent mean ± SD where n = 3, triplicate.

conditions (15.2% ± 1.2%) while H929 manifested intermediate levels of apoptosis (11.5% ± 2.5%). This data corresponded with observations made while culturing the individual MM cell lines. For example, the RPMI8226 cell line required more frequent replacement of the cell culture medium because it discoloured more quickly.

3.1.2. Cell surface phenotype of myeloma cell lines

The next stage of characterisation involved examining the baseline cell surface expression of CD38, CD138 and CD40. CD38 and CD138 antigens are phenotypic hallmarks associated with MM plasma cells. On the other hand, CD40 was investigated due to the association of its ligand (CD40L) with the stimulation of NF-κB activity (Coope et al. 2002; Tai et al. 2003; Hauer et al. 2005). In addition, although little is known of this antigen or its ligand, it was recently suggested that the amount of soluble CD40L present in MM patients is an indicator of MM disease stage (Kamińska et al. 2016).

Cells from each cell line were harvested, washed in PBS and then incubated with a combination of CD138-APC, CD38-PE and CD40-FITC conjugated monoclonal antibodies. A final wash in PBS was carried out to remove any unbound antibodies followed by analysis using flow cytometry.

A gating strategy was then applied to the collected data to ensure that only viable myeloma cells were selected for analysis (see Figure 3.3). Briefly, a population of viable cells was identified based on FSC-A and SSC-A and the doublets within this population excluded following gating based on FSC-A and FSC-height (FSC-H). Figure 3.3 demonstrates that the gating strategies were adjusted based on the individual cell lines because variation was observed among their respective flow cytometric profiles. This included variation in cell size (FSC-A), granularity due to baseline cell death (SSC-A) and the presence of doublets (FSC-A vs. FSC-H) within the different cell lines.

The selected population of viable single cells was then forward-gated

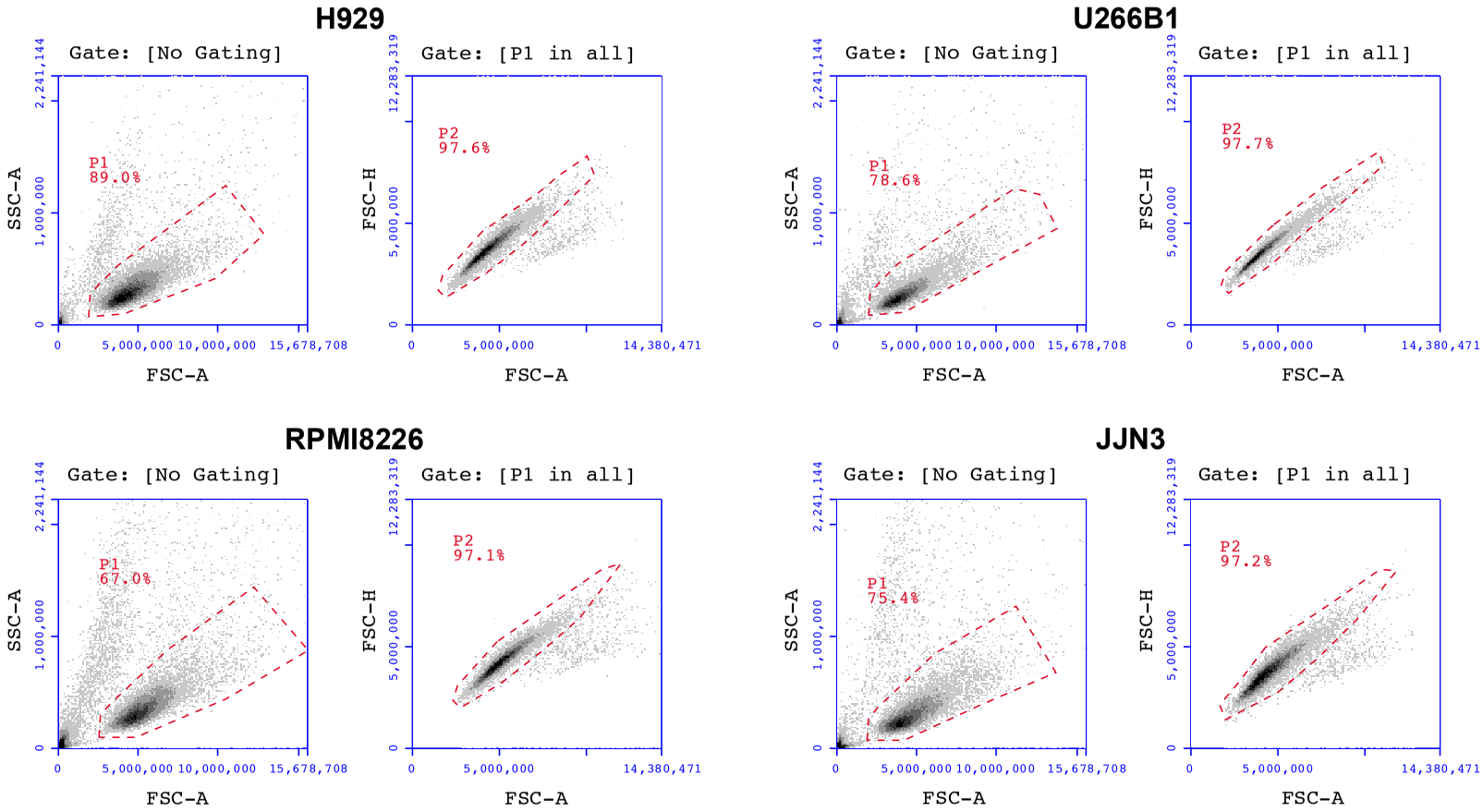

Figure 3.3 The gating strategy used for CD38, CD138 and CD40 flow cytometric data for each myeloma cell line.
Harvested MM cells from each cell line were stained with CD38-PE, CD138-APC and CD40-FITC conjugated antibodies and their respective expression was measured by flow cytometry. To gain an accurate MFI for each cell surface marker, gating was applied that was specific to individual cell lines. Viable myeloma cells were first gated in P1 based on their FSC-A and SSC-A profiles. Those cells gated in P1 then underwent a second level of scrutiny based on their FSC-A and FSC-H to exclude any doublets. The resultant P2 gate was used to create overlay histograms from which the MFI of each cell surface marker could be determined.

into a histogram plot for the expression of each antigen and the mean fluorescent intensity (MFI) values for CD38, CD138 and CD40 were recorded. Representative overlay histograms of each cell surface marker are shown in Figure 3.4A, 3.5A and 3.6A to demonstrate whether the antigens measured showed expression above background (unlabelled controls). Figure 3.4B, 3.5B and 3.6B show collated data from three separate phenotyping experiments carried out for each cell line.

Figure 3.4 shows that CD38 expression varied among the myeloma cell lines with RPMI8226 cells showing the highest expression of CD38 (382,022 ± 20,524) when compared to the other three cell lines. H929 (57,598 ± 4,502) and JJN3 (62,122 ± 6,585) both had relatively lower expression of CD38 and U266B1 had the lowest expression of CD38 (5,841 ± 935). Moreover, the CD38 expression observed for each MM cell was significantly different to that of the respective unlabelled control ($p < 0.001$, multiple t test followed by Holm-Sidak correction). However, based on the overlaid histogram presented in Figure 3.4A, the U266B1 cell line appeared to have a bimodal CD38 expression profile. This suggests that while most of the cells present within this cell line had a low level of CD38 expression, a small sub-population that expressed a higher level of CD38.

Figure 3.5 shows the CD138 expression profiles for each myeloma cell line; consistent with their plasma cell origin, all four cell lines analysed demonstrated a relatively high level of CD138 expression. However, as was the case for CD38, the expression of CD138 was heterogeneous between the cell lines. U266B1 had the highest average expression of CD138 (701,296 ± 60,920), H929 and RPMI8226 each have intermediate expression (564,907 ± 90,150 and 417,464 ± 66,040, respectively) and JJN3 has the lowest CD138 expression among the cell lines (288,862 ± 49,679). In addition, for all four MM cell lines shown in Figure 3.5B, the error bars span a large range for CD138 expression suggesting that there may exist day to day variation in the expression of this cell surface marker within each cell line.

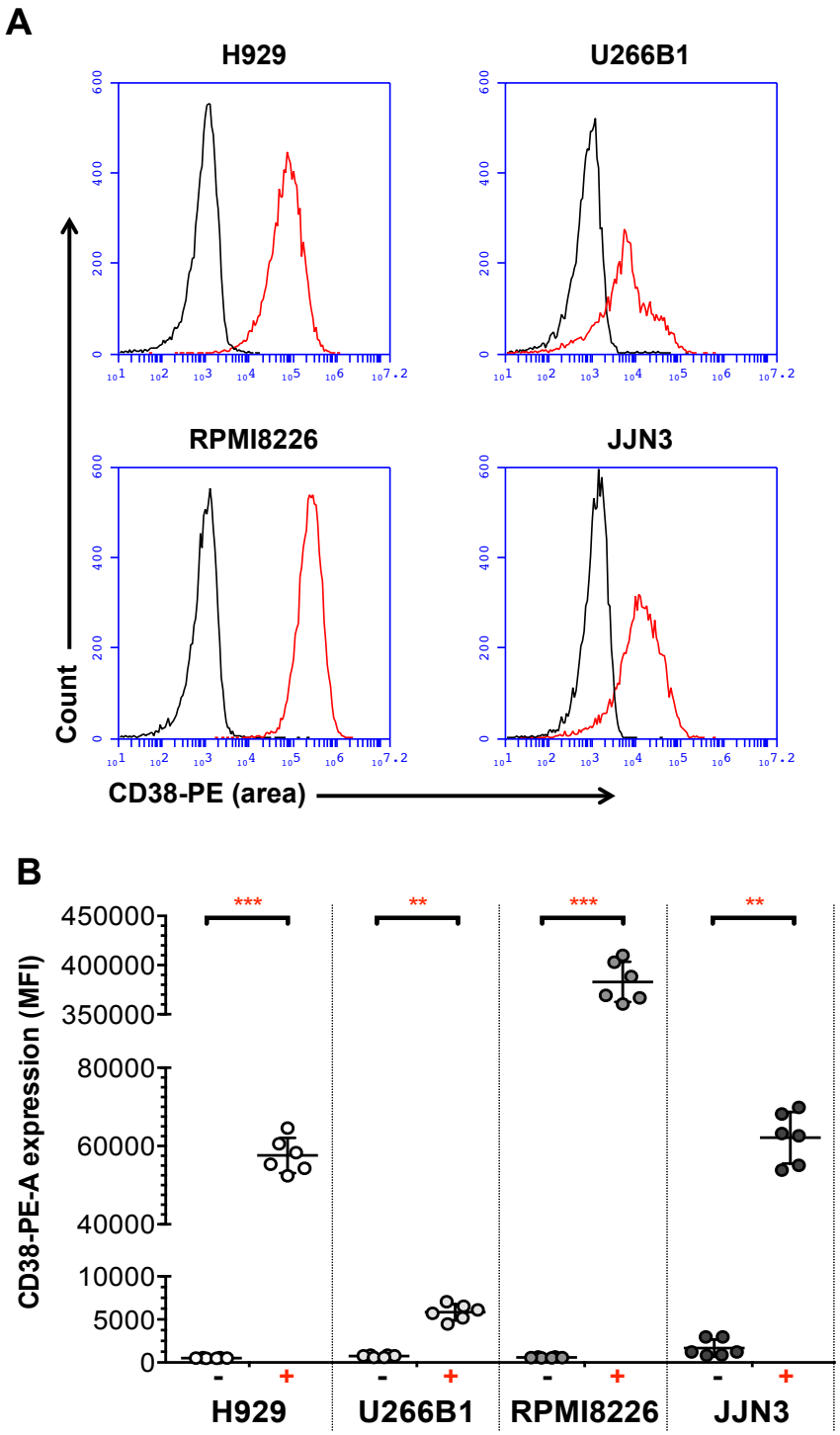

Figure 3.4 Baseline CD38 expression in the MM cell lines H929, U266B1, RPMI8226 and JJN3.

CD38 expression was investigated in each cell line by staining cells with an anti-CD38-PE conjugated antibody and then using flow cytometric analysis to measure MFI. (**A**) A representative overlay histogram is shown for each MM cell line (unstained control = ■, stained CD38-PE antibody sample = ■). (**B**) The average CD38-PE MFI for each cell line (unstained control = −, stained samples = +) where error bars represent SD (n = 3, duplicate), experimental duplicates shown. A multiple t test followed by Holm-Sidak correction was performed using Graphpad Prism 6.0 software to investigate the statistical significance values between the unlabelled control and CD38 stained sample for each MM cell line (n = 3, duplicates averaged). The results are reported above the graph (** = $p < 0.001$, *** = $p < 0.0001$).

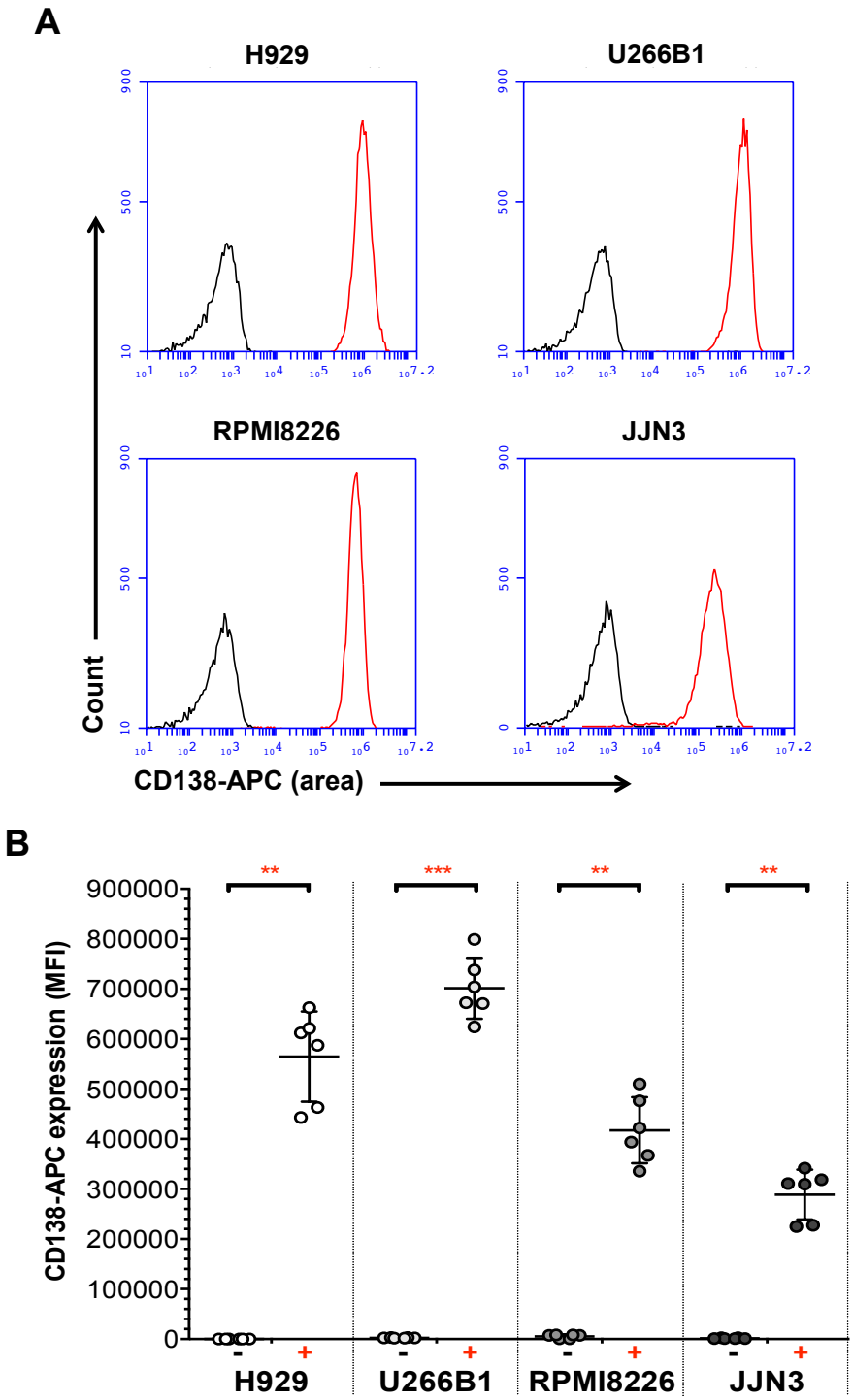

Figure 3.5 Baseline CD138 expression in the MM cell lines H929, U266B1, RPMI8226 and JJN3.

CD138 expression was investigated in each cell line by staining cells with an anti-CD138-APC conjugated antibody and then using flow cytometric analysis to measure MFI. (**A**) A representative overlay histogram is shown for each MM cell line (unstained control = ■, stained CD138-APC Ab sample = ■). (**B**) The average CD138-APC MFI for each cell line (unstained control = −, stained samples = +) where error bars represent SD (n = 3, duplicate), experiemental duplicates shown. A multiple t test followed by Holm-Sidak correction was performed using Graphpad Prism 6.0 software to investigate the statistical significance values between the unlabelled control and CD138 stained sample for each MM cell line (n = 3, duplicates averaged). The results are reported above the graph (** = $p < 0.001$, *** = $p < 0.0001$).

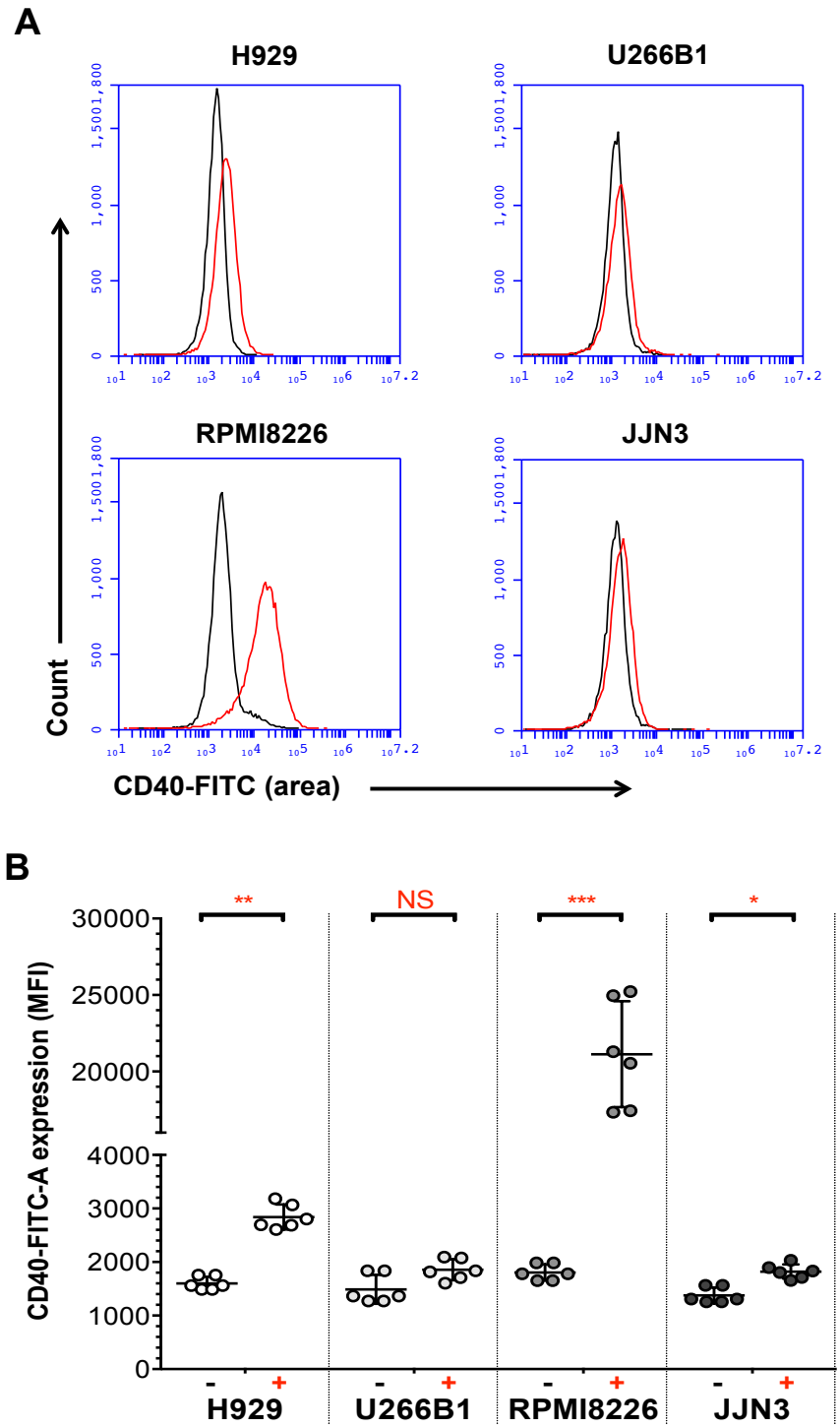

Figure 3.6 Baseline CD40 expression in the MM cell lines H929, U266B1, RPMI8226 and JJN3.

CD40 expression was investigated in each cell line by staining cells with an anti-CD40-FITC conjugated antibody and then using flow cytometric analysis to measure MFI. (**A**) A representative overlay histogram is shown for each MM cell line (unstained control = ■, stained CD40-FITC Ab sample = ■). (**B**) The average CD40-FITC MFI for each cell line (unstained control = −, stained samples = +) where error bars represent SD (n = 3, duplicate), experiemental duplicates shown. A multiple t test followed by Holm-Sidak correction was performed using Graphpad Prism 6.0 software to investigate the statistical significance values between the unlabelled control and CD40 stained sample for each MM cell line (n = 3, duplicates averaged). The results are reported above the graph (NS = not significant, * = $p < 0.05$, ** = $p < 0.01$, *** = $p < 0.001$).

Lastly, Figure 3.6 shows the CD40 expression of each myeloma cell line. RPMI8226 is the only one of the four cell lines analysed to express a relatively high level of CD40 (21,132 ± 3,857). Figure 3.6A and 3.6B show that U266B1 and JJN3 express CD40 at the lowest levels, although only JJN3 expresses CD40 to a level that is significantly different (p = 0.16 and p = 0.02, respectively, multiples t test followed by Holm-Sidak correction) to that of the unstained control (1,854 ± 215 and 1822 ± 127 as opposed to 1,489 ± 300 and 1,377 ± 166, respectively). In contrast, the overlay histogram for H929 in Figure 3.6A shows that the CD40-FITC antibody stained sample does not overlap with that of the unstained control suggesting that H929 may express a relatively low level of CD40. This is further confirmed by the collated data shown in Figure 3.6B for H929 when the CD40-FITC stained sample (2,840 ± 252) is compared to the unstained control (1,601 ± 138), this difference is significantly different (p = 0.0017, multiples t test followed by Holm-Sidak correction).

3.1.3. Basal NF-κB activity of myeloma cell lines

The final step in the characterisation of the myeloma cell lines involved investigating the basal NF-κB activity in each cell line. This was achieved using two techniques, electrophoretic mobility shift assay (EMSA) and enzyme linked immunosorbent assay (ELISA). For both assays, cells were harvested from each myeloma cell line and processed to generate nuclear extracts.

EMSA is semi-quantitative method of visualising NF-κB DNA binding activity. Briefly, 2μg of nuclear extract protein from each cell line was electrophoretically separated on a DNA retardation gel in the presence of NF-κB consensus oligonucleotides labelled with ^{32}P. The resultant DNA binding was then visualised using autoradiography. Figure 3.7A shows a representative EMSA that shows the NF-κB DNA binding activity within each cell line whereas Figure 3.7B shows the collated mean intensity of bands corresponding to the gel-retarded NF-κB DNA complexes derived from three separate EMSA experiments.

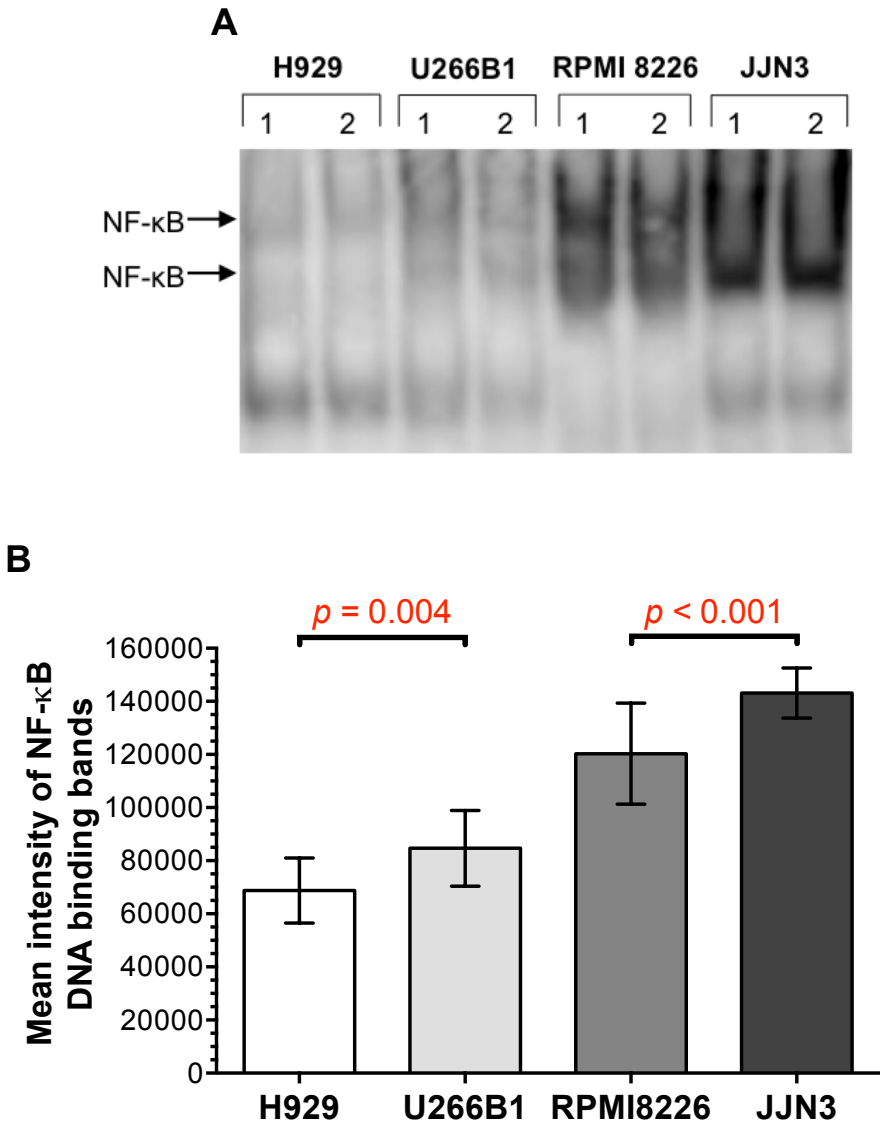

Figure 3.7 EMSA was performed on nuclear extract protein from the MM cell lines H929, U266B1, RPMI8226 and JJN3

(**A**) Representative EMSA showing the amount of NF-κB DNA binding for each cell line. The arrows indicate the positions of the bands corresponding to the gel-retarded NF-κB DNA complexes. (**B**) Image J software was used to quantify the mean intensity of bands corresponding to the gel-retarded NF-κB DNA complexes. A one-tailed, unpaired *t*-test was performed using Graphpad Prism 6.0 software to investigate the significant difference between the indicated cell lines. Values reported are mean intensity ± SD where $n = 3$.

Overall, Figure 3.7 illustrates that there was variation in the level of NF-κB DNA binding between the four myeloma cell lines. The bands indicating NF-κB DNA binding in H929 and U266B1 were of a relatively

low intensity (68,760 ± 12,224 and 84,666 ± 14,285, respectively), although the difference between the mean intensity bands was significant ($p = 0.004$). On the other hand, JJN3 had the strongest intensity band for NF-κB DNA binding (143,100 ± 9,425) when compared to the other three cell lines. RPMI8226 had an intermediate level intensity band (120,313 ± 19,019) that was more like the level of JJN3 than H929 and U266B1 cell lines but still significantly lower than the mean intensity band for the JJN3 cell line ($p < 0.001$).

An ELISA detecting active NF-κB subunits was also performed on the nuclear extract samples from each of the myeloma cell lines. This assay was a more quantitative technique than EMSA as it allowed quantification of active NF-κB subunit composition, therefore providing an insight as to which NF-κB pathway the cell lines were constitutively dependent on. The NF-κB family ELISA kit (Active Motif) was used and carried out according to the manufacturer's instructions. H929, U266B1 and RPMI8226 were each assayed at 1µg nuclear extract per well while JJN3 was assayed at a lower quantity of 0.5µg nuclear extract per well to accommodate for the fact that the EMSA suggested that it could have a relatively higher amount of NF-κB. Standard curves were generated using known quantities of recombinant p65 protein ($r^2 > 0.99$) and recombinant p50 protein ($r^2 > 0.96$) to allow NF-κB subunit quantification in nanograms per microgram of nuclear extract protein.

The results of three independent ELISA experiments are shown in Figure 3.8 for each MM cell line. Figure 3.8 demonstrates that p65, p50, p52, RelB and c-Rel NF-κB subunits were positively detected in all four myeloma cell lines suggesting that all cell lines possessed constitutive NF-κB activity. Moreover, the results reflected the pattern of heterogeneity in NF-κB activity that was observed by EMSA (Figure 3.7). Cumulatively, JJN3 appeared to have the highest level of active NF-κB subunits. In comparison, H929 had the lowest cumulative level of NF-κB activity among the cell lines. Both U266B1 and RPMI8226 cell lines had a relatively intermediate cumulative level of NF-κB activity.

The ELISA also suggested that the MM cell lines did not express higher levels of those subunits involved in the canonical NF-κB pathway (p65, p50 and c-Rel) compared to subunits involved in the non-canonical NF-κB pathway (p52 and RelB). This indicated that the NF-κB signalling observed in each cell line was most likely the result of a combination of both canonical and non-canonical NF-κB pathways. In terms of canonical pathway signalling, the levels of active p50 and c-Rel protein were relatively higher in all four myeloma cell lines compared to the levels of the levels of p65 NF-κB subunit protein. Similarly, U266B1, RPMI8226 and JJN3 expressed relatively increased levels of the non-canonical pathway subunit p52 in contrast to the level of RelB. H929 expressed the lowest levels of both non-canonical subunit proteins p52 and RelB when compared to the other cell lines.

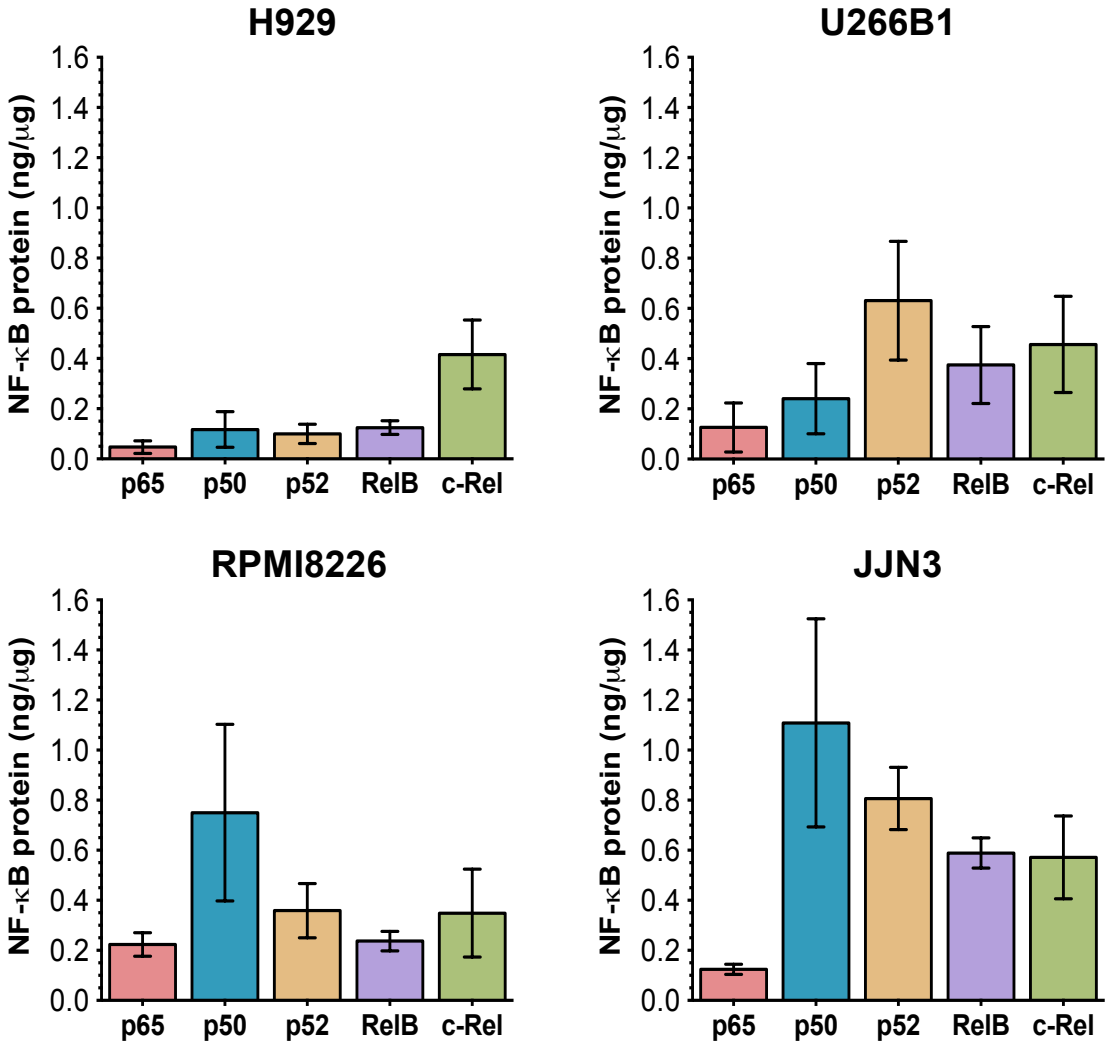

Figure 3.8 ELISA experiments detecting active NF-κB subunits were performed on each of the four MM cell lines.
ELISAs were carried out to allow p65, p50, p52 RelB and c-Rel subunit protein quantification. H929, U266B1 and RPMI8226 were assayed using 1μg nuclear extract/well and JJN3 at 0.5μg nuclear extract/well. Values reported are mean ± SD produced from duplicate values where n = 3.

3.2. Manipulation of myeloma cell lines with CD40L stimulation

Interactions of malignant plasma cells with the bone marrow microenvironment result in some of the hallmarks of MM pathophysiology e.g. the development of osteolytic bone lesions (Hideshima et al. 2007; Podar et al. 2007; Kuehl a Bergsagel 2012). Plasma cells expressing CD40 can interact with CD40L within this environment and CD40L has previously been shown to stimulate NF-κB activation, mainly via the non-canonical signalling pathway (Coope et al. 2002; Tai et al. 2003; Hauer et al. 2005). Therefore, the effect of CD40L stimulation on the cell surface phenotype and

NF-κB activity was investigated in the MM cell lines by co-culturing MM cells with fibroblasts expressing the CD40L.

3.2.1. Effect of CD40L stimulation on myeloma cell surface phenotype

Cells from each of the four cell lines were co-cultured with either CD40L or NTL transfected fibroblasts for 24h. An additional condition was added called 'LIQ' to act as a further control; this involved culturing MM cells in liquid monoculture as a comparator for the two co-culture conditions. At 24h, MM cells were removed from co-culture and LIQ conditions and washed in PBS. Subsequently, MM cells with incubated with CD38-PE and CD138-APC conjugated monoclonal antibodies before a final wash in PBS. CD38 and CD138 cell surface expression were analysed using flow cytometry to investigate whether CD40L stimulation altered the myeloma phenotype.

The gating strategy shown in Figure 3.3 was applied to the collected flow cytometric data to select viable myeloma cells and the MFI values for CD38 and CD138 determined. Figure 3.9 shows dot plots presenting the collated data from three separate phenotyping experiments carried out for all cell lines after 24h CD40L stimulation. Figure 3.9A shows that CD38 expression in the H929, U266B1, RPMI8226 and JJN3 cell lines was not significantly (p = 0.52, p = 0.99, p = 0.63 and p = 0.99, respectively) altered by co-culture with CD40L transfected fibroblasts.

Figure 3.9B shows the CD138 expression after 24h co-culture with and without fibroblasts transfected with NTL or CD40L. Similarly, H929, U266B1, RPMI8226 and JJN3 cells were again not significantly effected by NTL or CD40L fibroblast co-culture compared to baseline LIQ expression levels (p = 0.25, p = 0.70, p = 0.18 and p = 0.30, respectively). However, although not significant, H929 and RPMI8226 cells appeared to show a minor decrease in CD138 expression after co-culture with CD40L transfected fibroblasts compared to LIQ cultures (397,911 ± 99,606 and 289,459 ± 110,846 compared to 515,319 ± 49,662 and 421,179 ± 23,791, respectively).

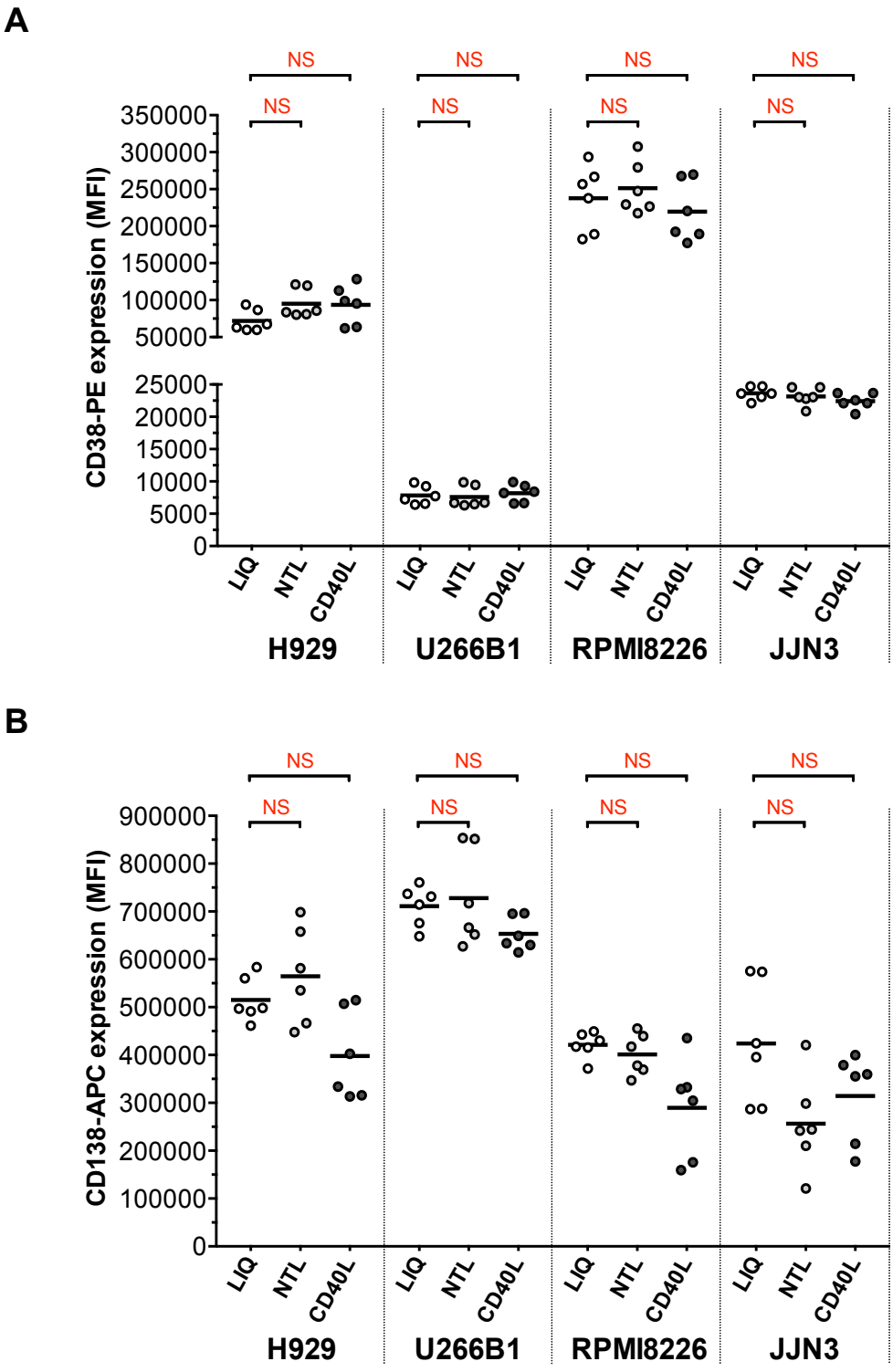

Figure 3.9 Effect of 24h CD40L stimulation on CD38 and CD138 cell surface expression on the MM cell lines H929, U266B1, RPMI8226 and JJN3.
At 24h, CD38 (**A**) and CD138 (**B**) expression was investigated using flow cytometric analysis after the MM cell lines H929, U266B1, RPMI8226 and JJN3 were co-cultured with and without CD40L or NTL transfected fibroblasts (n = 3, individual duplicates and overall mean shown). A two-way ANOVA followed by a Tukey's multiple comparisons test was performed using Graphpad Prism 6.0 software to investigate the statistical significance values between specific conditions for each MM cell line (n = 3, duplicates averaged). The results are reported above the graph (NS = not significant). (CD40L= cells co-cultured with CD40L transfected fibroblasts, NTL= cells co-cultured with NTL transfected fibroblasts, LIQ= MM cells cultured alone).

Overall, Figure 3.9 indicates that CD40L stimulation for 24h did not significantly alter the myeloma cell surface phenotype in the myeloma cell lines H929, U266B1, RPMI8226 and JJN3.

3.2.2. Effect of CD40L stimulation on NF-κB activity in MM cell lines

MM cell lines were co-cultured with and without CD40L or NTL transfected fibroblasts. After 24h, MM cells were removed from each condition and used to generate nuclear extracts. NF-κB family subunit ELISAs were then carried out on the nuclear extracts to investigate whether CD40L, in comparison to NTL, had increased NF-κB activity in the MM cell lines.

As with the previous experiments, H929, U266B1 and RPMI8226 were each assayed at 1μg nuclear extract per well while JJN3 cells were assayed using 0.5μg nuclear extract per well to reflect the increased basal NF-κB observed in these cells. Standard curves were generated using known quantities of recombinant p65 protein (r^2 >0.99) and recombinant p50 protein (r^2 >0.96) to allow NF-κB subunit quantification in ng/μg of nuclear extract protein. The results of these experiments are shown in Figures 3.11 and 3.12. One experiment in duplicate was performed to investigate the cell lines U266B1 and JJN3 because it was assumed that these cell lines were unlikely to respond to CD40L stimulation due to low level of CD40 expression. On the other hand, three separate experiments were performed for the H929 and RPMI8226 cell lines as these cell lines expressed higher levels of CD40. For each cell line, nuclear extract samples were assayed in duplicate in the NF-κB ELISA assays.

Figure 3.10 indicates that p65, p50, p52, RelB and c-Rel subunit activity were not significantly affected by 24h CD40L stimulation in H929 cells ($p > 0.05$). However, although not significant, the levels of p52 were decreased following 24h co-culture with CD40L transfected fibroblasts when compared to LIQ culture (0.620 ± 0.15 and 0.750 ± 0.24, respectively). However, a similar decrease was also observed after 24h co-culture with

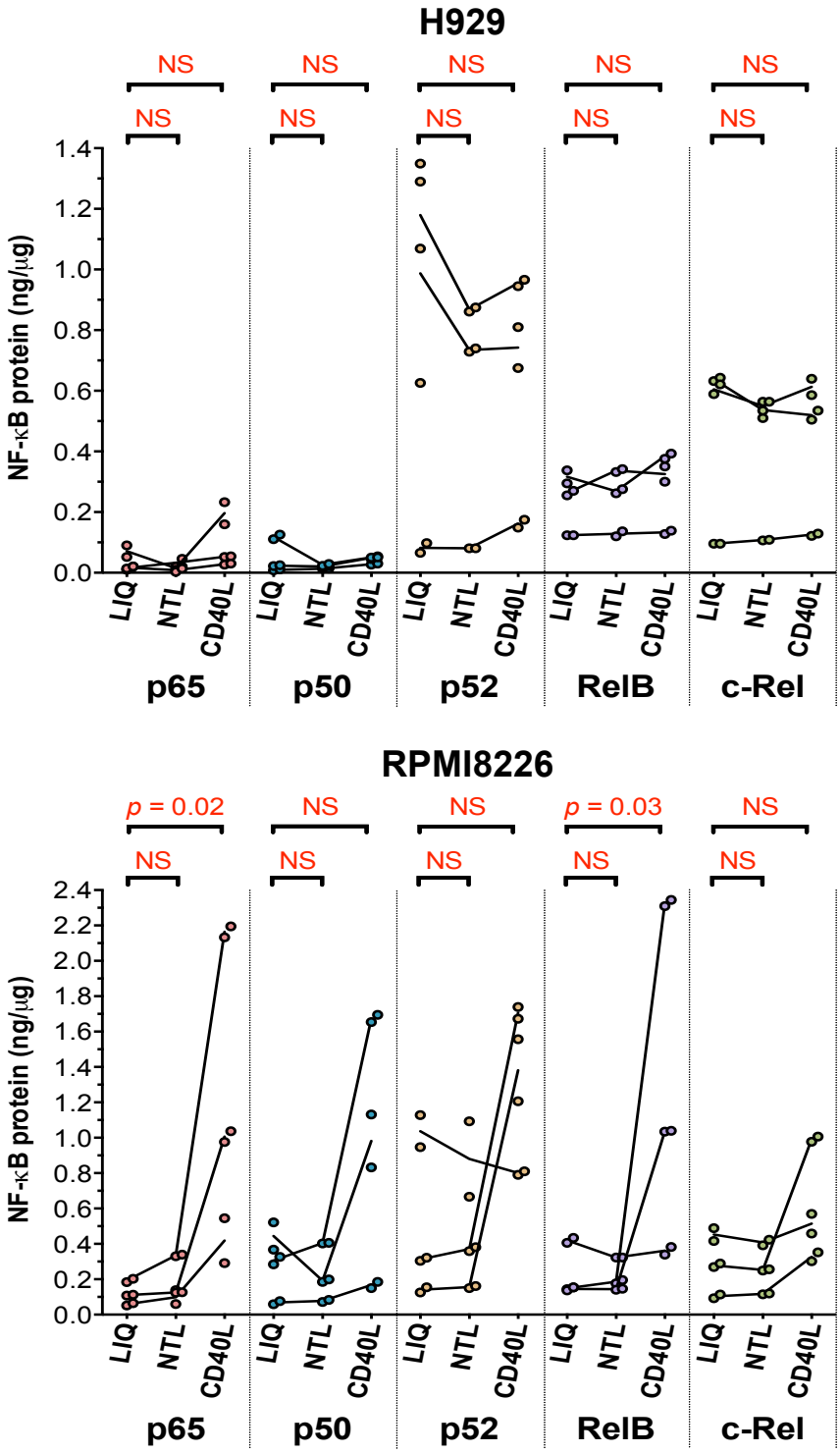

Figure 3.10 Effect of CD40L on NF-κB activity in the MM cell lines H929 and RPMI8226.
ELISAs detecting NF-κB subunits were performed 1μg/well on H929 and RPMI8226 nuclear extracts after 24h co-culture with and without CD40L or NTL transfected fibroblasts (n = 3, experimental duplicates shown and the mean of individual experiments are mapped with a line). A two-way ANOVA followed by a Tukey's multiple comparisons test was performed using Graphpad Prism 6.0 software to investigate the statistical significance values between specific conditions for each MM cell line (n = 3, duplicates averaged). The results are reported above each graph (NS = not significant). (CD40L= cells co-cultured with CD40L transfected fibroblasts, NTL= cells co-cultured with NTL transfected fibroblasts, LIQ= cells cultured alone).

NTL transfected fibroblasts when compared to LIQ culture conditions (0.561 ± 0.15 and 0.750 ± 0.24, respectively), suggesting that the decrease in p52 subunit activity was not caused by CD40L stimulation.

Figure 3.10 shows that NF-κB subunit expression in the nucleus of RPMI8226 cells was increased by 24h co-culture with CD40L transfected fibroblasts. All five NF-κB subunits showed a substantial increase in their active protein levels in response to co-culture with CD40L transfected fibroblasts. The most pronounced and significant increases were seen in the nuclear expression of p65 (p = 0.02) and RelB (p = 0.03) NF-κB subunits. As all NF-κB subunits were increased by 24h CD40L stimulation in RPMI8226 cells, this would suggest that both canonical and non-canonical NF-κB signalling were stimulated by CD40L.

Figure 3.11 shows the effect CD40L on NF-κB in the cell lines U266B1 and JJN3. The level of p65 in both JJN3 and U266B1 cells was not altered by co-culture with NTL or CD40L transfected fibroblasts when compared to the LIQ condition. However, in these cell lines p52, RelB and c-Rel NF-κB subunits all showed a slight increase in protein quantity after CD40L stimulation for 24h with p52 showing the most pronounced increase relative to RelB and c-Rel. On the other hand, p50 subunit protein was decreased after 24h co-culture with both NTL and CD40L transfected fibroblasts in both U266B1 and JJN3 cell lines.

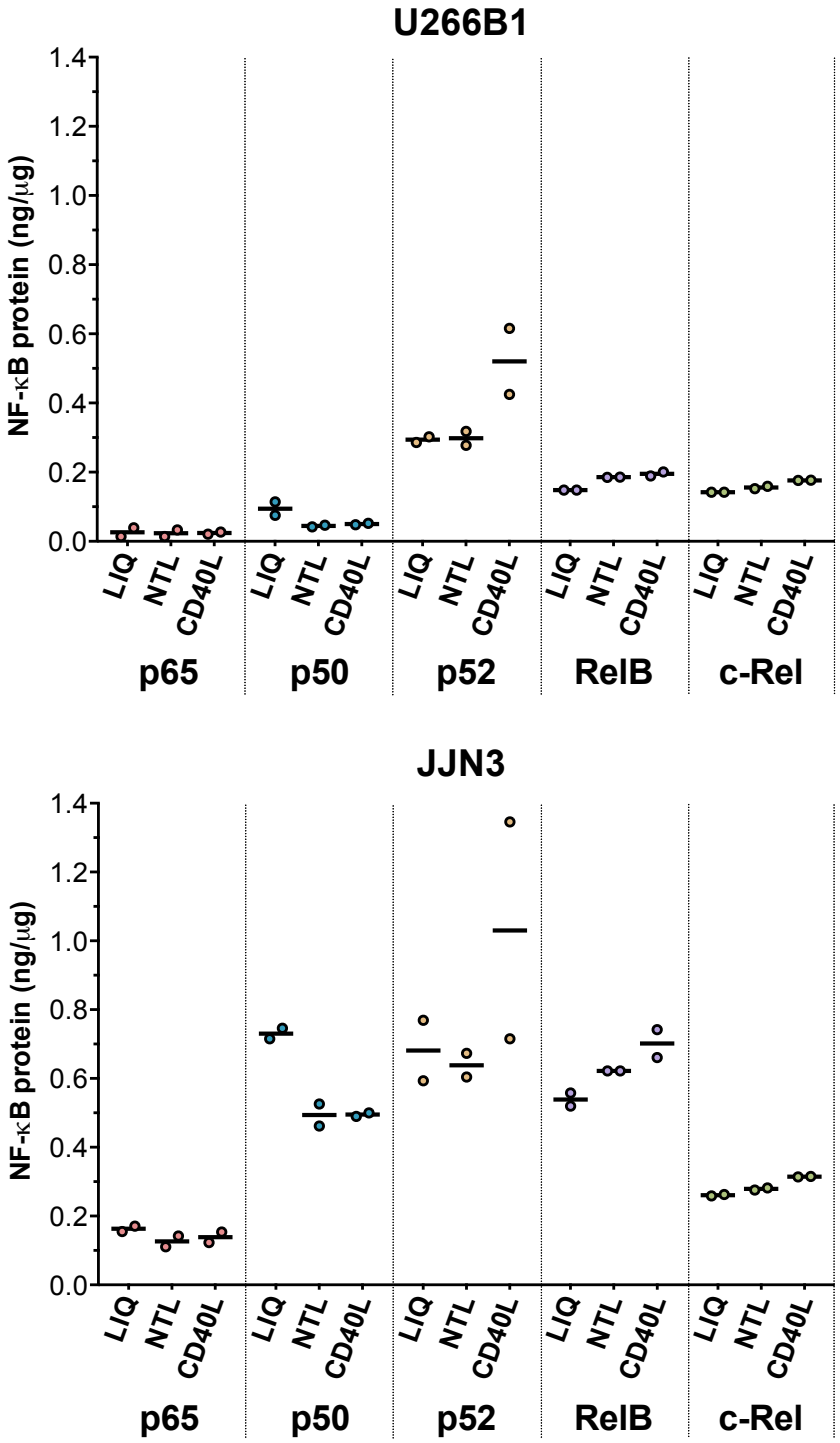

Figure 3.11 Effect of CD40L on NF-κB activity in the MM cell lines U266B1 and JJN3.
ELISAs detecting active NF-κB subunits were performed U266B1 and JJN3 nuclear extracts after 24h co-culture with and without CD40L or NTL transfected fibroblasts. U266B1 was assayed at 1μg/well and JJN3 at 0.5μg/well of nuclear extract protein where n = 1, duplicate. The graph shows n = 1, with individual experimental duplicates and overall mean. (CD40L= cells co-cultured with CD40L transfected fibroblasts, NTL= cells co-cultured with NTL transfected fibroblasts, LIQ= cells cultured alone).

3.3. The use of the non-specific NF-κB inhibitor BAY 11-7082 in myeloma cell lines

3.3.1. Cytotoxicity of BAY 11-7082 in MM cell lines

The first step in exploring the use of the non-specific NF-κB inhibitor BAY 11-7082 in MM cell lines involved assessing its cytotoxic potential. To investigate cytotoxicity, each MM cell line was treated within increasing concentrations of BAY 11-7082 ranging from 0.25μM to 15μM. After 48h, cells from each cell line were harvested and washed in PBS before staining with Annexin V-FITC and propidium iodide (PI). Cells were then analysed using flow cytometry to determine the percentage of apoptosis (Annexin V^+/PI^- + Annexin V^+/PI^+).

The raw data plots measured by the flow cytometer for the cell line H929 after 48h treatment with increasing concentrations of BAY 11-7082 are shown in Figure 3.12. Cells were first gated based on FSC-A and side SSC-A to exclude debris and these events were forward gated into bivariate plots of Annexin V (Annexin V-FITC-H) against propidium iodide (PI-H) (Figure 3.12). The scatter plots were split into quadrants so that the populations could be clearly identified and the percentage of apoptotic cells at each concentration of BAY 11-7082 were used to construct dose-response curves. Figure 3.13 presents the dose-response curves for each MM cell line and each graph was created from three separate experiments. The interpolated LD_{50} values and their respective 95% confidence intervals (CI) are reported for each cell line.

Figure 3.12 and 3.14 illustrate that BAY 11-7082 is cytotoxic in all the myeloma cell lines tested. Comparison of the LD_{50} values for each cell line indicated that the JJN3 cell line was relatively more resistant to apoptosis in response to BAY 11-7082 (LD_{50} = 3.38μM, 95% CI [2.71μM, 4.21μM]). However, the sensitivity of RPMI8226 cells to BAY 11-7082 was more similar to that of JJN3 than H929 and U266B1 cell lines (LD_{50} = 3.19μM, 95% CI [2.19μM, 4.64μM]). Conversely, Figure 3.13 shows that H929 and U266B1

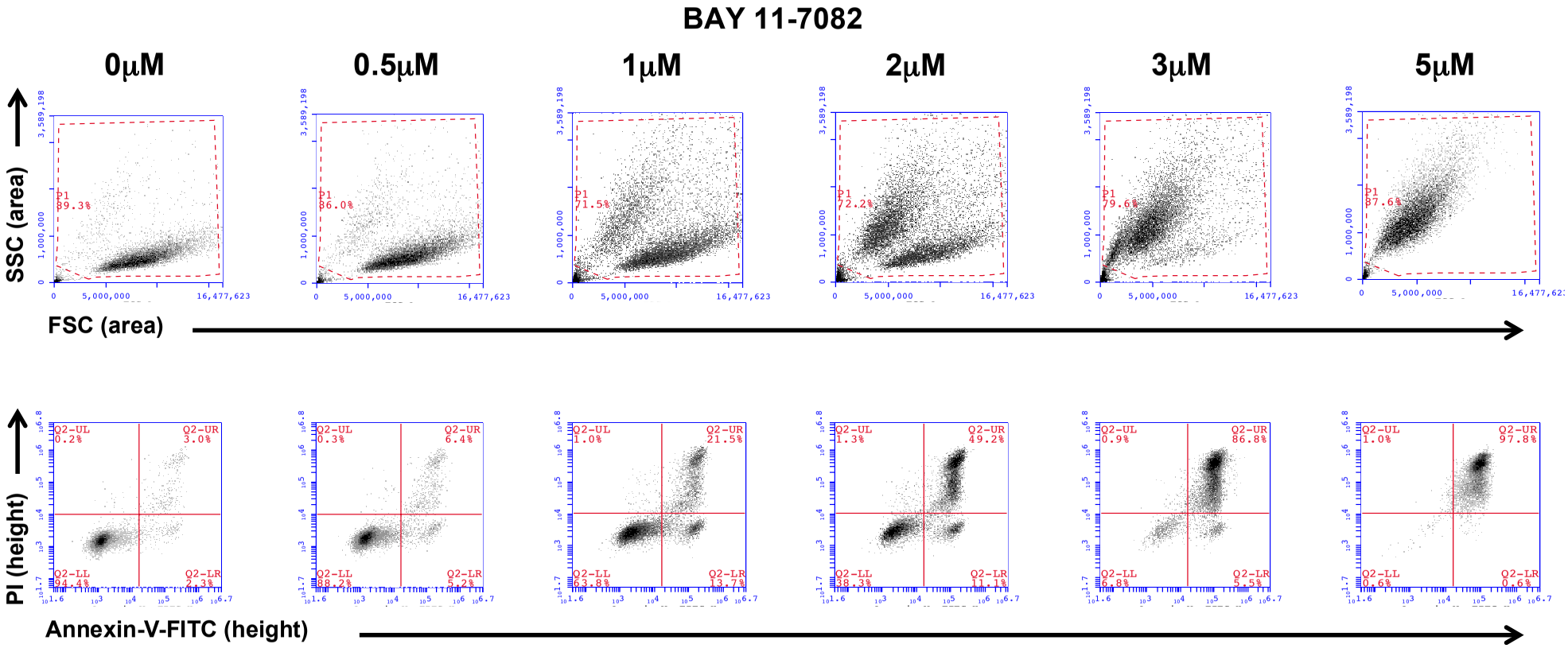

Figure 3.12 Flow cytometric data of the MM cell line H929 after 48h incubation with increasing concentrations of BAY 11-7082.
The MM cell line H929 was treated with increasing concentrations of BAY 11-7082 between 0.5μM and 5μM. At 48h, H929 cells were harvested and labelled with Annexin V-FITC and PI. Cell death was measured using Annexin V/PI positivity on an Accuri C6 flow cytometer. A representative example of the collected flow cytometric data for H929 after treatment with increasing concentrations of BAY 11-7082 is shown above. The first panel of scatter graphs shows the gating (P1) that was applied to exclude debris and select cells based on their forward scatter (FSC-A) and side scatter (SSC-A) profiles. The gating was then applied to scatter plots of Annexin-V-FITC-H and PI-H (the second panel of plots) to evaluate cytotoxicity. The percentage of apoptosis was quantified using Annexin V^+/PI^- (Q2-LR) + Annexin V^+/PI^+ (Q2-UR).

were the relatively most sensitive to apoptosis induced by BAY 11-7082. H929 and U266B1 had similar sensitivity as demonstrated by their LD_{50} values of 1.37μM (95% CI [1.16μM, 1.62μM]) and 1.93μM (95% CI [1.48μM, 2.52μM]), respectively.

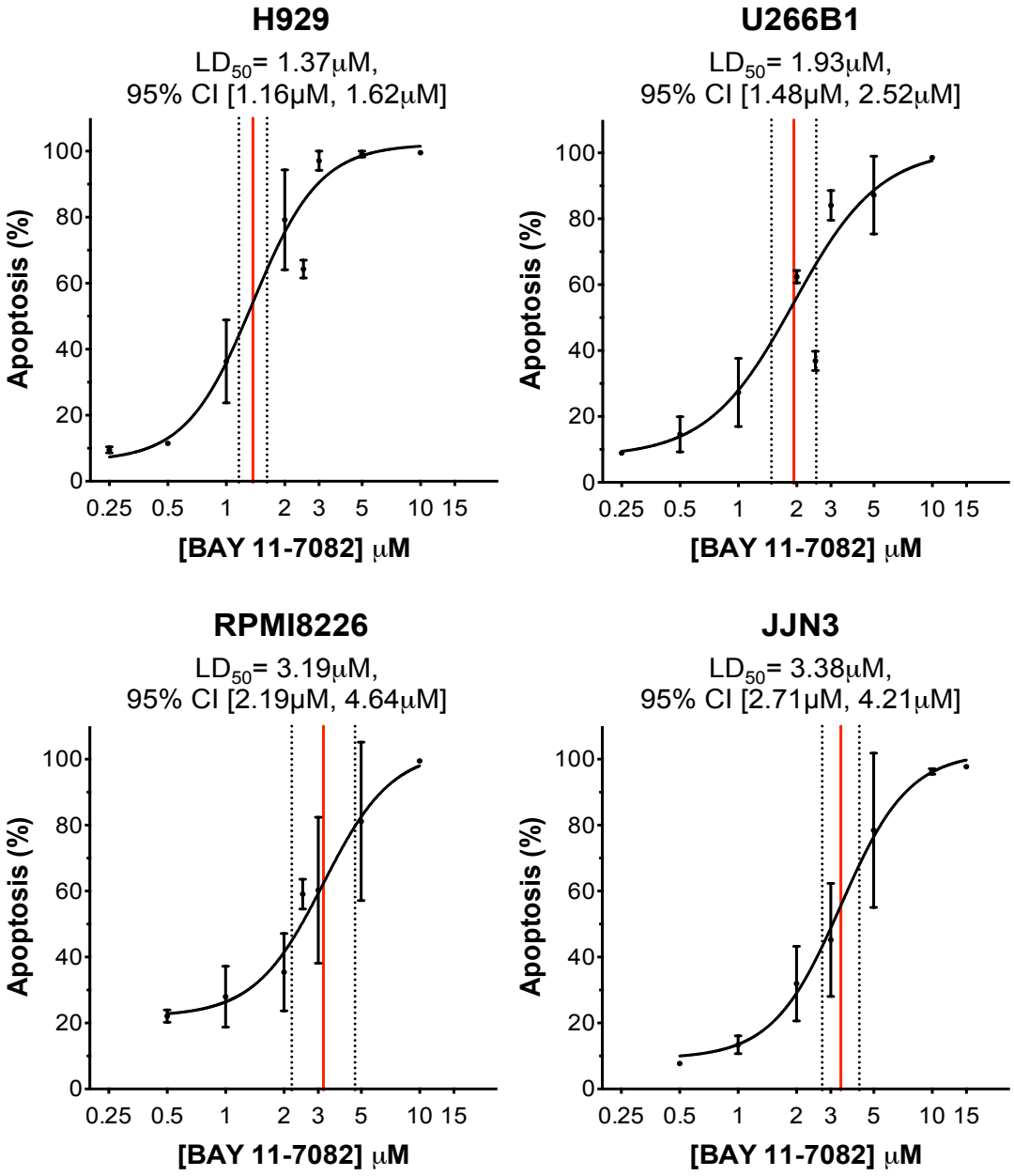

Figure 3.13 The cytotoxicity of BAY 11-7082 at 48h in the MM cell lines H929, U266B1, RPMI8226 and JJN3.
The cell lines H929, U266B1, RPMI8226 and JJN3 were treated with increasing concentrations of BAY 11-7082 between 0.25μM and 15μM. At 48h, cell death was measured using Annexin V/PI positivity on an Accuri C6 flow cytometer. The percentage of apoptotic cells at each concentration of BAY 11-7082 was then calculated and dose-response curves were constructed using GraphPad Prism 6.0. LD_{50} values were interpolated and are reported for each cell line alongside 95% CI. Error bars represent mean ± SD, where n = 3, triplicate.

3.3.2. Inhibition of NF-κB activity by BAY 11-7082

As BAY 11-7082 was cytotoxic at 48h in all four MM cell lines, the effect of this agent on NF-κB activity was assessed in the cell line RPMI8226 to investigate whether there was a correlation between apoptosis and the effect on NF-κB activity.

RPMI8226 cells were treated with increasing concentrations of BAY 11-7082 ranging from 0μM to 10μM in 2μM increments. At 4h, RPMI8226 cells from each concentration were harvested, washed in PBS to remove any BAY 11-7082 and nuclear extracts were derived from the washed cell pellets. This experiment was repeated three times and once all nuclear extracts were generated, they were assayed in duplicate at 1μg per well using NF-κB family subunit ELISA assays. This was carried out as per the manufacturer's instructions and standard curves were generated using known quantities of recombinant p65 protein (r^2 >0.99) and recombinant p50 protein (r^2 >0.96) to allow NF-κB subunit quantification. The subunit quantities were then normalised compared to the values at 0μM and data of these experiments are presented in Figures 3.15.

Figure 3.14 demonstrates that the quantities of all five NF-κB subunits were decreased in a dose-dependent manner after 4h exposure to increasing concentrations of BAY 11-7082. The p52 subunit showed the most significant decrease after 4h exposure to 10μM BAY 11-7082 (22.4% ± 4.9%, p < 0.001) when compared to 0μM. The p50 and RelB NF-κB subunits experienced the largest decrease in protein quantity (7.1% ± 10.4% at 10μM, p=0.003 and 8.6% ± 12.0% at 10μM, p = 0.003, respectively) compared to untreated levels. While p65 and c-Rel subunits experienced a significant decrease in protein level in response to 10μM BAY 11-7082, relatively the decrease in activity was the lowest observed among the NF-κB subunits (43.8% ± 9.2%, p = 0.005 and 46.2% ± 24.5%, p = 0.04, respectively).

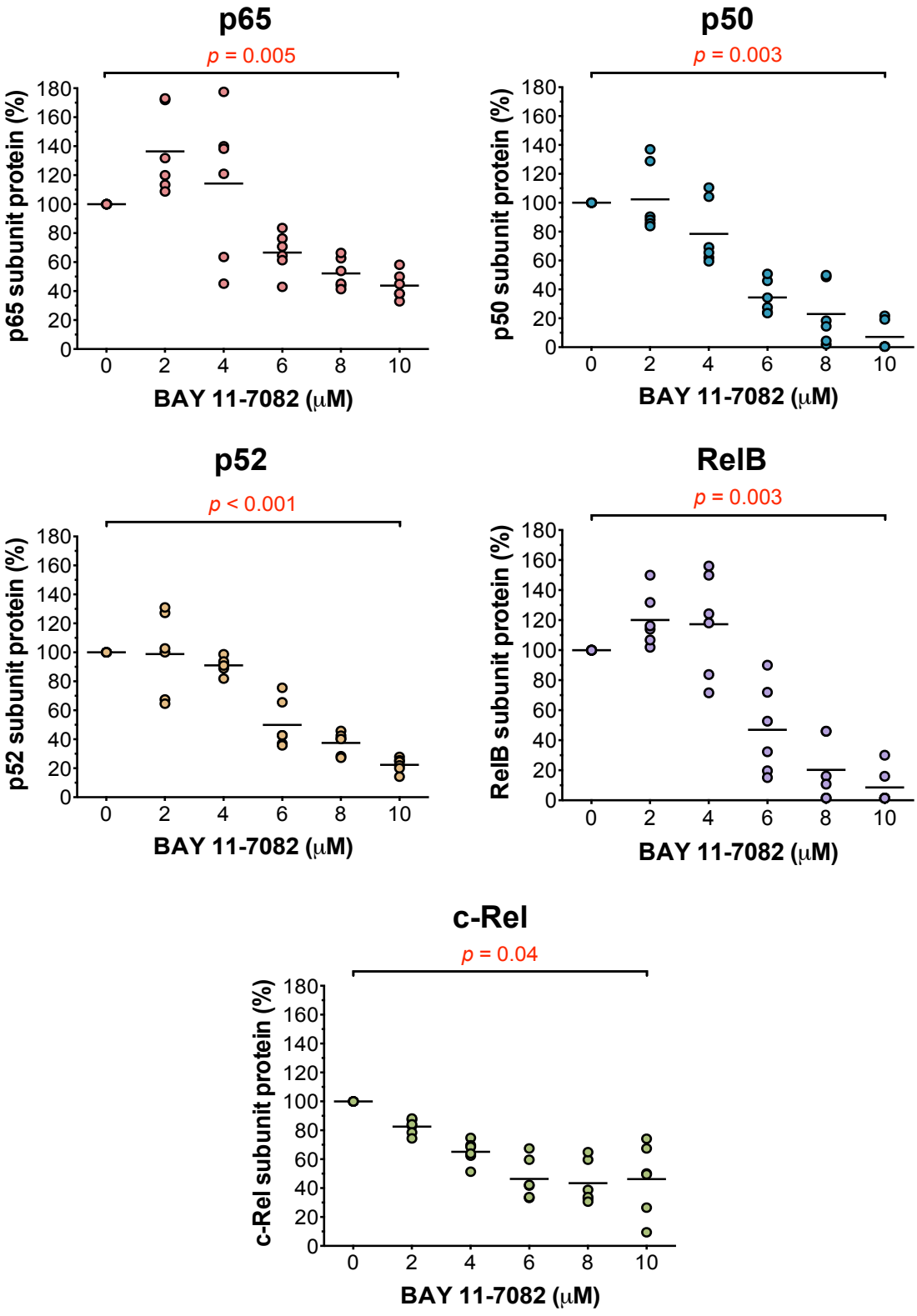

Figure 3.14 Effect of BAY 11-7082 on NF-κB activity in the MM cell line RPMI8226. RPMI8226 cells were incubated with increasing concentrations of BAY 11-7082 for 4h. RPMI8226 was then assayed at 1μg/well of nuclear extract protein using ELISAs detecting active NF-κB subunits. Quantified protein values were normalised compared to 0μM BAY 11-7082 to give the relative percentage of each NF-κB subunit. The percentages reported correspond to n = 3, duplicate with mean shown. A one-tailed unpaired t-test was performed using Graphpad Prism 6.0 software to investigate the statistical significance values between 0μM and 10μM BAY 11-7082 for each NF-κB subunit (n = 3, duplicates averaged).

Alongside the three experiments shown in Figure 3.14, the cytotoxicity induced by BAY 11-7082 in RPMI8226 cells was investigated at 24h. Briefly, cells were harvested, washed in PBS before staining with Annexin V-FITC and propidium iodide (PI). Annexin V/PI positivity was then analysed in triplicate by flow cytometer and the percentage of apoptotic cells at each concentration of BAY 11-7082 was calculated. The NF-κB ELISA data in Figure 3.14 was then plotted alongside the percentage of apoptosis at each concentration for each of the three experiments. The correlation between these two measurements was investigated by performing linear regression analysis.

Figure 3.15 displays the correlation between individual subunit quantities (ng/μg) and the percentage of apoptosis at each increasing dose of BAY 11-7082. The linear regression analysis for all five NF-κB subunits produced negative correlations that were all highly significant ($p < 0.001$). A pattern similar to that observed in Figure 3.14 for fold change and significance is observed when the linearity of each subunits linear regression was considered. For example, the correlation between apoptosis and the quantity of p50, p52 and RelB subunits produced the highest linearity ($r^2 = 0.74$, $r^2 = 0.72$ and $r^2 = 0.61$, respectively) whereas the negative correlation between the quantity of p65 and c-Rel subunits and apoptosis was relatively weaker ($r^2 = 0.57$ and $r^2 = 0.30$, respectively)

Overall, Figure 3.14 and Figure 3.15 suggest that BAY 11-7082 is dose-dependently inhibiting NF-κB activity generated through both the canonical and non-canonical pathways because this agent is significantly decreasing all active NF-κB subunits in RPMI8226 cells at 4h. The strong correlations seen between increasing concentrations of BAY 11-7082, inhibition of overall NF-κB activity at 4h and subsequent apoptosis at 24h implies that apoptosis in response to BAY 11-7082 in RPMI8226 cells may be a consequence of inhibition of NF-κB activity.

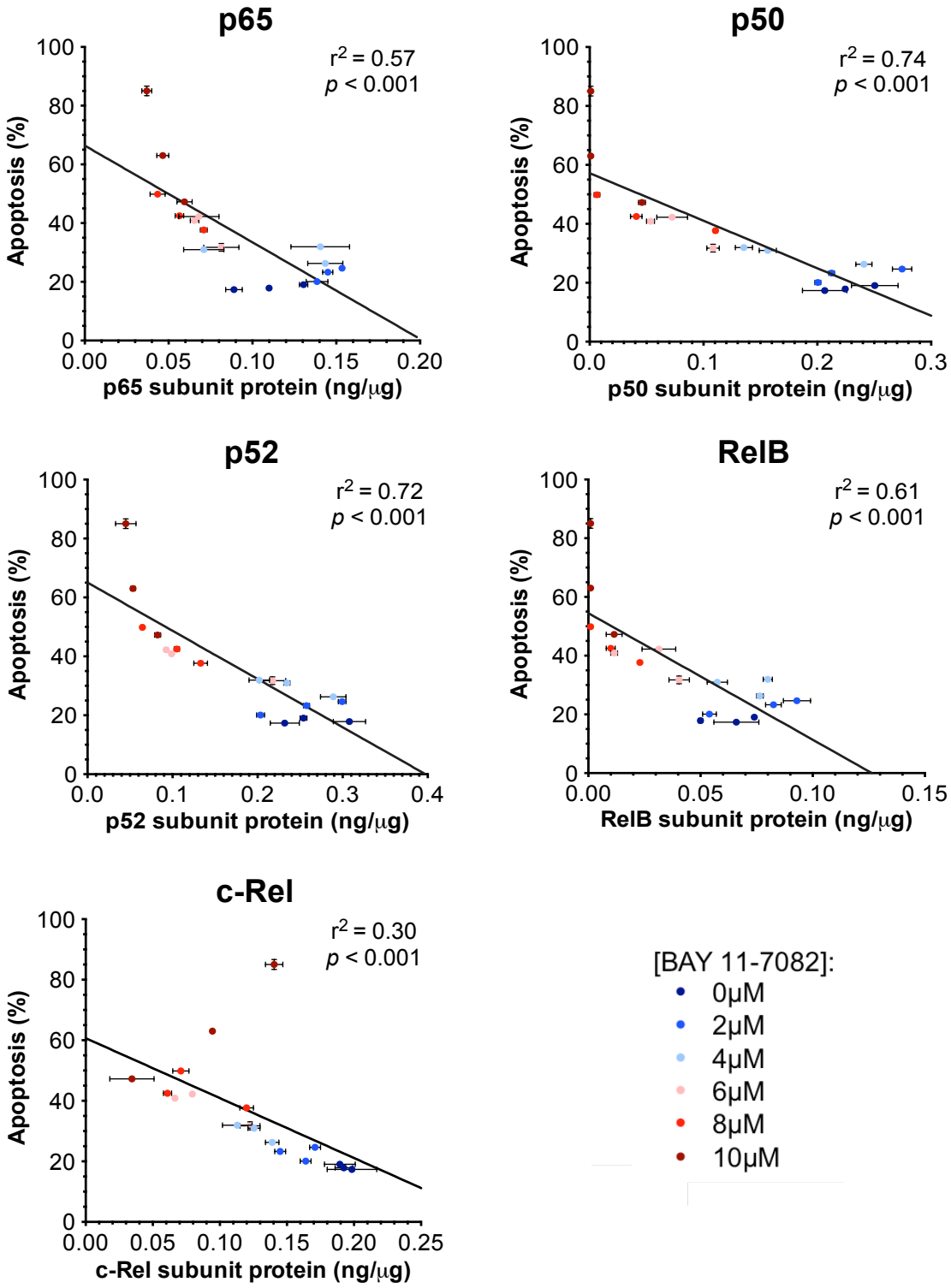

Figure 3.15 Correlation of BAY 11-7082 induced cytotoxicity at 24h with NF-κB activity at 4h in RPMI8226 cells.
RPMI8226 cells were incubated with increasing concentrations of BAY 11-7082. At 4h, nuclear extracts were generated and NF-κB subunit ELISAs were performed. Subsequently, at 24h the percentage of apoptotic cells was measured using Annexin V/ PI positivity for the corresponding conditions. The correlation between these measurements was investigated by linear regression using Graphpad Prism 6.0 software. The linearity (r^2) and p value are reported for each NF-κB subunit. The points plotted represent mean ± SEM for each experiment (n = 3).

3.4. Discussion

3.4.1. Characterisation of four multiple myeloma cell lines

The MM cell lines used throughout this thesis were chosen because they each represent distinct clinical features (and different NF-κB mutational profiles) manifested in MM (Drexler a Matsuo 2000; Annunziata et al. 2007; Keats et al. 2007). For example, H929 was selected because it possesses no known genetic abnormalities in the NF-κB pathway. On the other hand, U266B1, RPMI8226 and JJN3 are characterised by activating mutations affecting the NF-κB pathway (Annunziata et al. 2007; Keats et al. 2007). U266B1 and RPMI8226 possess inactivating TRAF3 mutations while JJN3 manifests an activating mutation in NF-κB inducing kinase (NIK).

Additionally, the cell lines were each derived from plasma cells originating from different anatomical niches of the disease, secrete different classes of immunoglobulin and even differ in the clinical stage of MM that they are derived from. For example, H929, U266B1 and RPMI8226 were obtained from patients diagnosed with MM and were derived from pleural effusion or peripheral blood samples (Matsuoka et al. 1967; Nilsson et al. 1970; Gazdar et al. 1986). Conversely, JJN3 is considered to be a more advanced stage of MM because it is derived from the bone marrow of a patient diagnosed with plasma cell leukaemia (Jackson et al. 1989).

As a result, it was predicted that each cell line would possess its own individual characteristics in terms of growth, phenotype and NF-κB activity. Therefore, to gain a better understanding of the MM cell lines, the first aim of this project was to characterise them.

It was noticed during the culture of each cell line that the apparent growth rates differed between the MM cell lines. The RPMI8226 and JJN3 cell lines showed the fastest growth rates as evidenced by the requirement to split the cultures more frequently than H929 and U266B1 cell lines. Therefore, the first step of cell line characterisation was to investigate the growth kinetics of each cell line by measuring cell cycle distributions and basal levels of apoptosis.

The data shown in Figure 3.1 suggested that RPMI8226 and JJN3 were the fastest growing myeloma cell lines because they had more cells in S phase and G_2/M phase of the cell cycle and a significantly lower percentage of cells in G_0/G_1 phase than H929 and U266B1 cell lines ($p < 0.05$, two-way ANOVA). Moreover, the percentages of cells in the G_0/G_1, S and G_2/M phases were not significantly different between RPMI8226 and JJN3 cell lines ($p = 0.14$, $p = 0.71$ and $p = 0.08$, respectively) suggesting that the growth rates of these two cell lines were similar.

H929 possesses the slowest growth rate and concordantly manifested significantly more cells within G_0/G_1 phase of cell cycle than U266B1, RPMI8226 and JJN3 cell lines ($p = 0.004$, $p < 0.001$ and $p < 0.001$, respectively). This suggests that at any one time more H929 cells were not actively cycling. In addition, U266B1 showed a similar growth rate to that of the H929 cell line and this was supported by the cell cycle profile, which showed that both the U266B1 and H929 cell lines had a similar percentage of cells in G_0/G_1, although this was still significantly different ($p = 0.004$, two-way ANOVA).

H929 has been previously reported to possess a doubling time of 50h (Gazdar et al. 1986), U266B1 a doubling time of 40-45h (Hellman et al. 1988) and a doubling time of 33.5h and 20-35h for RPMI8226 and JJN3 cell lines, respectively (Collins 2015; DSMZ 2016). The average doubling time of a MM cell line is 54h ± 36h (Drexler a Matsuo 2000) so the four cell lines that were characterised here reflect the expected spectrum of growth kinetics. As such, the data in Figure 3.1 supports my personal observations made whilst culturing the respective cell lines and also previous observations reported in the literature and within cell line databases.

Figure 3.2 suggests that all the MM cell lines experienced relatively low baseline apoptosis when cultured under standardised culture conditions. The U266B1 and JJN3 cell lines experienced the lowest levels of natural cell death whereas the H929 and RPMI8226 cell lines experienced more baseline apoptosis. RPMI8226 cells experienced the most baseline cell

death under optimal growth conditions and it was observed during cell culture that the medium that these cells were grown in was required to be replaced more regularly that the other cell lines due to discolouration. This did not appear to be associated with the growth kinetics of the cell line as RPMI8226 cells were not the most proliferative. It therefore remains possible that the growth conditions used for this cell line were sub-optimal.

Furthermore, plasma cells are antibody-producing cells and the RPMI8226 cell line has been previously shown to actively synthesise and secrete higher levels of immunoglobulin than the other MM cell lines (Matsuoka et al. 1968). In the same study, it was found that baseline cell death was associated with the higher levels of immunoglobulin synthesis. In theory, the increased immunoglobulin synthesis of the RPMI8226 cells may have a higher demand for nutrients, which could be responsible for the elevated cell apoptosis observed.

Overall, the growth characteristics of the four MM cell lines show heterogeneity both in terms of growth kinetics and baseline cell death under standardised growth conditions. Moreover, there did not seem to be an association between the level of baseline cell death and the rate of cell proliferation in each cell line. The cell proliferation of RPMI8226 and JJN3 cell lines were both relatively high but JJN3 cells experienced a low level of baseline cell death while RPMI8226 experienced the highest levels of cell death.

The phenotype of each myeloma cell line was also investigated by measuring the cell surface expression of three antigens; CD38, CD138 and CD40. CD38 and CD138 are common cell surface markers in MM and, as such, are used to identify malignant plasma cells in MM due to their consistent and relatively high expression (Lin et al. 2004). In vivo, CD38 is an activation marker that can function both enzymatically and through ligation to the adhesion molecule CD31, which is highly expressed on endothelial cells and B cells, to control MM cell migration, proliferation, differentiation and survival (Cesano et al. 1998; Deaglio et al. 1998;

Fernàndez et al. 1998; Horenstein et al. 2015). CD138, also known as syndecan-1, is expressed mainly on terminally differentiated B cells, making it a marker for plasma cells, although it is readily shed from the cell surface spontaneously or because of apoptosis induction (Jourdan et al. 1998; Yang et al. 2002; Ikeda et al. 2009). CD138 is an adhesion molecule that regulates cell, growth, proliferation and survival (Gharbaran 2015). CD40 is a cell surface marker that is not usually expressed on normal plasma cells but has been shown to be present in the early stages of MM, although its expression does not correlate to overall survival (Tong et al. 2000; Perez-Andres et al. 2009). In B cells, CD40 is required for B cell activation and terminal differentiation to plasma cells (O'Connor et al. 2003). The ligand of CD40 is CD40L (also called CD154) and interactions have previously been shown to stimulate NF-κB activity, mainly via the non-canonical signalling pathway (Coope et al. 2002; Tai et al. 2003; Hauer et al. 2005).

CD38, CD138 and CD40 cell surface antigens each contribute to the myeloma phenotype and it has been reported that 100% of existing MM cell lines express CD138, 89% positively express CD38 and 59% express CD40, (Drexler a Matsuo 2000). This study revealed variable expression of CD38 within the four cells lines. CD38 was most highly expressed in RPMI8226 cells, followed by H929 and JJN3, with the lowest level found in U266B1, which is in line with previous reports (Hata et al. 1994; Lagging et al. 1996; Deckert et al. 2014). However, the data were in slight contrast with a report published by (Gooding et al. 1999) where CD38 expression was lowest in JJN3, and U266B1 expressed an intermediate level of CD38. Furthermore, my results indicated that the U266B1 cell line contained a sub-population that expressed a higher level of CD38. It has previously been reported that the U266B1 cell line contained two sub-populations expressing different levels of the cell surface antigen CD38 (Lagging et al. 1996; Mahmoud et al. 1998). However, it is possible that at different passage numbers and under specific growth conditions, the U266B1 cells can express a higher or lower proportion of $CD38^{hi}$ cells thereby altering the overall MFI for this antigen. This could explain why Gooding *et al.* observed a higher expression of CD38 (Gooding et al. 1999).

The data in Figure 3.4 implies that U266B1 expressed the highest levels of CD138, H929 and RPMI8226 expressed intermediate levels, and JJN3 expressed the lowest levels of CD138. Although it can be concluded that CD138 expression was heterogeneous in these MM cell lines, the expression of this cell surface marker was relatively high in all cell lines. This is in slight contrast to previous data in which RPMI8226 was the cell line that expressed the most CD138 (Gooding et al. 1999; Ikeda et al. 2009). Moreover, it was suggested that the expression in JJN3 was more similar to that of RPMI8226 and H929 (Gooding et al. 1999). This difference may be the result of the gating used for measuring CD138 expression in JJN3 because it can be seen in Figure 3.4A that small sub-populations of cells are present with a lower level of CD138. When this is considered within the average MFI of CD138, it may lower the overall expression. The large error bars displayed alongside the data in Figure 3.4 also suggests that the level of CD138 expression in the cell lines was variable. CD138 is easily shed from the surface of MM cells and this may explain the variability in expression within an individual cell line (Jourdan et al. 1998; Yang et al. 2002; Ikeda et al. 2009).

In this thesis, the RPMI8226 cell line was the only MM cell line analysed that expressed a relatively high level of CD40. H929, U266B1 and JJN3 also expressed a lower level of CD40, but only H929 and JJN3 were significantly different to unstained control ($p < 0.01$, multiples t test). In keeping with these findings, RPMI8226 was previously shown to express relatively high levels of CD40 while U266B1 was shown to express a much lower level of this antigen (Tong et al. 1994; Fernandes et al. 2009).

In conclusion, the expression of CD38, CD138 and CD40 were found to be heterogeneous among the myeloma cell lines H929, U266B1, RPMI8226 and JJN3. Therefore, as CD38 (Kang et al. 2006; Tirumurugaan et al. 2008) and CD40 (Hinz et al. 2001) are both NF-κB regulated target genes, heterogeneous expression off these cell surface markers may suggest that NF-κB activity may also be differentially regulated in each MM cell line.

Consequently, baseline NF-κB activity was measured in each MM cell line and the NF-κB activity within the myeloma cell lines was also found to be heterogeneous. Based on EMSA and ELISA data, H929 possessed the lowest level of NF-κB activity, JJN3 was found to have the highest level of NF-κB activity, and both U266B1 and RPMI8226 possessed an intermediate level. These observations correlate with the genetic abnormalities associated with the respective cell lines and support previous findings (Annunziata et al. 2007; Keats et al. 2007; Demchenko et al. 2010) but contrast with previous EMSA data that showed U266B1 to have higher NF-κB DNA binding activity than RPMI8226 (Hideshima et al. 2006; Hideshima et al. 2009).

The results from the ELISAs confirm that the MM cell lines all possess constitutive NF-κB activity that arises as a combination of both the canonical and non-canonical NF-κB signalling pathways. This is in accordance with previously published data where it was reported that U266B1, RPMI8226 and JJN3 all rely on both NF-κB signalling pathways (Annunziata et al. 2007; Keats et al. 2007; Hideshima et al. 2009; Demchenko et al. 2010).

However, the ELISAs may not have been an appropriate tool to quantify the baseline levels of the NF-κB subunits p52, RelB and c-Rel in the MM cell lines. This is because their quantification in these experiments relied on using a p65 recombinant protein as a protein standard since a specific recombinant protein was not available for p52, RelB or c-Rel. For this reason, the levels of these subunits measured can only be assumed to be approximate quantities rather than specific quantities of each subunit. The ELISA's also showed variability between individual experiments and this was mainly a consequence of the quality of the standard curves generated from the p65 or p50 recombinant proteins for each experiment. As a result, this may add further error to the exact NF-κB subunit levels quantified in the ELISA's.

Furthermore, there may potentially be issues with the specificity of the antibodies provided in the NF-κB ELISA kits, as well as issues with the binding of specific NF-κB subunit dimers to the immobilised oligonucleotide. For these reasons, it has been discussed that the ELISA kits may be missing p52 homodimer binding (personal communication with Professor Neil Perkins). Consequently, there is a possibility that the ELISA's used may inaccurately under quantify the levels of some NF-κB subunits, especially those derived from the non-canonical pathway.

For the reasons discussed above, western blots could have been used in the place of the EMSA and ELISA techniques to more accurately determine the level of canonical and non-canonical pathway signalling in the MM cell line H929, U266B1, RPMI8226 and JJN3. Overall, with the use of the right combination of antibodies, this technique could have provided in depth information regarding the specific NF-κB pathway processing in each of the four MM cell lines. Antibodies targeting phosphorylated p100, p100 and p52 proteins could have provided information regarding non-canonical processing, whereas antibodies specific to IκBα, p65 and phosphorylated IκBα proteins could have given information on canonical pathway processing.

Finally, the main conclusion that can be drawn from the cell cycle, phenotype and NF-κB activity characterisation is that the MM cell lines H929, U266B1, RPMI8226 and JJN3 reflect the heterogeneity that is commonly observed in multiple myeloma.

3.4.2. Manipulation of myeloma cell lines with CD40L stimulation

The interaction of CD40 on malignant plasma cells with CD40L within the bone marrow microenvironment is an important interaction that can promote MM cell survival mainly through activation of non-canonical NF-κB signalling (Coope et al. 2002; Tai et al. 2003; Hauer et al. 2005). In addition, CD38 is a NF-κB regulated target gene so an increase in NF-κB activity through CD40L stimulation may alter the myeloma phenotype (Kang et al. 2006; Tirumurugaan et al. 2008). Therefore, the cell surface

phenotype and NF-κB activity was investigated in each MM cell line following co-culture of the MM cells with CD40L expressing fibroblasts.

The RPMI8226 cell line was found to possess the highest level of CD40 cell surface expression whereas the H929 cell line had minimal CD40 expression. For this reason, it was predicted that the RPMI8226 and H929 MM cell lines were more likely to respond to CD40L stimulation in terms of cell surface CD38 and CD138 expression and NF-κB activity compared to the U266B1 and JJN3 cell lines. Moreover, previous work has shown that CD40L stimulation increased CD38 expression in CLL B cells (Willimott et al. 2007; Patten et al. 2008). In contrast, at 24h, CD40L stimulation did not significantly alter cell surface CD38 or CD138 expression in H929, U266B1, RPMI8226 and JJN3 cells relative to unstimulated cells. Although not significant, the H929 and RPMI8226 cell lines did experience a minor decrease in CD138 expression following 24h CD40L stimulation. However, as CD138 is easily shed from the surface of MM cells (Jourdan et al. 1998; Yang et al. 2002; Ikeda et al. 2009), it is possible that the force used to extract the MM cell lines from the CD40L transfected fibroblasts may have contributed to the minor decrease observed.

Figure 3.10 showed that NF-κB activity was increased through CD40 activation in the RPMI8226 cell line because the levels of all active NF-κB subunits were increased following 24h CD40L stimulation, with the most prominent increases seen in the p65 and RelB subunits (p = 0.02 and p = 0.03, respectively). This indicates that CD40L stimulation is positively regulating NF-κB activity generated through both canonical and non-canonical signalling. This effect was not mirrored in the H929 cell line following CD40L stimulation and the active NF-κB subunit levels remained unchanged. The phenotype characterisation showed that RPMI8226 cells possess significantly higher levels of CD40 cell surface expression compared to H929 cells. Therefore, this may explain why the RPMI8226 cell line was more susceptible to an increase in NF-κB subunit levels in response to CD40 activation.

The results replicate previous findings that CD40 activation induced NF-κB activity generated through both the canonical and non-canonical signalling pathways (Coope et al. 2002; Tai et al. 2003; Hauer et al. 2005).

In conclusion, only NF-κB activity was significantly altered as a consequence of CD40L stimulation in the CD40 expressing MM cell line RPMI8226.

3.4.3. The use of the non-specific NF-κB inhibitor BAY 11-7082 in myeloma cell lines

One of the main aims of this thesis was to explore the use of NF-κB inhibitors in MM. As a first step, the effect of a commercially available non-specific NF-κB inhibitor, BAY 11-7082, was investigated in the myeloma cell lines. BAY 11-7082 has been shown to non-sepcifically inhibit NF-κB signalling by irreversibly inhibiting IκBα phosphorylation through the inhibition of IKK activation and this subsequently induced apoptosis in leukaemia cells (Pierce et al. 1997; Mori et al. 2002; Strickson et al. 2013). Therefore, as all the myeloma cell lines were shown to display constitutive NF-κB activity, it was predicted that inhibition of NF-κB would induce apoptosis but that the sensitivity of the MM cell lines may be heterogeneous.

The cytotoxicity of BAY 11-7082 was first investigated and it was found to induce dose-dependent cytotoxicity in all four MM cell lines tested, which replicates the previous studies showing that BAY 11-7082 was cytotoxic to MM cell lines (Dai et al. 2004b; Rauert-Wunderlich et al. 2013). As predicted, sensitivity to the NF-κB inhibitor varied among the cell lines. H929 was the most sensitive cell line to apoptosis induced by BAY 11-7082 and JJN3 was the most resistant cell line. U266B1 and RPMI8226 both displayed intermediate sensitivity to the agent but U266B1 showed sensitivity more similar to that of H929 whereas RPMI8226 was almost as resistant as JJN3.

The pattern observed in cytotoxicity inversely correlated with the level of constitutive NF-κB activity in each MM cell line. For example, JJN3

possessed the most NF-κB activity but was the most resistant myeloma cell line to BAY 11-7082 induced apoptosis. An explanation for this could relate to the function of NF-κB because the transcription factor regulates genes involved in anti-apoptosis and drug resistance (Gilmore 2007; Demchenko a Kuehl 2010). Therefore, cells with more NF-κB activity may be able to resist the inhibition caused by BAY 11-7082. However, this is contrast with other published data that suggests the inverse in which MM cell lines with a higher level of baseline activity of p65 and p52 subunits were more sensitive to apoptosis induced by IKK inhibition, although this was specific to IKKβ inhibition (Annunziata et al. 2007). As a result, Annunziata *et al.* reported that the JJN3 cell line was more sensitive to apoptosis induced through IKKβ inhibition when compared to the H929 cell line.

The correlation between apoptosis and the level of NF-κB inhibition by BAY 11-7082 was then investigated in the MM cell line RPMI8226, a MM cell line that possessed a comparatively intermediate NF-κB activity and a demonstrated a relatively intermediate sensitivity to BAY 11-7082. NF-κB subunit ELISA assays showed that p65, p50, p52, RelB and c-Rel active NF-κB subunits experienced a significant dose-dependent decrease in response to 10μM BAY 11-7082 ($p = 0.005$, $p = 0.003$, $p < 0.001$, $p = 0.003$ and $p = 0.04$, respectively). The largest fold changes were observed for p50 and RelB subunits, which are canonical and non-canonical associated NF-κB subunits, respectively. This suggests that BAY 11-7082 regulates NF-κB subunits involved in both NF-κB pathways and implies that BAY 11-7082 is an inhibitor of both canonical and non-canonical signalling pathways, which replicates previous findings (Jayandharan et al. 2011; Rauert-Wunderlich et al. 2013). As BAY 11-7082 is predicted to be an inhibitor of IKK activation, this would suggest that it is capable of inhibiting both IKKα and IKKβ activation, which would explain the dual inhibition observed for canonical and non-canonical NF-κB activity.

Moreover, Figure 3.15 shows that a highly significant negative correlation existed between NF-κB inhibition and the induction of apoptosis in response to BAY 11-7082. This suggests that inhibition of NF-κB activity

generated as a consequence of both canonical and non-canonical pathway signalling may contribute to the apoptotic effect induced by BAY 11-7082 in the MM cell lines. However, several studies have shown that BAY 11-7082 possesses other molecular targets and it is a possibility that this is contributing to the cytotoxicity of BAY 11-7082 in the MM cell lines (Lee et al. 2012; Rauert-Wunderlich et al. 2013; Strickson et al. 2013). For example, Stickson *et al.* 2013 showed that BAY 11-7082 is not a direct inhibitor of IKKα and IKKβ, but instead inhibits their activation by targeting components of the ubiquitin system, such as TRAF6, to prevent the formation of K63-pUb and linear-pUb chains. Moreover, as ubiquitination is involved in a wide range of signalling pathways, including proteasomal degradation and DNA damage, BAY 11-7082 inhibition of multiple ubiquitination events is more likely the cause of the concentration-dependent apoptosis measured in the MM cell lines (Strickson et al. 2013).

Chapter 4 – Evaluation of a series of novel IKKα inhibitors for the treatment of multiple myeloma

NF-κB signalling is generally described as occurring through two distinct pathways; the canonical and non-canonical NF-κB signalling pathways. The canonical pathway is mainly activated through IKKβ-mediated phosphorylation of the IκB proteins, which allows activated dimers of p65, p50 and c-Rel to translocate to the nucleus and then bind DNA κB elements (Adli et al. 2010). On the other hand, the non-canonical NF-κB pathway is mainly activated through NF-κB inducing kinase (NIK)-mediated phosphorylation of IKKα (Malinin et al. 1997; Ling et al. 1998). Activated IKKα then phosphorylates the precursor subunit p100, which leads to proteolytic processing of the p52 NF-κB subunit, which can form homo- or hetero-dimers with the RelB NF-κB subunit (Senftleben et al. 2001; Solan et al. 2002). The activated NF-κB p52/RelB dimers then translocate to the nucleus where they bind DNA κB elements to induce a transcriptional response.

Several studies have documented that MM tumours and cell lines possess a large number of genetic aberrations that lead to constitutive NF-κB activity, preferentially through activation of the non-canonical NF-κB pathway (Annunziata et al. 2007; Keats et al. 2007; Demchenko et al. 2010). Furthermore, constitutive RelB activation is observed in approximately 40% of MM cases and the phenotypic advantage of this has been found to be to promote MM cell survival by increasing the expression of anti-apoptotic NF-κB target genes such as cIAP2 (Cormier et al. 2013). Therefore, the dependence of MM cells on the non-canonical NF-κB pathway indicates its importance in MM disease progression and that inhibition of this NF-κB pathway may provide a promising therapeutic option in MM.

The NF-κB pathways can be specifically inhibited at several points; prevention of IκB protein degradation, inhibition of IKK activation and blockade of NF-κB DNA-binding (Godwin et al. 2013). Due to the crucial roles that IKK plays in the regulation of NF-κB activity, both through canonical and non-canonical pathway activation, inhibition of IKK activation may provide a promising therapeutic strategy.

Multiple IKKβ inhibitors have been evaluated in MM and these have been found to induce a number of anti-tumour effects, mainly through canonical NF-κB pathway inhibition. These include inhibiting cell proliferation and cell growth, inducing apoptosis and cell cycle arrest, overcoming IL-6 medicated cell growth and drug resistance, and down-regulating a number of NF-κB canonical pathway regulated genes, including IκBα, Bcl-2 and cyclin D1 (Hideshima et al. 2002; Bharti et al. 2003; Hideshima et al. 2006; Annunziata et al. 2007; Jourdan et al. 2007; Hideshima et al. 2009).

However, concerns over the safety profile of IKKβ inhibitors have prevented further development of these specific agents in MM. For example, complete ablation of the canonical pathway activity through IKKβ inhibition is likely to impair the function of the adaptive and innate immune system, due to the complexity through which NF-κB signalling can regulate immunity, and may also lead to IL-1β induced neutrophilia and inflammation (Greten et al. 2007; Vallabhapurapu a Karin 2009; Hsu et al. 2011). In addition, hepatic toxicity is a possible adverse event of IKKβ inhibitors because IKKβ knockout mouse models indicate that the embryonic lethality of this phenotype is a result of hepatocyte apoptosis (Li et al. 1999b; Tanaka et al. 1999).

Specific inhibitors of IKKα may be beneficial in overcoming some of the adverse events that are associated with canonical pathway inhibition (DiDonato et al. 2012). IKKα mainly governs the activation of the non-canonical NF-κB pathway so specific pharmacological inhibitors of IKKα would be expected to inhibit non-canonical NF-κB pathway activation in MM as opposed to canonical pathway activation (Senftleben et al. 2001; Solan et al. 2002).

In mice, deletion of IKKα induces perinatal lethality due to defects in skeletal and epidermal development, although this has been shown to be independent of NF-κB activation (Li et al. 1999a; Gerondakis et al. 2006). Replacing the kinase activation serine residues in IKKα with alanine residues to prevent the activation of IKKα, can overcome lethality by still allowing

expression of the protein itself (Cao et al. 2001). This produces a phenotype that is similar to that which arises in the absence of NIK or *nfkb2*, which encodes the p100 protein, in that defects are present in lymphoid organogenesis, germinal centre formation and generation of mature follicular dendritic cells (Senftleben et al. 2001; Bonizzi et al. 2004; Gerondakis et al. 2006). Moreover, these effects have been shown to arise because these processes are regulated by p52/RelB dimers through non-canonical NF-κB pathway activation (Bonizzi et al. 2004). In B-cells, IKKα has been shown to be essential for normal B-cell development and immature B-cells experience increased turnover due to apoptosis (Kaisho et al. 2001). The apoptosis has been demonstrated to be a consequence of decreased transcription of the anti-apoptotic protein Bcl-2 through ablation of BAFF-induced NF-κB non-canonical activation (Claudio et al. 2002a). Overall, this indicates a role for the non-canonical pathway in B-cell proliferation, maturation and apoptosis. In addition, dual IKK inhibition has been shown induce a more potent cytotoxic effect in MM cells when compared to IKKβ inhibition alone, which indicates that non-canonical pathway inhibition may be contributing to their overall apoptotic effect (Rauert-Wunderlich et al. 2013).

Therefore, my hypothesis was that the use of a novel IKKα inhibitor may represent a promising strategy for the treatment of MM. The specific aims of this chapter were to evaluate a series of pharmacological agents designed to inhibit IKKα in terms of their cytotoxicity, regulation of Mcl-1 expression and effect on NF-κB activity in the MM cell line, RPMI8226.

4.1. The kinase inhibitory profiles of the IKKα inhibitory agents

Prof. Simon MacKay at the University of Strathclyde kindly provided nine novel IKKα inhibitory pharmacological agents and these agents will be referred to from here on as the SU series of compounds. Table 4.1 shows the predicted inhibitory concentrations that induce 50% reduced function (IC_{50}) in the kinases IKKα, IKKβ and CDK9 for each of the nine SU compounds. Table 4.1 shows that each SU compound possesses a different kinase

inhibitory profile. SU1257 has a relatively unique inhibitory profile because it has been designed to be a structural analogue of the SU series but the compound does not possess IKKα, IKKβ or CDK9 inhibitory properties. For this reason, SU1257 represents an ideal control compound throughout the evaluation of the other SU series compounds.

Table 4.1 The predicted mechanistic data for the IKKα inhibitory SU series.
The IC_{50} value for the kinases IKKα, IKKβ and CDK9 for each of the nine SU compounds. A summary for each compound is also provided.

	IKKα	IKKβ	CDK9	Summary
SU1257	-	-	-	A structural analogue of the other SU compounds but without IKKα or IKKβ properties.
SU1053	28nM	4190nM	~1000nM	>140 times preferential inhibition of IKKα over IKKβ. A weak inhibitor of CDK9.
SU1261	10nM	680nM	16nM	>65 times preferential inhibition of IKKα over IKKβ. A potent inhibitor of CDK9.
SU1349	16nM	3352nM	13nM	An IKKα inhibitor with some weak inhibition of IKKβ. A potent inhibitor of CDK9.
SU1361	8nM	964nM	20nM	A dual IKKα and CDK9 inhibitor with weak IKKβ inhibitory properties
SU1365	26nM	1500nM	~20nM	A dual IKKα and CDK9 inhibitor with weak IKKβ inhibitory properties
SU1372	7nM	587nM	18nM	>80 times preferential inhibition of IKKα over IKKβ. A potent inhibitor of CDK9.
SU1411	~10nM	~500nM	~700nM	50 times preferential inhibition of IKKα over IKKβ. A weak inhibitor of CDK9.
SU1438	10nM	511nM	~700nM	>50 times preferential inhibition of IKKα over IKKβ. A weak inhibitor of CDK9.

Table 4.1 shows that SU1349 was the most potent inhibitor of CDK9 (IC_{50} = 13nM) and a potent inhibitor of IKKα (IC_{50} = 16nM). Similarly, SU1372 was the most potent IKKα inhibitor (IC_{50} = 7nM) but was also a relatively potent inhibitor of CDK9 (IC_{50} = 18nM). The compounds SU1261, SU1361 and SU1365 possessed comparable kinase inhibitory profiles. For example, all three compounds were potent inhibitors of IKKα (10nM, 8nM and 26nM,

respectively) and CDK9 (16nM, 20nM and ~20nM, respectively), but demonstrated weak inhibitory action against IKKβ (680nM, 964nM and 1500nM, respectively). SU1411 and SU1438 were both shown to be preferential IKKα inhibitors (IC_{50} = ~10nM) with weak inhibition of IKKβ (IC_{50} = ~500nM and IC_{50} = 511nM, respectively) and CDK9 (IC_{50} = ~700nM). Moreover, Table 4.1 shows that SU1053 was a weak inhibitor of both the IKKβ (IC_{50} = 4190nM) and CDK9 (IC_{50} = ~1000nM) kinases but was a relatively potent inhibitor of IKKα (IC_{50} =28nM).

4.2. Cytotoxicity of the SU series of IKKα inhibitory agents in the MM cell line RPMI8226

The high frequency of genetic abnormalities in MM that induce constitutive NF-κB activation, mainly through abnormalities affecting the non-canonical pathway, indicates a role for the non-canonical NF-κB signalling pathway in MM cell survival and disease progression (Annunziata et al. 2007; Keats et al. 2007; Demchenko et al. 2010). Moreover, it is predicted that the apoptotic effect induced by dual IKK inhibitors is a consequence of both canonical and non-canonical pathway inhibition (Rauert-Wunderlich et al. 2013).Therefore, the cytotoxicity of the nine novel IKKα inhibitors was compared in the RPMI8226 MM cell line. The RPMI8226 cell line was chosen as the MM cell line to investigate the SU series in because this MM cell line was found to possess an intermediate level of baseline NF-κB activity as a consequence of an inactivating TRAF3 mutation (Annunziata et al. 2007; Keats et al. 2007; Demchenko et al. 2010). Similarly, the RPMI8226 cell line was found to be intermediately sensitive to cytotoxicity induced by the non-specific NF-κB inhibitor BAY 11-7082 when compared to the H929, U266B1 and JJN3 MM cell lines.

RPMI8226 cells were incubated with increasing concentrations of each SU compound ranging from 0.5μM to 20μM. At 48h, the cells were harvested and washed in PBS before being labelled with Annexin V-FITC and propidium iodide (PI). The labelled cells were then analysed using flow

cytometry to determine the percentage of apoptosis (Annexin V^+/PI^- + Annexin V^+/PI^+ + Annexin V^-/PI^+) occurring at each concentration. Figure 4.1 shows the cytotoxicity of each IKKα inhibitory agent at 48h in the RPMI8226 cell line and the results shown are collated from two independent experiments.

Figure 4.1 shows that SU1257, SU1053 and SU1372 were the least cytotoxic compounds at 48h in the RPMI8226 cells and it was not possible to interpolate an accurate LD_{50} value from the data. For this reason, the LD_{50} value were described as >20μM. In addition, Figure 4.1 shows that the remaining six IKKα inhibitory agents induced cytotoxicity in a concentration-dependent manner in RPMI8226 cells at 48h. Comparison of the LD_{50} values for each SU compound indicates that SU1349 was the most cytotoxic agent (LD_{50} = 1.15μM) whereas SU1261 was the least cytotoxic of these agents (LD_{50} = 3.92μM). SU1361 and SU1365 both induce a relatively similar level of apoptosis in RPMI8226 cells at 48h, as evidenced by their comparable LD_{50} values (LD_{50} = 2.25μM and LD_{50} = 1.96μM, respectively). Although Table 4.1 indicates that SU1438 and SU1411 both possess similar kinase profiles in relation to IKKα, IKKβ and CDK9, Figure 4.1 shows that SU1411 was comparatively more cytotoxic than SU1438 in the RPMI8226 MM cell line at 48h (LD_{50} = 3.60μM and LD_{50} = 2.26μM, respectively).

Based on the kinase inhibitory data in Table 4.1 and the initial cytotoxicity screening profiles in Figure 4.1, six of the nine SU compounds were chosen for further characterisation concerning cytotoxicity, Mcl-1 expression and NF-κB activity. The chosen SU compounds were SU1257, SU1053, SU1349, SU1372, SU1411 and SU1438. SU1261, SU1361 and SU1365 were omitted from further investigation due to Table 4.1 suggesting that they each had a kinase inhibitory profile that was comparable to SU1349 and SU1372. For example, these compounds were potent inhibitors of CDK9 and IKKα, but weak inhibitors of IKKβ. Moreover, SU1349 was the most potent inhibitor of CDK9 whereas SU1372 was conversely the most potent inhibitor of IKKα.

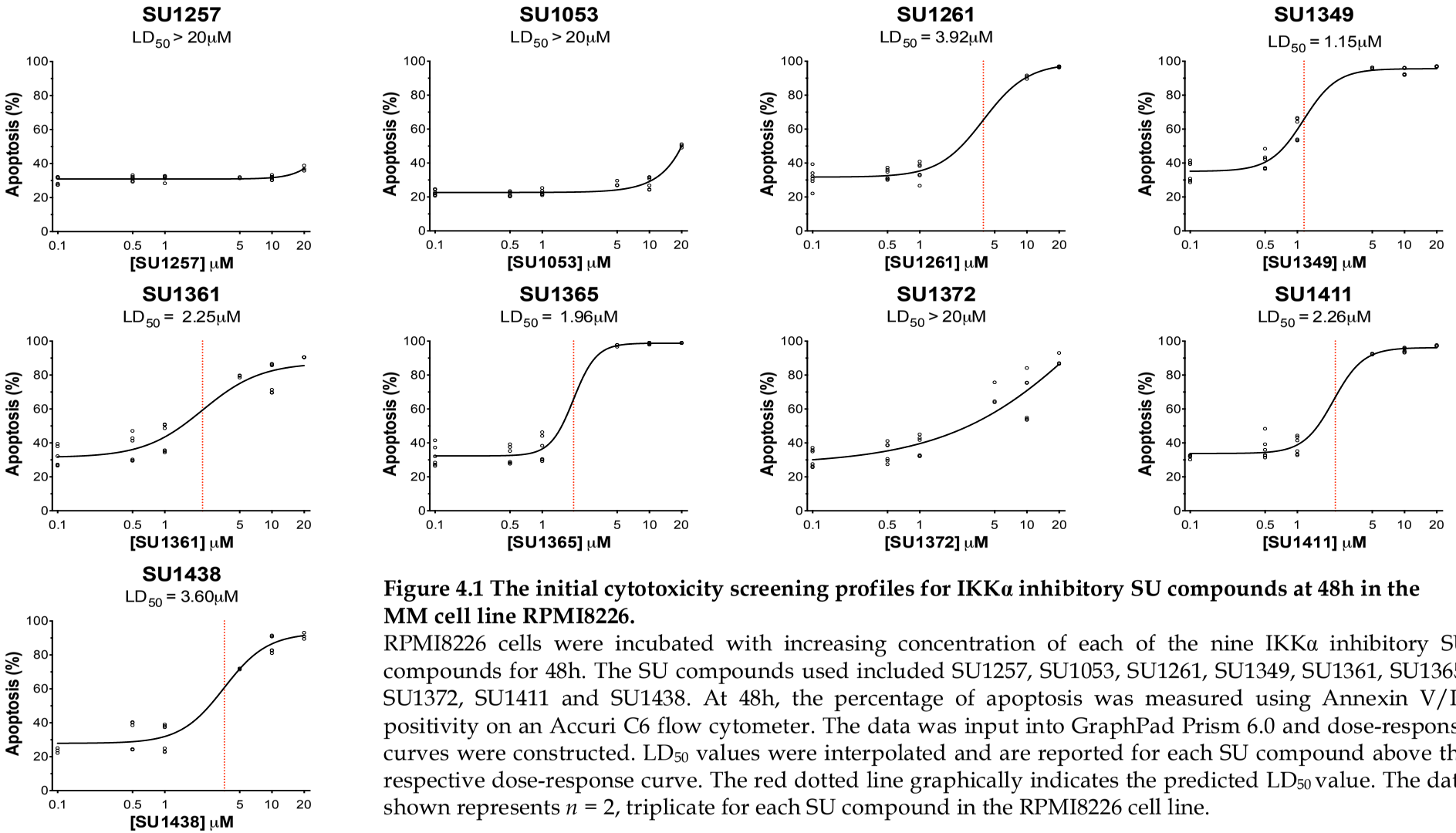

Figure 4.1 The initial cytotoxicity screening profiles for IKKα inhibitory SU compounds at 48h in the MM cell line RPMI8226.

RPMI8226 cells were incubated with increasing concentration of each of the nine IKKα inhibitory SU compounds for 48h. The SU compounds used included SU1257, SU1053, SU1261, SU1349, SU1361, SU1365, SU1372, SU1411 and SU1438. At 48h, the percentage of apoptosis was measured using Annexin V/PI positivity on an Accuri C6 flow cytometer. The data was input into GraphPad Prism 6.0 and dose-response curves were constructed. LD_{50} values were interpolated and are reported for each SU compound above the respective dose-response curve. The red dotted line graphically indicates the predicted LD_{50} value. The data shown represents n = 2, triplicate for each SU compound in the RPMI8226 cell line.

Therefore, the cytotoxicity of SU1257, SU1053, SU1349, SU1372, SU1411 and SU1438 in the RPMI8226 cell line was further investigated to allow the collated results to include a total of four independent experiments. This would allow a more robust calculation of the LD_{50} values as well as the 95% CI. Figure 4.2 shows the cytotoxicity profiles of each of the six chosen IKKα inhibitory agents at 48h in the RPMI8226 cell line and the results now represent four independent experiments.

Figure 4.2 indicates that it was still not possible to calculate accurate LD_{50} values for the least cytotoxic SU compounds SU1257, SU1053 and SU1372 and their predicted LD_{50} values were designed to be >20μM. Comparison of the remaining three SU compounds' LD_{50} values showed that SU1349 was the most cytotoxic compound in the RPMI8226 cells at 48h (LD_{50} = 1.92μM, 95% CI [1.32μM – 2.89μM]). Furthermore, SU1411 was comparatively more cytotoxic than SU1438, despite the similarity in their kinase inhibitory profiles (LD_{50} = 3.15μM, 95% CI [2.87μM – 3.46μM] and LD_{50} = 5.56μM, 95% CI [4.85μM – 6.38μM], respectively). The cytotoxicity of the three most cytotoxic SU series compounds in RPMI8226 cells at 48h is summarised in Figure 4.3. Figure 4.3 shows the mean LD_{50} values alongside 95% CI generated through Annexin-V/PI positivity (n = 4). In addition, an unpaired one-tailed t-test was performed on the data to investigate the statistical difference between the LD_{50} values calculated for each SU series compound in the RPMI8226 cell line.

Figure 4.3 shows that the SU1349 and SU1411 compounds did not induce significantly different cytotoxic effects in the RPMI8226 cell line (p = 0.821). On the other hand, the LD_{50} value interpolated for SU1438 was significantly higher than the LD_{50} value interpolated for SU1349 (p = 0.026) in the RPMI8226 cell line. Conversely, the LD_{50} value interpolated for SU1438 was not significantly different from the LD_{50} value interpolated for SU1411 in RPMI8226 cells (p = 0.066). In summary, the cytotoxicity of SU1349 was significantly greater than SU1438 but the cytotoxicity of SU1411 was relatively similar to both SU1349 and SU1418 in RPMI8226 cells.

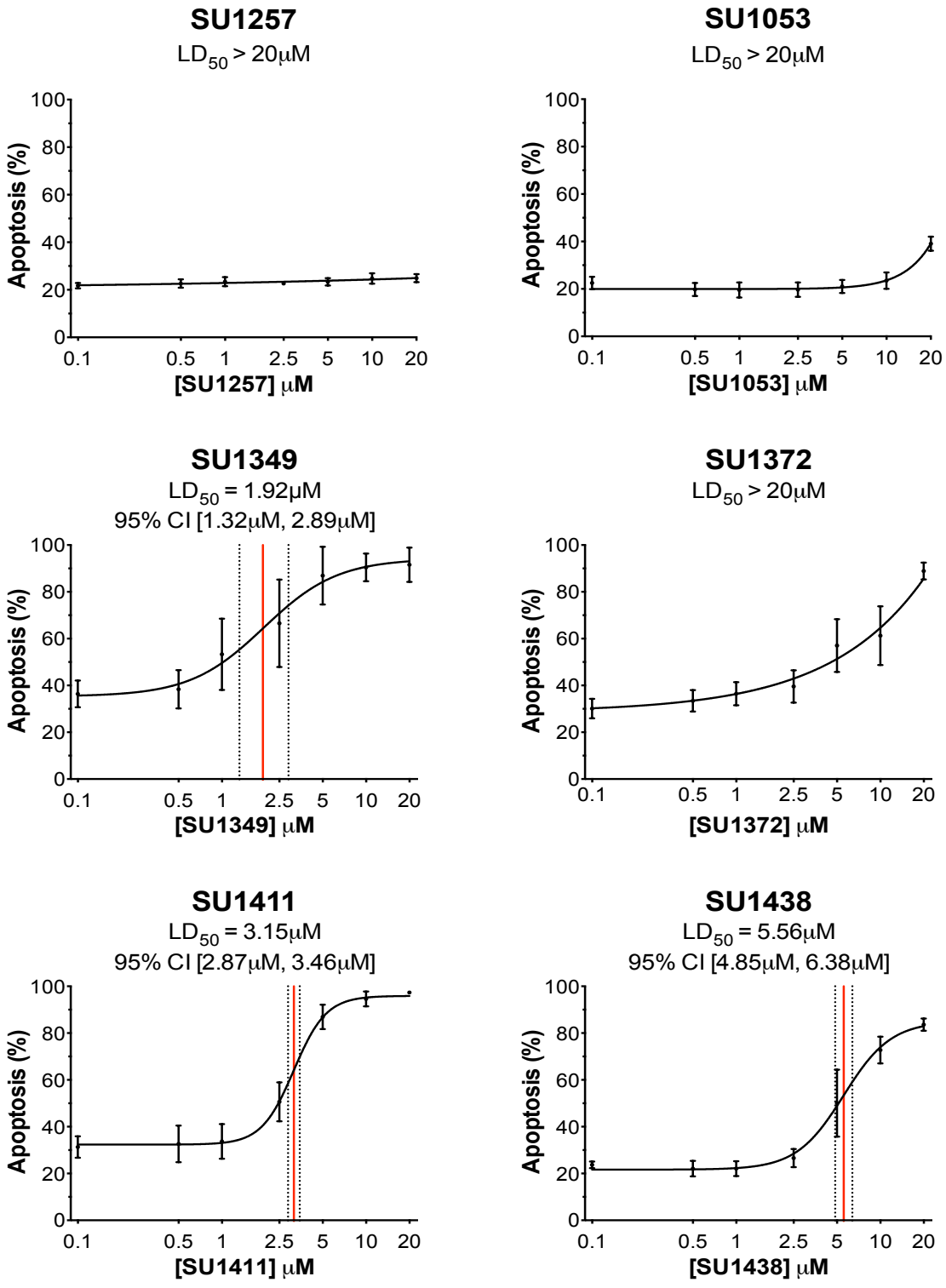

Figure 4.2 The cytotoxicity profiles of SU1257, SU1053, SU1349, SU1372, SU1411 and SU1438 at 48h in RPMI8226 cells.

To fully investigate the cytotoxicity profiles of each SU compound in RPMI8226 cells RPMI8226 cells were incubated with a more specific range of concentrations of SU compounds. At 48h, the percentage of apoptosis was measured using Annexin V/PI positivity on an Accuri C6 flow cytometer. The percentage of apoptotic cells at each concentration of SU compound was calculated and dose-response curves were constructed using Graphpad Prim 6.0. LD_{50} values were interpolated and are reported for each SU compound alongside 95% CI. Error bars represent mean ± SD, where n = 4.

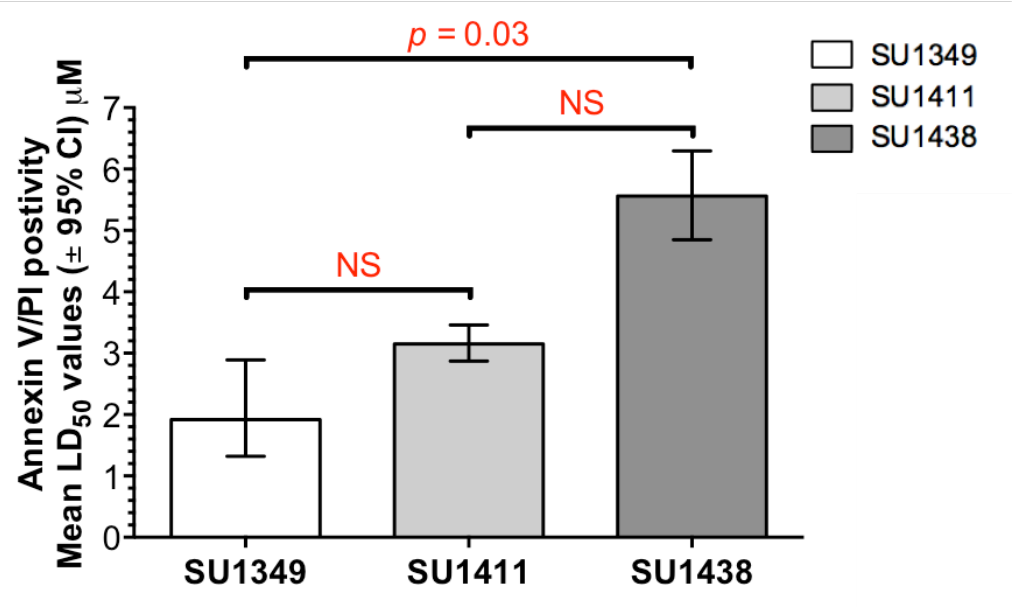

Figure 4.3 A summary of the relative cytotoxicity of SU1349, SU1411 and SU1438 in RPMI8226 cells at 48h.
The mean LD_{50} values generated through Annexin V/PI positivity are shown for increasing concentrations of SU1349, SU1411 and SU1438 in RPMI8226 cells at 48h. The results shown were interpolated using the dose-response curves in Figure 4.2 using Graphpad Prism 6.0. The values reported represent mean LD_{50} values ± 95% CI (µM) where n = 4. A one-way ANOVA followed by a Tukey's multiple comparison test was performed using Graphpad Prism 6.0 software to investigate the significant difference between the LD_{50} values calculated for the indicated SU series compounds in the RPMI8226 cell line.

4.3. Regulation of Mcl-1 expression in the MM cell line RPMI8226 by the SU series of IKKα inhibitory agents

In myeloma cells, Mcl-1 expression plays a critical role in maintaining cell viability (Derenne et al. 2002; Zhang et al. 2002). Furthermore, high expression of Mcl-1 in cancer cell lines has been linked to constitutively high NF-κB activity (Liu et al. 2014). In addition, previous studies have demonstrated that inhibition of NF-κB activity is accompanied by the down regulation of Mcl-1 expression in MM cell lines and may precede the activation of apoptotic pathways (Meinel et al. 2010). Therefore, Mcl-1 expression was quantified in the RPMI8226 cell line following 4h incubation (prior to any evidence of apoptosis induction) with increasing concentrations of each SU compound to investigate whether IKKα inhibition modulated the expression of Mcl-1.

RPMI8226 cells were treated separately with each of the IKKα inhibitory agents SU1257, SU1053, SU1349, SU1372, SU1411 and SU1438 at concentrations of 0.5μM, 1μM, 2.5μM and 5μM. At 4h, cells were harvested and then fixed and permeabilised before staining with an anti-Mcl-1-IgG1 antibody (Santa Cruz Biotechnology) followed by secondary labelling with a goat anti-mouse IgG1-FITC antibody (Santa Cruz Biotechnology). The stained RPMI8226 cells were then analysed using flow cytometry to quantify the intracellular Mcl-1 expression in cells treated with each concentration of SU compound.

A gating strategy was applied to the collected flow cytometry data to ensure that only viable, single cells were analysed. The serially gated cell populations were then assessed for Mcl-1 expression (MFI values) at each concentration of each SU compound. Figure 4.4 shows the representative overlaid histograms for Mcl-1 expression in untreated RPMI8226 cells and RPMI8226 cells treated with a 5μM of each SU compound for 4h.

Figure 4.4 shows that following 4h incubation with 5μM SU1257, Mcl-1 expression was not significantly altered in RPMI8226 cells relative to untreated cells. In contrast, the other SU compounds induced a decrease in Mcl-1 expression at 4h in RPMI8226 cells. Figure 4.4 shows that when used at a concentration of 5μM for 4h, SU1372 induced the greatest overall decrease in Mcl-1 expression in RPMI8226 cells.

To further investigate the regulation of Mcl-1 expression by the selected SU compounds, the Mcl-1-FITC MFI at each concentration of each IKKα inhibitor was determined and then expressed as a percentage of the untreated controls. Figure 4.5 shows the collated data from three separate experiments for RPMI8226 cells, outlining the dose-dependent regulation of Mcl-1 expression by the agents SU1257, SU1053, SU1349, SU1372, SU1411 and SU1438 at 4h.

Figure 4.5 shows that all six IKKα inhibitory agents analysed did not induce a significant decrease in Mcl-1 expression at 5μM relative to untreated cells following 4h treatment in RPMI8226 cells.

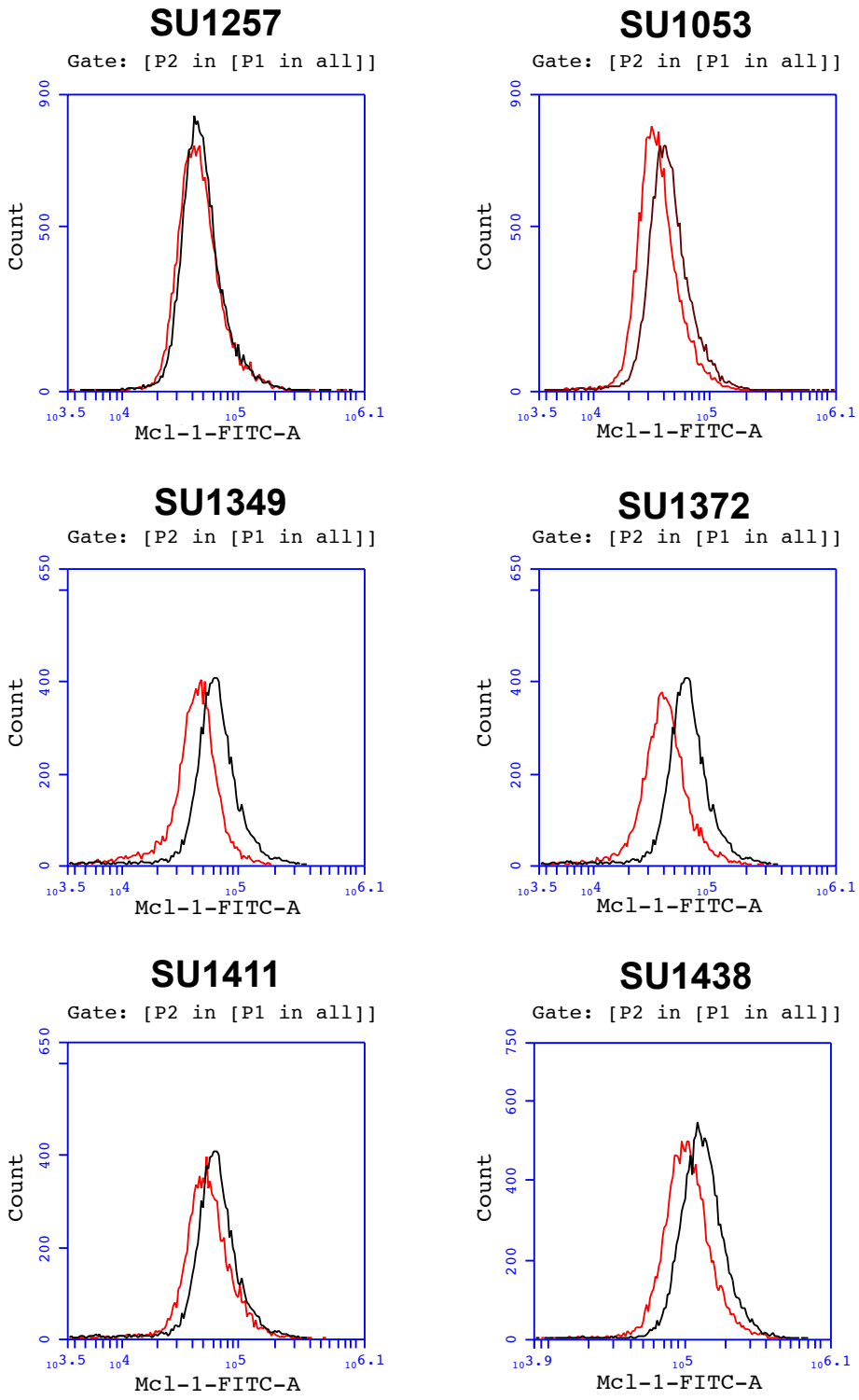

Figure 4.4 Representative overlay histograms of Mcl-1 expression in RPMI8226 cells at 4h after exposure to SU1257, SU1053, SU1349, SU1372, SU1411 and SU1438.
Mcl-1 expression was investigated in RPMI8226 cells after treatment with increasing concentrations of each of SU compound. At 4h, intracellular Mcl-1 expression was investigated by staining cells with an anti-Mcl-1-FITC conjugated antibody and the average MFI was measured by flow cytometry. To gain an accurate MFI for each cell surface marker, gating was applied to gate viable myeloma cells (P1) and exclude any doublets (P2). The resultant gating was used to create overlay histograms from which the MFI of Mcl-1 expression at each concentration could be determined. A representative overlay histogram is shown for each SU compound in RPMI8226 cells after 4h (untreated = ■, 5μM SU compound = ■).

Figure 4.5 indicates that 5μM SU1053 and SU1372 induced the largest average decrease in Mcl-1 expression compared to untreated RPMI8226 cells (76.4% ± 16.3% and 75.6% ± 7.4%, respectively) relative to the other SU agents, although the decrease in Mcl-1 expression was not significant for either agent (p = 0.24 and p = 0.12, respectively). For both SU1053 and SU1372, Figure 4.5 shows that this was accompanied by a dose-dependent decrease in Mcl-1 expression in RPMI8226 cells at 4h from concentrations of 1μM onwards, with respect to untreated RPMI8226 cells.

In addition, increasing concentrations of SU1349 induced a dose-dependent decrease in Mcl-1 expression in RPMI8226 cells at 4h from concentrations of 1μM onwards, that plateaued following exposure to 2.5μM and 5μM SU1349 (78.5% ± 7.8% and 80.4% ± 10.1%, respectively) when compared to untreated cells. However, the decrease in Mcl-1 expression induced by 5 μM SU1349 compared to untreated RPMI8226 cells was not significant (p = 0.18).

Figure 4.5 also shows that 5μM SU1257, SU1411 and SU1438 did not significantly (p = 0.40, p = 0.40 and p = 0.33, respectively) alter Mcl-1 expression at 4h compared to untreated RPMI8226 cells (93.3% ± 10.8%, 94.1% ± 11.8% and 88.2% ± 6.6%, respectively) and the three agents did not induce a dose-dependent reduction in Mcl-1 expression.

Overall, Figure 4.5 highlighted the potential inconsistency between the dose-dependent decrease and maximum decrease in normalised Mcl-1 expression at 5μM, and the calculated p values, especially for the SU compounds SU1349, SU1372 and SU1053.

In conclusion, Mcl-1 expression was decreased in a dose-dependent manner by SU1349 and SU1372 at 4h in RPMI8226 cells. In addition, SU1053, SU1411 and SU1438 induced a relatively weaker dose-dependent decrease in Mcl-1 expression in RPMI8226 cells whereas SU1257 did not affect Mcl-1 expression.

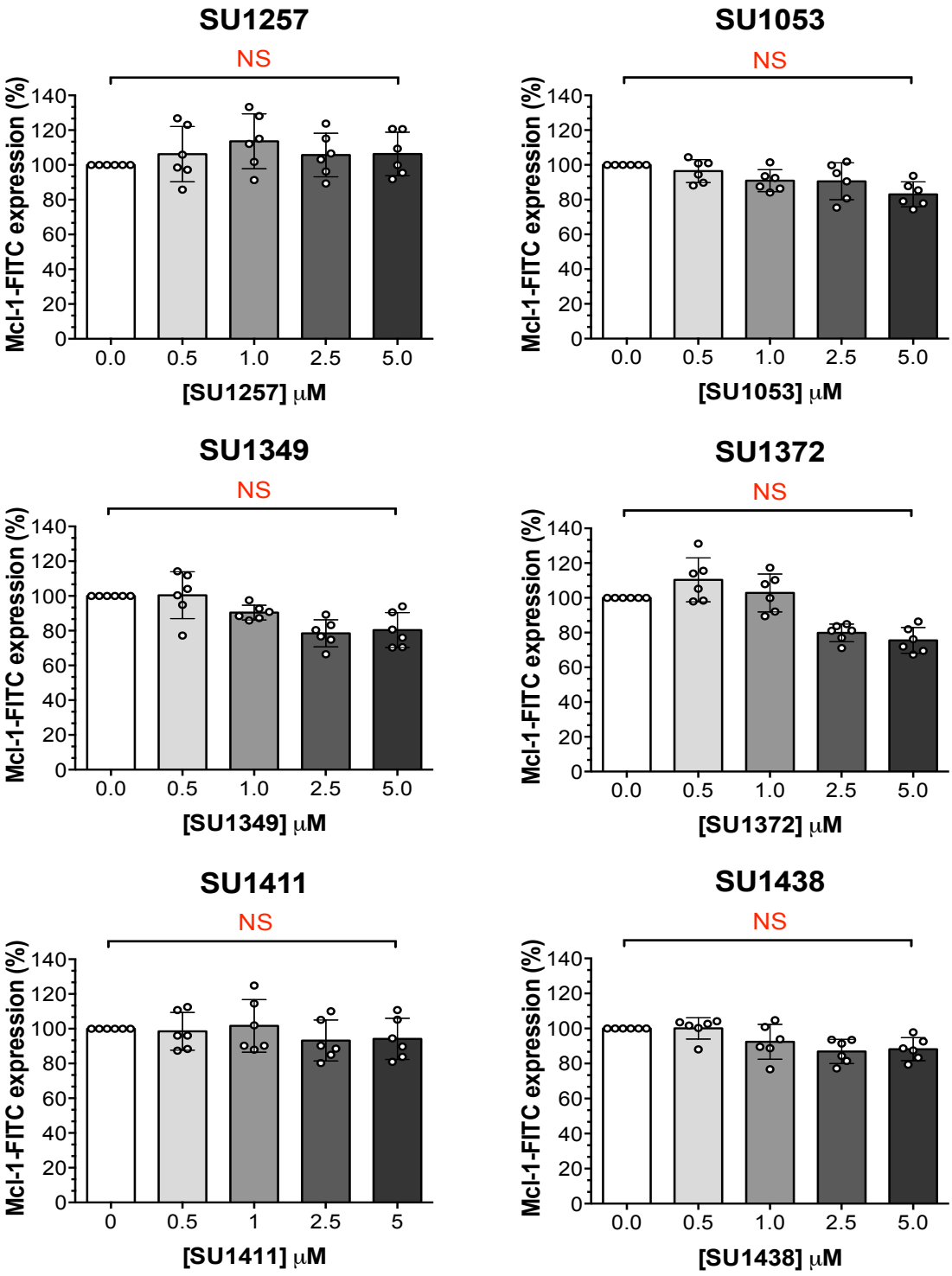

Figure 4.5 The dose-dependent regulation of Mcl-1 expression in RPMI8226 cells at 4h following treatment with SU1257, SU1053, SU1349, SU1372, SU1411 and SU1438. Mcl-1 expression was investigated in RPMI8226 cells after treatment with increasing concentrations of each of SU compound ranging from 0μM to 5μM. At 4h, intracellular Mcl-1 expression was investigated by staining RPMI8226 cells with an anti-Mcl-1-FITC conjugated antibody following fixation and permeabilisation. The average Mcl-1-FITC MFI at each concentration of SU compound was measured using an Accuri flow cytometer and normalised to the untreated control. A one-tailed unpaired *t*-test was performed using Graphpad Prism 6.0 software to investigate the statistical significance values between 0μM to 5μM for each SU compound in RPMI8226 cells at 4h (n = 3, duplicates averaged). The results are reported for each graph (NS = not significant, p > 0.05). Error bars represent mean ± SD where n = 3, experimental duplicates plotted.

4.4. Inhibition of NF-κB activity in the MM cell line RPMI8226 by the SU series of IKKα inhibitory agents

The association between cytotoxicity and the inhibition of constitutive NF-κB activity induced by the six SU compounds was investigated in more detail using an ELISA-based assay to detect the active NF-κB subunits p65, p50, p52 and RelB in nuclear extracts. These four subunits were selected to provide information on whether IKKα inhibition was effecting the canonical and/or the non-canonical NF-κB signalling pathway(s) in RPMI8226 cells.

RPMI8226 cells were incubated separately with each SU compound: SU1257 SU1053, SU1349, SU1372, SU1411 and SU1438, at concentrations of 0μM, 1μM, 2.5μM and 5μM. At 4h, cells were harvested and nuclear extracts generated. 1μg of RPMI8226 nuclear extract protein was assayed using the NF-κB family ELISA kit (Active Motif), as per the manufacturer's instructions. Standard curves were generated alongside the assay using known quantities of recombinant p65 protein ($r^2 > 0.99$) and recombinant p50 protein ($r^2 > 0.96$) to allow NF-κB subunit quantification in nanograms per microgram of nuclear extract protein.

Figures 4.7, 4.8, 4.9, 4.10, 4.11 and 4.12 show the quantities of active p65, p50, p52 and RelB NF-κB subunit proteins in the nucleus of RPMI8226 cells following 4h treatment with increasing concentrations of SU1257, SU1053, SU1349, SU1372, SU1411 and SU1438, respectively. For each Figure, the data shown consists of the collated data from three separate experiments where the individual nuclear extract samples were assayed in duplicate.

4.4.1. Inhibition of NF-κB activity in RPMI8226 cells by SU1257

Figure 4.6 shows that 5μM SU1257 significantly decreased the levels of p65 (p = 0.034) in the nuclear extracts of RPMI8226 cells relative to the untreated control samples. Figure 4.6 also shows that this was accompanied by a dose-dependent decrease in active p65 protein.

Conversely, Figure 4.6 demonstrates that the p50, p52 and RelB NF-κB subunits showed no significant decrease in nuclear protein levels following 4h with 5μM SU1257 relative to the untreated group (p = 0.053, p = 0.128 and p = 0.144, respectively). However, all three NF-κB subunits appeared to show a dose-dependent decrease in active protein level.

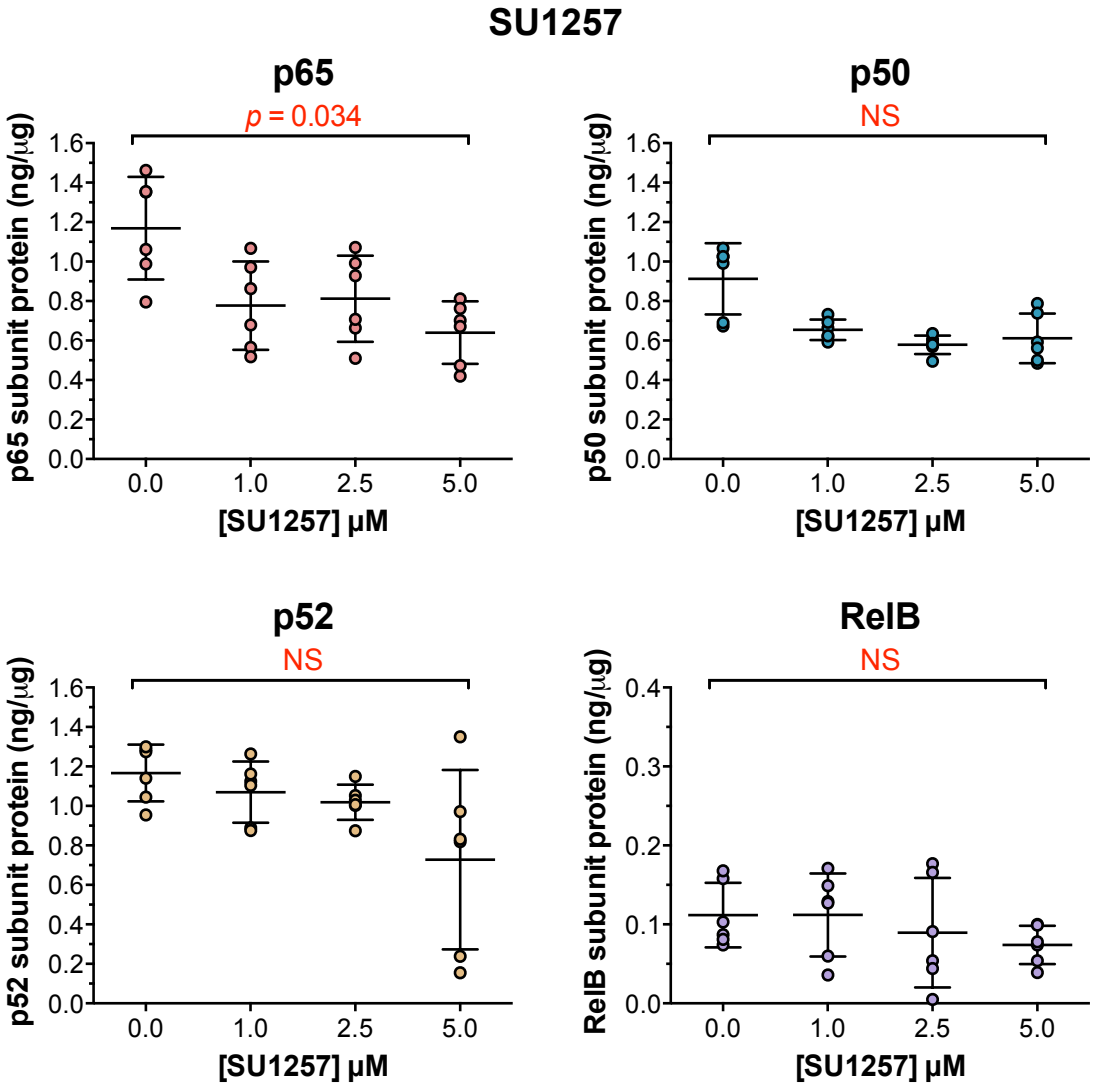

Figure 4.6 Effect of SU1257 on NF-κB activity in RPMI8226 MM cells at 4h. RPMI8226 cells were exposed to increasing concentrations of the SU compound SU1257 for 4h. RPMI8226 cells were then harvested and used to generate nuclear extract samples. The MM cell line was then assayed at 1μg/well of nuclear extract protein using ELISAs detecting the active NF-κB subunits p50, p65, p52 and RelB. A one-tailed unpaired *t*-test was performed using Graphpad Prism 6.0 software to investigate the statistical significance values between 0μM to 5μM for SU1257 in RPMI8226 cells for each NF-κB subunit (n = 3, duplicates averaged). The results are reported above the graph (NS = not significant, p > 0.05). Values reported are mean ± SD produced from duplicate measurements where n = 3, experimental duplicates shown.

4.4.2. Inhibition of NF-κB activity in RPMI8226 cells by SU1053

Figure 4.7 demonstrates that 5μM SU1053 significantly decreased the levels of p50, p52 and RelB in RPMI8226 cells relative to the untreated samples (p = 0.035, p = 0.007 and p = 0.016, respectively). As can be seen in Figure 4.7, SU1053 induced a dose-dependent inhibition of p50, p52 and RelB nuclear protein levels in RPMI8226 cells, although the dose-dependent decrease was relatively stronger for p52 activity following SU1053 treatment. In contrast, Figure 4.7 shows that the level of nuclear p65 was not significantly different in RPMI8226 cells treated with SU1053 when compared to untreated controls (p = 0.305).

4.4.3. Inhibition of NF-κB activity in RPMI8226 cells by SU1349

Figure 4.8 shows that 5μM SU1349 significantly decreased the levels of active p65 (p = 0.024) and p52 (p = 0.021) in RPMI8226 cells relative to the untreated samples in a dose-dependent manner. Figure 4.8 also shows that the level of active p50 protein was significantly decreased following treatment with SU1349 (p = 0.038), although not in a dose-dependent manner, but instead the p50 level plateaued at concentrations of 1μM, 2.5μM and 5μM (0.54 ± 0.04ng/μg, 0.68 ± 0.01ng/μg and 0.61 ± 0.09ng/μg) compared to untreated RPMI8226 cells (1.04 ± 0.22ng/μg). Conversely, Figure 4.8 indicates that the average level of active RelB protein was increased by 5μM SU1349 in RPMI8226 cells relative to the untreated samples, although this was not significant (p = 0.111). However, this increase could be a result of one set of duplicate measurements skewing the overall average of RelB protein measured at 5μM SU1349.

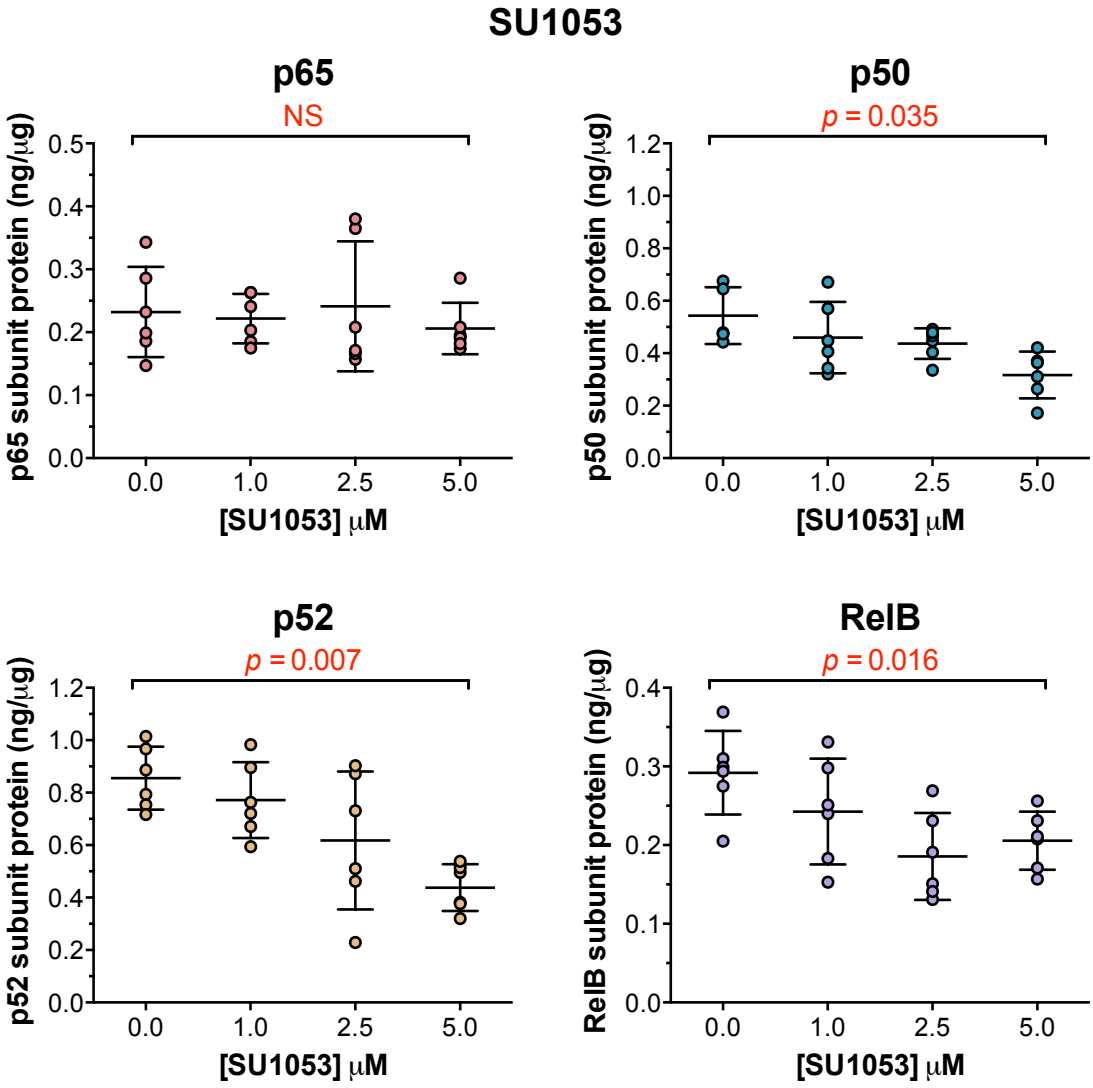

Figure 4.7 Effect of SU1053 on NF-κB activity in RPMI8226 MM cells at 4h.
RPMI8226 cells were exposed to increasing concentrations of the SU compound SU1053 for 4h. RPMI8226 cells were then harvested and used to generate nuclear extract samples. The MM cell line was then assayed at 1µg/well of nuclear extract protein using ELISAs detecting the active NF-κB subunits p50, p65, p52 and RelB. A one-tailed unpaired *t*-test was performed using Graphpad Prism 6.0 software to investigate the statistical significance values between 0µM to 5µM for SU1053 in RPMI8226 cells for each NF-κB subunit (n = 3, duplicates averaged). The results are reported above the graph (NS = not significant, $p > 0.05$). Values reported are mean ± SD produced from duplicate measurements where n = 3, experimental duplicates shown.

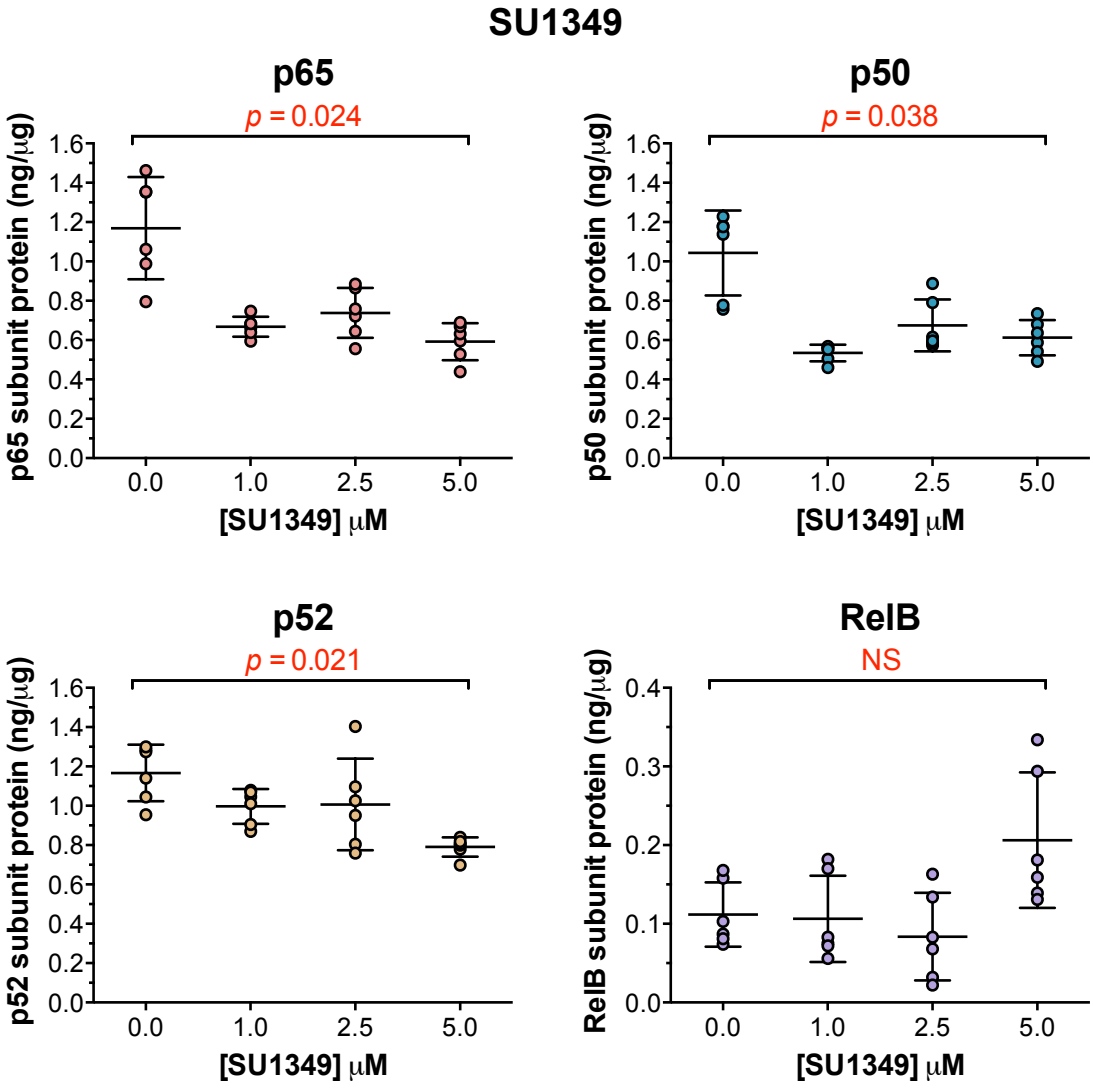

Figure 4.8 Effect of SU1349 on NF-κB activity in RPMI8226 MM cells at 4h.
RPMI8226 cells were exposed to increasing concentrations of the SU compound SU1349 for 4h. RPMI8226 cells were then harvested and used to generate nuclear extract samples. The MM cell line was then assayed at 1µg/well of nuclear extract protein using ELISAs detecting the active NF-κB subunits p50, p65, p52 and RelB. A one-tailed unpaired *t*-test was performed using Graphpad Prism 6.0 software to investigate the statistical significance values between 0µM to 5µM for SU1349 in RPMI8226 cells for each NF-κB subunit (n = 3, duplicates averaged). The results are reported above the graph (NS = not significant, $p > 0.05$). Values reported are mean ± SD produced from duplicate measurements where n = 3, experimental duplicates shown.

4.4.4. Inhibition of NF-κB activity in RPMI8226 cells by SU1372

Figure 4.9 demonstrates that 5μM SU1372 significantly decreased the levels of p65, p50 and p52 in RPMI8226 cells relative to the untreated samples (p = 0.018, p = 0.023 and p = 0.049, respectively). For the active levels of p65 and p50 proteins in RPMI8226 cells, Figure 4.9 shows that there was a comparatively strong dose-dependent decrease. On the other hand, Figure 4.9 demonstrates that 5μM SU1372 increased the amount of nuclear RelB protein in RPMI8226 cells relative to the untreated samples, although this was not significant (p = 0.059). The pattern shown suggests that although 1μM SU1372 initially decreased RelB activity relative to the untreated sample (0.07 ± 0.04ng/μg compared to 0.11 ± 0.04ng/μg, respectively), a dose-dependent increase in nuclear RelB protein was observed with concentrations of 2.5μM and 5μM SU1372 (0.15 ± 0.07ng/μg and 0.19 ± 0.05ng/μg, respectively). However, Figure 4.9 again shows that this may be due to one set of duplicate measurements at each concentration skewing the overall average of RelB protein measured at 5μM SU1372.

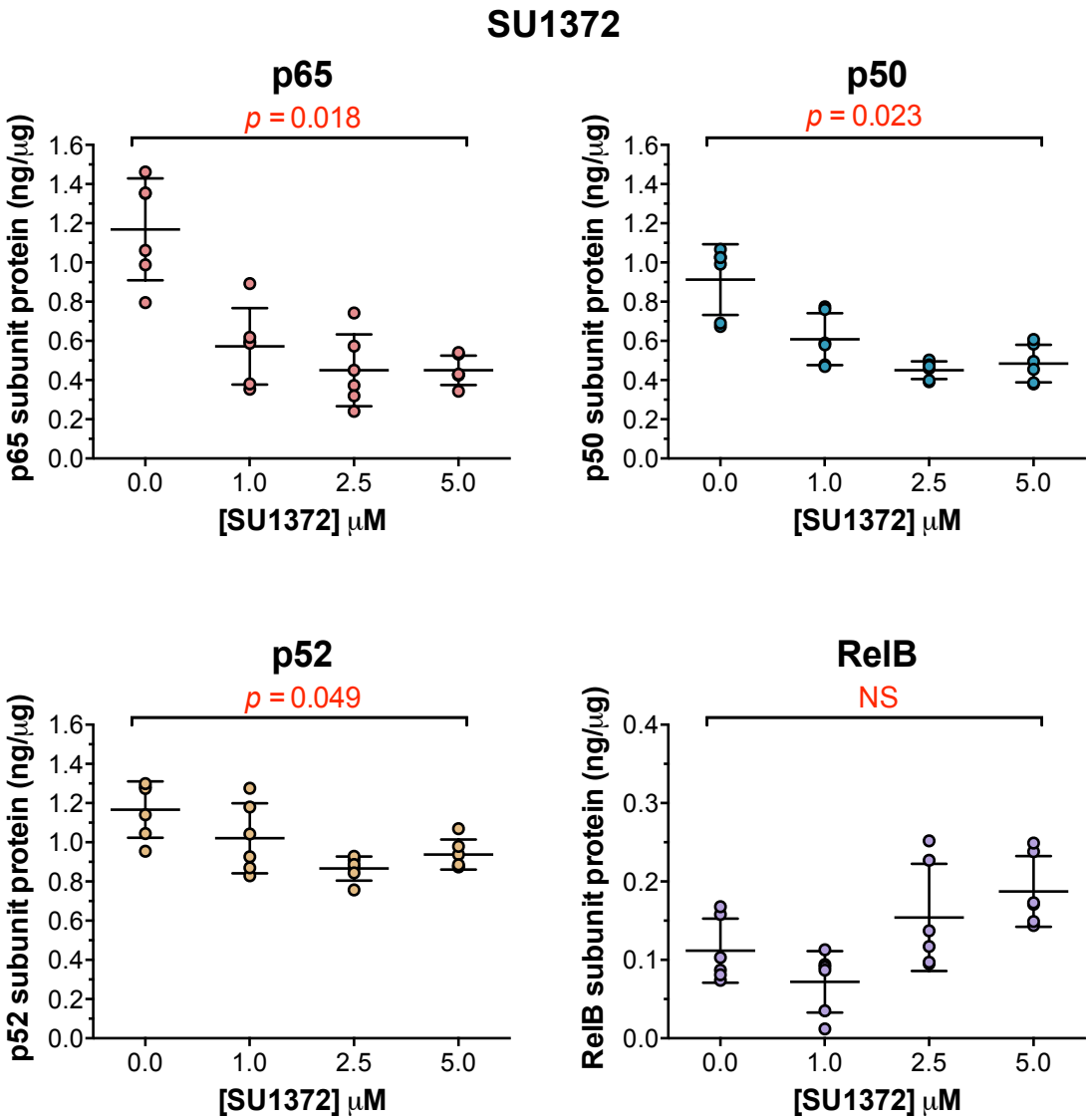

Figure 4.9 Effect of SU1372 on NF-κB activity in RPMI8226 MM cells at 4h.
RPMI8226 cells were exposed to increasing concentrations of the SU compound SU1372 for 4h. RPMI8226 cells were then harvested and used to generate nuclear extract samples. The MM cell line was then assayed at 1µg/well of nuclear extract protein using ELISAs detecting the active NF-κB subunits p50, p65, p52 and RelB. A one-tailed unpaired *t*-test was performed using Graphpad Prism 6.0 software to investigate the statistical significance values between 0µM to 5µM for SU1372 in RPMI8226 cells for each NF-κB subunit (n = 3, duplicates averaged). The results are reported above the graph (NS = not significant, $p > 0.05$). Values reported are mean ± SD produced from duplicate measurements where n = 3, experimental duplicates shown.

4.4.5. Inhibition of NF-κB activity in RPMI8226 cells by SU1411

Figure 4.10 shows that 5μM SU1411 significantly decreased the levels of p65, p50 and p52 activity (p = 0.014, p = 0.014 and p = 0.015, respectively) in RPMI8226 cells relative to the untreated samples. For all three NF-κB subunits, Figure 4.10 shows that SU1411 induced a relatively strong dose-dependent decrease in RPMI8226 cells.

In Figure 4.10, the level of nuclear RelB protein was also decreased in a dose-dependent manner in RPMI8226 cells following 4h treatment with SU1411, although to a weaker extent than that observed for p65, p50 and p52 activity. However, the decrease that SU1411 induced in RelB activity at 5μM was significantly different to the untreated level of nuclear RelB protein (p = 0.039).

4.4.6. Inhibition of NF-κB activity in RPMI8226 cells by SU1438

Figure 4.11 demonstrates that 5μM SU1438 significantly decreased the levels of p65 and RelB activity in RPMI8226 cells when compared to untreated nuclear protein levels (p = 0.027 and p = 0.002, respectively). Moreover, both significant changes in p65 and RelB activity that were induced by 5μM SU1438 were accompanied by dose-dependent decreases.

In contrast, the levels of active p50 and p52 subunit were not significantly altered by treatment for 4h with 5μM SU1438 when compared to untreated RPMI8226 cells (p =0.126 and p = 0.472, respectively). Figure 4.11 shows that nuclear p50 protein was not dose-dependently decreased by SU1438, but instead the decrease plateaued following treatment with 1μM, 2.5μM and 5μM (0.32 ± 0.12ng/μg, 0.34 ± 0.11ng/μg and 0.35 ± 0.17ng/μg, respectively) relative to untreated controls (0.54 ± 0.11ng/μg). Figure 4.11 also shows that, although the level of active p52 subunit decreased following treatment with 1μM SU1438 when compared to the untreated control, the level of p52 activity then increased with 2.5μM and 5μM SU1438 (0.79 ± 0.16ng/μg, 0.85 ± 0.15ng/μg, respectively).

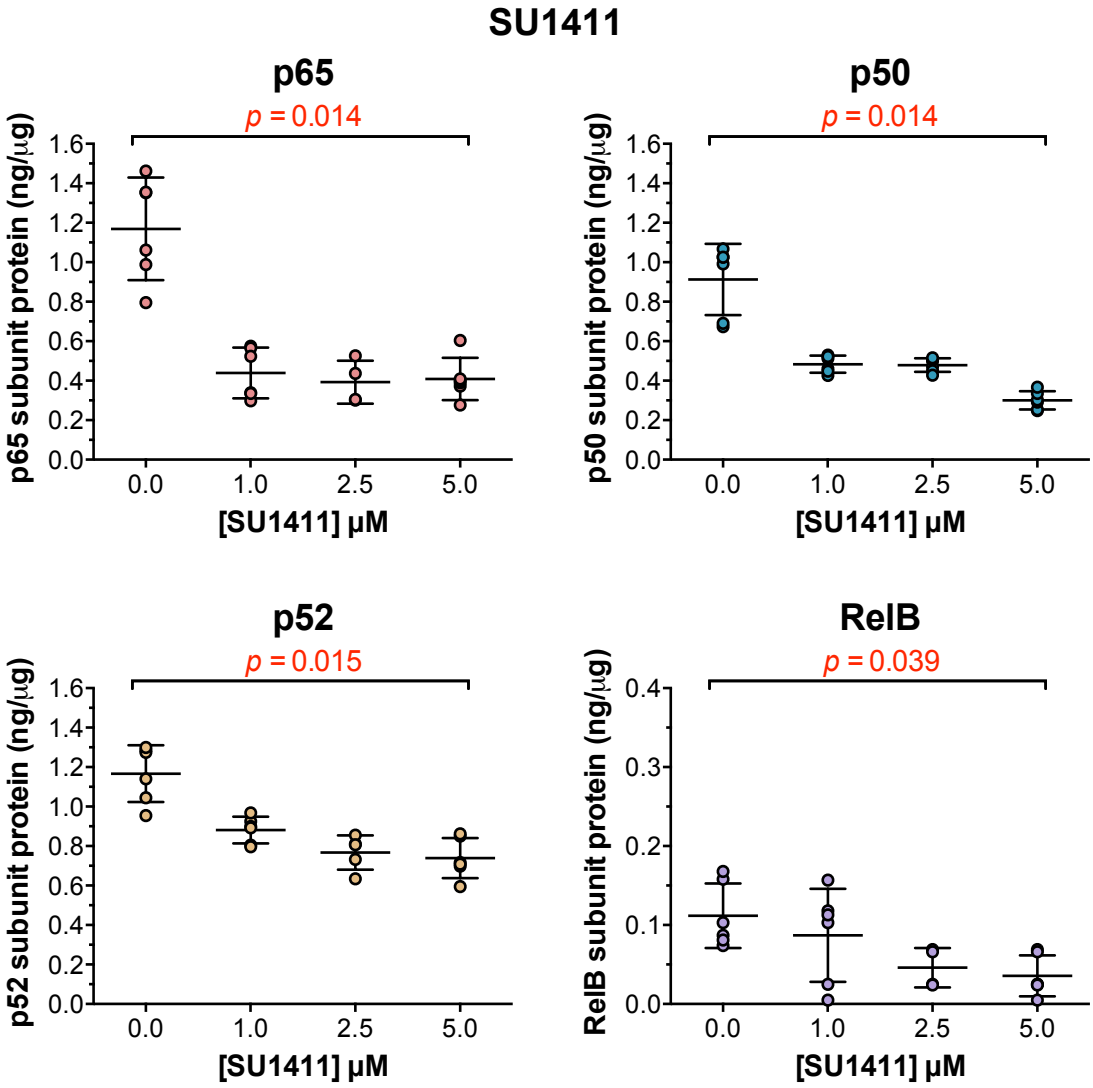

Figure 4.10 Effect of SU1411 on NF-κB activity in RPMI8226 MM cells at 4h. RPMI8226 cells were exposed to increasing concentrations of the SU compound SU1411 for 4h. RPMI8226 cells were then harvested and used to generate nuclear extract samples. The MM cell line was then assayed at 1µg/well of nuclear extract protein using ELISAs detecting the active NF-κB subunits p50, p65, p52 and RelB. A one-tailed unpaired *t*-test was performed using Graphpad Prism 6.0 software to investigate the statistical significance values between 0µM to 5µM for SU1411 in RPMI8226 cells for each NF-κB subunit (n = 3, duplicates averaged). The results are reported above the graph (NS = not significant, $p > 0.05$). Values reported are mean ± SD produced from duplicate measurements where n = 3, experimental duplicates shown.

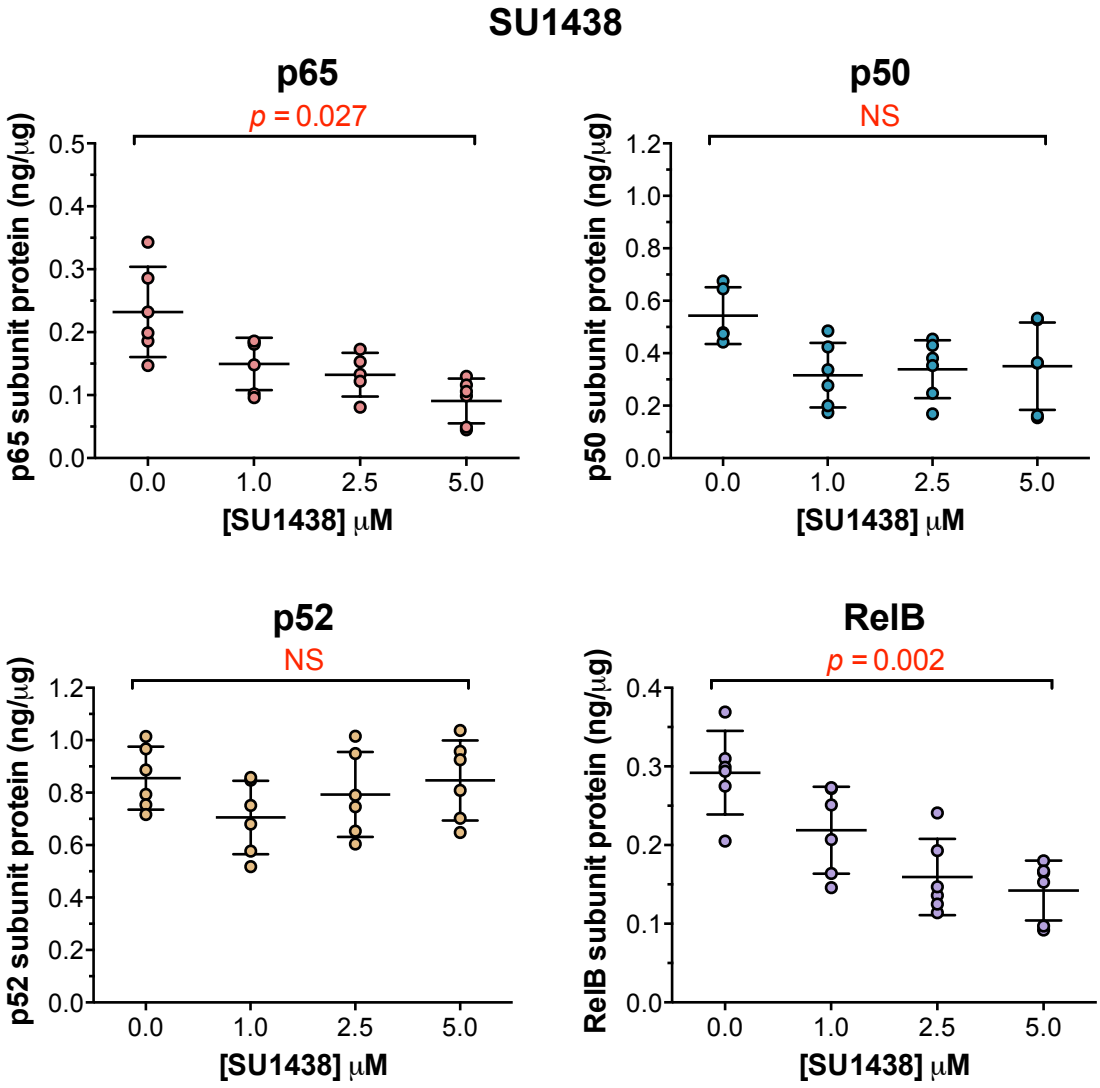

Figure 4.11 Effect of SU1438 on NF-κB activity in RPMI8226 MM cells at 4h.
RPMI8226 cells were exposed to increasing concentrations of the SU compound SU1438 for 4h. RPMI8226 cells were then harvested and used to generate nuclear extract samples. The MM cell line was then assayed at 1µg/well of nuclear extract protein using ELISAs detecting the active NF-κB subunits p50, p65, p52 and RelB. A one-tailed unpaired *t*-test was performed using Graphpad Prism 6.0 software to investigate the statistical significance values between 0µM to 5µM for SU1438 in RPMI8226 cells for each NF-κB subunit (n = 3, duplicates averaged). The results are reported above the graph (NS = not significant, $p > 0.05$). Values reported are mean ± SD produced from duplicate measurements where n = 3, experimental duplicates shown.

4.4.7. Summary of inhibition of NF-κB activity in RPMI8226 cells by the SU series of IKKα inhibitory agents as measured by ELISA

Table 4.2 summarises the data presented in Figures 4.7-4.12, which showed the inhibition of NF-κB subunit activity induced by the IKKα inhibitory agents SU1257, SU1053, SU1349, SU1372, SU1411 and SU1438 at 4h in RPMI8226 cells. As a result, Table 4.2 outlines the statistical significance between 5μM of each IKKα inhibitory agent and untreated sample for the active NF-κB subunits p65, p50, p52 and RelB and, if relevant, the general direction of the alteration in subunit activity.

Table 4.2 shows that when used at a concentration of 5μM in RPMI8226 cells for 4h, five of the six selected IKKα inhibitory agents significantly decreased the levels of at least one NF-κB subunit classically associated with both the canonical and non-canonical NF-κB pathways. This indicates that the IKKα inhibitory agents SU1053, SU1349, SU1372, SU1411 and SU1438 induced an inhibitory effect on both the canonical and non-canonical NF-κB pathways.

The only SU agent that did not induce significant regulation of canonical and non-canonical NF-κB pathway associated subunits was SU1257. This agent significantly decreased the activity of only the p65 NF-κB subunit, although this was only just within the boundary for significance ($p = 0.04$). This indicates that SU1257 did not significantly inhibit the non-canonical NF-κB pathway, but may be inhibiting p65 mediated canonical pathway activity.

Table 4.2 A summary of inhibition of NF-κB activity in RPMI8226 cells by the SU series of IKKα inhibitory agents.
The data shown in Figure 4.6-4.11 is summarised in the table below. The table displays the regulation of the active NF-κB subunits p65, p50, p52 and RelB in RPMI8226 cells following 5μM of the SU agents SU1257 SU1053, SU1349, SU1372, SU1411 and SU1438 when compared to the untreated sample. The NF-κB pathway that each NF-κB subunit is classically associated with is indicated. The *p* values stated are of a one-tailed unpaired *t*-test that was performed using Graphpad Prism 6.0 software to investigate the statistical significance values between 0μM and 5μM for each SU agent for each NF-κB subunit (n = 3, duplicates averaged) (NS = not significant, $p > 0.05$). If relevant, the direction of NF-κB subunit regulation at 5μM SU agent compared to untreated RPMI8226 cells is shown (🡻 = decreased, 🡹 = increased, n/a = no correlation evident in the associated Figures 4.6-4.11).

	Canonical NF-κB pathway				**Non-canonical NF-κB pathway**			
	p65		**p50**		**p52**		**RelB**	
	p value	Direction	*p* value	Direction	*p* value	Direction	*p* value	Direction
SU1257	0.034	🡻	NS	n/a	NS	n/a	NS	n/a
SU1053	NS	n/a	0.035	🡻	0.007	🡻	0.016	🡻
SU1349	0.024	🡻	0.038	🡻	0.021	🡻	NS	n/a
SU1372	0.018	🡻	0.023	🡻	0.049	🡻	NS	n/a
SU1411	0.014	🡻	0.014	🡻	0.015	🡻	0.039	🡻
SU1438	0.027	🡻	NS	n/a	NS	n/a	0.002	🡻

4.4.8. Inhibition of NF-κB activity in RPMI8226 cells by SU1257, SU1349 and SU1411 as measured by western blot analysis

The association between cytotoxicity and the inhibition of constitutive NF-κB activity induced by the SU compounds SU1257, SU1349, and SU1411 was also briefly investigated using western blot analysis detecting the NF-κB proteins phosphorylated p100 (p-p100), total p100, IκBα, phosphorylated p65 (p-p65) and total p52. Theses proteins were detected to provide information on whether SU1257, SU1349 and SU1411 were effecting the processing of canonical and/or the non-canonical NF-κB subunits in RPMI8226 cells. As IKKα is responsible for phosphorylating p100 to the active subunit p52, the level of p-p100, total p100 and total p52 protein was analysed as an output of non-canonical NF-κB activity. Conversely, p-p65 and IκBα were measured to assess canonical pathway activity. IκBα is also known to be downstream gene product of NF-κB activity.

RPMI8226 cells were incubated separately with each SU compound: SU1257, SU1349 and SU1411, at concentrations of 0μM, 1μM, 2.5μM and 5μM. At 4h, cells were harvested and whole cell lysates were generated. 4μg of RPMI8226 whole cell lysate protein from each condition was assayed using western blot analysis. The levels of p-p100, total p100, p-p65, total p52 and IκBα were evaluated in each sample. In all experiments, β-actin protein was assessed as a control.

Figure 4.12 shows a representative western blot showing the quantities of active p-p100, total p100, p-p65, total p52 and IκBα NF-κB proteins in RPMI8226 cells following 4h treatment with increasing concentrations of SU1257, SU1349 and SU1411.

Figure 4.12 demonstrates that SU1411 and SU1349 both substantially decreased levels of p-p100, p-p65 and IκBα in a dose-dependent manner in RPMI8226 cells. Figure 4.12 also indicates that the SU compound SU1411 also decreased the level of β-actin across increasing concentrations in RPMI8226, indicating the possibility of unequal protein loading. However, the decrease in β-actin across increasing concentrations of SU1411 was not

as prominent as the decrease p-p100, p-p65 and IκBα proteins, suggesting that unequal protein loading was not fully responsible for the decrease in the proteins visualised.

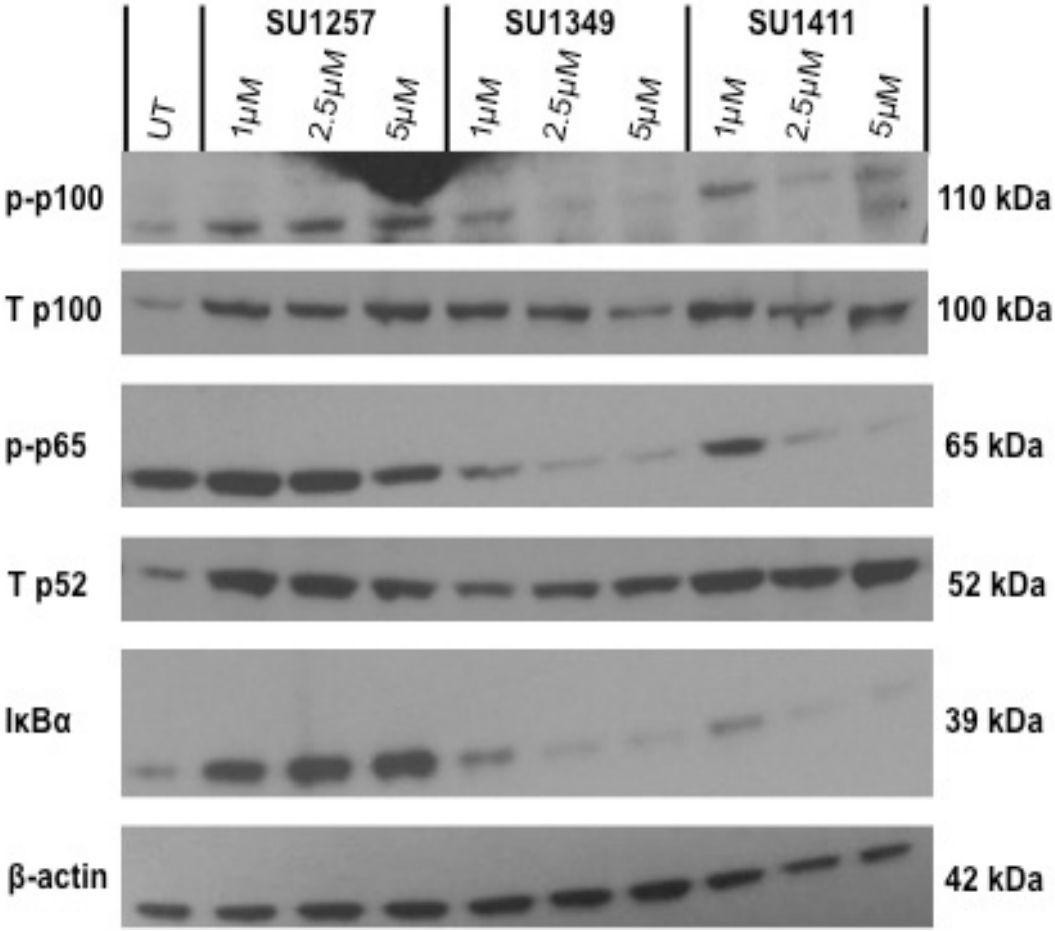

Figure 4.12 Representative western blot showing the effect of SU1257, SU1349, and SU1411 on NF-κB activity in RPMI8226 MM cells at 4h.
RPMI8226 cells were exposed to increasing concentrations of the SU compounds SU1257, SU1349 and SU1411 for 4h at the concentrations of 0μM, 1μM, 2.5μM and 5μM. RPMI8226 cells were then harvested and used to generate whole cell lysates. SDS-PAGE and western blot analysis was used to investigate the level of NF-κB pathway proteins in 4μg whole cell lysates from RPMI8226 cells generated from each condition. The levels of phospho (p)-p100, total (T) p100, p-p65, T p52 and IκBα were evaluated in each sample. In all experiments, β-actin was used as a control. Protein bands are labelled for corresponding NF-κB protein and molecular weight. UT = untreated (0μM).

Figure 4.12 also shows that total p100 protein decreased while total p52 increased following treatment with increasing concentrations of SU1349 and SU1411 for 4h in RPMI8226 cells. This indicates that the two SU agents are not specifically inhibiting the non-canonical NF-κB pathway because the

changes in the levels of these proteins suggest that p100 processing is continuing.

Figure 4.12 shows that SU1257 also induced a decrease in p-p65 in a dose-dependent manner in RPMI8226 cells. In contrast to SU1349 and SU1411, Figure 4.12 also shows that SU1257 induced a dose-dependent decrease in total p52 protein but did not appear to effect the levels of total p-p100, total p100, IκBα or β-actin in RPMI8226 cells.

In summary, western blot analysis showed a dose-dependent decrease in both canonical and non-canonical NF-κB activity after treatment with increasing concentrations of the SU compounds SU1349 and SU1411 in RPMI8226 cells, although the results indicate that the agents may be more specifically effecting the canonical NF-κB pathway. In addition, Figure 4.12 suggests that SU1257 seemingly decreased only canonical NF-κB activity.

4.5. The effect of increasing concentrations of SU1257 and SU1053 on cytotoxicity and Mcl-1 expression in RPMI8226 cells

The data so far suggested that the IKKα inhibitory agents SU1257 and SU1053 were the least cytotoxic inhibitors when compared to SU1349, SU1372, SU1411 and SU1438. Moreover, when SU1257 and SU1053 were investigated for cytotoxicity at 48h at the maximum concentration of 20μM (Figure 4.2), the percentage of apoptosis induced was well below 50% (24.1% ± 1.8% and 40.9% ± 7.2%, respectively). Therefore, it was not initially possible to interpolate an LD_{50} value for cytotoxicity for these two SU inhibitory agents so these two compounds were re-assessed for cytotoxicity at two higher concentrations of 50μM and 100μM to allow an accurate assessment of their respective LD_{50} values.

Alongside these experiments, Mcl-1 expression was also investigated at 4h using 10μM and 20μM of SU1257 and SU1053. This was performed to confirm the results of Figure 4.5, in which both SU1257 and SU1053 did not significantly alter Mcl-1 expression at the maximum concentration of 5μM, and investigate whether Mcl-1 remained unchanged at higher concentrations of each agent.

RPMI8226 cells were treated separately with SU1257 and SU1053 at concentrations of 0.1μM, 0.5μM, 1μM, 2.5μM, 5μM, 10μM, 20μM, 50μM and 100μM. At 4h, RPMI8226 cells were harvested from the concentrations of 0.5μM, 1μM, 2.5μM, 5μM, 10μM and 20μM and then fixated and permeabilised before staining with an anti-Mcl-1-IgG_1 antibody (Santa Cruz Biotechnology) followed by secondary labelling with a goat anti-mouse IgG_1-FITC antibody (Santa Cruz Biotechnology). The stained RPMI8226 cells were then analysed using flow cytometry to quantify the intracellular Mcl-1 expression at each concentration of each compound.

A gating strategy was applied to the collected flow cytometric data to ensure that only viable, single RPMI8226 cells were analysed. The serially gated cell populations were then assessed for Mcl-1 expression (MFI values) at each concentration. The Mcl-1-FITC MFI values at each concentration for

each SU agent was determined and normalised to the untreated MFI for RPMI8226 cells. Figure 4.13A shows the collated data from three separate experiments for RPMI8226 cells (n = 1, duplicate for 10μM and 20μM SU1257 only), outlining the dose-dependent regulation of Mcl-1 expression by the agents SU1257 and SU1053 at 4h when used at increased concentrations.

The same experiments were continued to 48h, at which point RPMI8226 cells were harvested from all concentrations used and washed in PBS before being labelled with Annexin V-FITC and PI. The labelled cells were then analysed using flow cytometry to determine the percentage of apoptosis (Annexin V^+/PI^- + Annexin V^+/PI^+ + Annexin V^-/PI^+) occurring at each concentration. Figure 4.13B shows the cytotoxicity of SU1257 and SU1053 at 48h in the RPMI8226 cell line with the two increased concentrations of 50μM and 100μM analysed and the results shown were collated from four independent experiments.

Figure 4.13A shows that when used at two increased concentrations of 10μM and 20μM, SU1257 induced a modest decrease in Mcl-1 expression in RPMI8226 cells (81.4% ± 2.5% and 85.7% ± 0.9%, respectively) relative to the normalised untreated sample, although no statistical evaluation was performed as the experiment was n =1 in duplicate. In contrast, SU1053 induced a moderate dose-dependent decrease with increasing concentrations that continued past 5μM. At the highest concentration of 20μM, SU1053 decreased Mcl-1 expression at 4h in RPMI8226 cells to 63.6% ± 18.0%, although this was still not significantly different from the untreated control sample (p = 0.085).

Figure 4.13B shows the dose-response curve for SU1257 when the higher concentrations of 50μM and 100μM were added. It was still not possible to accurately interpolate an LD_{50} value as the maximum percentage apoptosis induced at 100μM SU1257 was 57.1% ± 1.5% in RPMI8226 cells. This suggests that SU1257 was relatively non-cytotoxic in RPMI8226 cells.

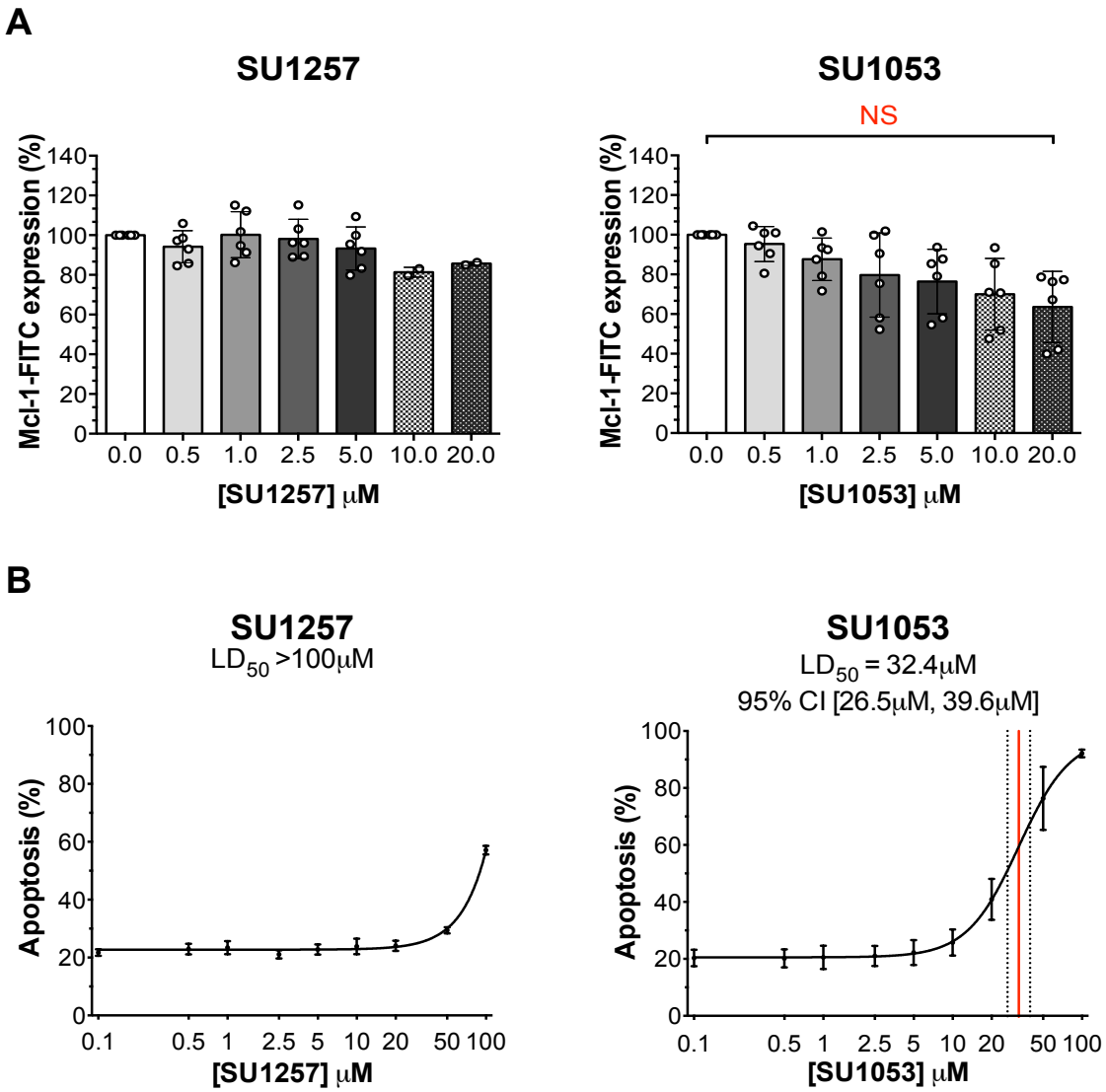

Figure 4.13 The cytotoxicity profiles and regulation of Mcl-1 expression in RPMI8226 cells after exposure to SU1257 and SU1053 at increased concentrations. To fully investigate SU1257 and SU1053 in RPMI8226 cells, these two SU compounds were incubated with RPMI8226 cells at higher increasing concentrations. (**A**) At 4h, intracellular Mcl-1 expression was measured on an Accuri C6 flow cytometer and normalised to the untreated control. A one-tailed unpaired *t*-test was performed using Graphpad Prism 6.0 software to investigate the statistical significance values between 0μM to 20μM for SU1053 in RPMI8226 cells (n = 3, duplicates averaged). The results are reported above the graph (NS = non-significant, $p < 0.05$). Error bars represent SD where n = 3, duplicate (n = 1, duplicate for 10μM and 20μM SU1257), experimental duplicates plotted. (**B**) At 48h, cytotoxicity was investigated using Annexin V/PI positivity on an Accuri C6 flow cytometer. The percentage of apoptotic cells at each concentration of SU compound was calculated and dose-response curves were constructed using Graphpad Prim 6.0. Where possible, LD_{50} values were interpolated and are reported alongside 95% CI. Error bars represent mean ± SD, where n = 4, experimental duplicates shown.

On the other hand, Figure 4.13B shows that at increased concentrations of 50μM and 100μM, SU1053 continued to induce a dose-dependent increase in cytotoxicity following a concentration of 5μM and an LD_{50} value was positively interpolated (LD_{50} = 32.4μM, 95% CI [26.5μM, 39.6μM]). Overall Figure 4.13B suggests that while SU1053 is relatively less cytotoxic than some of the other SU compounds, it does become cytotoxic at higher concentrations.

4.6. Discussion

In this chapter, a series of novel IKKα inhibitory compounds were evaluated in the MM cell line RPMI8226. The RPMI8226 cell line was chosen because this MM cell line was found to possess an intermediate level of baseline NF-κB activity in Chapter 3 and possesses an inactivating TRAF3 mutation, so it was hypothesised that this MM cell line would be susceptible to IKKα inhibition by virtue of constitutive activation of the non-canonical NF-κB pathway (Annunziata et al. 2007; Keats et al. 2007; Demchenko et al. 2010). Overall, nine novel IKKα inhibitory compounds were evaluated (kindly provided by Prof. Simon MacKay, University of Strathclyde). Each of the SU compounds used were specifically designed to target IKKα, although each had a unique kinase inhibitory profile.

4.6.1. Cytotoxicity of the SU agents in RPMI8226 cells

The cytotoxicity of all nine SU agents was first screened in RPMI8226 cells following 48h incubation with increasing concentrations of each agent (n =2) and it was hypothesised that the cytotoxicity of each SU compound would correlate with their respective IKKα, IKKβ and CDK9 kinase inhibitory profiles. Therefore, the aim was that the pairing of the available kinase inhibitory data with initial cytotoxicity in RPMI8226 cells, would allow a decision on a smaller selection of IKKα inhibitory agents to take forward for further investigation.

Three of the SU compounds, SU1257, SU1053 and SU1372, induced a low level of cytotoxicity in RPMI8226 cells such that accurate LD_{50} values

could not be calculated. Conversely, the remaining six SU agents, SU1261, SU1349, SU1361, SU1365, SU1411 and SU1438, were more potent and induced cytotoxicity in a concentration-dependent manner in RPMI8226 cells. However, the conclusion was that the kinase inhibitory profiles did not completely correlate with the cytotoxicity induced in the initial screening. For example, both SU1349 and SU1372 had similar kinase inhibitory profiles with respect to CDK9 and IKKα and IKKβ, but their respective cytotoxicity profiles in RPMI8226 cells were markedly different. Based on initial LD_{50} values, SU1349 was the most cytotoxic agent whereas SU1372 was relatively one of least cytotoxic agents. This suggests that the cytotoxicity induced by these agents may not be a consequence of their inhibition of CDK9, IKKα and IKKβ, and the SU compounds may be inducing their effects through off-target kinase inhibition, particularly in the case of SU1349.

Similarly, the kinase profile data suggested that SU1411 and SU1438 had similar inhibitory profiles because they both preferentially inhibited IKKα over IKKβ and CDK9. However, the initial cytotoxicity data for LD_{50} values suggested that SU1411 was more cytotoxic than SU1438. For this reason, these four SU compounds were included in the selection of agents for further analysis. SU1257 and SU1053 were also chosen; SU1257 due to its unique inhibitory profile and SU1053 because it showed the weakest inhibition of both the IKKβ and CDK9 kinases but was a relatively potent inhibitor of IKKα.

In conclusion, the chosen SU compounds included SU1257, SU1053, SU1349, SU1372, SU1411 and SU1438 and the cytotoxicity of these six agents was further investigated to allow a more robust comparison of the variation in cytotoxicity ($n = 4$). SU1257, SU1053 and SU1372 remained the least cytotoxic compounds in RPMI8226 cells and it was not possible to interpolate an accurate LD_{50} value for these agents. However, when SU1053 was reassessed at two increased concentrations of 50μM and 100μM, an LD_{50} value was successfully interpolated. This indicated that although SU1053 was relatively non-cytotoxic, it become more cytotoxic at higher

concentrations. The same was not true for increased concentrations of 50μM and 100μM SU1257 so this agent was classified as essentially non-cytotoxic in RPMI8226 MM cells.

Further investigation revealed that the pattern of cytotoxicity for SU1349, SU1411 and SU1438 was consistent with the initial screening. SU1438 was significantly less cytotoxic than SU1349, whereas SU1349 and SU1411 induced a comparatively similar level of cytotoxicity in RPMI8226 cells, although SU1411 was also comparatively similar in cytotoxicity to SU1438. Overall, except for SU1257, this suggested that the kinase inhibitory profiles did not completely explain the cytotoxicity induced by the SU compounds.

Although the use of specific IKKα inhibitors in MM has not yet been described elsewhere, it has been demonstrated that knockdown or depletion of IKKα in MM cells does not effect their overall survival or viability (Annunziata et al. 2007; Rauert-Wunderlich et al. 2013), but may instead impact on MM cell growth and proliferation (Hideshima et al. 2009). In addition, knockdown of IKKα in B-cells has been shown to be non-toxic (Senftleben et al. 2001). This correlates with the pattern observed in terms of SU compound cytotoxicity and the relationship with their IKKα kinase inhibitory profile. For example, the lack of cytotoxicity induced by SU1053 and SU1372, both of which are selective potent inhibitors of IKKα, suggests that IKKα inhibition is not the dominant cause of apoptosis in the RPMI8226 MM cell line.

CDK9, unlike other Cdc2-like kinases, does not participate in cell cycle regulation but is instead involved in cell differentiation through regulation of RNA transcription (de Falco a Giordano 1998; Napolitano et al. 2000). Inhibition of CDK9 has been shown to induce cytotoxicity in MM cells through inhibition of transcription and Mcl-1 protein levels, although the CDK9 inhibitors used in these studies were more potent towards CDK9 than the SU agents (Manohar et al. 2011; Dolloff et al. 2012; Jorda et al. 2014). In contrast, the data for the SU compounds suggests that CDK9

inhibition does not seem to be one of the main contributing causes of apoptosis in RPMI8226 cells. This is evident in the disparity in cytotoxicity between SU1349 and SU1372, both of which have kinase inhibitory profiles indicating that they are similarly potent inhibitors of CDK9.

4.6.2. Mcl-1 regulation by the SU agents in RPMI8226 cells

To begin exploring the effect of IKKα inhibition on NF-κB activity, the dose-dependent regulation of Mcl-1 expression at 4h was quantified in RPMI8226 cells for each of the six selected SU IKKα inhibitory agents. Mcl-1 is an important anti-apoptotic protein that is relevant in the survival and progression of MM (Derenne et al. 2002; Zhang et al. 2002; Meinel et al. 2010). Moreover, a constitutive level of NF-κB activity correlates with the expression of Mcl-1 in MM cell lines (Liu et al. 2014). Therefore, it was hypothesised that the regulation of Mcl-1 expression in RPMI8226 cells by the SU agents would correlate with their cytotoxicity.

At all of the concentrations of SU1257 tested, the level of Mcl-1 expression remained comparable to the untreated controls, which was consistent with the lack of cytotoxicity observed with this agent in RPMI8226 MM cells. On the other hand, SU1053, SU1349, SU1372 and SU1438 all decreased Mcl-1 expression in a dose-dependent manner, although the level of down-regulation was variable among the SU compounds and did not directly correlate with cytotoxicity. The largest overall decrease in Mcl-1 expression (at 5μM) was seen with SU1053, although this was not significant. The dose-dependent decrease in Mcl-1 expression by SU1053 continued when higher concentrations of 10μM and 20μM were analysed, although this was still not significant ($p = 0.24$).

SU1349 and SU1372 showed a similar down-regulation pattern in terms of Mcl-1 expression with increasing concentrations. Several studies have shown that CDK9 inhibition significantly decreases Mcl-1 expression, which contributes to cell apoptosis (Manohar et al. 2011; Dolloff et al. 2012; Jorda et al. 2014). SU1349 and SU1372 are both potent inhibitors of CDK9 and both induced a strong dose-dependent down-regulation in Mcl-1

expression at 4h, which may suggest that CDK9 inhibition is contributing to this effect.

Both SU1411 and SU1438 did not decrease Mcl-1 expression in a dose-dependent manner but did induce a relatively weak decrease in Mcl-1 expression at 5μM when compared to the untreated controls. Similar to their cytotoxic effects, SU1411 and SU1438 induced different decreases in Mcl-1 expression, despite the similarity in their kinase inhibitory profiles. Overall, this shows that the apoptosis induced by most of the SU IKKα inhibitors does not correlate with the level of down-regulation of Mcl-1 expression so Mcl-1 down-regulation is unlikely to be the main cause of apoptosis. In addition, neither do the kinase inhibitory profiles of most of the SU compounds correlate with the level of down-regulation in Mcl-1 expression that was induced in RPMI8226 MM cells.

4.6.3. NF-κB activity regulation by the SU agents in RPMI8226 cells

In order to further characterise the IKKα inhibitory pharmacological agents, the dose-dependent effect of each agent on NF-κB activity was investigated in more detail using an ELISA-based method for detecting the active NF-κB subunits p65, p50, p52 and RelB in the MM cell line RPMI8226.

The results demonstrated that five of the six selected IKKα inhibitory agents significantly decreased the levels of at least one NF-κB subunit classically associated with both the canonical and non-canonical NF-κB pathways. This suggests that SU1053, SU1349, SU1372, SU1411 and SU1438 inhibited both the canonical and non-canonical NF-κB pathways. The remaining SU agent, SU1257, only significantly decreased p65 activity, indicating that SU1257 was not significantly inhibiting the non-canonical pathway activation.

As mentioned previously, the ELISA possessed caveats that meant that it may not have been an appropriate tool to quantify the effect that the SU compounds induced on NF-κB activity. For example, there were potential issues with method of subunit quantification used for the ELISA's, the specificity of the antibodies provided in the NF-κB ELISA kit and issues

with the binding of specific NF-κB subunit dimers to the immobilised oligonucleotide (personal communication with Professor Neil Perkins). Therefore, western blot analysis was also used to visualise the dose-dependent effect of SU1257, SU1411 and SU1349 on NF-κB proteins. This technique also showed that SU1349 and SU1411 induced a does-dependent decrease in canonical and non-canonical NF-κB associated proteins, although inhibition of the canonical pathway seemed the most prominent. In addition, similar to ELISA, western blot analysis also revealed that SU1257 dose-dependently decreased p-p65 protein, indicating that SU1257 inhibits the canonical NF-κB pathway.

However, western blotting was only used to visualise the effect that the SU compounds SU1257, SU1349 and SU1411 had on NF-κB activity in the MM cell line RPMI8226. Therefore, to fully explore the SU compounds effect on NF-κB activity more western blotting could have been utilised to investigate the effect that the SU compounds SU1053, SU1438 and SU1372 had on NF-κB pathway processing in RPMI8226 cells. Furthermore, with the use of the right combination of antibodies (such as those used in Figure 4.12), western blotting could have provided more in depth information regarding the specific NF-κB pathway processing following treatment with these IKKα inhibitory compounds. For example, antibodies targeting phosphorylated p100, and total p100 and p52 proteins could have provided definitive proof of non-canonical pathway inhibition by SU1053, SU1438 and SU1372 as p100 functions as both the precursor of p52 and a RelB-specific inhibitor.

The five SU agents that regulated both canonical and non-canonical associated NF-κB subunits were all potent inhibitors of IKKα, with at least a 50-fold preference towards IKKα inhibition when compared to IKKβ. IKKα is mainly responsible for the phosphorylation of the precursor subunit p100 to the activated p52 NF-κB subunit, which can form homo- or hetero-dimers with the RelB NF-κB subunit (Senftleben et al. 2001; Solan et al. 2002). In addition, knockdown of IKKα in B-cells substantially decreased the level of p52 subunit while conversely increasing p100 protein (Senftleben et al.

2001). For this reason, it was hypothesised that IKKα inhibition by these five SU agents would preferentially inhibit the non-canonical associated NF-κB subunits, resulting in a dose-dependent decrease in nuclear p52 and RelB protein.

However, the variable inhibition of non-canonical NF-κB subunits induced by the SU agents did not readily relate to the IKKα inhibition profiles for each agent. For example, although SU1438 was as potent an IKKα inhibitor as SU1411, ELISA indicated that it did not significantly inhibit p52 activity whereas SU1411 did. Furthermore, SU1053, the least potent IKKα inhibitor, induced the most significant overall decrease in p52 activity (p = 0.007). Moreover, ELISA showed that all five agents induced a significant dose-dependent down-regulation of at least one of the canonical NF-κB pathway proteins, p65 or p50. This was regulatory pattern was confirmed using western blot analysis, which showed that both SU1349 and SU1411 induced a substantial dose-dependent decrease in p-p65, IκBα and p-p100 proteins. Conversely, total p52 protein was dose-dependently increased by SU1349 and SU1411 in RPMI8226 cells, which may indicate lack of specificity towards non-canonical NF-κB inhibition by these SU agents.

Therefore, the presence of canonical pathway inhibition by the SU agents may indicate that inhibition of IKKα in the MM cell line RPMI8226 may also be inhibiting canonical pathway activity generated through p65 and p50 activation. Several studies have demonstrated that both IKKα and IKKβ can carry out phosphorylation of IκBα, although IKKα is the least efficient kinase and cannot replace IKKβ (DiDonato et al. 1997; Mercurio et al. 1997; Régnier et al. 1997; Lam et al. 2008). Additionally, it has been reported that both IKKα and IKKβ can phosphorylate the p65 subunit to promote transactivation potential (Perkins 2006). However, the lack of correlation in effect on NF-κB activity and IKKα inhibitory potential may indicate the possibility of additional kinase targets for the SU agents that may regulate NF-κB activity.

Another irregularity that emerged when considering the effects of the SU compounds on the non-canonical pathway was the increase in RelB activity induced by SU1349 and SU1372. These two agents have similar kinase inhibitory profiles and differ from the other SU agents in the respect that they each possess potent inhibitory action against CDK9. This may indicate that CDK9 inhibition is involved in the inhibition of the non-canonical NF-κB pathway, especially through inhibition of RelB activity. However, it is more likely that variation between ELISA experiments for these two SU compounds is the reason because for both the RelB ELISA results for these compounds, outliers can be identified that may have skewed the statistical result.

4.6.4. Conclusion

The aim of this chapter was to evaluate a series of pharmacological agents designed to inhibit IKKα in terms of their cytotoxicity, regulation of Mcl-1 expression and effect on NF-κB activity in the MM cell line, RPMI8226. This chapter has shown that the majority of IKKα inhibitory SU agents were dose-dependently cytotoxic in RPMI8226 cells, although the level of cytotoxicity did not correlate with dose-dependent down-regulation of the anti-apoptotic protein Mcl-1 or NF-κB activity. This suggests that another mechanism exists by which the IKKα inhibitors induce their cytotoxicity. Moreover, the effects induced by these agents could not be explained completely by their kinase inhibitory profiles.

The exception to this was SU1257, an agent that been designed to be a structural analogue of the other compounds but has no IKKα or IKKβ inhibitory properties. SU1257 was shown to be relatively non-toxic even when used at increased concentrations, did not alter Mcl-1 expression, and did not significantly inhibit the non-canonical NF-κB pathway. Therefore, the kinase inhibitory profile for this agent matches the effects that this agent induces in MM and warrants its use as a control compound in experiments investigating these agents.

In conclusion, these agents may provide a promising strategy for MM treatment but the specific cause of apoptosis will need to be further investigated.

Chapter 5 – The effect of the SU series of IKKα inhibitory agents on global gene expression in MM cells.

Microarray-based techniques are capable of simultaneously assessing the gene expression of thousands of different genes through the measurement of mRNA expression in a single reaction (Slonim a Yanai 2009). This removes the difficulty of pre-selecting and measuring putative genes of interest, including specific tumour suppressor genes and/or oncogenes, for analysis as microarray-based techniques allow for global gene expression to be quantified in a single experiment. In addition, the completion of multiple gene sequencing projects has provided the information required for the specific annotation of arrays and improvements to the actual design of the individual gene probes on the microarray chips (Hubank 2004). Microarrays can therefore provide in-depth information on the underlying biological pathways that are altered both in disease and by pharmacological agents. Moreover, the data generated through microarray-based techniques is usually highly reproducible and quantitative.

Microarray-based techniques have been used to investigate global gene expression in several haematological malignancies to clarify the specific expression abnormalities that give rise to cancer biology and to sub-stratify specific tumour types. Examples include chronic lymphocytic leukaemia and various B-cell lymphomas (Dürig et al. 2003; Jelinek et al. 2003; Staudt a Dave 2005). In MM, microarray-based techniques have been used to reveal the specific gene expression profiles that are responsible for differentiating MM cells from normal plasma cells and identify the transcriptional characteristics associated with poor prognosis (Zhan et al. 2002; Shaughnessy et al. 2005). In addition, global gene expression profiling has also been shown to provide predictive prognostic markers and identify new therapeutic targets within relevant signalling pathways in MM (Decaux et al. 2008; Hose et al. 2011). Moreover, several studies have specifically used microarray-based techniques to understand the role of the NF-κB pathways in MM through analysis of aberrant gene expression (Annunziata et al. 2007; Keats et al. 2007; Demchenko et al. 2010).

The previous chapter characterised the SU series of pharmacological agents in terms of their cytotoxicity and altered nuclear NF-κB expression. The next step was to develop a deeper understanding of the mode of action of the SU series. The SU series was designed to target the NF-κB pathway through inhibition of IKKα. For this reason, the effect of these compounds on global gene expression was investigated using Affymetrix GeneChip® HTA 2.0 gene expression analysis.

The overall aim of this experiment was to investigate whether the individual agents targeted distinct sets of genes or whether a common set of genes was altered by the SU compounds, but perhaps in a quantitatively different fashion. Therefore, this chapter will cover the following key steps:

1. Experimental design and sample generation.
2. Quality control of the Affymetrix Gene Chips
3. Comparison of altered gene expression
4. Selection of genes for qRT-PCR validation
5. qRT-PCR results
6. Comparison of qRT-PCR and Affymetrix Gene Chips

5.1. Affymetrix GeneChip® HTA 2.0 gene expression analysis

5.1.1. Experimental design and sample generation

Five compounds from the SU series were chosen for global gene expression analysis. These were SU1257, SU1053, SU1438, SU1411 and SU1349. SU1257 does not possess IKKα, IKKβ or CDK9 inhibitory properties (Table 4.1) and was found to be non-cytotoxic in the RPMI8226 cell line. SU1349 was shown to be a potent inhibitor of both CDK9 and IKKα (Table 4.1), and was the most cytotoxic SU series compound in RPMI8226 cells. SU1411 and SU1438 preferentially inhibited IKKα with weak inhibition of IKKβ and CDK9 (Table 4.1). Nevertheless, SU1411 was found to be more cytotoxic than SU1438 in RPMI8226 cells following exposure for 48h.

Of the cytotoxic compounds, SU1053 was the weakest inhibitor of both the IKKβ and CDK9 kinases but was a relatively potent inhibitor of

IKKα (Table 4.1); SU1053 was significantly less cytotoxic than SU1411 and SU1438.

The RPMI8226 MM cell line was selected for the global gene expression analysis because this MM cell line was found to possess an intermediate level of NF-κB activity so was used to characterise the SU series compounds in the previous chapter. Three treatments of each pharmacological agent were performed and samples were generated with doses-response experiments performed in parallel.

RPMI8226 cells were incubated alone and in the presence of increasing concentrations of the SU compounds SU1257, SU1053, SU1438, SU1411 and SU1349. At 4h, cells were harvested from untreated and from cells treated with 2.5μM of each SU compound to generate TRIzol® lysates. Samples were subsequently processed for RNA extraction once three replicate sets for each treatment were collected. Each SU compound was used at a concentration of 2.5μM because this was found to be a concentration where most of the SU series compounds effected viability, Mcl-1 expression and NF-κB activity in the RPMI8226 cell line.

Prior to RNA extraction, dose-dependent cytotoxicity in the parallel samples was measured at 48h by flow cytometry using Annexin V/PI positivity for all experiments in which a 4h TRIzol® lysate was generated. The aim of this was to ensure that the SU compounds were inducing the expected cytotoxic effect prior to commitment to undertaking the microarray analysis. The cytotoxicity dose-response curves for all samples used in the microarray analysis are shown in Appendix Figure I. It shows that all samples treated with SU compound samples induced the expected cytotoxicity at 48h.

Following RNA extraction, RNA quality was assessed using an Agilent 2100 Bioanalyzer System. All the RNA extracts generated for the microarray analysis achieved an RNA integrity value of 10, which is the highest quality value possible. Thus, high quality samples were available for global gene expression analysis.

Once all the samples were validated, the resulting RNA extracts were analysed by Affymetrix GeneChip® Human Transcriptome Array (HTA) 2.0 as per the manufacturer's instructions by Dr Amanda Redfern, Central Biotechnology Services (CBS), Cardiff University. This particular type of microarray was chosen due to the high level of information it delivers; not just gene expression levels, but also alternate splicing events. For the purposes of this study, the focus of analysis revolved around the alteration of gene expression that each individual SU compound induced at 4h in the RPMI8226 cell line.

In summary, 18 individual samples were analysed using Affymetrix GeneChip® HTA 2.0 corresponding to n = 3 for each treatment condition. Overall, six treatment conditions were analysed. These were untreated (UT) RPMI8226 cells and RPMI8226 cells treated with 2.5μM of SU1257, SU1053, SU1438, SU1411 or SU1349 for 4h.

5.1.2. Quality control and normalisation of the Affymetrix GeneChip® HTA 2.0 microarray data

The data from the Affymetrix GeneChip® HTA 2.0 analysis was returned by CBS in the form of a series of CEL files. These were opened and analysed using the statistical software environment, R. An assessment of the quality of the raw data from each of the individual Affymetrix GeneChips was performed.

A histogram of distribution of the Log_2 transformed perfect match (PM) probe intensities for each sample array analysed was plotted to compare the variation in PM probe intensity between the 18 individual sample arrays (Figure 5.1A). This shows the overall signal from the individual sample arrays and can indicate one or a subset of arrays has given a different signal across the chip. Figure 5.1A demonstrates that the general shape of all 18 sample arrays was similar, which would be expected for replicate arrays derived from a cell line. However, the centre of the distribution histogram for each sample array differed slightly suggesting that the dataset would benefit from normalisation.

Therefore, the PM probe intensities for all 18 sample arrays were normalised using RMA normalisation. To check that the RMA normalisation was effective, a histogram of the distribution of Log_2 PM probe intensities for each individual sample array was plotted using the RMA normalised data (Figure 5.1B). Figure 5.1B shows that following normalisation the distribution of signals follows a Gaussian bell-shaped curve.

A boxplot of the RMA normalised sample arrays (Figure 5.1C) demonstrates that the median, lower quartile and upper quartile of RMA normalised Log_2 PM probe intensities were comparable across all 18 individual sample arrays. This indicates that the RMA normalisation for the 18 individual sample arrays had been effective.

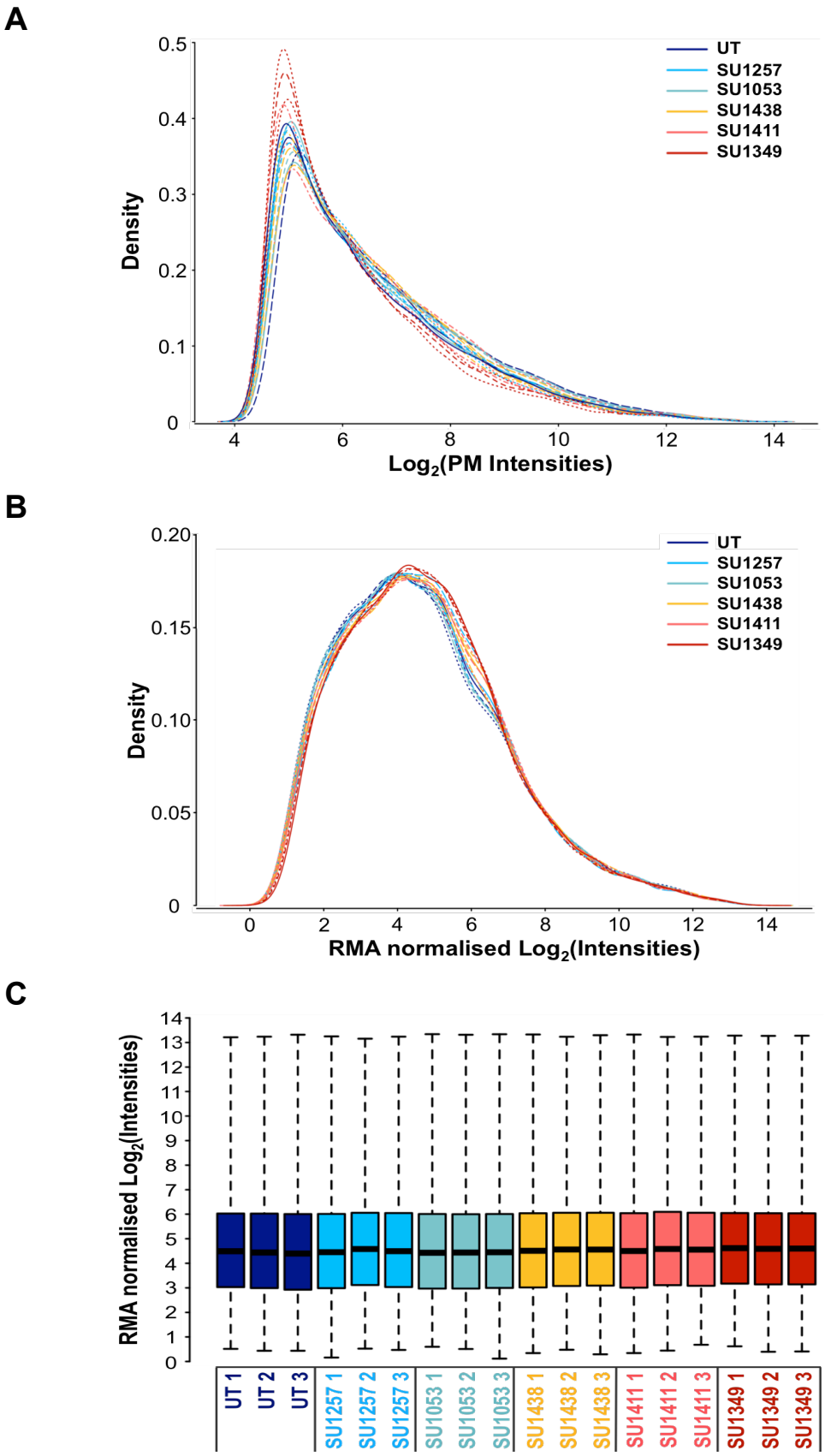

Figure 5.1 Quality control of the Affymetrix HTA 2.0 individual sample arrays. (**A**) A histogram was plotted of the microarray data to compare the distribution of Log_2 transformed PM probe intensities between individual sample arrays. A histogram (**B**) and a boxplot (**C**) demonstrating the effect RMA normalisation had on the distribution on Log_2 intensities between different sample arrays. The data shown represent n = 3 for each condition. (UT = untreated).

5.1.3. Investigating the global gene expression effects of the SU series

Following RMA normalisation of data from the 18 Affymetrix GeneChips, an analysis on the global effects of the SU compounds was performed. The objective of this analysis was to determine how the pharmacological agents grouped by their effects on overall gene expression across the whole GeneChip. This allowed an investigation of whether the individual sample arrays reflected their treatment condition and whether group replicates were homogenous. Two methods were used: (1) the generation of a distance matrix followed by clustering and (2) a principal component analysis.

5.1.3.1. Distance matrix and hierarchical cluster analysis of microarrays

The Log_2 PM probe intensities were used to calculate the Euclidean distance between each sample and plotted using the 'corrplot' package (Wei a Simko 2016). The distances were assembled into a matrix to produce Figure 5.2A. The most distant set of arrays from untreated cells was found in cells treated with SU1349, with most of the SU1349 replicates having a distance greater than 100 when compared to the other GeneChips.

Figure 5.2A shows that changes between 60 and 100 were caused by both SU1438 and SU1411-treated arrays. In comparison, UT, SU1257 and SU1053-treated arrays all showed lower distance matrix values (typically ranging from 50 to 80). One exception to this pattern was the SU1257 (array 2), which indicates that this sample was an outlier.

The distance matrix was then used to generate a hierarchical cluster diagram using the complete linkage cluster method (Figure 5.2B). Hierarchical clustering is a technique that can identify and represent different patterns within the data. The clustering used in Figure 5.2B was unsupervised clustering because no previous information was assumed about the data and the samples were arranged based on sample variation in the PM probe intensities. The cluster analysis initially produced two main branches that were subsequently split into two sub-branches each.

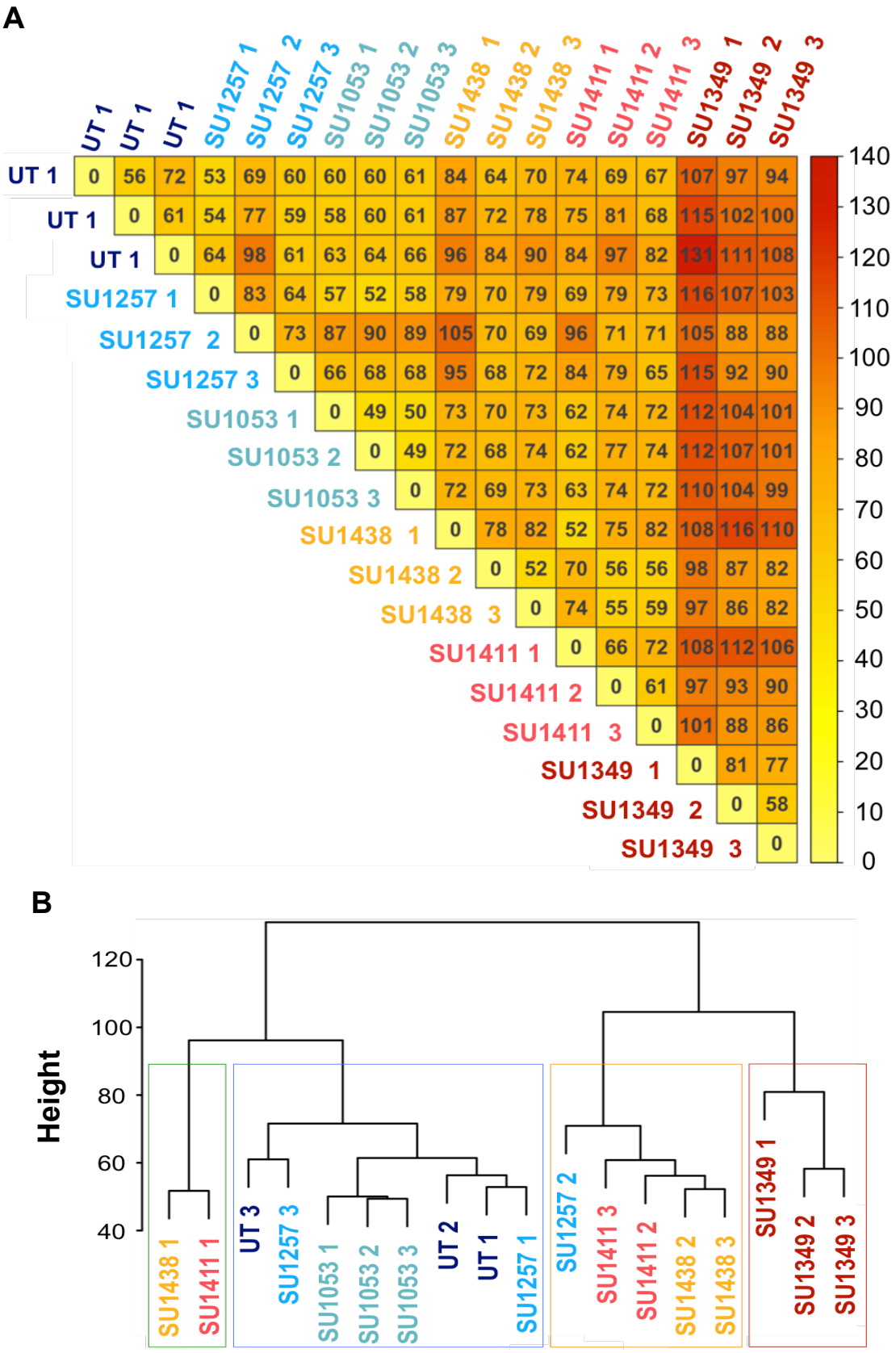

Figure 5.2 Distance matrix and hierarchical cluster analysis of the microarray data. The RMA normalised microarray data was used to produce a distance matrix using the Euclidean method (**A**). The distance matrix was then subjected to a hierarchical cluster analysis using the complete linkage clustering method (**B**). The four main branches within the hierarchical cluster analysis are highlighted. The data shown represents *n*=3 for each condition.

The four branches are highlighted in Figure 5.2B by the coloured boxes. Similar to Figure 5.2A, SU1349 treated samples were identified as most different and distinct from the other treatments because they clustered together in one of the four branches. In addition, Figure 5.2B shows that eight of the nine arrays for UT, SU1257 and SU1053 clustered on the same branch demonstrating that these groups showed a similar global gene expression signatures that were distinct from the SU1349-treated branch. An exception was one of the SU1257 treated arrays, SU1257 (array 2), which clustered on the other of the two main cluster branches, indicating that it showed a distinct global gene expression signature. This again suggests that SU1257 (array 2) was an outlier.

Figure 5.2B also shows that four of SU1438 and SU1411-treated arrays clustered on the same branch as the SU1349-treated samples suggesting a degree of similarity in global gene expression. The SU1438 (array 1) and SU1411 (array 1)-treated sample arrays clustered closer to the UT, SU1053 and SU1257-treated arrays. This indicates that these two arrays possessed some additional variation in global gene expression.

5.1.3.2. Principal component analysis of arrays

A principal component analysis (PCA) was performed on the RMA normalised sample data to extend the assessment of the global changes in gene expression. This method identifies patterns within the PM probe intensities and uses these to transform the data into its principal components. The principal components are then used to express the data in such a way that highlights the similarities and differences among the 18 individual sample arrays.

Table 5.1 and Figure 5.3A show the top 10 principal components produced from analysis of the 18 sample arrays using PCA. Figure 5.3A and Table 5.1 demonstrate that cumulatively, principal components 1 to 10 contributed to a total of 82.5% of the variance between the individual microarrays. Overall, principal component 1 and 2 were cumulatively responsible for 45.4% of the variability within the data.

Table 5.1 Results of the principal component analysis on the microarray data
The variances of the 10 largest principal components produced by PCA of the microarray data are shown in the table below.

Principal Component	Standard deviation	Proportion of Variance	Cumulative Proportion
1	154.0	33.6%	33.6%
2	91.3	11.8%	45.4%
3	84.5	10.1%	55.5%
4	65.7	6.1%	61.6%
5	54.0	4.1%	65.7%
6	52.94	4.0%	69.7%
7	49.9	3.5%	73.2%
8	48.1	3.3%	76.5%
9	46.7	3.1%	79.6%
10	45.3	2.9%	82.5%

Therefore, the PCA was visualised by principal components 1 and 2 (Figure 5.3B). Generally, the arrays can be grouped based on their respective treatment group as indicated in Figure 5.3B using the ovals. Based on the visualisation by principal components 1 and 2, the three SU1349-treated arrays were distinct from the other sets of SU compound treated arrays. Similarly, SU1438 and SU1411-treated arrays are presented in a manner that suggests that both compounds induced comparable alterations in global gene expression. Visualisation of both UT and SU1053 treated samples by principal components 1 and 2 showed that these six arrays are closely related and can be grouped together. In contrast, the three SU1257 arrays were difficult to cluster as a comparable group of similarly treated arrays. This is a consequence of one array appearing quite distant when visualised by the principal components 1 and 2, which supports the observation from hierarchical cluster analysis with regards to SU1257 (array2).

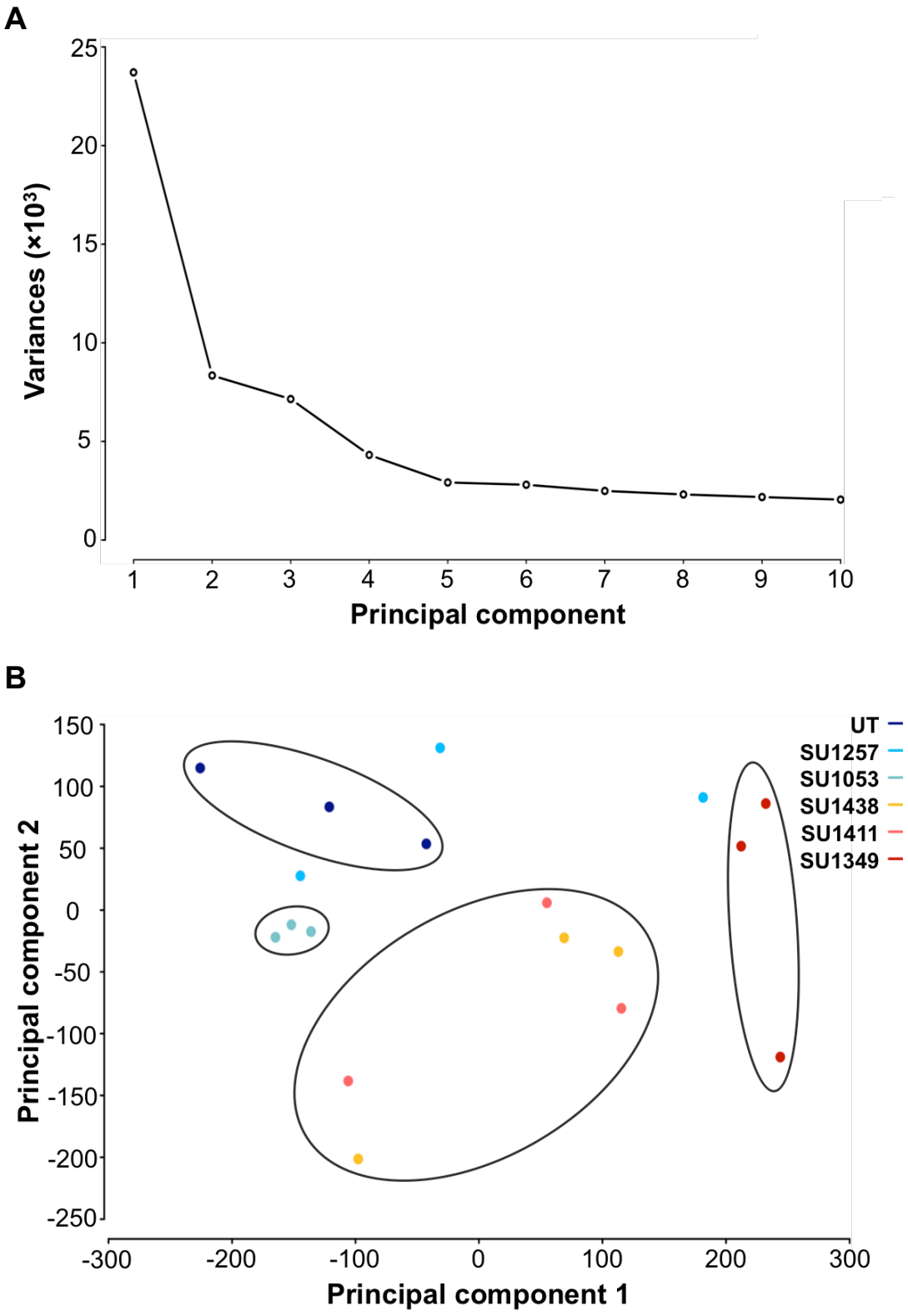

Figure 5.3 Principal component analysis of Affymetrix HTA 2.0 data.
A PCA was performed on the RMA normalised data to investigate the overall variability between the individual sample arrays. (**A**) A plot of the variances associated with each principal component was produced from the results of the PCA. (**B**) A scatter graph showing the grouping of individual sample arrays based on principal component 1 and 2, which contributed to the most variability within the data. Individual sample arrays within the same treatment group were circled where possible. The data shown represents n = 3 for each condition.

In conclusion, the distance matrix and PCA revealed three groups of distinct gene expression changes caused by the SU series of compounds:

1. SU1349 had the most distinct set of changes indicating a qualitative difference from UT and the other compounds in the changes caused.

2. SU1438 and SU1411 caused changes in gene expression when compared to UT but these were distinct to those induced by SU1349 treatment.

3. Both SU1053 and SU1257 caused more subtle changes in global gene expression with some extra variation in one of the SU1257 samples.

5.1.4. Visualisation of differentially expressed probesets

The next step of the analysis involved the visualisation of differentially expressed (DE) probesets. The treatment group replicates were averaged, the array probes were condensed to their respective probesets and DE probesets were identified within each UT vs. treated comparison. Two different methods were used for the visualisation of the DE probesets; (1) Volcano plots and (2) Venn diagrams.

5.1.4.1. Visualising changes with Volcano plots

The DE probesets were first visualised using volcano plots showing fold change (Log_2 (FC)) and statistical significance ($-Log_{10}$ (p value)) for each treated contrast compared to UT (Figure 5.4). Lines at $x = 1$ and $x = -1$ were added to highlight those probesets that had a two-fold change (Log_2 (FC) ≥ 1) in either direction.

The volcano plots in Figure 5.4 have been arranged based on the cytotoxicity of that SU compound in RPMI8226 cells with SU1257 being the least cytotoxic and SU1349 being the most cytotoxic. Overall, Figure 5.4 demonstrates that as the cytotoxicity of the SU compound increased so did the number of probesets breaching the threshold of a Log_2 (FC) ≥ 1 with a significance of $p \leq 0.05$.

Figure 5.4 shows that the UT vs. SU1257 contrast has the fewest probesets experiencing a Log_2 (FC) ≥ 1 paired with $p \geq 0.05$, which produced a relatively flat shape. In contrast, SU1349 induced the most significant changes in probeset expression relative to UT. Compared with the other four SU compounds, the volcano plot for UT vs. SU1349 showed the most probesets with a Log_2 (FC) ≥ 1 in both directions and the most probesets with a significant ($p \leq 0.05$) alteration in expression. The UT vs. SU1053 contrast generated a volcano plot that has more probesets showing significant changes than that of UT vs. SU1257. Moreover, UT vs. SU1438 and UT vs. SU1411 produce volcano plots that were relatively similar in shape and size. This suggests that the quantitative nature of the changes induced by SU1438 and SU1411 were comparable.

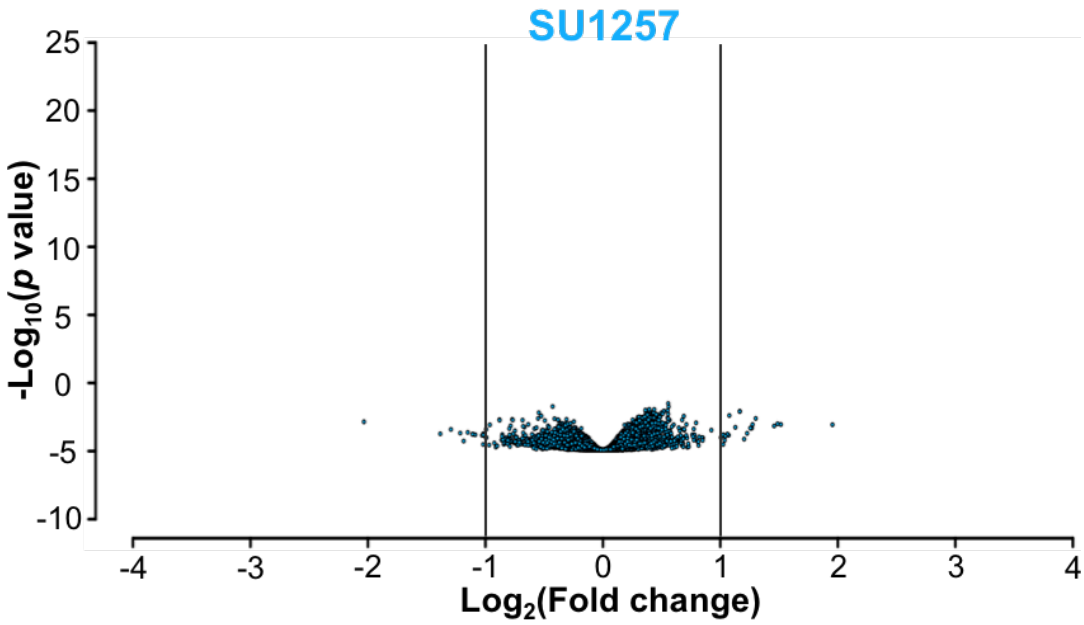
SU1257
25
20
15
10
5
0
-5
-10
-Log10(p value)
-4
-3
-2
-1
0
1
2
3
4
Log2(Fold change)

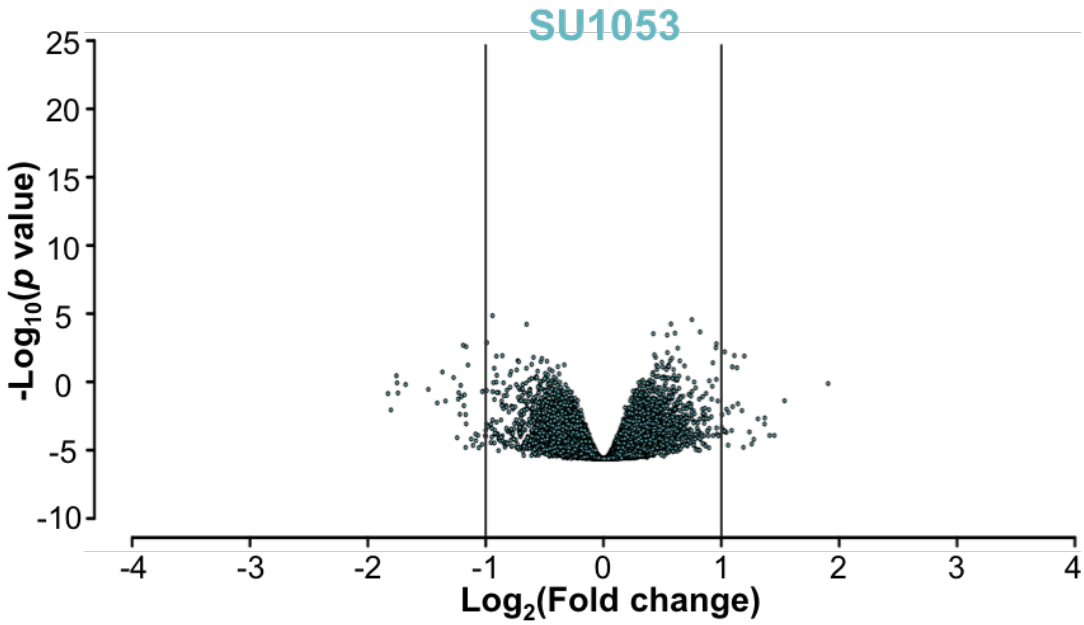
SU1053
25
20
15
10
5
0
-5
-10
-Log10(p value)
-4
-3
-2
-1
0
1
2
3
4
Log2(Fold change)

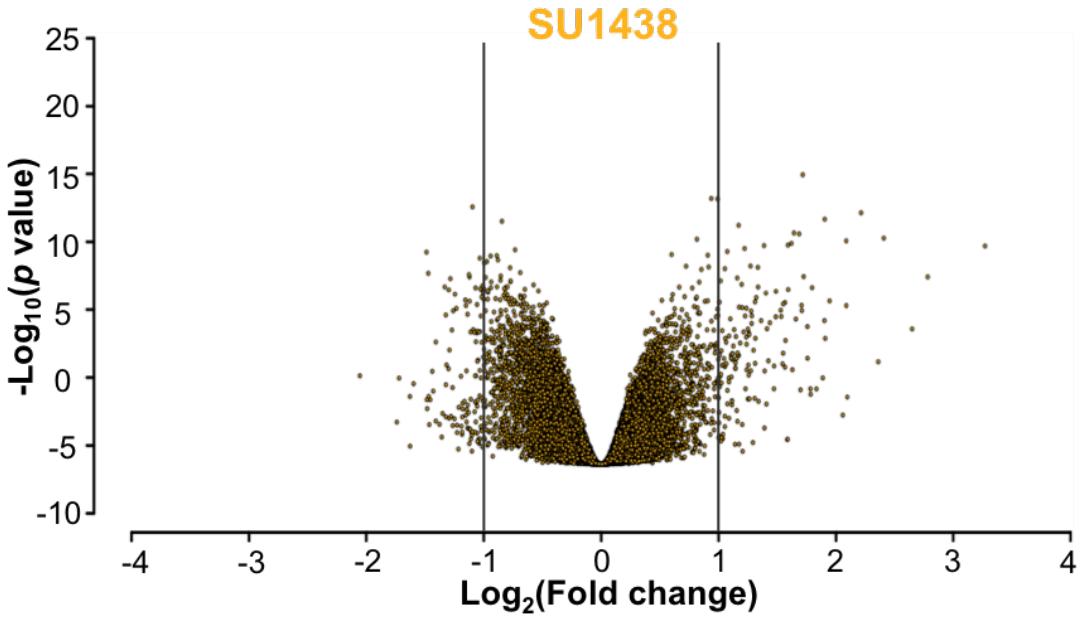
SU1438
25
20
15
10
5
0
-5
-10
-Log10(p value)
-4
-3
-2
-1
0
1
2
3
4
Log2(Fold change)

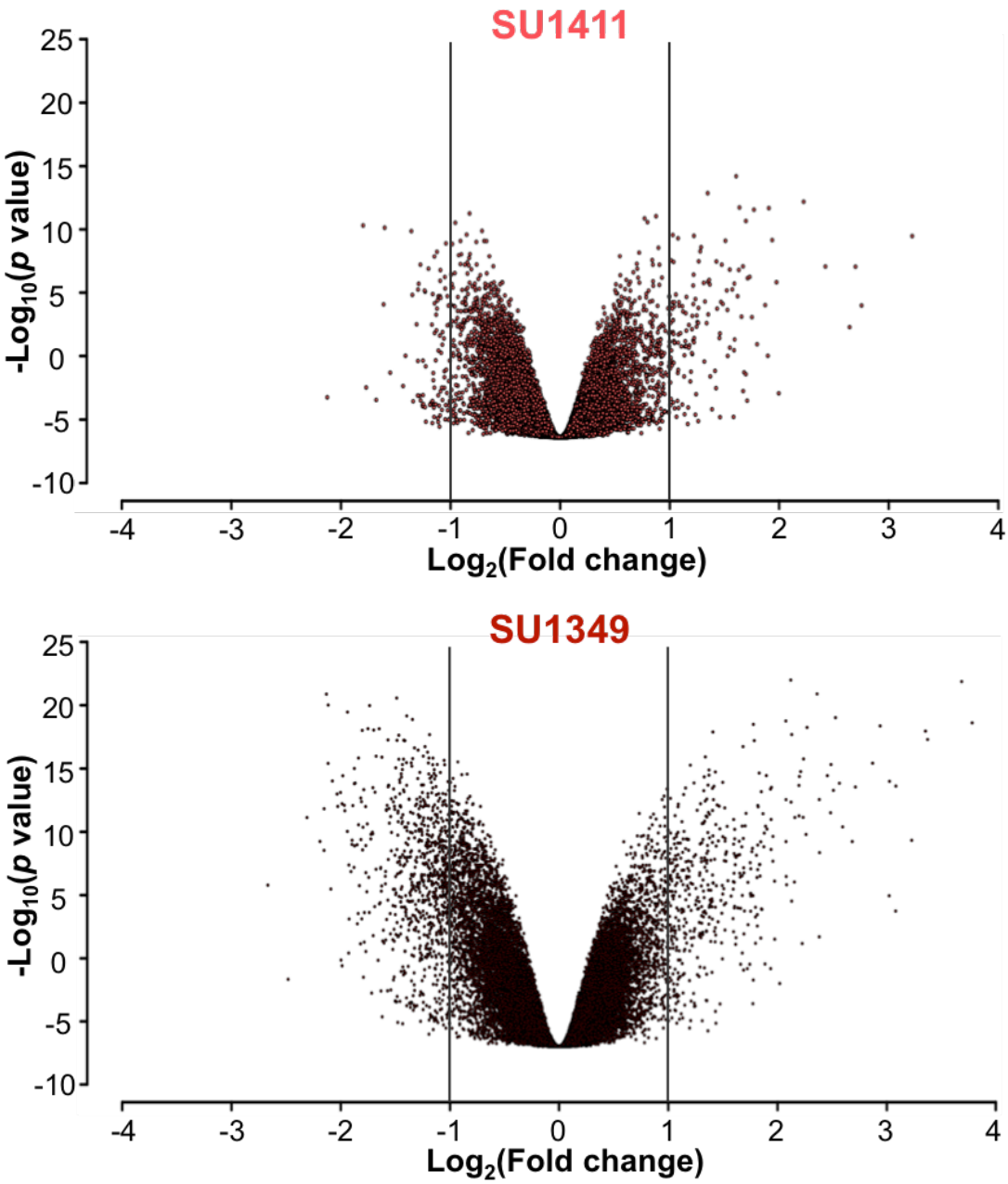

Figure 5.4 Volcano plots of the contrasts for UT sample arrays vs. treated arrays to identify differentially expressed (DE) probesets.
The individual arrays corresponding to UT and treated were grouped (where n = 3) and then multiple linear models were fitted to each group to condense Affymetrix HTA 2.0 probesets. Once in this state, empirical Bayes moderated t-statistics test was performed for each contrast (UT vs. SU1257, UT vs. SU1053, UT vs. SU1438, UT vs. SU1411 and UT vs. SU1349) to investigate the difference between treated arrays and UT arrays. Volcano plots of the results of the test were plotted to help in identification of DE probesets. Lines at x = 1 and x = -1 were plotted to show those probesets with a Log_2 (FC) of one or greater in either direction.

5.1.4.2. Visualising gene expression changes using Venn diagrams

The overlaps in altered probesets were visualised by plotting a Venn diagram of the significantly ($p \leq 0.05$) upregulated and down-regulated probesets (Figure 5.5). UT vs. SU1349 possesses the highest number of altered probesets in total (426 upregulated; 756 down-regulated). UT vs. SU1438 and UT vs. SU1411 specifically shared 42 upregulated and 22 down-regulated DE probesets. However, in total, they had 88 upregulated and 25 down-regulated DE probesets in common because 49 (46 upregulated and 3 down-regulated DE probesets) were shared with SU1349. Figure 5.5 also shows that UT vs. SU1257 possessed the fewest altered probesets (4 upregulated) and UT vs. SU1053 also has relatively few DE probesets (5 upregulated, 17 down-regulated).

In conclusion, DE probesets, defined as Log_2 (FC) ≥ 1 in either direction and $p \leq 0.05$, were present for all treated samples when compared with UT controls although the number of DE probesets varied depending on the SU compound. The variation in the number of DE probesets appeared to parallel the level of cytotoxicity; SU1257 induced the least altered probesets and SU1349 induced the most.

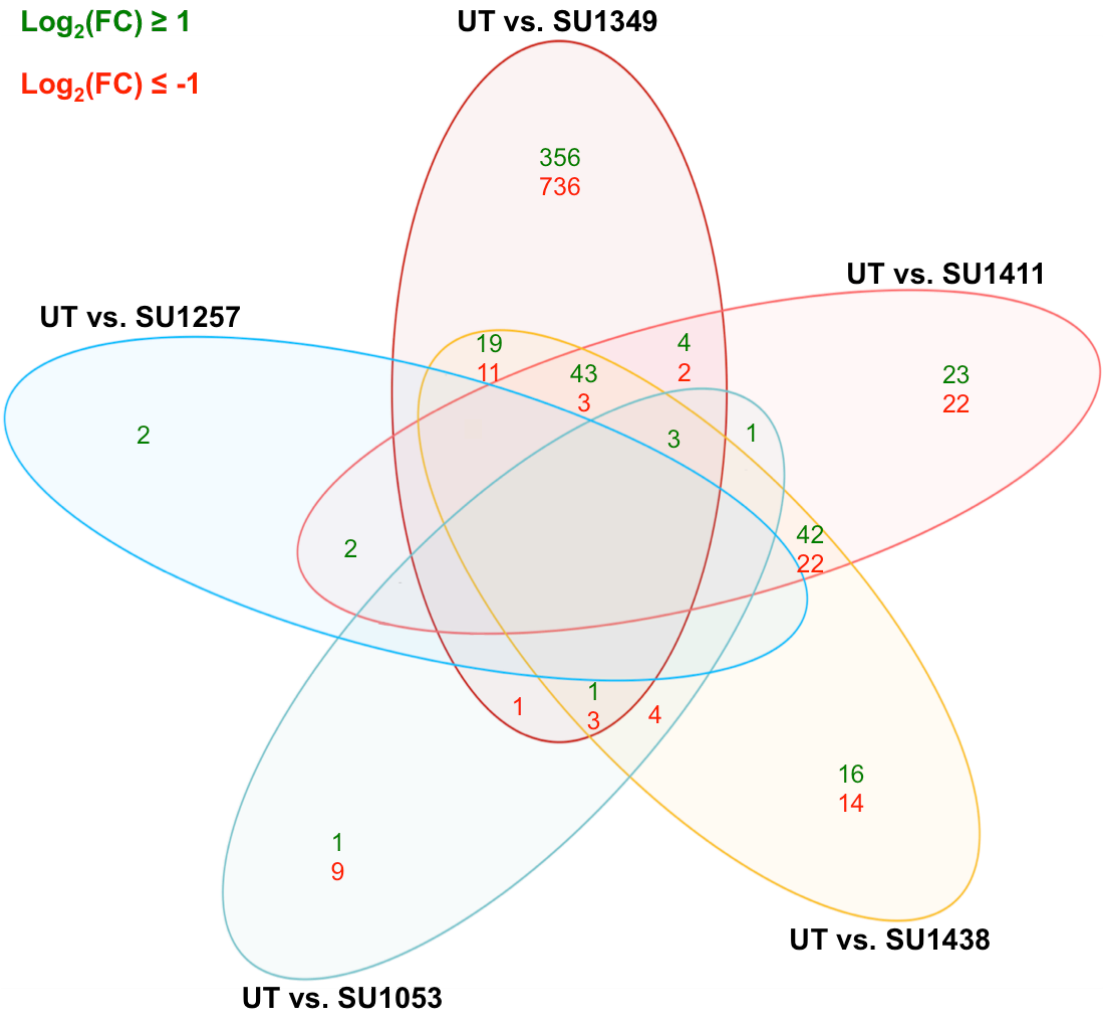

Figure 5.5 Venn diagram showing the number of differentially expressed (DE) probesets for each compound when using Log_2 (FC) > 1 and p < 0.05 thresholds.
The results of the empirical Bayes moderated t-statistics test was sorted to include only those probesets that experienced a two-fold change in either direction (down-regulated = Log_2 (FC) ≤ -1, upregulated = Log_2 (FC) ≥ 1) and a p ≤ 0.05. A multiple comparison test was performed followed by Benjamini and Hochberg correction to investigate the similarities in the DE probesets between the UT and treated contrasts and used to plot a Venn diagram. The number of probesets that were upregulated (Log_2 (FC) ≥ 1) are shown in green and down-regulated probesets (Log_2 (FC) ≤ 1) are shown in red. Zero values have been omitted for clarity.

5.1.5. Annotation of differentially expressed (DE) genes relating to DE probesets

With the identification of the DE probesets, the next step involved converting the probesets to their respective gene names and annotating the genes. The Affymetrix GeneChip® HTA 2.0 includes probesets that correspond to gene expression changes and alternate splicing events. For this analysis, only the probesets matching human genes were used.

The identification pipeline generated a gene list that contained 556 annotated genes and the 'gplots' package (Warnes et al. 2016) in R was used to generate the heat map of the global gene alterations shown in Figure 5.6. Figure 5.6 shows that the annotated genes followed the same pattern that was observed for the probesets in Figure 5.4 and Figure 5.5. For example, SU1257 showed the lowest number of altered genes with a Log_2 (FC) ≥ 1 in either direction whereas SU1349 differentially regulated the most annotated genes.

For this reason, only SU1438, SU1411 and SU1349 were analysed further as these caused more gene alteration and more cytotoxicity in the RPMI8226 MM cell line. The gene lists for these SU compounds are visualised in the Venn diagram (Figure 5.7). The data indicates that the SU compounds down-regulated more genes than they upregulated in RPMI8226 myeloma cells.

The list of DE genes specific for the UT vs. SU1349 contrast was too long (83 upregulated and 419 down DE genes) to be placed in the Venn diagram in Figure 5.7; a list of these DE genes is available in Appendix Tables I and II. Eight genes (6 upregulated and 2 down-regulated DE genes) were shared by all three of compounds. SU1438 and SU1411 shared 24 DE genes (10 upregulated and 14 down-regulated DE genes). In addition, the SU1349 shared more DE genes with SU1438 (2 upregulated and 8 down-regulated DE genes) than with SU1411 (1 upregulated and 1 down-regulated DE genes).

Overall, each SU compound showed some unique characteristics in terms of gene regulation but they also shared common regulatory pathways.

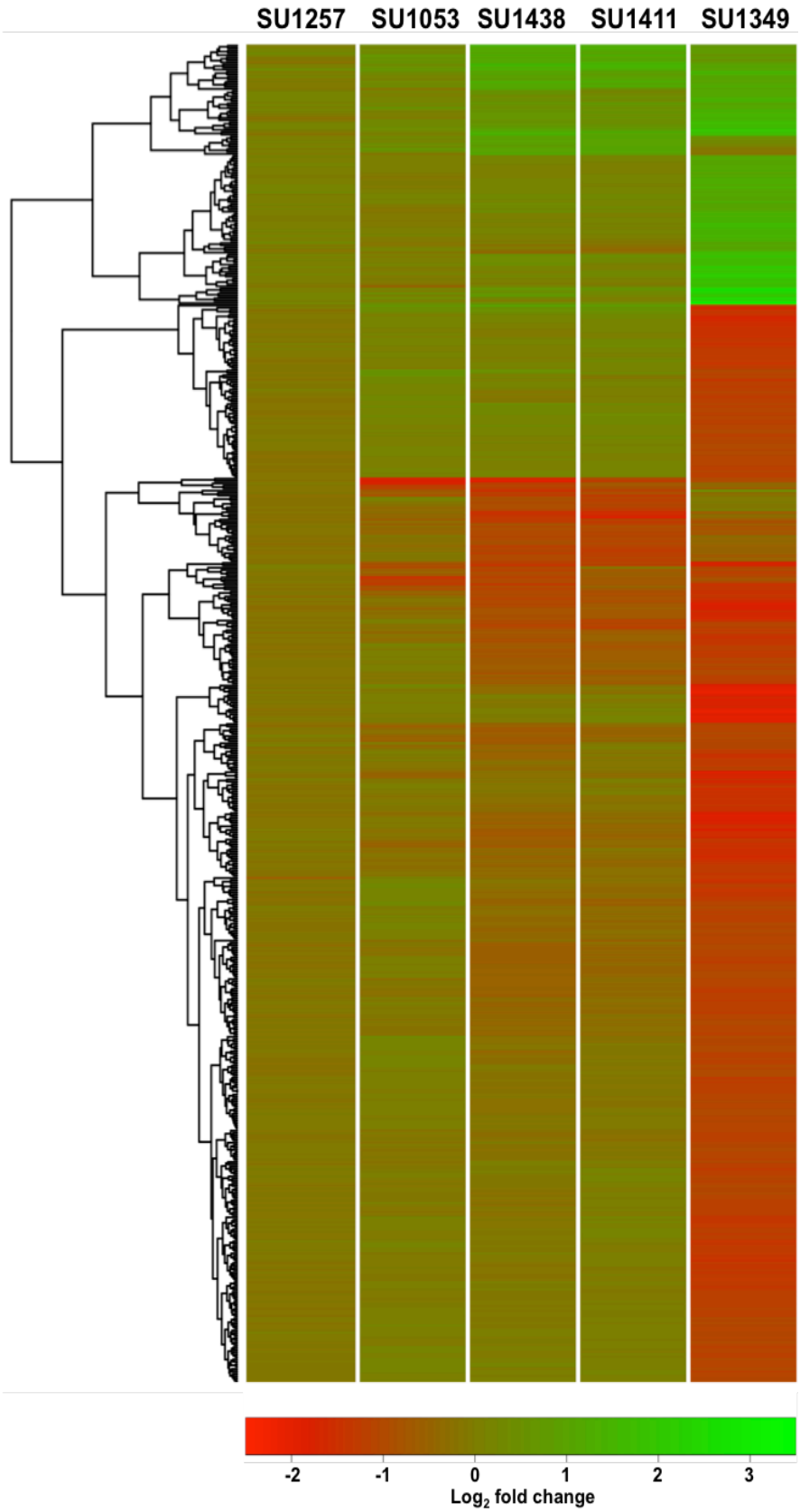

Figure 5.6 Global gene alterations in 556 differentially expressed (DE) genes induced by the SU compounds when compared to UT controls

The probesets of the empirical Bayes moderated t-statistics were labelled with gene symbols and the DE genes located ($p \leq 0.05$ and Log_2 (FC) ≥ 1, in either direction). This generated a list of 556 genes that were DE in at least one of the SU-treated samples when compared to UT controls. The heat map was generated using the 'gplots' package in R Studio and shows the global gene alterations in 556 DE genes.

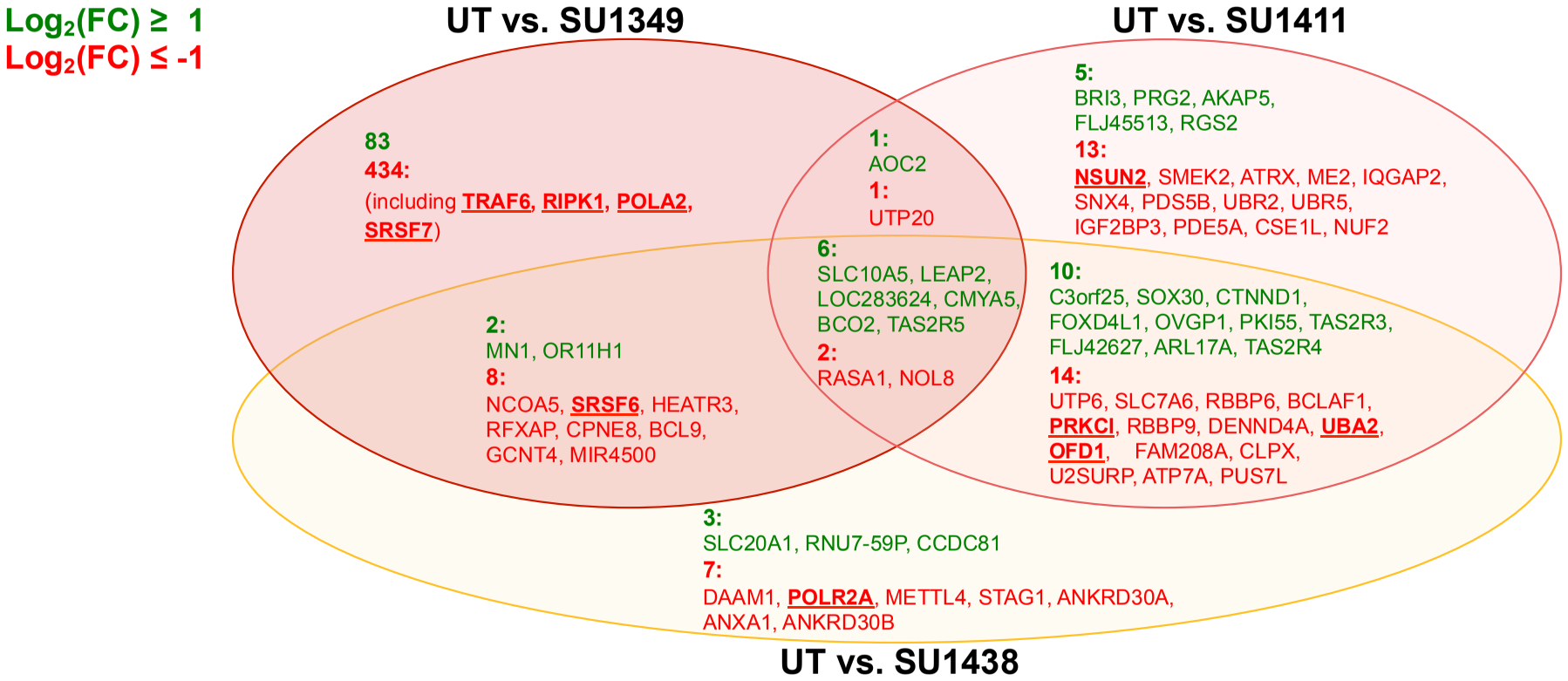

Figure 5.7 Venn diagram showing the identity of differentially expressed (DE) genes for each contrast when Log_2 (FC) ≥ 1 in either direction, and $p < 0.05$ for the three more cytotoxic compounds.

The results of the empirical Bayes moderated t-statistics test were sorted to include only probesets where $p \leq 0.05$ and Log_2 (FC) ≥ 1 in at least one of the contrast groups for UT vs. SU1438, UT vs. SU1411 and UT vs. SU1349. The probesets were labelled with gene symbols to allow identification of DE genes within the microarray data. A multiples comparison test was performed followed by Benjamini-Hochberg correction to investigate the similarities in the DE genes between the cytotoxic compound groups in relation to the untreated control group. The results were plotted in the Venn Diagram. The genes that were upregulated (Log_2 (FC) ≥ 1) are shown in green and down-regulated probesets (Log_2 (FC) ≤ -1) are shown in red. The gene lists were produced using R Studio and the Venn diagram was prepared using Microsoft PowerPoint. Genes of interest that were used for qPCR validation are shown in bold and underlined.

5.1.6. Selection of DE genes to be used for validation in qRT-PCR

The microarray analysis to date revealed qualitative and quantitative changes in gene expression as a result of exposure to the SU compounds. Therefore, DE genes were selected for validation by quantitative RT-PCR using a four-step process:

1. Enrichment analysis of Gene Ontology (GO) terms
2. Pathway enrichment analysis of DE genes
3. Expression levels of the DE genes
4. Specific association of DE genes with the SU compounds, SU1438, SU1411 and SU1349.

5.1.6.1. Enrichment analysis of biological Gene Ontology terms

First, an enrichment analysis of the DE regulated gene lists for SU1438, SU1411 and SU1349 was carried out using the online enrichment tool Enrichr (Chen et al. 2013; Kuleshov et al. 2016). To retrieve the gene lists used in this analysis, the DE genes were separated based on Log_2 (FC). For SU1438 and SU1411, this was a Log_2 (FC) ≥ 1 in either direction but this threshold produced 522 genes for SU1349. This list of DE genes was too long to be used for the enrichment analysis in Enrichr so for SU1349 a cut-off of Log_2 (FC) ≥ 1.5 in either direction was applied. This produced manageable gene lists of 52, 52 and 92 genes for SU1438, SU1411 and SU1349, respectively. The new SU1349 gene list consisting of 92 DE genes can be found in Appendix Table III.

The Gene Ontology (GO) terms for the above lists of genes was analysed using the online tool Enrichr (Chen et al. 2013; Kuleshov et al. 2016). Appendix Figure II shows the number of DE genes associated with the eight GO categories for each treatment condition following sorting of the GO terms using R. Appendix Tables IV, V and VI show the identity of the DE genes for each treatment condition and the number of GO categories each DE gene is involved in. Based on this information, smaller lists of DE genes were selected based on involvement in >7 GO terms or if they were associated with the GO terms: cell cycle, transcription,

signalling or apoptosis. These GO terms were specifically chosen due to their association with NF-κB signalling. This reduced the genes lists to 21, 25 and 41 genes for SU1438, SU1411 and SU1349 respectively. The new DE gene lists are shown in Appendix Table VII for each of the more cytotoxic SU compounds.

5.1.6.2. Pathway profiles for the SU1438, SU1411 and SU1349 GO gene lists

These revised DE gene lists for SU1438, SU1411 and SU1349 were re-inserted into the Enrichr analysis tool and a pathway enrichment analysis was performed. The Appendix Tables VIII, IX and X display the full list of the results for the pathway enrichment analysis for the SU1438, SU1411 and SU1349 DE gene lists, respectively. DE genes were selected for further analysis based on whether they regulated pathways connected to transcription, apoptosis, cell cycle or directly modulated NF-κB signalling. This reduced the gene lists to 8, 6 and 9 genes for SU1438, SU1411 and SU1349, respectively (Appendix Tables XI, XII and XIII).

5.1.6.3. Expression levels of the SU1438, SU1411 and SU1349 DE gene lists

Finally, 10 DE genes that would be used for microarray validation using qRT-PCR were chosen from the final gene lists for these SU compounds. For this, genes were identified based on high expression and fold change (Appendix Tables XI, XII and XIII), and specific association with the SU compounds, SU1438, SU1411 and SU1349. Only those genes that were expressed to a relatively high level in both UT and treated samples were considered for qRT-PCR because this would ensure that these genes would be positively detected.

Figure 5.8 presents a summary of the Log_2 expression of each of the 10 final DE genes that were used for validation of the microarray in the qRT-PCR experiments for all the array groups, including the UT, SU1257 and SU1053 array groups. As can be seen in Figure 5.8, all 10 selected DE genes were highly expressed in UT RPMI8226 cells.

TRAF6, RIPK1, POLA2 and SRSF7 are DE genes specifically associated with the action of SU1349 (Figure 5.7). Figure 5.8 also demonstrates that down regulation of TRAF6 and RIPK1 was specifically related to the action of SU1349, whereas both SU1438 and SU1411 down-regulate POLA2 and SRSF7 genes but to a lesser extent. Although POLR2A was previously shown to be a unique DE gene for SU1438 (Figure 5.7), Figure 5.8 shows that SU1053, SU1411 and SU1349 also down-regulate POLR2A. SRSF6 expression was altered by both SU1438 and SU1349 (when Log_2 (FC) ≥ 1 and $p \leq 0.05$) (Figure 5.7), this is also reiterated in Figure 5.8 where SRSF6 transcription was markedly repressed by SU1438 and SU1349. Treatment with SU1053 and SU1411 also caused a reduction in SRSF6 transcription but to a lesser extent.

PRKCI, OFD1 and UBA2 were differentially down-regulated in response to both SU1438 and SU1411 (Figure 5.7). Figure 5.8 confirms that OFD1, PRKCI and UBA2 were all substantially down-regulated by both SU1438 and SU1411 but remained relatively unaffected following treatment with SU1053 and SU1349. The final selected DE gene was NSUN2, which was found to be a DE gene unique to SU1411 (Figure 5.7). Figure 5.8 shows that SU1411 induced the highest level of down-regulation in NSUN2 transcription but also suggests that SU1438 substantially down-regulated NSUN2 relative to UT controls.

Table 5.2 lists the transcriptional product of each of the 10 chosen DE genes, along with the function of the subsequent protein. Table 5.2 demonstrates that all DE genes chosen have a role in regulating NF-κB activation, apoptotic pathways, DNA replication, transcription or protein modification.

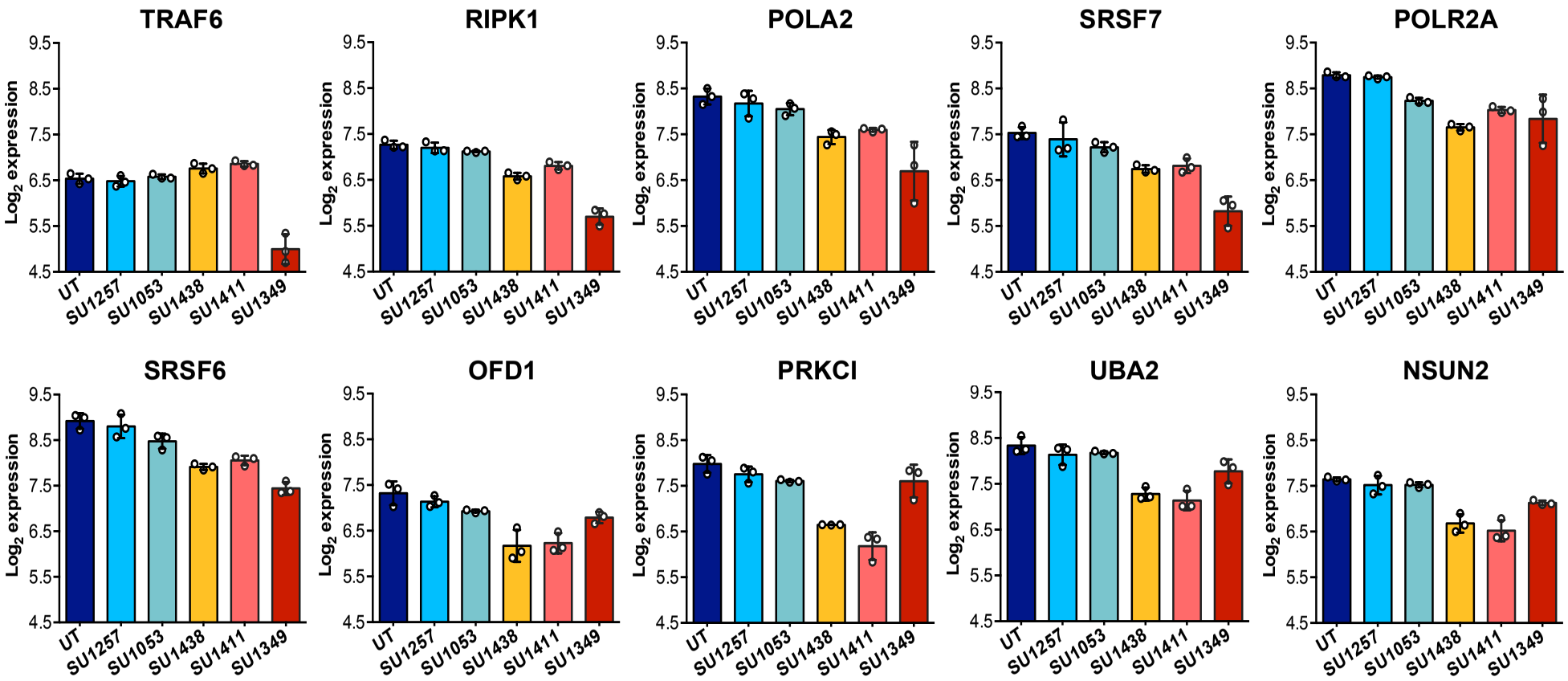

Figure 5.8 Log_2 expression of the 10 differentially expressed (DE) microarray genes selected for validation in qRT-PCR.
The Log_2 expression of 10 selected DE genes in RPMI8226 cells following 4h with and without treatment with SU1438, SU1411 and SU1349. All the selected DE genes produce a Log_2 (FC) ≥ 1 that is significant ($p \leq 0.05$) following treatment with one of cytotoxic compounds relative to the untreated group. Each DE gene has been selected based on its specificity to certain treatment groups and its correlation to NF-κB related pathways and gene ontologies. Errors bars represent SD where n=3. The graphs were constructed using Graphpad Prism 6.0 software.

Table 5.2 The transcriptional product and protein function of the 10 differentially expressed genes selected for validation in qRT-PCR
This table was adapted from the information provided on UniProt database, available at http://www.uniprot.org/uniprot/Q08J23 (The UniProt Consortium 2017).

Gene	Transcriptional product	Protein function
TRAF6	**TNF receptor-associated factor 6**	An E3 ubiquitin ligase that mediates the synthesis of K63-linked-polyubiquitin chains conjugated to proteins. This protein mediates ubiquitination of free/unanchored polyubiquitin chain leading to MAP3K7, NF-κB and JUN activation. As an adapter protein, TRAF6 can mediate signal transduction initiated via TNF receptor, IL-1 receptor and IL-17 receptor. In addition, it regulates osteoclast differentiation by mediating the activation of adapter protein complex 1 and NF-κB, in response to RANKL stimulation.
RIPK1	**Receptor-interacting serine/threonine-protein kinase 1**	RIPK1 is a serine-threonine kinase that transduces inflammatory and cell-death signals following death receptor ligation, activation of pathogen recognition receptors, and DNA damage. Ubiquitination by TRAF2 via K63-link chains acts as a critical enhancer of communication with downstream signal transducers in the MAPK and NF-κB pathways.
POLA2	**DNA polymerase alpha subunit B**	POLA2 may play an essential role at the early stage of chromosomal DNA replication by coupling the polymerase alpha/primase complex to the cellular replication machinery.
SRSF7	**Serine/arginine-rich splicing factor 7**	This protein is required for pre-mRNA splicing but can also modulate alternative splicing in vitro. It may function as export adapter involved in mRNA nuclear export, such as of histone H2A.
POLR2A	**DNA-directed RNA polymerase II subunit RPB1**	POLR2A is a DNA-dependent RNA polymerase that catalyses the transcription of DNA into RNA. It is the largest and catalytic component of RNA polymerase II, which synthesizes mRNA precursors and many functional non-coding RNAs. As a result, Pol II is the central component of the basal RNA polymerase II transcription machinery.
SRSF6	**Serine/arginine-rich splicing factor 6**	SRSF6 plays a role in constitutive splicing and modulates the selection of alternative splice sites. It plays a role in wound healing and in the regulation of keratinocyte differentiation and proliferation via its role in alternative splicing.
OFD1	**Oral-facial-digital syndrome 1 protein**	OFD1 is a component of the centrioles controlling mother and daughter centrioles length and is involved in the biogenesis of the cilium, a centriole-associated function. OFD1 plays an important role in development by regulating Wnt signalling.
PRKCI	**Protein kinase C iota type**	PRKCI is a calcium- and diacylglycerol-independent serine/ threonine-protein kinase that plays a general protective role against apoptotic stimuli. This protein is involved in NF-κB activation, cell survival, differentiation and polarity, and contributes to the regulation of microtubule dynamics in the early secretory pathway.
UBA2	**SUMO-activating enzyme subunit 2**	UBA2 is involved in pathway protein sumoyltaion, which is part of protein modification. It mediates ATP-dependent activation of SUMO proteins followed by formation of a thioester bond between a SUMO protein and a conserved active site cysteine residue on UBA2/SAE2.
NSUN2	**tRNA (cytosine(34)-C(5))-methyltransferase**	This protein is an RNA methyltransferase that methylates tRNAs, and possibly RNA polymerase III transcripts, and may act downstream of Myc to regulate epidermal cell growth and proliferation. NSUN2 is required for proper spindle assembly and chromosome segregation, independently of its methyltransferase activity.

5.2. Validation of the microarray data using qRT-PCR

Primer pairs specific for the 10 target DE genes and an additional endogenous control gene (RSP14) were designed using NCBI/Primer-BLAST (Ye et al. 2012). A representative example of the melting curve and amplification plot for the endogenous control gene and each of the target DE genes are shown in Appendix Figures III – XIII.

The samples used in the qRT-PCR experiments were created from the identical experiments used to generate the TRIzol® lysates for the Affymetrix GeneChip® HTA 2.0. Therefore, they should provide a robust means of validating the microarray data because they were collected from the same RPMI8226 cells under the same treatment conditions at the same time. The TRIzol® lysates were processed to RNA extracts and the RNA integrity of the eluted RNA was checked by CBS at Cardiff University using an Agilent 2100 Bioanalyzer System. Appendix Figure XIV shows that all the processed samples had a RIN ≥ 9.7, which suggests the eluted RNA was of a high quality. The eluted RNA was subsequently reverse transcribed into cDNA and then analysed using specific primers by qRT-PCR.

Figure 5.9 and Figure 5.10 show the fold changes for each of the 10 DE genes following exposure to the five compounds in the SU series: SU1257, SU1053, SU1438, SU1411 and SU1349. Figure 5.9 and Figure 5.10 both show that SU1257 did not significantly alter any of the 10 genes analysed using qRT-PCR. In addition, SU1053 treatment was responsible for significantly down-regulating only SRSF7 expression ($p = 0.021$).

Figures 5.9 and 5.10 shows that qRT-PCR measured a relatively large decrease in TRAF6, RIPK1, POLA2, SRSF7 and SRSF6 expression following treatment with SU1349, although only the down-regulation of TRAF6 expression was significant ($p = 0.034$). An explanation for this may be the large variation between the replicates for SU1349 treatment, which is indicated by the relatively large error bars shown for these genes in Figure 5.10. In addition, Figure 5.10 shows that SU1438 similarly significantly down-regulated TRAF6 expression ($p = 0.041$).

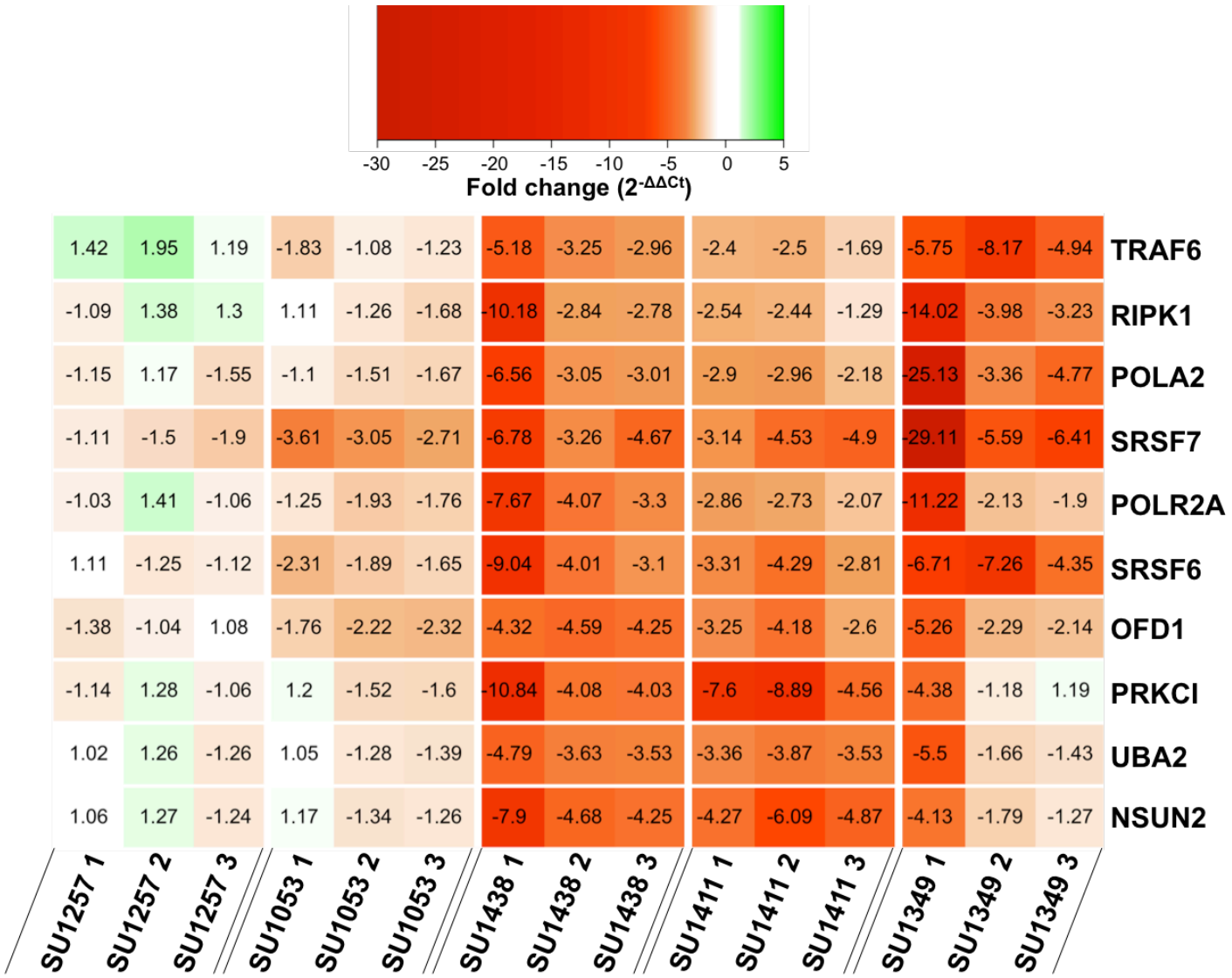

Figure 5.9 Heat map analysis of the 10 DE microarray genes in RPMI8226 cells after 4h treatment with SU compounds using qRT-PCR.

The 10 DE genes picked from the results of the microarray analysis were validated using qRT-PCR. The expression of the DE genes was investigated after RPMI8226 cells were exposed to each SU compound for 4h. The fold changes reported were calculated using the comparative threshold cycle (Ct) method ($2^{-\Delta\Delta Ct}$). The endogenous control used for the calculation was RSP14. A heat map was plotted of the fold change where n = 3, duplicate.

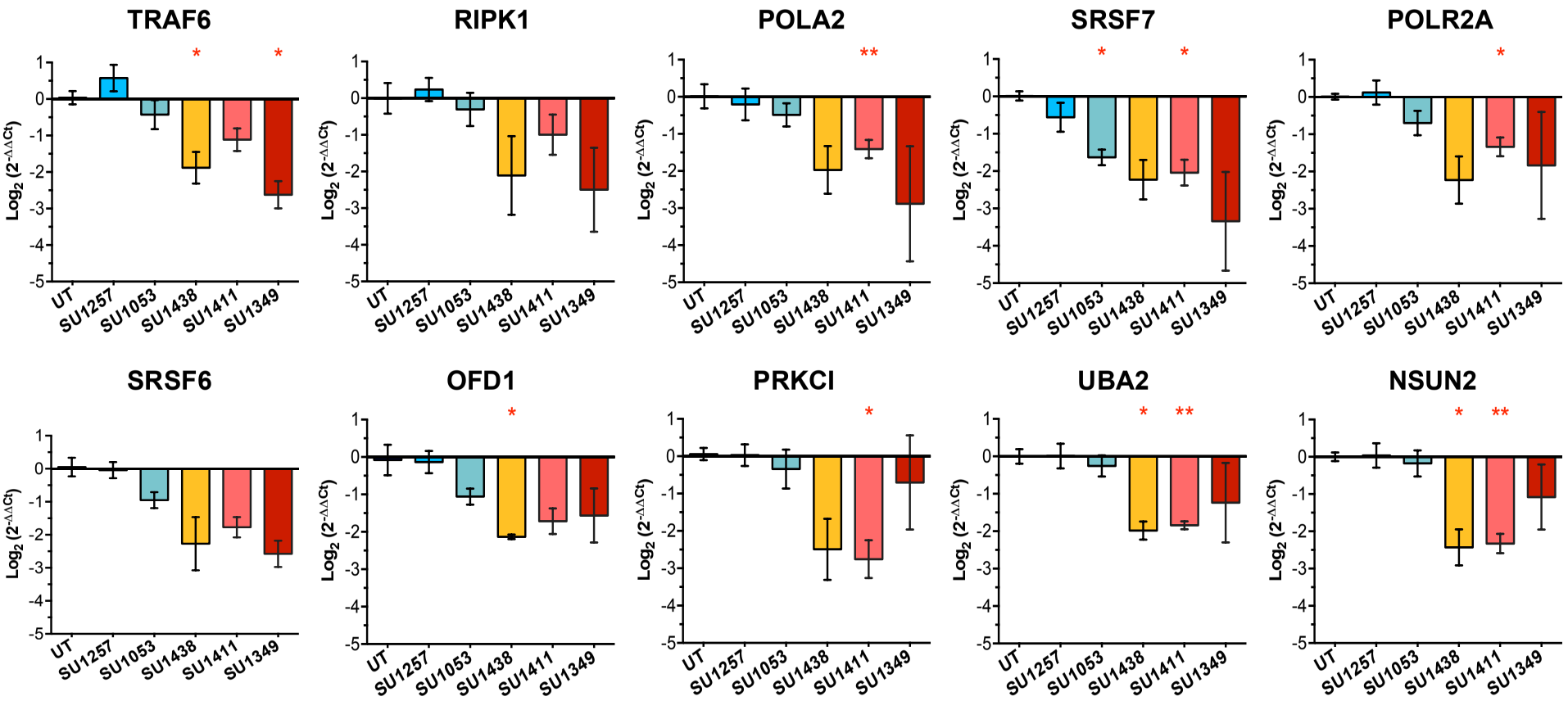

Figure 5.10 Validation of DE microarray genes in RPMI8226 cells after 4h treatment with SU compounds using qRT-PCR.
The fold changes calculated using the $2^{-\Delta\Delta Ct}$ method were averaged and Log_2 transformed. A one-way, paired ANOVA followed by a Dunnet multiple comparisons test was performed using Graphpad Prism 6.0 software to investigate the statistical difference between UT vs. SU compound treated gene expression. Significant results are displayed above the graphs ($p \leq 0.05$ = * and $p \leq 0.01$ = **). Errors bars represent SD where $n = 3$, in duplicate. The graphs were constructed using Graphpad Prism 6.0 software.

Figures 5.9 and 5.10 suggest that SU1438 treatment was also responsible for significantly decreasing the expression of OFD1 (p = 0.040) and NSUN2 (p = 0.041), the latter of which was also significantly down-regulated by SU1411 treatment (p = 0.003). In addition, Figure 5.9 and 5.10 show that SU1411 was also responsible for significantly down-regulating POLA2 (p = 0.005), POLR2A (p = 0.043), SRSF7 (p = 0.018), PRKCI (p = 0.022) and UBA2 (p = 0.008).

The relationship between the microarray gene expression levels and qRT-PCR gene expression levels among the UT and SU compound treated samples was explored to allow validation of the microarray data. Figure 5.11 plots the microarray gene expression (Log_2 expression) and qRT-PCR fold change (Log_2 ($2^{-\Delta\Delta Ct}$)) for each sample group and DE gene.

Figure 5.11 shows that there was a correlation in nine of the 10 genes. The exception was TRAF6 where qRT-PCR did not replicate the expression changes observed in the microarray for the SU series compounds SU1411 and SU1438, and SU1053. This may be due to the difference in the relative sensitivities of the two assays or the differences in the normalisation methods that each assay employs (Morey et al. 2006).

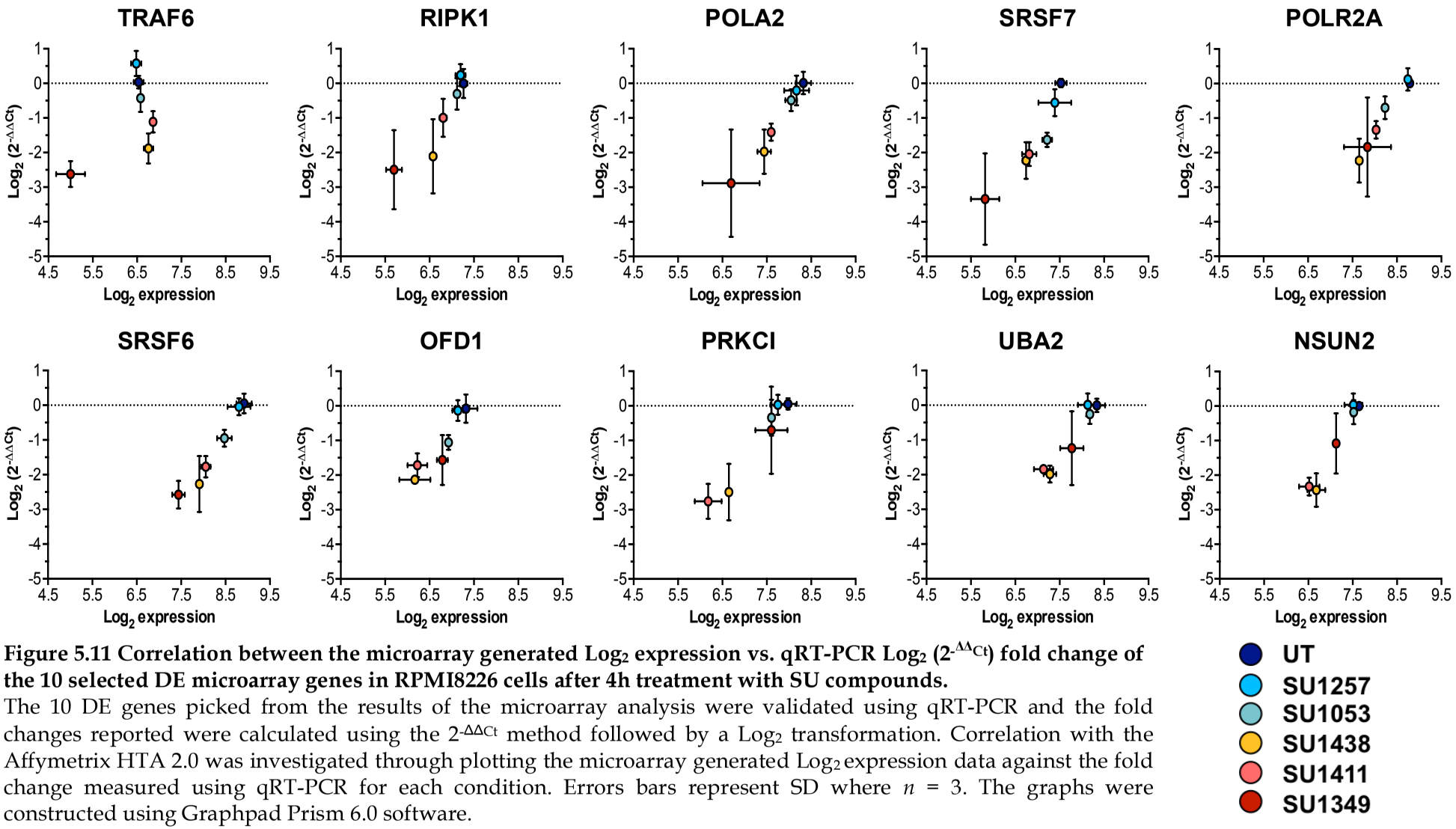

Figure 5.11 Correlation between the microarray generated Log_2 expression vs. qRT-PCR Log_2 ($2^{-\Delta\Delta Ct}$) fold change of the 10 selected DE microarray genes in RPMI8226 cells after 4h treatment with SU compounds.

The 10 DE genes picked from the results of the microarray analysis were validated using qRT-PCR and the fold changes reported were calculated using the $2^{-\Delta\Delta Ct}$ method followed by a Log_2 transformation. Correlation with the Affymetrix HTA 2.0 was investigated through plotting the microarray generated Log_2 expression data against the fold change measured using qRT-PCR for each condition. Errors bars represent SD where n = 3. The graphs were constructed using Graphpad Prism 6.0 software.

5.3. Discussion

The aim of this chapter was to investigate whether individual agents targeted distinct sets of genes or whether a common set of genes was altered by the SU compounds, but perhaps in a quantitatively different fashion. To achieve this, the Affymetrix GeneChip® HTA 2.0 was used to assess global gene expression in untreated RPMI8226 cells and RPMI8226 cells following treatment with SU1257, SU1053, SU1349, SU1411 and SU1438.

5.3.1. Quality control of the microarray experiment

A potential pitfall in microarray-based techniques is the small number of replicates because these experiments are often time-consuming and expensive. Therefore, throughout the process of carrying out the microarray analysis in this thesis, multiple quality control assessments were performed to ensure that variability in the gene expression analysis was minimised. The aim was that this would allow a robust global gene expression analysis to be performed, where any alterations in gene expression identified would be unlikely to have arisen through accidental associations or due to inherent variation caused by poorly controlled experimental conditions.

Variability can arise through three main sources in a microarray-based gene expression analysis: experimental, technical or analytical (Hubank 2004). The Affymetrix GeneChip® HTA 2.0 was carried out on RNA samples from the untreated and treated RPMI8226 cells. The experimental design of a microarray experiment is an important step that is often overlooked in microarray-based studies (Slonim a Yanai 2009). For this reason, careful consideration was given to the selection of the MM cell line to be used and the concentration and exposure time chosen for each SU compound. In addition, all microarray samples were taken on the same day from one MM cell line, ensuring equal passage number, and all samples were prepared at the same time.

To reduce experimental variability, prior to RNA extraction, dose-dependent cytotoxicity in parallel samples was measured at 48h. This was

performed to ensure that the SU compounds were inducing the expected cytotoxic effects so that samples not responding as previously observed were not included in the microarray analysis. This ensured validation of the samples used in the microarray analysis to guarantee that any alterations in gene expression were representative of the inhibitory action of the SU compounds. Appendix Figure I demonstrated that all samples used in the microarray analysis induced the expected cytotoxicity in RPMI8226 cells, based on the characterisation described in Chapter 4.

In addition, the quality of the RNA was measured to ensure that poor RNA quality was not a factor that contributed to technical variation within the microarray analysis. RNA is inherently less stable than DNA and can be affected by many factors, including poor sample preparation and pre-analysis storage. All RNA extracts used in the Affymetrix GeneChip® HTA 2.0 analysis were of the highest quality (RNA integrity = 10), which minimised technical variability.

Once the Affymetrix GeneChip® HTA 2.0 had been performed and the resulting data retrieved as CEL files, all subsequent analysis was performed using the statistical software environment, R (R-Core-Team 2014). R is a highly versatile piece of software that provides a variety of statistical and graphical techniques, and is constantly being developed and refined by leading statisticians. Many packages that are useful in microarray data analysis are available for use in R through Bioconductor, another open-source platform that offers a collection of software packages scripted in the R language for computational biology and bioinformatics (Gentleman et al. 2004). For this reason, R remains one of the most advanced tools for the analysis of microarray-based techniques such as Affymetrix GeneChip® HTA 2.0. However, one disadvantage of R is that it does not have a graphical user interface and instead relies on an understanding of the R programming language to write R scripts to perform statistical and graphical analysis, which can prove to be time consuming.

R was used to first assess the quality of the raw data produced by each of the individual Affymetrix GeneChips to ensure that the measures took to reduce experimental and technical variability had been a success. This confirmed that the 18 separate GeneChip arrays were similar and comparable, which would be expected for arrays derived from an identical cell line. Therefore, this indicated that technical variability had been successfully minimised and the individual sample arrays were comparable, which further validated the microarray-based experiment.

In conclusion, all quality control techniques applied confirmed that experimental and technical variability was minimised appropriately, and verified the use of further graphical and statistical manipulation of the microarray data.

5.3.2. Assessing qualitative and quantitative alterations in gene expression measured by the microarray analysis

The initial step of the microarray analysis in R investigated the global effects of the SU compounds in RPMI8226 cells and determined how the transcriptional effects of the pharmacological agents grouped based on overall gene expression across the whole GeneChip. This indicated that three groups of distinct gene expression changes caused by the SU series of compounds could be clearly identified; (1) SU1349 had the most distinct set of changes indicating a qualitative difference from UT and the other compounds in the gene changes caused, (2) SU1438 and SU1411 caused a change in gene expression when compared to UT but in a distinct way to SU1349 treatment, and (3) SU1053 and SU1257 caused more subtle changes in gene expression with some extra variation in one of the SU1257 samples.

Initial visualisation of the qualitative changes in probesets showed that each SU IKKα inhibitory agent was responsible for indicating DE probesets in RPMI8226 cells, when compared to the untreated group. Moreover, the number of DE probesets correlated with the cytotoxicity of the SU agent in RPMI8226 cells. For example, SU1257 induced the least DE probesets and was relatively non-cytotoxic in RPMI8226 cells. On the other hand, the most cytotoxic SU agent, SU1349, induced the greatest number of

DE probesets in RMPI8226 cells. Overall, this may suggest that some of the DE probesets may be related to genes that contribute to the apoptosis induced by these agents in MM cells despite the samples being taken after just 4h of exposure to SU compound. However, Figure 5.4 showed that SU1438 and SU1411 produce DE volcano plots that were relatively similar in shape and size, which suggests that the quantitative nature of the changes induced by SU1438 and SU1411 may be comparable. Conversely, this may indicate that the DE probesets do not relate to DE genes that are involved in the induction of apoptosis by the SU agents because the cytotoxicity of SU1438 and SU1411 was shown to be significantly different in Chapter 4.

The quantitative nature of the DE probesets induced by each SU agent compared to the untreated group were visualised by plotting a Venn diagram of the number of upregulated and down-regulated probesets (Figure 5.5). As was suggested by the volcano plots, the Venn diagram indicated that the number of DE expressed probesets correlates with the cytotoxicity of the SU compound in RPMI8226 cells. Interestingly, the three most cytotoxic agents, SU1438, SU1411 and SU1349, shared a significant number of the same DE probesets. Moreover, each SU compound possessed unique DE probesets. Therefore, identification of the possible DE genes relating to the DE probesets could indicate specific genes that are involved in the mechanism of action of these agents.

For this reason, the probesets were annotated to their respective human genes. Once annotated, 556 annotated genes were identified as DE by at least one SU compound and Figure 5.6 was plotted to qualitatively assess the global gene alterations induced by the five SU compounds in RPMI8226 cells. Qualitatively, the pattern shown mirrored the pattern observed for the DE probesets in Figure 5.4, in that the number of DE genes increased with the increasing cytotoxicity of the SU compounds.

The number of DE genes induced by the three more cytotoxic SU compounds was assessed in more detail to quantitatively determine the

exact number of DE genes and their identities (Figure 5.7). Quantitatively, these SU compounds down-regulated more genes and DE genes were both shared and unique for each SU compound. Moreover, the most DE genes were shared by both the SU1438 and SU1411. Chapter 4 showed that both agents possessed a relatively similar inhibitory profile so the fact that they shared a relatively high number of DE genes could be indicative of their shared mechanism of action. Interestingly, SU1438 relative to SU1411 shared more DE genes with SU1349, although these compounds have significantly different cytotoxic potential and inhibitory profiles.

The number of genes that were differentially regulated by SU1349 was significantly much higher than the number regulated individually by both SU1438 and SU1411. Quantitatively, this may indicate that the increased kinase inhibitory potency for CDK9, shown in Chapter 4, could be responsible for inducing a higher number of DE genes. However, it is more likely that the increased number of DE genes may also be explained by SU1349 having more off-target effects than predicted in the inhibitory profile, which contributes to its increased cytotoxic potential in MM cells. SU1053 was shown in Chapter 4 to possess a similar inhibitory profile to SU1349, although it induced substantially less cytotoxicity in RPMI8226 cells. This chapter has shown that number of genes that were differentially regulated by SU1349 was significantly much higher than the number regulated individually by SU1053. Therefore, it seems likely that the relatively increased cytotoxicity of some of the SU compounds is likely to arise because of off-target inhibitory effects.

In conclusion, the gene expression analysis revealed qualitative and quantitative changes in gene expression that were both shared among the SU agents and that were unique to each SU agent. Overall, the pattern that emerged was that an increase in the number of DE probesets or the number of DE genes, correlated with the cytotoxicity of that SU agent in RPMI8226 cells. However, it is likely that the cytotoxicity induced by these agents is caused, at least in part, because of off-target kinase inhibitory effects.

5.3.3. Assessing qualitative and quantitative alterations in gene expression measured by the microarray analysis

The quantitative and qualitative changes in global gene expression that were revealed by the analysis required validation using a smaller and more reproducible technique. The technique that was chosen to validate the microarray analysis was quantitative RT-PCR. Data verification using a method such as qRT-PCR is recommended for use with microarray analysis (Hubank 2004). Therefore, to validate the microarray analysis using qRT-PCR, a small selection of 10 representative DE genes belonging to the SU1438, SU1411 and SU1349 contrasts were selected.

The DE genes to be used in the qRT-PCR validation were chosen based on four main factors; gene ontology, pathway profiles, expression levels and association with specific SU compounds. The online enrichment tool, Enrichr, was chosen to be used in the microarray analysis because this tool is relatively newer than other available enrichment tools and has a database that is frequently updated (Kuleshov et al. 2016). In addition, Enrichr provides a variety of in depth enrichment information on the gene lists inserted and has a relatively friendly user interface. One of the drawbacks of using this tool was that the SU1349 vs. untreated contrast (522 genes) was too large to be used to select qRT-PCR genes due to the list being too comprehensive to insert into the Enrichr tool. Therefore, further filtering (Log_2 (FC) ≥ 1.5, in either direction) was required to reduce the SU1349-regulated gene list. Although this allowed creation of a more manageable list (92 genes), it resulted in the exclusion of many DE genes. Shortening the SU1349 DE gene list also reduced the comparability with the SU1438 and SU1411 compounds' DE gene lists, which were created using the initial filtering (Log_2 (FC) ≥ 1, in either direction) and were of a more manageable size (52 and 52 genes, respectively).

The 10 selected DE genes were used in qRT-PCR experiments that analysed the level of these genes in RPMI8226 cells, following treatment with SU1257, SU1053, SU1411, SU1438 and SU1349. To reduce experimental and technical variation the samples used in the qRT-PCR experiments were created from the identical experiments used to generate the TRIzol® lysates

for the Affymetrix GeneChip® HTA 2.0. Therefore, ensuring a robust validation of the microarray analysis using matched samples. As a further quality assurance, the quality of the RNA was checked and this was found to be of a high quality, where RIN ≥ 9.7. This was slightly less than the quality of the RNA used within the microarray analysis (RIN = 10). This may be a consequence of the longer storage time of the RNA whilst the microarray computational analysis was taking place, which may have resulted in a slight loss in RNA stability and quality.

Overall, the results of the qRT-PCR indicated that this technique successfully validated the microarray analysis because similar gene expression changes were observed for the same set of 10 DE microarray genes in both experiments. Moreover, when the relationship between the microarray gene expression levels and qRT-PCR gene expression levels among the UT and SU compound treated samples was explored, this indicated that there was a correlation in nine of the 10 genes. The exception was TRAF6 where qRT-PCR did not replicate the expression changes observed in the microarray for the SU series compounds SU1411 and SU1438, and SU1053.

In conclusion, the qRT-PCR successfully validated the microarray analysis and demonstrated that variability in gene expression following treatment with the SU agents in RPMI8226 cells was most likely due real biological regulation by these agents. Therefore, this study has produced the first high quality microarray dataset analysing the use of novel IKKα inhibitors in MM.

5.3.4. Final conclusions

This chapter has successfully highlighted that the SU compounds differentially regulate the expression of multiple genes; some which were shared and some were unique to specific agents. In addition, it was shown that an increased amount of DE genes was associated with the increase in cytotoxicity of an SU agent in RPMI8226 MM cells. However, the data presented in this chapter has also indicated that the effects of the SU

compounds is more likely to be due to off-target kinase inhibition rather than direct NF-κB inhibition.

The quality control carried out throughout the course of the microarray analysis has also been successful in reducing variability and was shown to have contributed to producing a high-quality microarray dataset. The selection of 10 DE genes from the microarray data were validated using qRT-PCR and this further verified the quality of the dataset. As a result, this study has produced the first high quality microarray dataset analysing the use of novel IKKα inhibitors in MM. Therefore, the work undertaken in this thesis chapter lays the groundwork for further research into the global gene expression regulation of the SU IKKα inhibitory agents SU1257, SU1053, SU1438, SU1411 and SU1349 in the MM cell line RPMI8226.

Chapter 6 – Evaluation of a novel NIK inhibitor for the treatment of multiple myeloma

NF-κB inducing kinase (NIK) is a MAP3K-related protein kinase that activates NF-κB mainly through the phosphorylation of IKKα, which predominantly results in non-canonical NF-κB pathway signalling (Malinin et al. 1997; Ling et al. 1998). NIK is also capable of phosphorylating IKKβ to activate the canonical pathway but NIK has less affinity for this IKK so IKKα is the preferred substrate (Ling et al. 1998; Senftleben et al. 2001). In normal cells, NIK is present at undetectable levels due to TRAF3, which is a negative regulator of NIK (Liao et al. 2004). TRAF3 interacts with NIK to induce the proteasomal degradation of NIK, which mainly inhibits non-canonical NF-κB pathway signalling but may additionally negatively regulate canonical pathway signalling (Liao et al. 2004; Zarnegar et al. 2008).

Several studies have documented that MM tumours and cell lines possess a high number of genetic aberrations leading to NIK overexpression and stabilisation (Annunziata et al. 2007; Keats et al. 2007; Demchenko et al. 2010). This is a result of inactivating mutations in negative regulators of NIK, such as TRAF3, and activating mutations in NIK and positive regulators of NIK, such as CD40. The overexpression of NIK in MM contributes to the increased NF-κB signalling observed because higher constitutive levels of NIK allows the phosphorylation of both IKKα and IKKβ resulting in both non-canonical and canonical NF-κB pathway signalling (Annunziata et al. 2007; Keats et al. 2007; Demchenko et al. 2010).

TRAF3 deficiency has been shown to substantially enhance the survival of B cells (Xie et al. 2007; Gardam et al. 2008). Furthermore, the enhancement in survival was associated with the stabilisation and subsequent overexpression of NIK that allows constitutive activation of non-canonical pathway signalling independent of external stimuli (He et al. 2006).

Moreover, the knockdown of NIK expression in MM cell lines that expressed a high level of NIK protein induced cell apoptosis; the same effect was not observed in those cell lines that contained a low level of NIK

expression (Annunziata et al. 2007). This supports the concept that NIK overexpression contributes to increased survival and tumourigenesis in MM cells and MM cells with high NIK levels are dependent on NIK. The survival signals induced by NIK are likely to be through activation of both the canonical and non-canonical NF-κB pathway signalling (Annunziata et al. 2007; Demchenko et al. 2010).

Deletion or inactivating mutations of the TRAF3 gene are common events in MM and are a characteristic of the RPMI8226 and U266B1 MM cell lines (Annunziata et al. 2007; Keats et al. 2007; Demchenko et al. 2010). U266B1 cells possess a frame-shift mutation in TRAF3 that results in the transcribed TRAF3 protein lacking the functioning NIK-binding domain. On the other hand, the TRAF3 protein is undetectable in RPMI8226 cells due to a bi-allelic deletion of TRAF3. The TRAF3 deficiency present in both of these MM cell lines has been shown to contribute to their relatively high level of NF-κB activity (Annunziata et al. 2007; Keats et al. 2007; Demchenko et al. 2010). Furthermore, the JJN3 cell line possesses an activating unbalanced rearrangement of NIK that results in a NIK protein that lacks the TRAF3-binding domain (Annunziata et al. 2007; Keats et al. 2007; Demchenko et al. 2010). This means that, although TRAF3 is still expressed to a high level in JJN3 cells, the mutant NIK protein is unable to interact with TRAF3 and this gives rise to both NIK overexpression and increased NF-κB activity (Annunziata et al. 2007; Keats et al. 2007; Sasaki et al. 2008; Demchenko et al. 2010).

The over expression of NIK in U266B1, RPMI8226 and JJN3 MM cell lines likely contributes to their relatively increased NF-κB activity when compared to H929 as this is a MM cell line that does not possess NIK activating mutations (Annunziata et al. 2007; Keats et al. 2007; Demchenko et al. 2010).

Therefore, my hypothesis was that the use of a novel NIK inhibitor, CW15337, may represent a promising strategy for the treatment of MM, particularly in the context of NIK activation. The specific aims of this chapter

were to evaluate the use of this pharmacological agent in terms of cytotoxicity, regulation of Mcl-1 expression and effect on NF-κB activity in the four MM cell lines, each representing different clinical features of MM. In addition, the relative effects of CW15337 on the transcription of genes that were significantly altered following exposure to the IKKα inhibiting SU compounds were also investigated.

6.1. Cytotoxicity of CW15337 in MM cell lines

NIK overexpression as a result of TRAF3 deficiency has been shown to enhance B cell survival through constitutive activation of the non-canonical NF-κB pathway that is independent of ligand activation (He et al. 2006; Xie et al. 2007; Gardam et al. 2008). Moreover, Annunziata *et al.* demonstrated that MM cell lines that overexpress NIK were sensitive to apoptosis induced by knockout of NIK (Annunziata et al. 2007). This suggests that NIK overexpression contributes to MM cell survival and MM cells with NIK overexpression become dependent on NIK for their survival. Additionally, several studies have demonstrated that NIK inhibition induces apoptosis in MM cell lines (Demchenko et al. 2014; Takeda et al. 2016). Therefore, the cytotoxicity of the novel NIK inhibitor, CW15337, was investigated in the four MM cell lines, H929, U266B1, RPMI8226 and JJN3, to investigate whether sensitivity to apoptosis would vary according to the TRAF3 and NIK status of each MM cell line.

Each MM cell line was incubated with increasing concentrations of CW15337 ranging from 0.5μM to 10μM. At 48h, MM cells were harvested and washed in PBS before being labelled with Annexin V-FITC and PI. The labelled cells were then analysed using flow cytometry to determine the percentage of apoptosis (Annexin V^+/PI^- + Annexin V^+/PI^+ + Annexin V^-/PI^+) occurring at each CW15337 concentration. Figure 6.1 shows the cytotoxicity of CW15337 at 48h in each MM cell line and the results shown are collated from three independent experiments.

Figure 6.1 shows that the novel NIK inhibitor induced cytotoxicity in a concentration-dependent manner in all of the MM cell lines analysed.

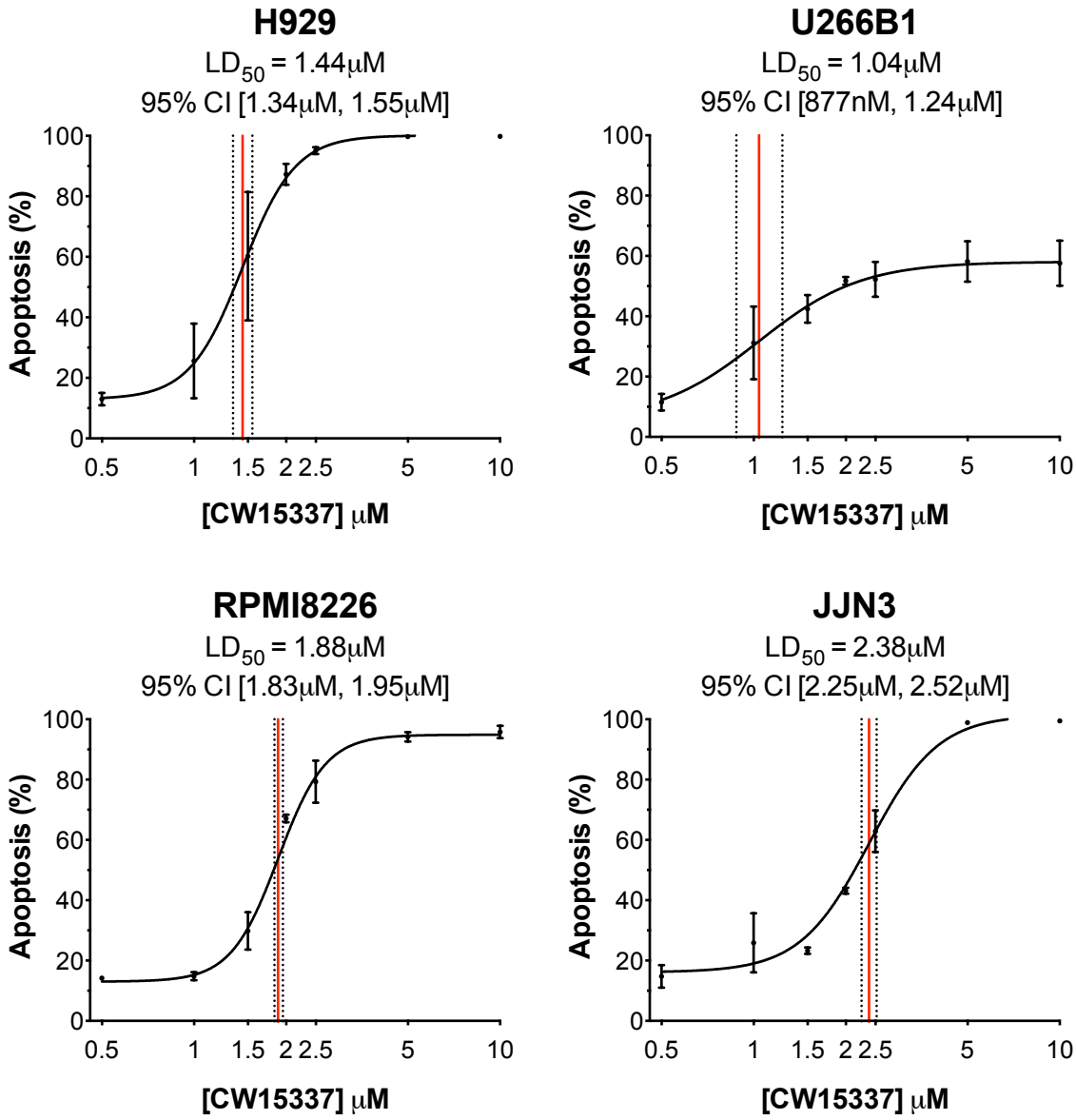

Figure 6.1 The cytotoxicity of the NIK inhibitor CW15337 at 48h in MM cell lines. The MM cell lines H929, U266B1, RPMI8226 and JJN3 were treated with increasing concentrations of CW15337 between 0.5μM and 10μM. At 48h, cell death was measured using Annexin V/PI positivity on an Accuri C6 flow cytometer. The percentage of apoptotic cells at each concentration of CW15337 was then calculated and dose-response curves were constructed using GraphPad Prism 6.0. LD_{50} values were interpolated and are reported for each cell line alongside 95% CI. Error bars represent mean ± SD, where n = 3, triplicate.

Comparison of the LD_{50} values for each MM cell line shows that JJN3 was the most resistant cell line to apoptosis induced by CW15337 (LD_{50} = 2.38μM, 95% CI [2.25μM, 2.52μM]). The LD_{50} values for H929 (LD_{50} = 1.44μM, 95% CI [1.34μM, 1.55μM]) and RPMI8226 (LD_{50} = 1.88μM, 95% CI [1.82μM, 1.94μM])

are relatively similar and represent a relatively intermediate level of sensitivity to apoptosis in response to CW15337.

Based on LD_{50} value alone, U266B1 (LD_{50} = 1.04μM, 95% CI [887nM, 1.24μM]) was the most sensitive MM cell line to cytotoxicity induced by CW15337. However, Figure 6.1 shows that the dose-response curve for U266B1 plateaued at a level of apoptosis of 57.6% ± 7.52% at 10μM compared to the peak apoptosis for H929, RPMI8226 and JJN3 at 10μM (99.8% ± 0.1%, 95.8% ± 2.0% and 99.4% ± 0.4%, respectively). This could either suggest a subset of cells within the U266B1 cell line that are inherently resistant to cytotoxicity induced by CW15337 or that there was a technical issue with the Annexin-V/PI labelling of this cell line.

Therefore, to further explore this phenomenon, the raw flow cytometric data plots were investigated in more detail. Figure 6.2 shows a representative example of the collected raw data used to create the dose-response curve shown for U266B1 in Figure 6.1. The first panel of scatter plots in Figure 6.2 shows the gating that was used to identify viable and apoptotic U266B1 cells based on their FSC-A and SSC-A profiles. The second panel shows the corresponding scatter plots of Annexin-V-FITC-H and PI-H that are used to more specifically evaluate cytotoxicity (Annexin V^+/PI^- (Q2-LR) + Annexin V^+/PI^+ (Q2-UR) + Annexin V^-/PI^+ (Q1-UL)).

Figure 6.2 highlights the inconsistency between the FSC-A and SSC-A profiles and the corresponding scatter plots of Annexin-V-FITC-H and PI-H in the U266B1 cell line following treatment with CW15337. The FSC-A and SSC-A profiles shown in Figure 6.2 indicate that U266B1 cells experience a more prominent dose-dependent increase in apoptosis induced by CW15337 than was shown in Figure 6.1. The FSC-A and SSC-A profile for U266B1 cells treated with 10μM CW15337 shows that 94.1% of U266B1 cells had undergone FSC-A and SSC-A changes consistent with the induction of apoptosis. In contrast, the corresponding scatter plot of Annexin-V-FITC-H and PI-H in Figure 6.2 indicates that only 55.7% of U266B1 cells were apoptotic after 48h treatment with 10μM CW15337.

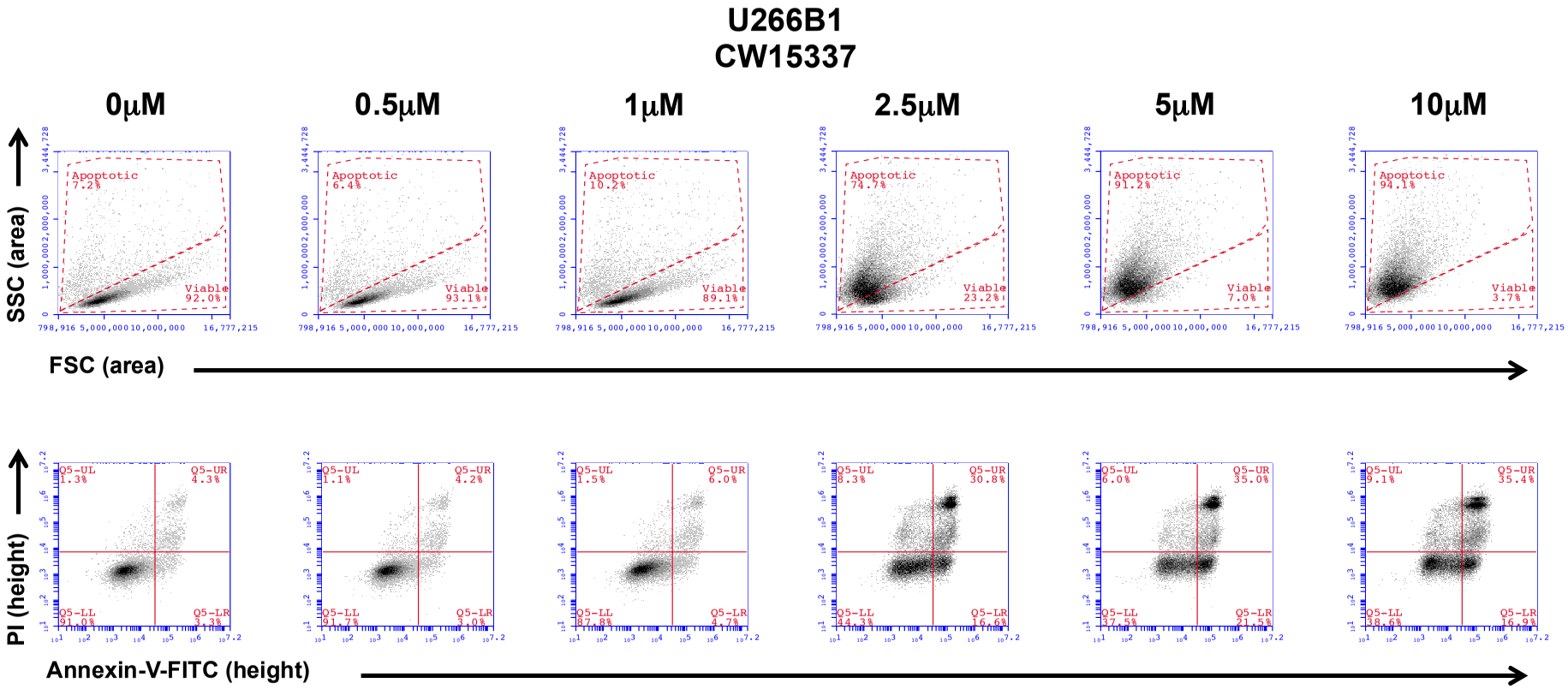

Figure 6.2 Flow cytometric data of the MM cell line U266B1 after 48h incubation with increasing concentrations of CW15337.
The MM cell line U266B1 was treated with increasing concentrations of the NIK inhibitor CW15337 between 0.5μM and 10μM. At 48h, U266B1 cells apoptosis was measured using Annexin V/PI positivity on an Accuri C6 flow cytometer and representative examples of the collected flow cytometric data are shown above. The first panel of scatter graphs shows examples of the gating set up to identify viable and apoptotic U266B1 cells based on their forward scatter (FSC-A) and side scatter (SSC-A) profiles. The second panel shows the corresponding scatter plots of Annexin-V-FITC-H and PI-H that are used to more specifically evaluate cytotoxicity. The percentage of apoptosis was quantified using Annexin V^+/PI^- (Q2-LR) + Annexin V^+/PI^+ (Q2-UR) + Annexin V^-/PI^+ (Q1-UL).

In conclusion, Figure 6.2 suggests that it was more likely an issue with the Annexin V-FITC and PI staining used to assess cell apoptosis in the U266B1, which resulted in an underestimation of the cytotoxicity of CW15337 as calculated in Figure 6.1. There was no evidence to support the notion of a resistant sub-population of U266B1 cells.

For this reason, the cytotoxicity of CW15337 in all MM cell lines was reassessed by calculating the percentage of apoptotic cells at 48h based on the FSC-A and SSC-A profiles measured by flow cytometry. The data used for calculating FSC-A and SSC-A apoptosis corresponds to the same three independent experiments that were used to create Figure 6.1.

Overall, the LD_{50} values obtained through both the FSC-A and SSC-A viability method and the Annexin-V/PI positivity method were similar for the MM cell lines H929, RPMI8226 and JJN3 (Table 6.1). In addition, Figure 6.3 shows that a linear regression analysis of LD_{50} values calculated using Annexin V/PI positivity and FSC-A and SSC-A apoptosis produced a correlation with a high linearity ($r^2 = 0.79$). This indicates that both methods show strong concordance and it was appropriate to evaluate the cytotoxic effects if CW15337 using the FSC-A and SSC-A method.

Therefore, Figure 6.4 shows the resulting dose-response curves plotted for each MM cell line using the FSC-A and SSC-A method of calculating apoptosis at each concentration of CW15337. Figure 6.4 shows that CW15337 was cytotoxic in all the MM cell lines after 48h treatment in a dose-dependent manner. Figure 6.4 shows that in H929, U266B1, RPMI8226 and JJN3 cells, CW15337 induces a relatively similar maximum apoptosis at 10μM (99.5% ± 0.1%, 94.9% ± 2.7%, 98.1% ± 0.9% and 99.5% ± 0.1%, respectively).

Table 6.1 Comparison between the LD_{50} values calculated using the FSC-A and SSC-A apoptosis method and the Annexin-V/PI positivity method of assessing apoptosis. The LD_{50} values for each of the two methods are shown for the H929, U266B1, RPMI8226 and JJN3 MM cell lines alongside 95% CI.

	Annexin V/PI positivity	FSC-A and SSC-A apoptosis
H929	LD_{50} = 1.44μM 95% CI [1.43μM - 1.55μM]	LD_{50} = 1.49μM 95% CI [1.39μM - 1.60μM]
U266B1	LD_{50} = 1.04μM 95% CI [877nM - 1.24μM]	LD_{50} = 1.52μM 95% CI [1.35μM - 1.71μM]
RPMI8226	LD_{50} = 1.88μM 95% CI [1.83μM - 1.95μM]	LD_{50} = 1.87μM 95% CI [1.80μM - 1.95μM]
JJN3	LD_{50} = 2.38μM 95% CI [2.25μM - 2.52μM]	LD_{50} = 2.73μM 95% CI [2.60μM - 2.87μM]

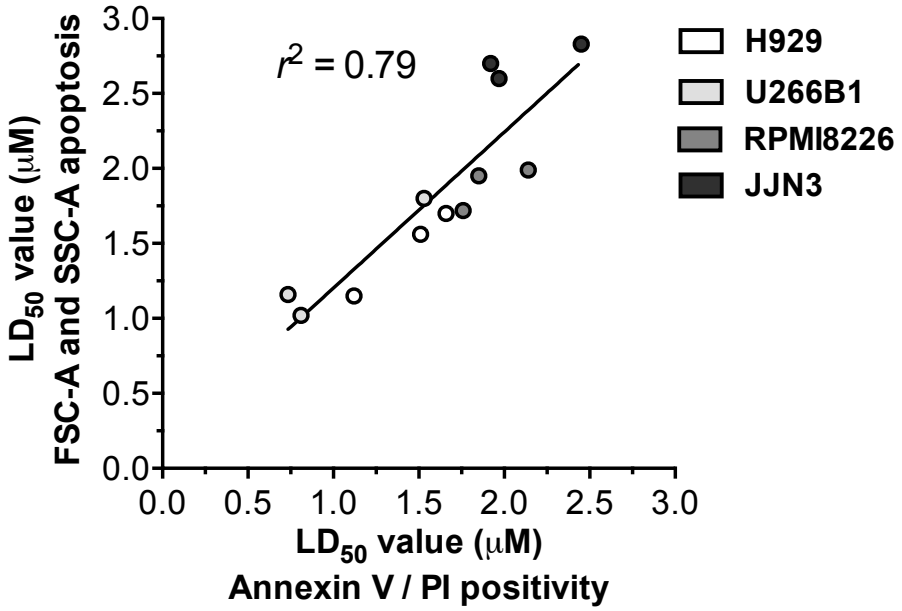

Figure 6.3 Correlation of the LD_{50} values calculated using the Annexin-V/PI positivity and the FSC-A and SSC-A apoptosis method.
The correlation between the LD_{50} values calculated using the Annexin-V/PI positivity and those calculated using the FSC-A and SSC-A apoptosis method was explored for the MM cell lines H929, U266B1, RPMI8226 and JJN3 using a linear regression analysis in Graphpad Prism 6.0. The points plotted represent the LD_{50} values calculated for each cell line using each method (n = 3). The resulting linearity (r^2) is reported alongside the graph.

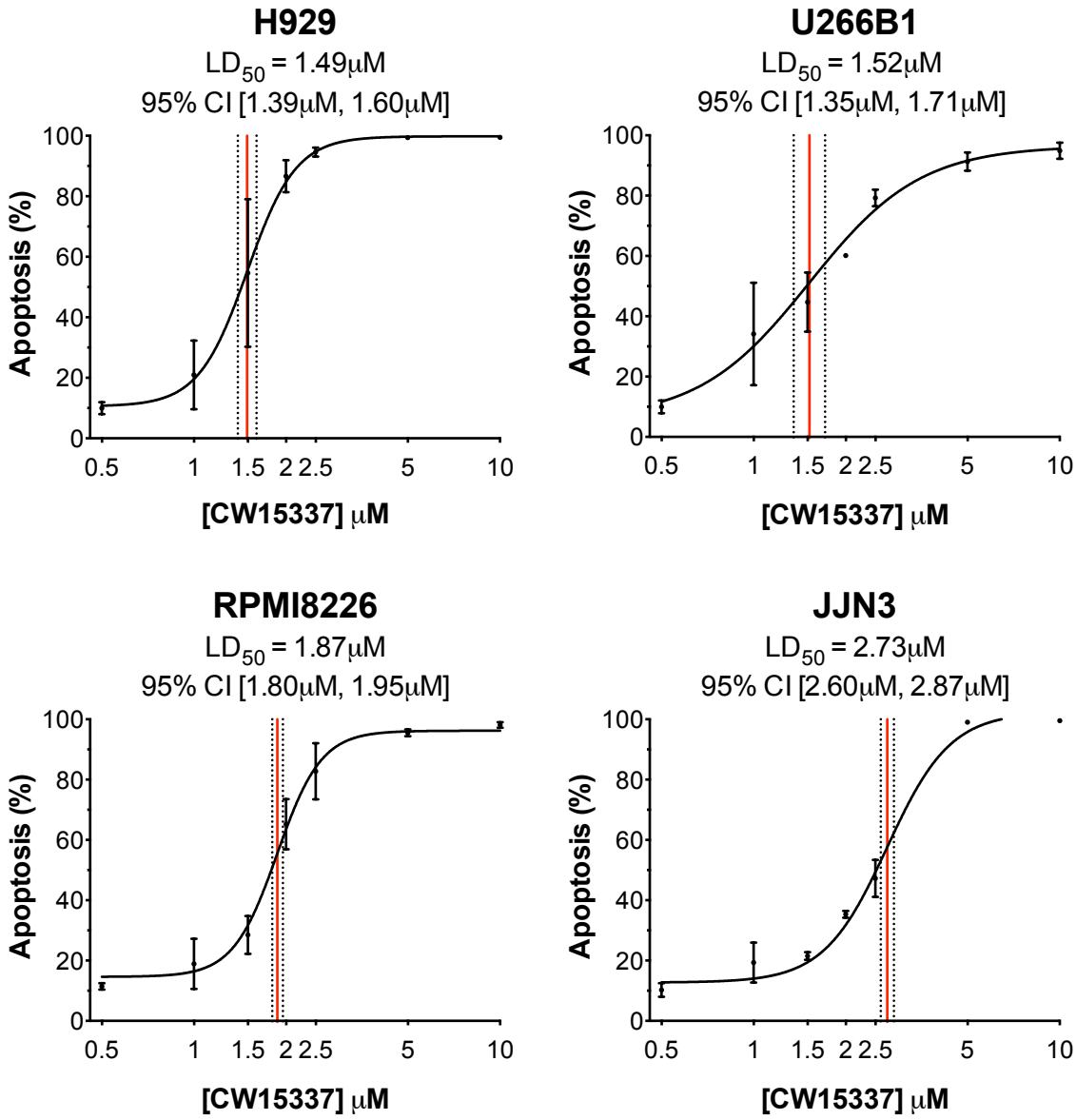

Figure 6.4 The cytotoxicity of CW15337 at 48h in the MM cell lines H929, U266B1, RPMI8226 and JJN3 when FSC-A and SSC-A are used to calculate apoptosis.
The data shown in Figure 6.1 was re-analysed so that cell death was measured as a percentage of apoptotic cells at each concentration based on FSC-A and SSC-A gating. The percentage of apoptotic cells at each concentration of CW15337 was input into GraphPad Prism 6.0 and dose-response curves were constructed. LD_{50} values were interpolated and are reported for each cell line alongside 95% CI. Error bars represent mean ± SD, where n = 3, triplicate.

Comparison of the LD_{50} values in Figure 6.4 indicates that H929 (LD_{50} = 1.49μM, 95% CI [1.39μM - 1.60μM]) and U266B1 (LD_{50} = 1.52μM, 95% CI [1.35μM - 1.71μM]) cell lines experience a relatively high sensitivity to apoptosis induced by CW15337 whereas the RPMI8226 cell line (LD_{50} = 1.87μM, 95% CI [1.80μM - 1.95μM]) has relatively more resistance to

apoptosis induced by CW15337. The LD_{50} value shown in Figure 6.4 for the JJN3 cell line (LD_{50} = 2.73μM, 95% CI [2.60μM - 2.87μM]) suggests that this MM cell line is the most resistant to apoptosis induced by CW15337.

The relative sensitivity of each MM cell line to CW15337 is summarised in Figure 6.5, which shows the mean LD_{50} values alongside 95% CI generated using FSC-A and SSC-A method of calculating apoptosis for each MM cell line. In addition, a one-way ANOVA followed by a Tukey's multiple comparison test was performed on the data to investigate the statistical difference between the LD_{50} values calculated for each MM cell line. Figure 6.5 shows that H929 and U266B1 cells do not experience a significantly different sensitivity to apoptosis induced by CW15337 (p = 0.921). Furthermore, the LD_{50} value interpolated for the RPMI8226 cell line compared to that of the U266B1 cell line was also not significantly different (p = 0.125). However, Figure 6.5 also shows that the LD_{50} value calculated for the JJN3 cell line is significantly higher than the LD_{50} value of the RPMI8226 cell line in response to CW15337 treatment (p = 0.023).

In conclusion, CW15337 was cytotoxic at 48h in all MM cell lines tested. For the MM cell lines H929, RPMI8226 and JJN3, the level of apoptosis calculated by both Annexin V-FITC and PI staining (Figure 6.1) and FSC-A and SSC-A profiles (Figure 6.4) showed a strong correlation (r^2 = 0.84) (Figure 6.3). However, Figure 6.1, 6.2 and 6.4 indicate that there was an issue with the Annexin V-FITC and PI staining used to calculate the cytotoxicity specifically in the U266B1 cell line in response to CW15337. To more accurately assess the cytotoxicity of the NIK inhibitor in U266B1 cells, and to more reliably compare the relative cytotoxic effects on the four cell lines, the FSC-A and SSC-A profiles were used to calculate apoptosis. By this method it was revealed that the H929, U266B1 and RPMI8226 MM cell lines shared a similar sensitivity to apoptosis induced by CW15337 (Figure 6.4 and Figure 6.5).

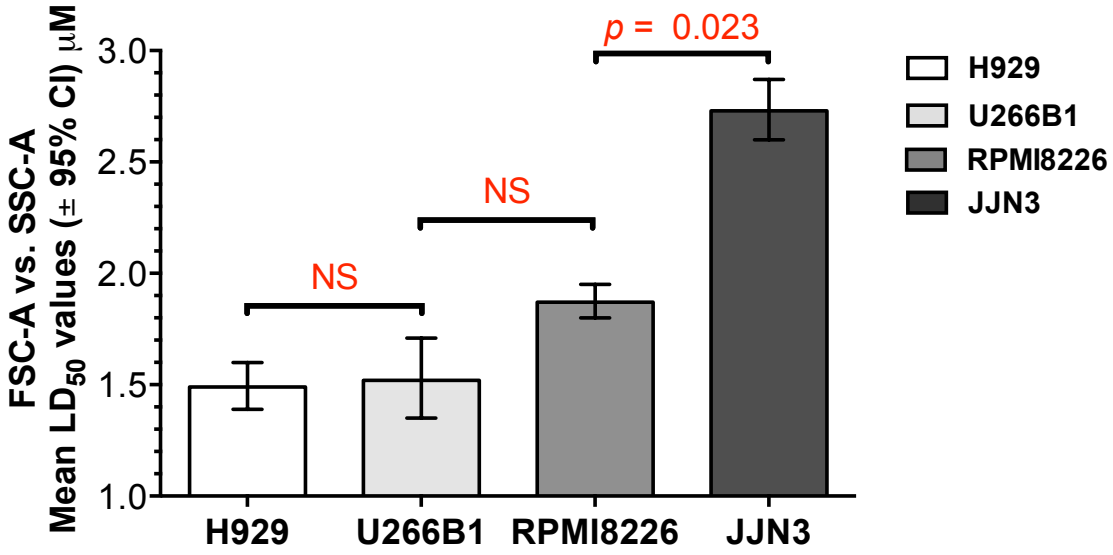

Figure 6.5 A summary of the relative sensitivity of each MM cell line to apoptosis induced by CW15337.

The mean LD_{50} values generated through the FSC-A and SSC-A method of assessing apoptosis are shown for the MM cell lines H929, U266B1, RPMI8226 and JJN3 in response to increasing concentration of CW15337 for 48h. The results shown were interpolated using the dose-response curves in Figure 6.4 using Graphpad Prism 6.0. The values reported represent mean LD_{50} values ± 95% CI (μM) where n = 3, triplicate. A one-way ANOVA followed by a Tukey's multiple comparison test was performed using Graphpad Prism 6.0 software to investigate the significant difference between the LD_{50} values calculated for the indicated cell lines.

6.2. CW15337 regulation of Mcl-1 expression in MM cell lines

In myeloma cells, Mcl-1 expression plays a critical role in maintaining cell viability (Derenne et al. 2002; Zhang et al. 2002). Furthermore, high expression of Mcl-1 in cancer cell lines has been linked to constitutively high NF-κB activity (Liu et al. 2014). In addition, previous studies have demonstrated that inhibition of NF-κB activity is accompanied by the down regulation of Mcl-1 expression in MM cell lines and may precede the activation of apoptotic pathways (Meinel et al. 2010). Therefore, Mcl-1 expression was quantified in MM cell lines after 4h incubation (prior to any evidence of apoptosis induction) with increasing concentrations of the NIK inhibitor, CW15337 to investigate whether NIK inhibition modulated the expression of Mcl-1 in the MM cell lines.

MM cells from the MM cell lines H929, U266B1, RPMI8226 and JJN3 were treated with CW15337 at concentrations of 0.5μM, 1μM, 2.5μM and 5μM. At 4h, cells from each MM cell line were harvested and then fixated and permeabilised before staining with an anti-Mcl-1-IgG1 antibody (Santa Cruz Biotechnology) followed by secondary labelling with a goat anti-mouse IgG1-FITC antibody (Santa Cruz Biotechnology). The stained cells were then analysed using flow cytometry to quantify the intracellular Mcl-1 expression at each concentration of CW15337 in each MM cell line.

A gating strategy was applied to the collected flow cytometric data to ensure that only viable, single MM cells were analysed. The serially gated MM cell populations were then assessed for Mcl-1 expression (MFI values) at each concentration of CW15337. Figure 6.6 shows the representative overlay histograms of Mcl-1 expression in each MM cell line for the untreated and 5μM CW15337 treated MM cells at 4h. Figure 6.6 shows that all of the MM cell lines used have a relatively high baseline level of Mcl-1 expression. Moreover, all MM cell lines experience a similar decrease in Mcl-1 expression following 4h incubation with 5μM CW15337 relative to the untreated baseline level.

As all MM cell lines have a high expression of Mcl-1, the relationship between the specific baseline Mcl-1 expression and sensitivity to apoptosis induced by CW15337 treatment was investigated in each MM cell line. The aim of this was to evaluate whether baseline Mcl-1 expression could be a predictor of a MM cell lines response to NIK inhibition. The Mcl-1-FITC MFI in untreated MM cells was calculated and plotted against the mean LD_{50} value interpolated for each MM cell line. A linear regression analysis was performed and the results are shown in Figure 6.7.

Figure 6.7 shows that the H929 cell line possesses the highest average level of baseline Mcl-1 expression compared to the other three cell lines, although the error calculated was large. Figure 6.7 also shows that U266B1 cells have the second highest level of average Mcl-1 expression that is relatively more similar to Mcl-1 expression in the H929 cell line. The RPMI8226 and JJN3 cell lines relatively have lower levels of average Mcl-1 expression in untreated cells. Overall, the RPMI8226 cell line has the lowest baseline Mcl-1 expression of all the MM cell lines. The linear regression analysis indicates that there is a low negative correlation between the average baseline Mcl-1 expression and the calculated LD_{50} value in response to CW15337 for each MM cell line ($r^2 = 0.21$), which indicates that baseline Mcl-1 expression weakly determines MM cell line sensitivity to apoptosis induced through NIK inhibition.

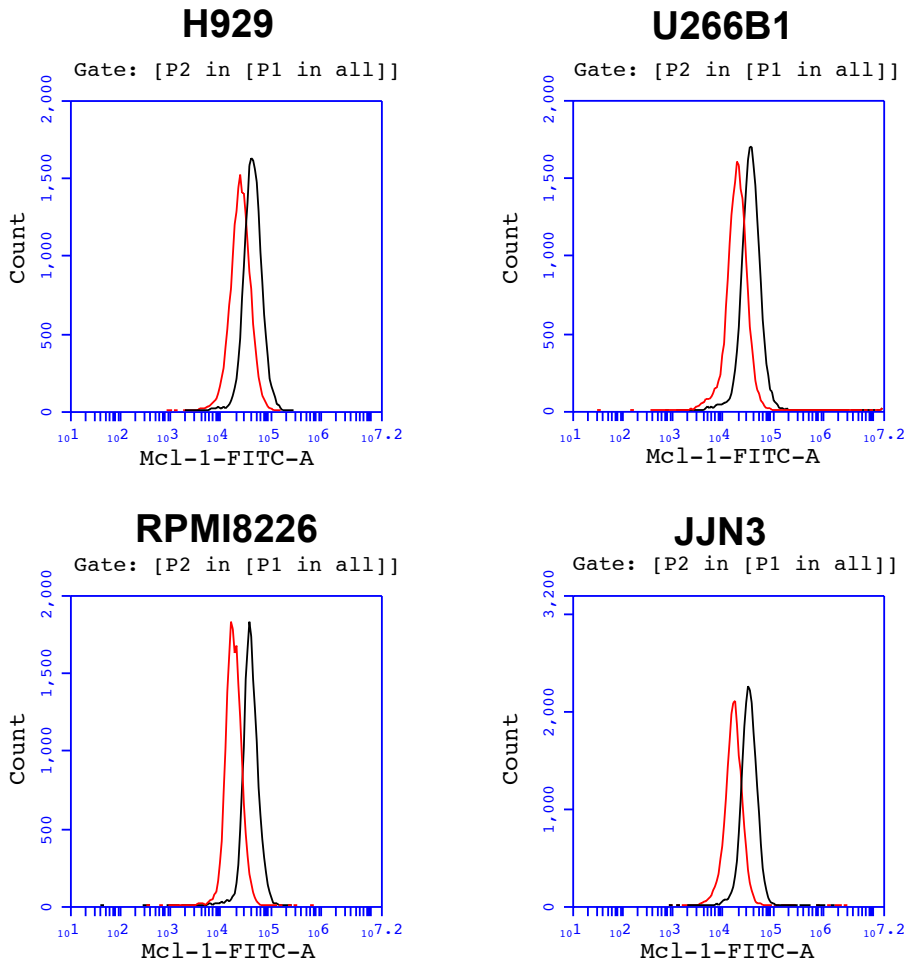

Figure 6.6 Representative overlay histograms of Mcl-1 expression in MM cell lines after 4h exposure to the NIK inhibitor CW15337.
Mcl-1 expression was investigated in H929, U266B1, RPMI8226 and JJN3 cells after treatment with increasing concentrations of CW15337. At 4h, intracellular Mcl-1 expression was investigated by staining cells with an anti-Mcl-1-FITC conjugated antibody and the average MFI was measured by flow cytometry. To gain an accurate MFI for each cell surface marker, gating was applied to gate viable myeloma cells (P1) and exclude any doublets (P2). The resultant gating was used to create overlay histograms from which the MFI of Mcl-1 expression at each concentration could be determined. A representative overlay histogram is shown for each MM cell line after 4h treatment with 5μM CW15337 (untreated = ■, 5μM CW15337 = ■).

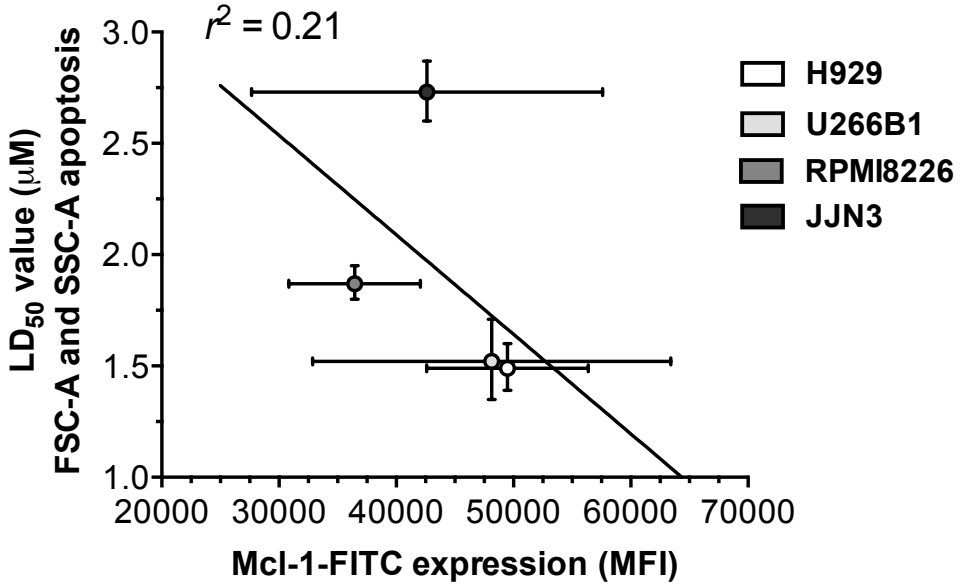

Figure 6.7 Correlation between baseline Mcl-1 expression and the LD_{50} values calculated for apoptosis induced by CW15337 in each MM cell line.
The relationship between the specific baseline Mcl-1 expression and sensitivity to apoptosis induced by CW15337 treatment was investigated in each MM cell line. The points plotted represent Mcl-1-FITC expression (MFI) (mean ± SD) against the LD_{50} values calculated for apoptosis induced by CW15337 (LD_{50} value ± 95% CI) for each MM cell line ($n = 3$). A linear regression analysis was performed in Graphpad Prism 6 and the resulting linearity (r^2) is reported alongside the graph.

The Mcl-1-FITC MFI at each concentration of the NIK inhibitor was determined and normalised to the untreated MFI for each MM cell line. Figure 6.8 shows the collated data from three separate experiments for each MM cell line outlining the dose-dependent regulation of Mcl-1 expression by CW15337 at 4h. Figure 6.8 shows that all four MM cell lines experienced a dose-dependent decrease in Mcl-1 expression relative to untreated cells following 4h treatment with CW15337. The highest concentration of CW15337 (5μM) induced a highly significant decrease in Mcl-1 expression in the H929 and RPMI8226 cell lines ($p = 0.004$ and $p = 0.004$, respectively) relative to untreated MM cells.

Figure 6.8 indicates that the H929 MM cell line underwent the largest decrease in Mcl-1 expression after 5μM CW15337 compared to the untreated group (50.0% ± 6.1%) relative to the other MM cell lines. The RPMI8226 cell line also underwent a relatively large decrease in Mcl-1 expression at 5μM CW15337 (51.1% ± 9.2%) relative to untreated MM cells and experiences the

most consistent dose-dependent down-regulation of Mcl-1 expression compared to the other cell lines.

Figure 6.8 shows that both U266B1 and JJN3 MM cells underwent a dose-dependent down-regulation of Mcl-1 expression, although this decrease was not significant when the highest concentration of CW15337 (5μM) was compared to untreated MM cells (p = 0.124 and p = 0.105, respectively). The dose-dependent decrease in Mcl-1 expression induced by CW15337 in JJN3 cells is shown in Figure 6.8 to plateau following exposure to 2.5μM and 5μM CW15337 (58.6% ± 6.8% and 58.1% ± 6.4%, respectively) relative to untreated JJN3 cells. Figure 6.8 also indicates that the U266B1 cell line experienced a maximum decrease in Mcl-1 expression at 5μM similar to that of the JJN3 cell line, when compared to untreated Mcl-1 expression in each cell line (57.4% ± 13.2% and 58.1% ± 6.4%, respectively).

In conclusion, the NIK inhibitor significantly down-regulated Mcl-1 expression in a dose-dependent manner in the MM cell lines H929 and RPMI8226 after 4h treatment. Moreover, the normalised change in overall Mcl-1 expression measured at 5μM CW15337 was relatively similar for each of the four MM cell lines. Therefore, Figure 6.6 and 6.8 suggest that NF-κB activity may be inhibited by CW15337 in each MM cell line at 4h in a dose-dependent manner.

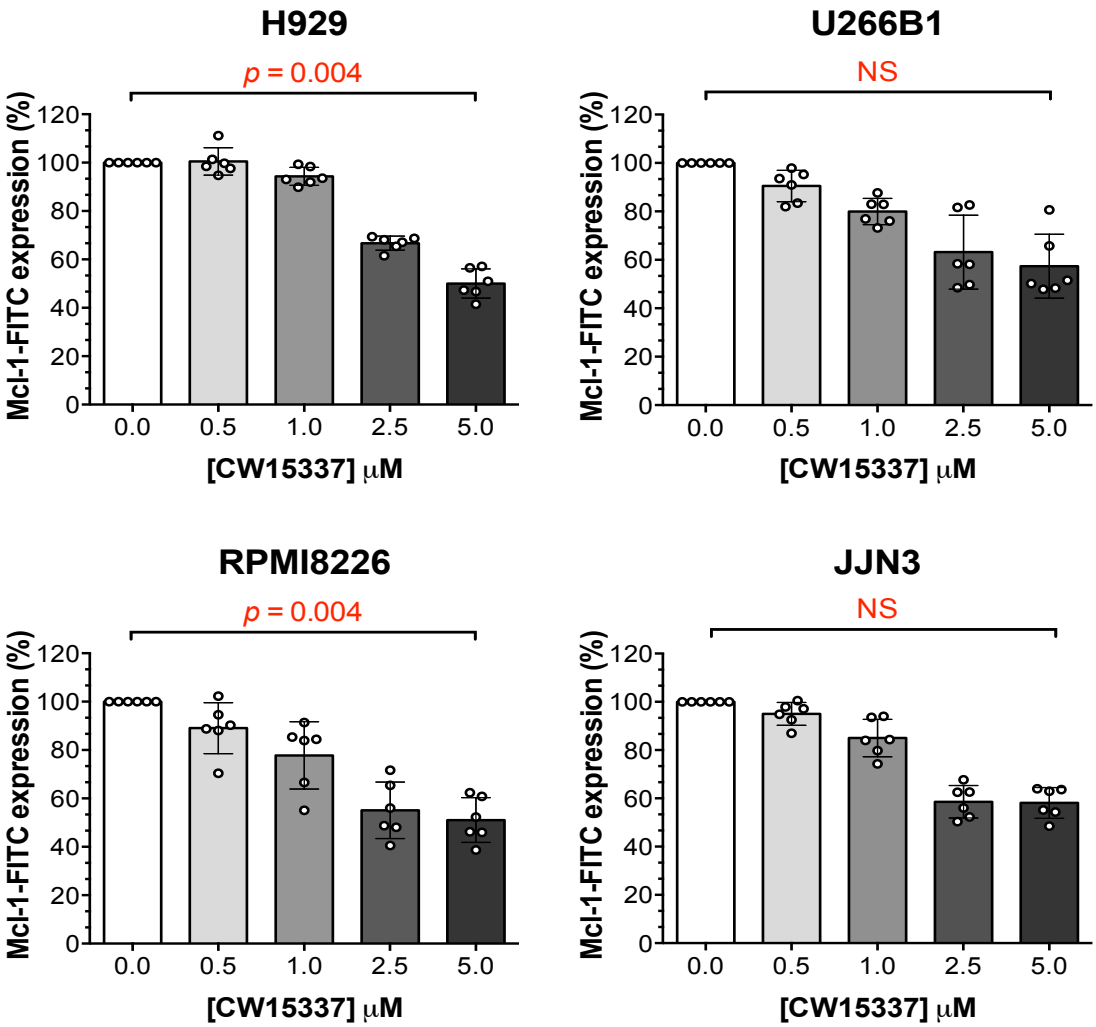

Figure 6.8 The dose-dependent regulation of Mcl-1 expression in MM cell lines after 4h treatment with CW15337.

Mcl-1 expression was investigated in the H929, U266B1, RPMI8226 and JJN3 cell lines after treatment with increasing concentrations of CW15337 ranging from 0μM to 5μM. At 4h, intracellular Mcl-1 expression was investigated by staining cells with an anti-Mcl-1-FITC conjugated antibody following fixation and permeabilisation. The Mcl-1-FITC MFI at each concentration of SU compound was measured using an Accuri flow cytometer and normalised to the untreated control. A one-tailed unpaired *t*-test was performed using Graphpad Prism 6.0 software to investigate the statistical significance values between 0μM to 5μM of CW15337 in each MM cell line at 4h (n = 3, duplicates averaged). The results are reported above the graph (NS = not significant, p > 0.05).. Error bars represent SD where n = 3, duplicate and experimental duplicates are shown.

6.3. Inhibition of NF-κB activity by CW15337

The association between cytotoxicity and the inhibition of constitutive NF-κB activity induced by CW15337 was investigated in more detail using an ELISA detecting the active NF-κB subunits p65, p50, p52 and RelB. These four subunits were specifically chosen because they would provide information as to whether NIK inhibition was effecting canonical or non-canonical generated NF-κB activity. The RPMI8226 MM cell line was used for these experiments because it had an intermediate level of constitutive NF-κB activity and also possessed a bi-allelic mutation in TRAF3 resulting in NIK activation.

RPMI8226 cells were incubated with the NIK inhibitor at concentrations of 1μM, 2.5μM and 5μM. At 4h, RPMI8226 cells from each concentration of CW15337 were harvested and converted to nuclear extracts. 1μg of RPMI8226 nuclear extract protein was assayed using the NF-κB family ELISA kit (Active Motif), as per the manufacturers instructions. Standard curves were generated alongside the assay using know quantities of recombinant p65 protein ($r^2 > 0.99$) and recombinant p50 protein ($r^2 > 0.96$) to allow NF-κB subunit quantification in nanograms per microgram of nuclear extract protein.

Figure 6.9 shows the quantities of active p65, p50, p52 and RelB NF-κB subunit proteins in RPMI8226 cells following 4h treatment with CW15337 at concentrations of 1μM, 2.5μM and 5μM. The data shown consists of the collated data from three separate experiments where the individual nuclear extract samples were assayed in duplicate.

Figure 6.9 shows that both the p52 and RelB subunits experienced a dose-dependent inhibition across all increasing concentrations of CW15337 in RPMI8226 cells, although only the RelB subunit experienced a significant decrease by 5μM CW15337 when compared to the untreated samples (p = 0.002).

Conversely, the p65 and p50 NF-κB subunits did not show a significant change in nuclear protein levels following 5μM CW15337 relative to the untreated group (p = 0.269 and p = 0.224, respectively). Furthermore, no dose-dependent regulation of p65 and p50 was observed.

Overall, Figure 6.9 demonstrates that 5μM CW15337 preferentially decreased the levels of p52 and RelB NF-κB subunits in a dose-dependent manner in RPMI8226 cells. The specific dose-dependent decrease of these subunits suggests that CW15337 predominantly inhibited the non-canonical NF-κB signalling pathway.

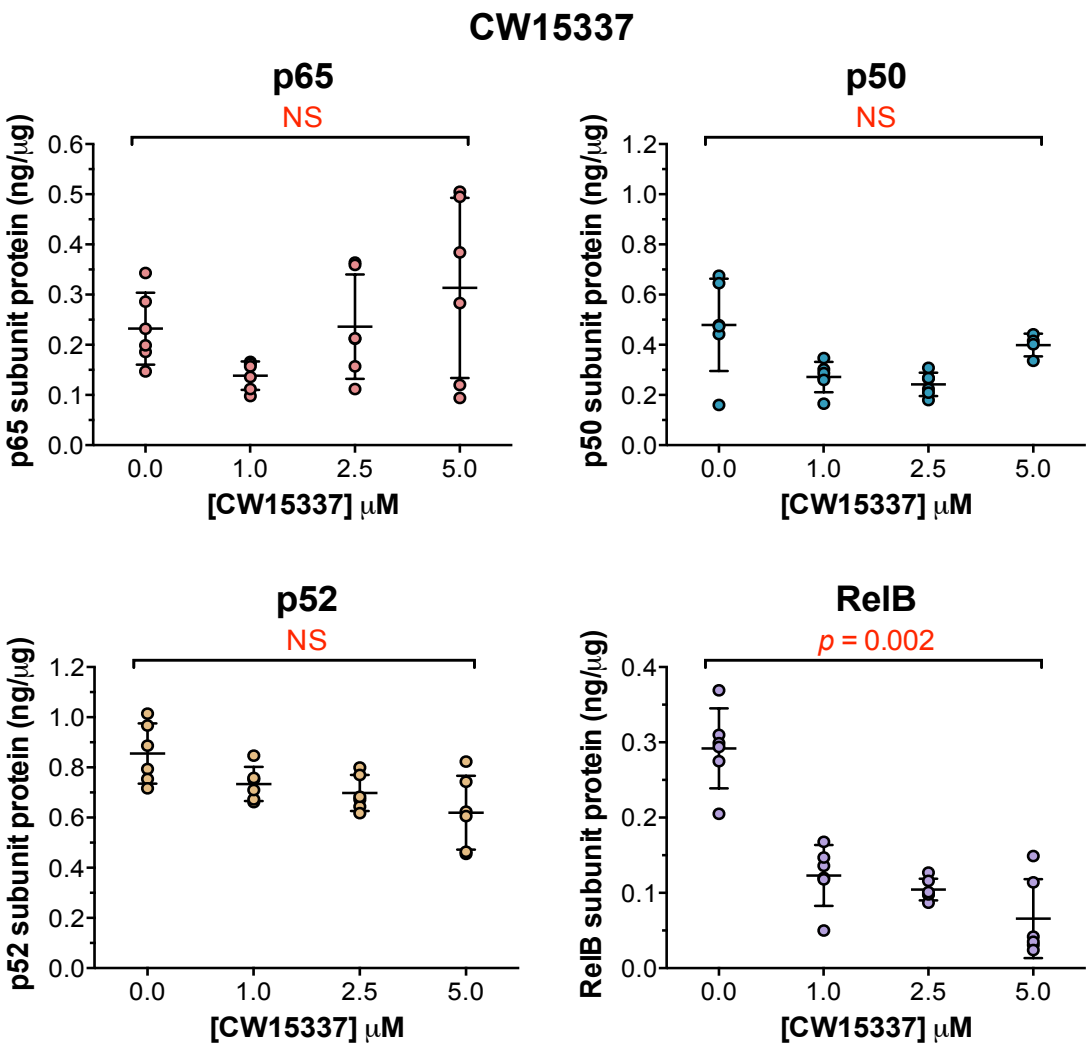

Figure 6.9 Effect of CW15337 on NF-κB activity in RPMI8226 MM cells at 4h. RPMI8226 cells were exposed to increasing concentrations of CW15337 for 4h. RPMI8226 cells were then harvested and used to generate nuclear extract samples. The MM cell line was then assayed at 1µg/well of nuclear extract protein using ELISAs detecting the active NF-κB subunits p50, p65, p52 and RelB. A one-tailed unpaired *t*-test was performed using Graphpad Prism 6.0 software to investigate the statistical significance values between 0µM to 5µM for CW15337 in RPMI8226 cells for each NF-κB subunit (n = 3, duplicates averaged). The results are reported above the graph (NS = not significant, $p > 0.05$). Values reported are mean ± SD produced from duplicate measurements where n = 3, experimental duplicates shown.

6.4. Gene expression following CW15337 treatment using qRT-PCR

NIK mainly regulates NF-κB activity through the activation of IKKα, which subsequently activates the non-canonical signalling pathway (Ling et al. 1998; Senftleben et al. 2001). Therefore, the effect of the NIK inhibitor on previously validated IKKα-regulated genes was compared with the IKKα inhibitory SU compounds using qRT-PCR analysis.

The genes analysed included those identified as significantly altered following exposure to the SU compounds in the previous chapter (TRAF6, RIPK1, POLA2, SRSF7, POLR2A, SRSF6, OFD1, PRKCI, UBA2 and NSUN2). The effect of CW15337 (2.5μM) on specific gene transcription was assessed in RPMI8226 cells and the results compared with those obtained with SU1257, SU1053, SU1411, SU1438 and SU1349.

Briefly, RPMI8226 cells were incubated alone and in the presence of 2.5μM of CW15337. At 4h, cells were harvested from untreated and 2.5μM treated conditions to generate TRIzol® lysates that were subsequently processed to RNA extracts using an RNeasy mini kit (Qiagen), according to the manufacturers instructions. The eluted RNA was reverse transcribed into cDNA using a high capacity cDNA reverse transcription kit (Applied Biosystems). A reaction master mix was prepared for each primer pair containing the cDNA, primer pairs and SYBR® Green I dye and this was loaded into the wells of a 96-well reaction plate. The reaction plate was then analysed using ViiA™ 7 Real-Time PCR System (Applied BioSystems). The qRT-PCR results were used to generate the relative fold change in each target gene using the $2^{-\Delta\Delta Ct}$ method (Livak a Schmittgen 2001) where the endogenous control gene was RSP14.

The $2^{-\Delta\Delta Ct}$ fold change for each of the 10 genes analysed using qRT-PCR following treatment with 2.5μM CW15337 for 4h in RPMI8226 cells are shown in the heatmap in Figure 6.10. The results are shown alongside the qRT-PCR data previously produced for the SU compounds SU1257,

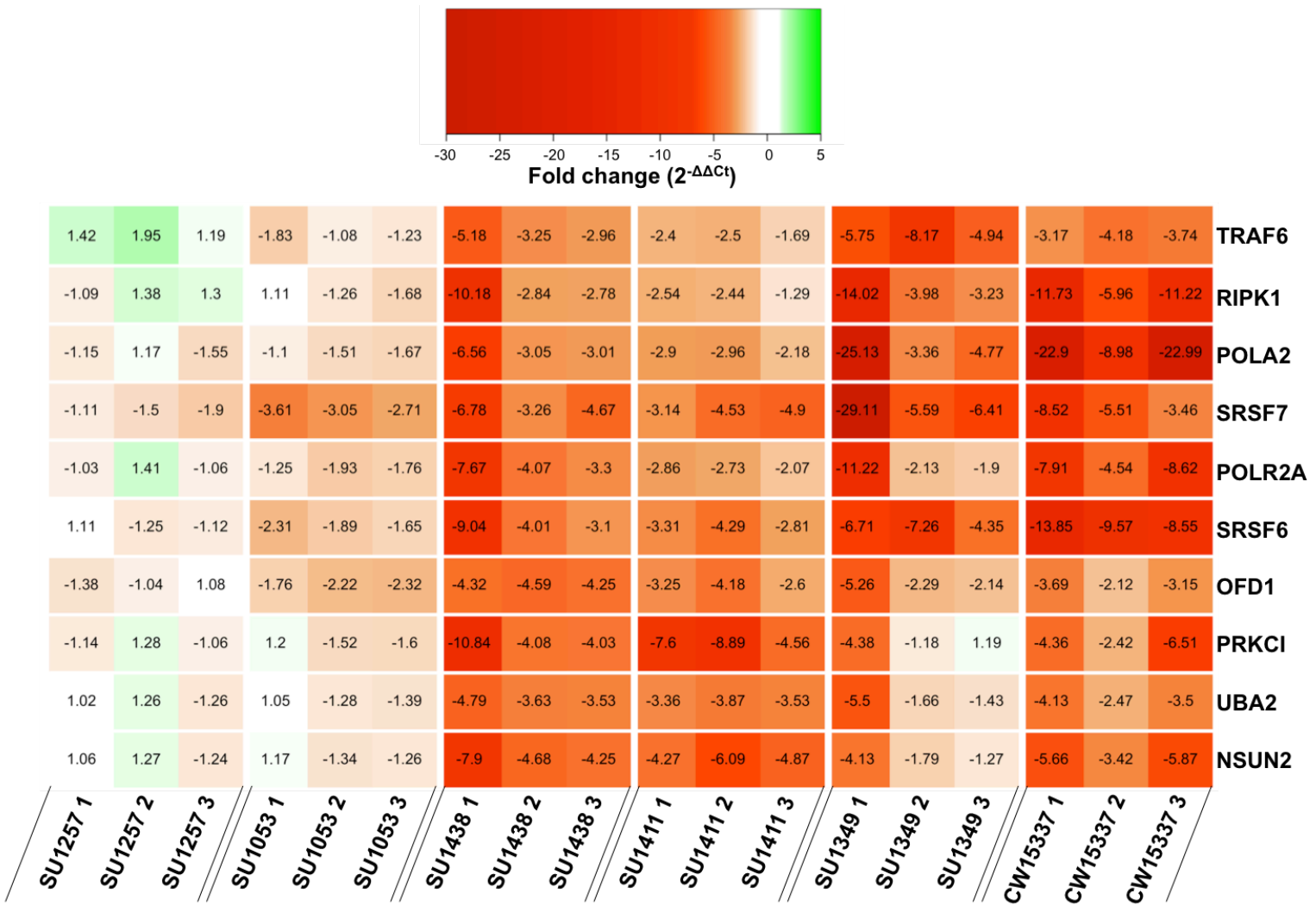

Figure 6.10 qRT-PCR analysis of the 10 DE microarray genes in RPMI8226 cells after 4h treatment with 2.5µM CW15337.

The 10 DE genes picked from the results of the microarray analysis were quantified using qRT-PCR following treatment with 2.5µM CW15337 for 4h in RPMI8226 cells. The fold changes reported were calculated using $2^{-\Delta\Delta Ct}$ method. The endogenous control used for the calculation was RSP14. A heatmap was plotted of the fold change where n=3, duplicate. The results shown previously for the SU compounds SU1257, SU1053, SU1438, SU1411 and SU1349 have been placed alongside CW15337 for comparison.

SU1053, SU1438, SU1411 and SU1349 in RPMI8226 cells to allow for a side-by-side comparison of the effect of each compound on specific gene regulation. The results shown for the NIK inhibitor represent three separate experiments that were analysed in duplicate in the qRT-PCR.

Figure 6.10 shows that CW15337 has a regulatory profile that possesses the most similarities with the three most cytotoxic SU compounds (SU1438, SU1411 and SU1349). Moreover, CW15337 appeared to encompass a combination of all three of the SU compounds' regulatory profiles. For this reason, the statistical significance values were investigated using a Two-way ANOVA to compare the fold change in gene transcription that CW15337 treatment induced with the fold changes induced by SU1438, SU1411 and SU1349 treatment for each of the 10 genes measured using qRT-PCR. Table 6.2 displays the results of this analysis.

Figure 6.10 shows that CW15337 treatment caused a similar down regulation in RIPK1, POLA2, SRSF7 and SRSF6 as that induced by SU1349. However, the average fold change in RIPK1, POLA2 and SRSF6 induced by CW15337 (-9.6 ± 3.2, -18.3 ± 8.1 and -10.7 ± 2.8, respectively) was relatively higher than that induced by SU1349 (-7.1 ± 6.0, -11.1 ± 12.2 and -6.1 ± 1.5, respectively), although Table 6.2 shows that only POLA2 was significantly (p = 0.0031) altered by CW15337 compared to SU1349. In contrast, CW15337 induced significantly less change in the transcription of SRSF7 when compared to SU1349 down regulation (-5.8 ± 2.5 and -13.7 ± 13.3, respectively, p = 0.0009). However, this could be due to the relatively large variation in SU1349 qRT-PCR replicate samples skewing the average fold change. Moreover, TRAF6 gene transcription was most markedly decreased following treatment with SU1349 (-6.3 ± 1.7), although this was not significantly different when compared to CW15337 (p = 0.74). Moreover, the changes in TRAF6 induced by CW15337 were more similar to the fold change observed with SU1438 (-3.7 ± 0.5 and -3.8 ± 1.2, respectively, $p > 0.99$).

Table 6.2 Two-way ANOVA comparing the fold change in the transcription of each gene induced by CW15337 with fold change induced by SU1438, SU1411 and SU1349.

A two-way ANOVA followed by Tukey's multiple comparisons test was performed in Graphpad Prism to investigate the statistical significance values between the fold change in gene transcription that CW15337 treatment induced compared with the fold changes induced by SU1438, SU1411 and SU1349 as measured using qRT-PCR (n = 3). The adjusted p value and the resulting significance summary ($p \leq 0.05$ = *, $p \leq 0.01$ = **, $p \leq 0.001$ = *** and $p \leq 0.0001$ = ****) are reported for each comparison.

		Adjusted p value	Summary
TRAF6	CW15337 vs. SU1438	> 0.9999	ns
	CW15337 vs. SU1411	0.9668	ns
	CW15337 vs. SU1349	0.7393	ns
RIPK1	CW15337 vs. SU1438	0.1936	ns
	CW15337 vs. SU1411	0.0016	**
	CW15337 vs. SU1349	0.7476	ns
POLA2	CW15337 vs. SU1438	< 0.0001	****
	CW15337 vs. SU1411	< 0.0001	****
	CW15337 vs. SU1349	0.0031	**
SRSF7	CW15337 vs. SU1438	0.9963	ns
	CW15337 vs. SU1411	0.9516	ns
	CW15337 vs. SU1349	0.0009	***
POLR2A	CW15337 vs. SU1438	0.8916	ns
	CW15337 vs. SU1411	0.174	ns
	CW15337 vs. SU1349	0.906	ns
SRSF6	CW15337 vs. SU1438	0.0653	ns
	CW15337 vs. SU1411	0.0032	**
	CW15337 vs. SU1349	0.1596	ns
OFD1	CW15337 vs. SU1438	0.9753	ns
	CW15337 vs. SU1411	> 0.9999	ns
	CW15337 vs. SU1349	> 0.9999	ns
PRKCI	CW15337 vs. SU1438	0.9158	ns
	CW15337 vs. SU1411	0.7417	ns
	CW15337 vs. SU1349	0.6092	ns
UBA2	CW15337 vs. SU1438	0.9995	ns
	CW15337 vs. SU1411	> 0.9999	ns
	CW15337 vs. SU1349	0.9998	ns
NSUN2	CW15337 vs. SU1438	0.9994	ns
	CW15337 vs. SU1411	> 0.9999	ns
	CW15337 vs. SU1349	0.7418	ns

In addition, Figure 6.10 shows that CW15337 decreased the expression of POLR2A, OFD1, PRKCI, UBA2 and NSUN2, which were previously found to be genes that were repressed by treatment with SU1438 and SU1411. Moreover, Table 6.2 shows that the magnitude of the fold changes induced by CW15337 in these five genes was not significantly different to those induced by SU1438 and SU1411 gene regulation. The fold change in POLR2A that CW15337 induced (-7.02 ± 2.2) was marginally higher than that induced by SU1438 (-5.0 ± 2.3) and SU1411 (-2.6 ± 0.4) in RPMI8226 cells. The average fold change of OFD1, UBA2 and NSUN2 genes induced by CW15337 (-3.0 ± 0.8, -3.4 ± 0.8 and -5.0 ± 1.4, respectively) were more similar to those caused by treatment with SU1411 (-3.3 ± 0.8, -3.6 ± 0.3 and -5.1 ± 0.9, respectively). The relative transcription of PRKCI showed an average fold change in response to CW15337 (-4.4 ± 2.1) that was relatively smaller than that induced by both SU1438 (-6.3 ± 3.9) and SU1411 (-7.0 ± 2.2).

In conclusion, Figure 6.10 suggests that CW15337 is a potent regulator of the 10 SU compound associated genes. The CW15337 down regulated both SU1349 and SU1438/SU1411 associated genes and for the RIPK1, POLA2, POLR2A and SRSF6 genes the down regulation measured was relatively more pronounced. Taken together, these data indicate that CW15337 has a similar effect on the transcriptional programme of a selected subset of genes in RPMI8226 cells when compared with the IKKα inhibitors SU1438, SU1411 and SU1349.

6.5. Discussion

The use of a novel NIK inhibitor, CW15337 was evaluated in four MM cell lines, each representing different NF-κB signatures due to the lack or presence of genetic abnormalities effecting NIK. Cytotoxicity was first assessed in all MM cell lines after 48h incubation with increasing concentrations of CW15337. The U266B1, RPMI8226 and JJN3 MM cell lines manifest constitutive NF-κB activity and possess increased expression of NIK, either due to activating mutations of NIK itself or due to the loss of a TRAF3 binding domain. Consequently, it was hypothesised that these three

MM cell lines may be more susceptible to cytotoxicity induced by NIK inhibition.

CW15337 was cytotoxic in all four MM cell lines at 48h in a concentration-dependent manner, although the sensitivity to apoptosis induced by the NIK inhibitor was heterogeneous between the MM cell lines. Contrary to the proposed hypothesis, the H929 cell line was the most sensitive to the cytotoxic effects of the NIK inhibitor CW15337 whereas the JJN3 cell line was relatively more resistant. The U266B1 and RPMI8226 cell lines showed intermediate sensitivity to CW15337-induced apoptosis. Overall, this indicates that those MM cell lines containing TRAF3 inactivating or NIK activating mutations, which give rise to NIK dependency, were comparatively more resistant to cytotoxicity induced by CW15337 NIK inhibition. Moreover, NIK inhibition is more cytotoxic in the NIK independent MM cell line H929.

This correlates with the study by Demchenko *et al.* who also showed that NIK inhibition by two novel NIK inhibitors in MM cell lines possessing more NIK protein were less sensitive to cytotoxicity induced by NIK inhibition compared to those MM cell lines that contained less NIK protein (Demchenko et al. 2014). In contrast, the same study demonstrated that NIK independent MM cell lines, such as H929, did not experience a decrease in viability in response to NIK inhibition. In addition, the cytotoxicity results for CW15337 also contrast with those obtained by Annunziata *et al.* who determined that NIK silencing in the NIK dependent MM cell line JJN3 was cytotoxic but did not induce cytotoxicity in the H929 MM cell line (Annunziata et al. 2007). Therefore, the finding that H929 was the most sensitive MM cell line to cytotoxicity induced by the NIK inhibitor is contrary to previous studies. However, the dichotomy between the data in this thesis and the existing literature may be a consequence of the off-target effects of CW15337. For example, the kinome screening data shown in Appendix Figure XV demonstrates that CW15337 has many kinase targets, including JAK2 and MAP4K2.

The results in Chapter 3 revealed that H929 had the lowest constitutive level of NF-κB activity, whereas U266B1 and RPMI8226 possessed intermediate levels although U266B1 cells showed NF-κB activity closer to that of the H929 cell line. The JJN3 cell line possessed the highest level of NF-κB activity of the four cell lines and was the most resistant to the effects of CW15337. Therefore, the pattern of CW15337 cytotoxicity was inversely correlated with the level of NF-κB activity possessed by each MM cell line. An explanation for this could relate to the function of NF-κB because the transcription factor regulates genes involved in anti-apoptosis (Gilmore 2007; Demchenko a Kuehl 2010). Therefore, cells with more NF-κB activity may be able to resist the inhibition caused by CW15337 by first depleting its increased reserves that act to buffer the induced cell death. However, this does not fully explain why the results for H929 differ from previous findings.

To begin exploring the effect of NIK inhibition on NF-κB activity, the CW15337 dose-dependent regulation of Mcl-1 expression at 4h was quantified in each MM cell line. Mcl-1 is an anti-apoptotic protein that must be maintained in MM cells to sustain viability (Derenne et al. 2002; Zhang et al. 2002). In addition, inhibition of NF-κB activity is accompanied by the down-regulation of Mcl-1 expression and may contribute to the activation of apoptotic pathways (Meinel et al. 2010).

The baseline Mcl-1 expression was quantified in the MM cell lines and was shown to be expressed in all four cell lines. This was consistent with each MM cell line possessing a constitutive level of NF-κB activity (Liu et al. 2014). Moreover, all MM cell lines experienced a dose-dependent decrease in Mcl-1 expression relative to untreated myeloma cells in response to 4h incubation with CW15337. This was accompanied by a highly significant decrease in Mcl-1 expression in the H929 and RPMI8226 MM cell lines at the highest concentration of CW15337 (5μM) relative to the untreated control. However, the percentage of change in Mcl-1 expression at 5μM was relatively similar between the MM cell lines and did not correlate with the cell line specific pattern of sensitivity to apoptosis induced by CW15337. Nevertheless, linear regression analysis revealed a weak negative correlation between baseline

Mcl-1 expression and LD_{50} value calculated through apoptosis induced by CW15337 in the MM cell lines. This suggests that baseline Mcl-1 expression may be a predictor of cytotoxic sensitivity to NIK inhibition, although more data would be required to make a robust conclusion, preferably in primary MM cells rather than cell lines.

The levels of other anti-apoptotic proteins, such as Bcl-X_L, have also been shown to correlate with constitutive NF-κB activity induced by NIK overexpression in B cells (Sasaki et al. 2008). Similar to the results obtained for Mcl-1 in response to CW15337, Bcl-X_L was down regulated by NIK inhibition in MM cell lines and this corresponded with apoptosis and a decrease in NF-κB activity (Takeda et al. 2016). Bcl-X_L expression was not measured in this present study so it remains unclear whether CW15337 also induces a decrease in the expression of this anti-apoptotic protein. However, the significant dose-dependent decrease in Mcl-1 expression observed suggests that CW15337 NIK inhibition may correspond with a decrease in NF-κB activity in the MM cell lines tested, which may contribute to the cytotoxicity of CW15337.

For this reason, the dose-dependent effect of CW15337 on NF-κB activity was investigated in more detail using an ELISA detecting the active NF-κB subunits p65, p50, p52 and RelB in the MM cell line RPMI8226. The results demonstrated that only the non-canonical NF-κB pathway experienced a concentration-dependent decrease, although only the RelB subunit was significantly affected by NIK inhibition by CW15337. However, as already discussed, the ELISA possessed caveats that meant that it might not have been an appropriate tool to quantify CW15337 inhibition of NF-κB activity. Therefore, western blotting could have been used as an additional tool to fully characterise the effect that CW15337 induced on NF-κB pathway processing in RPMI8226 cells. More specifically, by quantifying phosphorylated p100, and total p100 and p52 proteins following treatment with CW15337, this technique could have provided definitive proof of non-canonical pathway inhibition because p100 functions as both the precursor of p52 and a RelB-specific inhibitor.

NIK mainly regulates the activation of the non-canonical NF-κB pathway (Ling et al. 1998; He et al. 2006) so it is consistent that only p52 and RelB subunits would be down regulated by NIK inhibition. On the other hand, it has been suggested that NIK silencing or inhibition decreases the level of overall NF-κB activity generated through both canonical and non-canonical signalling (Annunziata et al. 2007; Demchenko et al. 2014). At least in the RPMI8226 MM cell line used in this study, CW15337 did not significantly effect the canonical NF-κB pathway because the levels of p65 and p50 are not significantly altered by NIK inhibition.

Several studies have shown that the non-canonical pathway is the main NF-κB pathway that regulates anti-apoptotic pathways (He et al. 2006; Xie et al. 2007; Gardam et al. 2008). Therefore, it seems possible that CW15337-mediated inhibition of NIK, and hence the depletion of non-canonical NF-κB signalling, may contribute to the induction of apoptosis in the MM cell lines.

NIK is responsible for phosphorylating IKKα to activate the non-canonical NF-κB pathway (Ling et al. 1998; Senftleben et al. 2001). Given that CW15337 inhibited only non-canonical NF-κB pathway activity, it was hypothesised that CW15337 may share mechanistic similarities with the SU compounds explored in this thesis, as they also inhibit non-canonical signalling through IKKα inhibition. To investigate this, the transcriptional inhibition pattern caused by exposure to the SU compounds were compared with CW15337 using qRT-PCR analysis. The qRT-PCR analysis suggested that CW15337 was also a potent regulator of the 10 SU compound associated genes. Furthermore, the gene expression profile for CW15337 was most similar to the three most cytotoxic SU compounds, SU1349, SU1411 and SU1438. However, four of the SU compound differentially regulated genes experienced a more marked down regulation in response to CW15337 compared to their associated SU compounds. These genes included the SU1349 associated genes RIPK1 and POLA2 and also differentially expressed genes POLR2A and SRSF6 that are differentially regulated by both SU1349 and SU1438.

To maintain experimental consistency and allow adequate comparison, gene expression was investigated in the RPMI8226 cell line following 4h 2.5μM CW15337. This concentration was chosen based on the average LD_{50} values obtained for the SU compounds in the RPMI8226, which were comparatively less cytotoxic than CW15337. This may contribute to the relatively more potent down regulation of the four genes observed following treatment with CW15337 but this is unlikely as other genes, such as TRAF6, SRSF7 and PRKCI, experienced a smaller fold change than that the gene associated SU compound.

Overall, the comparison of CW15337 regulated gene expression with that of the SU compounds suggests that CW15337 had a similar gene expression profile to SU1349, SU1411 and SU1438. These were the three most cytotoxic SU compounds tested in this series and so this could suggest that all the pharmacological agents regulated similar pathways that contributed to their cytotoxic nature. However, CW15337 had a quantitatively distinct pattern of gene regulation to the SU compounds, suggesting that its mechanism of action may differ slightly from that of the IKKα inhibitors.

The aim of this chapter was to investigate the use of a novel NIK inhibitor, CW15337, in four MM cell lines with different clinical features of MM to evaluate the potential of a NIK inhibitor as a therapeutic agent. This chapter has successfully shown that CW15337 was potently, and dose-dependently, cytotoxic in all the MM cell lines tested and this was coupled with a dose-dependent down-regulation of the expression of the anti-apoptotic protein Mcl-1. CW15337 dose-dependently inhibited only the non-canonical NF-κB pathway, which likely contributes to the cytotoxic effect of the pharmacological agent.

Chapter 7 – Conclusions and final discussion

7.1. Summary of key findings

1. The commercially available non-specific NF-κB inhibitor BAY 11-7082 was cytotoxic in all four MM cell lines tested, H929, U266B1, RPMI8226 and JJN3, and the cytotoxicity of this agent was associated with inhibition of both the canonical and non-canonical NF-κB pathways.
2. Most of the novel IKKα inhibitory SU compounds were dose-dependently cytotoxic in RPMI8226 cells but their potency was not obviously related to either the inhibition of NF-κB or the down-regulation of the anti-apoptotic protein Mcl-1.
3. Characterisation of the SU compounds, excluding SU1257, showed that the effects induced by these agents could not be entirely explained by their kinase inhibitory profiles for IKKα, IKKβ and CDK9.
4. Microarray analysis revealed qualitative and quantitative changes in gene expression induced by the individual SU compounds. Some of the genes affected were common to all the SU compounds tested and some were unique to individual SU compounds.
5. 10 genes that were altered by treatment with the SU compounds were selected for qRT-PCR validation. 9/10 of the genes showed the same pattern of expression as that observed in the microarray analysis.
6. The NIK inhibitor, CW15337, was dose-dependently cytotoxic in all four MM cell lines, although the apoptotic responses were heterogeneous. Cytotoxicity of CW15337 correlated with a dose-dependent decrease in both Mcl-1 expression and non-canonical NF-κB pathway in MM cell lines. Gene expression analysis using qRT-PCR showed that CW15337 had a similar gene expression profile to the SU1349, SU1411 and SU1438 IKKα inhibitory SU compounds, suggesting the possibility of a shared mechanism of action.

7.2. Final discussion

7.2.1. Characterisation of NF-κB inhibitors in MM cell lines

The work carried out in this thesis was the first project within our research group to use the four MM cell lines H929, U266B1, RPMI8226 and JJN3. Therefore, the initial step of this project involved characterisation of the MM cell lines in terms of growth characteristics, cell surface phenotype and NF-κB activity profiling. The aim was to gain an understanding of the individual characteristics of each MM cell line to allow planning of future experiments using these cell lines. The main finding of this section of work was that heterogeneity was observed between the four MM cell lines in all the characteristics evaluated; this was important as it reflected the heterogeneity that is commonly observed in MM.

The key aim of this thesis was to characterise NF-κB inhibitors in the MM cell lines with a view to evaluate their use as therapeutic agents in this hematological malignancy. To achieve this, over the course of this thesis, a workflow was developed for characterising potential NF-κB inhibitors in MM cell lines. This workflow included assessment of cytotoxicity, NF-κB activity, the expression of the survival protein Mcl-1 and selected gene expression changes by qRT-PCR. A key step in this workflow was the investigation of a possible correlation between cytotoxicity and NF-κB activity. Using this workflow, the following inhibitors were investigated: the commercial non-specific NF-κB inhibitor BAY 11-7082; a series of first-in-class IKKα inhibitors; and a novel NIK inhibitor in MM cell lines.

When looked at together, this work supports the concept of NF-κB as a promising therapeutic target in MM. The non-specific NF-κB inhibitor BAY 11-7082, NIK inhibitor CW15337 and most of the SU compounds induced dose-dependent cytotoxicity in the MM cell lines. For BAY 11-7082 and CW15337, the cytotoxicity correlated with significant and dose-dependent changes in NF-κB activity. With respect to BAY 11-7082, a significant negative correlation existed between inhibition of all five nuclear NF-κB subunits and the induction of apoptosis, suggesting that inhibition of both the canonical and the non-canonical NF-κB pathways may contribute to

the apoptotic effect induced by BAY 11-7082 in the MM cell lines. However, it is more than likely that off-target inhibitory effects are responsible for the dose-dependent cytotoxicity of this agent as opposed to NF-κB inhibition (Lee et al. 2012; Rauert-Wunderlich et al. 2013; Strickson et al. 2013). By way of contrast, the NIK inhibitor, CW15337, significantly and dose-dependently down-regulated non-canonical NF-κB subunit activity in RPMI8226 cells, whereas canonical NF-κB subunits were not significantly affected by NIK inhibition. In addition, the apoptosis induced by CW15337 was accompanied by a dose-dependent decrease in Mcl-1 expression in all four MM cell lines. An interesting finding was that sensitivity of the MM cell lines to apoptosis induced by both BAY 11-7082 and CW15337 was heterogeneous, and was inversely associated with the baseline level of overall constitutive NF-κB activity that each MM cell line possessed.

Characterisation of the SU compounds in the MM cell line RPMI8226 suggested that, unlike BAY 11-7082 and CW15337, the cytotoxicity of these agents did not correlate with the dose-dependent down-regulation of NF-κB activity or expression of the anti-apoptotic protein Mcl-1. Furthermore, the cytotoxicity of each compound could not be completely explained by their respective inhibitory profiles with regards to IKKα, IKKβ and CDK9 inhibition. For example, an interesting finding was that SU compounds that appeared to have comparable kinase inhibitory profiles, such as the potent IKKα inhibitors SU1053 and SU1349, were shown in Chapter 4 to induce contrasting levels of cytotoxicity in RPMI8226 cells. This suggested that the SU compounds, especially those with higher potency, inhibited other molecular targets, which contributed to their cytotoxicity. Moreover, the fact that SU1053 was one of the least cytotoxic SU compounds, despite its potency as an IKKα inhibitor, may suggest that targeting IKKα alone may not be sufficient for the effective treatment of MM.

Therefore, to gain a deeper understanding of the mode of action of the SU compounds, global gene expression was investigated using an Affymetrix GeneChip® HTA 2.0 gene chips. The microarray analysis of the SU compounds tested revealed qualitative and quantitative changes in gene

expression. Some of the genes affected were common to all compounds and others were unique to each SU agent. Another key finding was that the number of genes that were differentially regulated by SU1349 was significantly much higher than the number regulated individually by SU1053, SU1438 and SU1411. Moreover, the pattern that emerged was that an increase in the number of differentially regulated genes correlated with the cytotoxicity of that SU agent in RPMI8226 cells. Therefore, it seems likely that the relatively increased cytotoxicity of some of the SU compounds, similar to BAY 11-7082 (Lee et al. 2012; Rauert-Wunderlich et al. 2013; Strickson et al. 2013), is likely to arise as a consequence of off-target inhibitory effects.

A selection of 10 genes were chosen based on their biological regulation by the SU compounds in RPMI8226 cells. These genes were used to successfully validate the microarray data using qRT-PCR and were also used to assess the relative effects of CW15337 in the same cell line. Comparative analysis of these 10 genes showed that CW15337 had a similar effect to SU1349, SU1411 and SU1438, which were the three more cytotoxic SU compounds. However, CW15337 had a quantitatively distinct pattern of gene regulation when compared to the SU compounds, suggesting that its mechanism of action may differ slightly from that of the IKKα inhibitors. This was confirmed by the fact that CW15337 only inhibited the non-canonical pathway signalling, whereas the SU compounds inhibited both the canonical and non-canonical NF-κB pathways. On the other hand, Supplementary Figure XV demonstrates that CW15337 has many kinase targets, including JAK2 and MAP4K2, which may contribute to the comparatively different regulation of the 10 genes selected from the microarray analysis. For this reason, a genome-wide investigation of the effects of CW15337 is merited to investigate whether, similar to BAY 11-7082 (Lee et al. 2012; Rauert-Wunderlich et al. 2013; Strickson et al. 2013) and SU1349, more off-target inhibition is evident.

Overall, the data in this thesis shows that the novel NIK inhibitor CW15337 was comparatively more potent at inducing cytotoxicity in the MM cell lines when compared to the non-specific pan IKK inhibitor BAY 11-7082

and the novel IKKα inhibitors evaluated in this project. Moreover, relative to the SU compounds, CW15337 was a more potent inhibitor of Mcl-1 expression and induced more selective inhibition of the non-canonical NF-κB pathway in MM cell lines, which likely contributes to the apoptotic effect of this agent. Therefore, the data presented in this thesis would suggest that NIK inhibition represents a promising therapeutic strategy for targeting MM.

7.2.2. Limitations of this study and suggested future work

The initial hypothesis for the work surrounding the evaluation of NF-κB inhibitors in MM, was that the MM cell lines that possessed a high-level of NF-κB activity would be inherently more dependent on these signalling pathways for survival. Therefore, NF-κB inhibition would selectively target MM cells that relied more heavily on constitutive NF-κB activity. This is sometimes referred to as oncogene addiction (Torti a Trusolino 2011). An interesting finding of this thesis was that MM cell lines that possessed a relatively high level of constitutive NF-κB activity were comparatively more resistant to apoptosis induced by the non-specific NF-κB inhibitor BAY 11-7082 and the NIK inhibitor CW15337. This could potentially present a flaw in the rationale for targeting MM using specific NF-κB inhibitors and may indicate that cells that possess lower levels of NF-κB activity, such as non-malignant cells, may be sensitive to NF-κB inhibition, resulting in adverse toxicity. For this reason, one of the next steps for this work would be to evaluate the use of the novel SU compounds and CW15337 in normal B-cells to determine whether a positive therapeutic index exists between malignant cells and normal cells.

A more complete structure activity analysis would also be important; this was not possible in the present study as the chemical structures of the individual SU compounds were not divulged due to outstanding intellectual property issues. Furthermore, the kinase inhibitory profile data, kindly provided by Prof. Simon Mackay, only included information on IKKα, IKKβ and CDK9. This means that it is possible that these agents may potently inhibit other targets, including other kinases, which might explain the findings reported in this thesis.

A critique of the work carried in this thesis would be the dominant use of MM cell lines as opposed to primary material. Initially, I planned to use primary MM cells derived from patients to provide a more realistic evaluation of the NF-κB inhibitors. However, it became apparent in the earlier stages of this project that the experiments used to characterise the NF-κB inhibitors used a relatively large number of cells, which made routine use of clinical samples impossible.

Consequently, the RPMI8226 cell line was used for the characterisation of the SU compounds. I would have liked to also evaluate the SU compounds in the other MM cell lines to allow a comparison of their sensitivity and to investigate whether, like BAY 11-7082 and CW15337, the sensitivity to apoptosis induced by the SU compounds varied between these cell lines. However, the time constraints of this project pressed me into selecting a 'representative' MM cell line to allow appropriate evaluation of the nine novel SU compounds. RPMI8226 was chosen because this cell line was found to possess an intermediate level of constitutive NF-κB activity (Chapter 3) and possessed genetic abnormalities associated with constitutive non-canonical NF-κB signalling (Annunziata et al. 2007; Keats et al. 2007; Demchenko et al. 2010). Another reason why the RPMI8226 cell line was chosen for the SU compound characterisation was that this MM cell line was found to express CD40, and CD40L stimulation induced a significant increase in both the canonical and non-canonical NF-κB activity. Interaction of malignant plasma cells with the BMM provides a supportive tumour environment, and CD40L stimulation is one factor that contributes to this effect *in vivo* (Coope et al. 2002; Tai et al. 2003; Hauer et al. 2005). Therefore, further work could include investigating the role that prior CD40L stimulation has on the sensitivity of the RPMI8226 cell line to apoptosis induced by the NF-κB inhibitors evaluated throughout this thesis. This would address the question as to whether increased NF-κB activity could increase the resistance of this cell line to cytotoxicity induced by the NF-κB inhibitors, and may highlight the role of the tumour microenvironment in protecting MM cells from potential therapies targeting the NF-κB pathway.

Another limitation of the work carried out in this thesis is the dependence on the techniques EMSA and ELISA to characterise NF-κB activity in the four MM cell lines, and the dependence mainly on ELISA to quantify the effect of the NF-κB inhibitors in the MM cell line RPMI8226. As discussed throughout this thesis, the ELISA potentially possessed caveats that meant that the sole use of this technique might not have been appropriate to fully answer the research questions posed. As shown briefly in Chapter 4, by using the right combination of antibodies (p-p100, p100, p52, IκBα and p-p65), western blotting could have provided more in depth information about specific NF-κB pathway processing. For this reason, it would have been more appropriate to have used western blotting as an additional or replacement technique for more definitively determining both canonical and non-canonical NF-κB pathway processing in the MM cell lines at baseline, and following treatment with the NF-κB inhibitors.

Despite the limitations already described, this study produced the first genome-wide microarray dataset analysing the use of novel IKKα inhibitors in MM. The analysis performed in this thesis focused on the DE gene expression induced by the SU compounds. Therefore, many other parts of the dataset could be analysed including alternate splicing events, various microRNA and more analysis of the pathways indicated by regulation of DE genes. This would potentially allow a greater understanding of the effects of the SU compounds in MM.

7.2.3. The future of NF-κB targeting in the treatment of MM

Overall, my final thoughts are that targeting the NF-κB pathways in MM could be described as a double-edged sword. Although targeting NF-κB may provide a promising therapeutic strategy for the treatment of MM due to the reliance that this disease has on NF-κB activation, NF-κB is involved in the regulation of a number of biological processes and global inhibition of NF-κB has been shown to induce a number of toxicities related to immune suppression and inflammation (DiDonato et al. 2012). Therefore, the development of NF-κB inhibitors that selectively target specific components

of the NF-κB pathway could potentially minimise the serious toxicities that are associated with global inhibition.

In keeping with this concept, multiple IKKβ inhibitors have been shown to be moderately successful in targeting MM (Hideshima et al. 2002; Bharti et al. 2003; Hideshima et al. 2006; Annunziata et al. 2007; Jourdan et al. 2007; Hideshima et al. 2009). However, concerns over their safety profiles has prevented further development of these specific agents (Li et al. 1999a; Li et al. 1999b; Tanaka et al. 1999; Greten et al. 2007; Vallabhapurapu a Karin 2009; Hsu et al. 2011). For this reason, specific inhibition of the non-canonical NF-κB pathway may provide an alternative method for therapeutically targeting MM.

On the other hand, this thesis indicates that targeting IKKα alone may not provide a suitable treatment for MM, and instead inhibiting the non-canonical NF-κB pathway using specific NIK inhibitors, such as CW15337, may be more beneficial. However, more work is required to understand the effects that NIK inhibition may have on non-malignant cells, to avoid adverse toxicities, and explore the protective role that the tumour microenvironment may play in protecting MM cells from the anti-tumour effects of NIK inhibition. Due to the heterogenic nature of MM, the use of NIK inhibitors should be evaluated in a larger selection of MM cell lines and MM patient samples to determine the range of responses to NIK inhibition. This could help to identify patient characteristics, stage and/or genetic abnormalities that identify patients who might benefit from frontline treatment with a NIK inhibiting agent. This would be particularly beneficial if NIK inhibition was found to be effective in the high-risk MM patient group because in this patient population progression-free survival is limited (Kumar et al. 2008; Naymagon a Abdul-Hay 2016).

Further to the above, the use of a both IKKα and NIK inhibitors should be explored in combination with the current MM treatments such as bortezomib, pomalidomide and dexamethasone, all of which have been suggested to act synergistically with specific NF-κB inhibitors (Keifer et al.

2001; Mitsiades et al. 2002a; Mitsiades et al. 2002c). Bortezomib and IKKα or NIK inhibitors would be particularly interesting combinations to investigate in MM because Bortezomib has been shown to induce some of its therapeutic activity through the inhibition of the canonical NF-κB signalling pathway (Hideshima et al. 2001; Hideshima et al. 2002). Therefore, this combination may inhibit global NF-κB inhibition in MM to induce the most extreme anti-cancer effects while providing the potential to minimise adverse events. This may provide the most efficacious treatment combination to eradicate MM cells and prevent the emergence of treatment resistant sub-clonal populations in MM, which usually leads to patient relapse or refractory disease (Egan et al. 2012; Magrangeas et al. 2013).

References

Adli, M. et al. 2010. IKKalpha and IKKbeta each function to regulate NF-kappaB activation in the TNF-induced/canonical pathway. *PLoS One* 5(2), t. e9428.

Andree, H. A. et al. 1990. Binding of vascular anticoagulant alpha (VAC alpha) to planar phospholipid bilayers. *J Biol Chem* 265(9), tt. 4923-4928.

Annunziata, C. M. et al. 2007. Frequent engagement of the classical and alternative NF-kappaB pathways by diverse genetic abnormalities in multiple myeloma. *Cancer Cell* 12(2), tt. 115-130.

Bergsagel, P. L. et al. 2005. Cyclin D dysregulation: an early and unifying pathogenic event in multiple myeloma. *Blood* 106(1), tt. 296-303.

Bergsagel, P. L. et al. 2013. Improving overall survival and overcoming adverse prognosis in the treatment of cytogenetically high-risk multiple myeloma. *Blood* 121(6), tt. 884-892.

Bharti, A. C. et al. 2003. Curcumin (diferuloylmethane) down-regulates the constitutive activation of nuclear factor-kappa B and IkappaBalpha kinase in human multiple myeloma cells, leading to suppression of proliferation and induction of apoptosis. *Blood* 101(3), tt. 1053-1062.

Bianchi, G. a Anderson, K. C. 2014. Understanding biology to tackle the disease: Multiple myeloma from bench to bedside, and back. *CA Cancer J Clin* 64(6), tt. 422-444.

Boccadoro, M. et al. 2005. Preclinical evaluation of the proteasome inhibitor bortezomib in cancer therapy. *Cancer Cell Int* 5(1), t. 18.

Bommert, K. et al. 2006. Signalling and survival pathways in multiple myeloma. *Eur J Cancer* 42(11), tt. 1574-1580.

Bonizzi, G. et al. 2004. Activation of IKKalpha target genes depends on recognition of specific kappaB binding sites by RelB:p52 dimers. *EMBO J* 23(21), tt. 4202-4210.

Brieva, J. A. et al. 1991. Human in vivo-induced spontaneous IgG-secreting cells from tonsil, blood and bone marrow exhibit different phenotype and functional level of maturation. *Immunology* 72(4), tt. 580-583.

Brioli, A. et al. 2014a. The impact of intra-clonal heterogeneity on the treatment of multiple myeloma. *Br J Haematol* 165(4), tt. 441-454.

Brioli, A. et al. 2014b. Biology and treatment of myeloma. *Clin Lymphoma Myeloma Leuk* 14 Suppl, tt. S65-70.

Cao, Y. et al. 2001. IKKalpha provides an essential link between RANK signaling and cyclin D1 expression during mammary gland development. *Cell* 107(6), tt. 763-775.

Carlotti, F. et al. 2000. Dynamic shuttling of nuclear factor kappa B between the nucleus and cytoplasm as a consequence of inhibitor dissociation. *J Biol Chem* 275(52), tt. 41028-41034.

Carvalho, B. S. a Irizarry, R. A. 2010. A framework for oligonucleotide microarray preprocessing. *Bioinformatics* 26(19), tt. 2363-2367.

Cassese, G. et al. 2003. Plasma cell survival is mediated by synergistic effects of cytokines and adhesion-dependent signals. *J Immunol* 171(4), tt. 1684-1690.

Cesano, A. et al. 1998. Role of CD38 and its ligand in the regulation of MHC-nonrestricted cytotoxic T cells. *J Immunol* 160(3), tt. 1106-1115.

Chapman, M. A. et al. 2011. Initial genome sequencing and analysis of multiple myeloma. *Nature* 471(7339), tt. 467-472.

Chauhan, D. et al. 1996. Multiple myeloma cell adhesion-induced interleukin-6 expression in bone marrow stromal cells involves activation of NF-kappa B. *Blood* 87(3), tt. 1104-1112.

Chauhan, D. et al. 1995. Regulation of interleukin 6 in multiple myeloma and bone marrow stromal cells. *Stem Cells* 13 Suppl 2, tt. 35-39.

Chen, E. Y. et al. 2013. Enrichr: interactive and collaborative HTML5 gene list enrichment analysis tool. *BMC Bioinformatics* 14, t. 128.

Chen, F. E. a Ghosh, G. 1999. Regulation of DNA binding by Rel/NF-kappaB transcription factors: structural views. *Oncogene* 18(49), tt. 6845-6852.

Chen, L. F. a Greene, W. C. 2004. Shaping the nuclear action of NF-kappaB. *Nat Rev Mol Cell Biol* 5(5), tt. 392-401.

Chen, Z. et al. 1995. Signal-induced site-specific phosphorylation targets I kappa B alpha to the ubiquitin-proteasome pathway. *Genes Dev* 9(13), tt. 1586-1597.

Chng, W. J. et al. 2014. IMWG consensus on risk stratification in multiple myeloma. *Leukemia* 28(2), tt. 269-277.

Claudio, E. et al. 2002a. BAFF-induced NEMO-independent processing of NF-kappa B2 in maturing B cells. *Nat Immunol* 3(10), tt. 958-965.

Claudio, J. O. et al. 2002b. A molecular compendium of genes expressed in multiple myeloma. *Blood* 100(6), tt. 2175-2186.

Collins, J. M. 2015. *National Institute of Cancer, Discovery & Development Service, NCI-60 Human Cancer Cell Line Screen* [Ar-Lein]. https://dtp.cancer.gov/discovery_development/nci-60/cell_list.htm: Ar gael ar: [Cyrchwyd: 27/09/2016].

Coope, H. J. et al. 2002. CD40 regulates the processing of NF-kappaB2 p100 to p52. *EMBO J* 21(20), tt. 5375-5385.

Cormier, F. et al. 2013. Frequent engagement of RelB activation is critical for cell survival in multiple myeloma. *PLoS One* 8(3), t. e59127.

CRUK. 2014. *Cancer Research UK (CRUK), Myeloma incidence statistics* [Ar-Lein]. Ar gael ar: http://www.cancerresearchuk.org/health-professional/cancer-

statistics/statistics-by-cancer-type/myeloma/incidence - heading-One [Cyrchwyd: September].

Dai, S. et al. 2004a. The IkappaB kinase (IKK) inhibitor, NEMO-binding domain peptide, blocks osteoclastogenesis and bone erosion in inflammatory arthritis. *J Biol Chem* 279(36), tt. 37219-37222.

Dai, Y. et al. 2004b. Interruption of the NF-kappaB pathway by Bay 11-7082 promotes UCN-01-mediated mitochondrial dysfunction and apoptosis in human multiple myeloma cells. *Blood* 103(7), tt. 2761-2770.

Davies, F. a Baz, R. 2010. Lenalidomide mode of action: linking bench and clinical findings. *Blood Rev* 24 Suppl 1, tt. S13-19.

de Falco, G. a Giordano, A. 1998. CDK9 (PITALRE): a multifunctional cdc2-related kinase. *J Cell Physiol* 177(4), tt. 501-506.

Deaglio, S. et al. 1998. Human CD38 (ADP-ribosyl cyclase) is a counter-receptor of CD31, an Ig superfamily member. *J Immunol* 160(1), tt. 395-402.

Decaux, O. et al. 2008. Prediction of survival in multiple myeloma based on gene expression profiles reveals cell cycle and chromosomal instability signatures in high-risk patients and hyperdiploid signatures in low-risk patients: a study of the Intergroupe Francophone du Myélome. *J Clin Oncol* 26(29), tt. 4798-4805.

Deckert, J. et al. 2014. SAR650984, a novel humanized CD38-targeting antibody, demonstrates potent antitumor activity in models of multiple myeloma and other CD38+ hematologic malignancies. *Clin Cancer Res* 20(17), tt. 4574-4583.

Delhase, M. et al. 1999. Positive and negative regulation of IkappaB kinase activity through IKKbeta subunit phosphorylation. *Science* 284(5412), tt. 309-313.

Demchenko, Y. N. et al. 2014. Novel inhibitors are cytotoxic for myeloma cells with NFkB inducing kinase-dependent activation of NFkB. *Oncotarget* 5(12), tt. 4554-4566.

Demchenko, Y. N. et al. 2010. Classical and/or alternative NF-kappaB pathway activation in multiple myeloma. *Blood* 115(17), tt. 3541-3552.

Demchenko, Y. N. a Kuehl, W. M. 2010. A critical role for the NFkB pathway in multiple myeloma. *Oncotarget* 1(1), tt. 59-68.

Deng, L. et al. 2000. Activation of the IkappaB kinase complex by TRAF6 requires a dimeric ubiquitin-conjugating enzyme complex and a unique polyubiquitin chain. *Cell* 103(2), tt. 351-361.

Derenne, S. et al. 2002. Antisense strategy shows that Mcl-1 rather than Bcl-2 or Bcl-x(L) is an essential survival protein of human myeloma cells. *Blood* 100(1), tt. 194-199.

DiDonato, J. A. et al. 1997. A cytokine-responsive IkappaB kinase that activates the transcription factor NF-kappaB. *Nature* 388(6642), tt. 548-554.

DiDonato, J. A. et al. 2012. NF-κB and the link between inflammation and cancer. *Immunol Rev* 246(1), tt. 379-400.

Dimopoulos, M. A. et al. 2016. Carfilzomib and dexamethasone versus bortezomib and dexamethasone for patients with relapsed or refractory multiple myeloma (ENDEAVOR): a randomised, phase 3, open-label, multicentre study. *Lancet Oncol* 17(1), tt. 27-38.

Dispenzieri, A. et al. 2010. Prevalence and risk of progression of light-chain monoclonal gammopathy of undetermined significance: a retrospective population-based cohort study. *Lancet* 375(9727), tt. 1721-1728.

Dispenzieri, A. et al. 2013. Smoldering multiple myeloma requiring treatment: time for a new definition? *Blood* 122(26), tt. 4172-4181.

Dobrzanski, P. et al. 1994. Differential interactions of Rel-NF-kappa B complexes with I kappa B alpha determine pools of constitutive and inducible NF-kappa B activity. *EMBO J* 13(19), tt. 4608-4616.

Dolcet, X. et al. 2005. NF-kB in development and progression of human cancer. *Virchows Arch* 446(5), tt. 475-482.

Dolloff, N. G. et al. 2012. Sangivamycin-like molecule 6 exhibits potent anti-multiple myeloma activity through inhibition of cyclin-dependent kinase-9. *Mol Cancer Ther* 11(11), tt. 2321-2330.

Dou, Q. P. a Li, B. 1999. Proteasome inhibitors as potential novel anticancer agents. *Drug Resist Updat* 2(4), tt. 215-223.

Drexler, H. G. a Matsuo, Y. 2000. Malignant hematopoietic cell lines: in vitro models for the study of multiple myeloma and plasma cell leukemia. *Leuk Res* 24(8), tt. 681-703.

DSMZ. 2016. *JJN-3 catalogue data sheet* [Ar-Lein]. https://http://www.dsmz.de/catalogues/details/culture/ACC-541.html: Ar gael ar: [Cyrchwyd: 27/09/2016].

Dürig, J. et al. 2003. Expression of ribosomal and translation-associated genes is correlated with a favorable clinical course in chronic lymphocytic leukemia. *Blood* 101(7), tt. 2748-2755.

Ea, C. K. et al. 2006. Activation of IKK by TNFalpha requires site-specific ubiquitination of RIP1 and polyubiquitin binding by NEMO. *Mol Cell* 22(2), tt. 245-257.

Egan, J. B. et al. 2012. Whole-genome sequencing of multiple myeloma from diagnosis to plasma cell leukemia reveals genomic initiating events, evolution, and clonal tides. *Blood* 120(5), tt. 1060-1066.

Egan, P. et al. 2016. Towards Stratified Medicine in Plasma Cell Myeloma. *Int J Mol Sci* 17(10).

Fadok, V. A. et al. 1992. Exposure of phosphatidylserine on the surface of apoptotic lymphocytes triggers specific recognition and removal by macrophages. *J Immunol* 148(7), tt. 2207-2216.

Feng, R. et al. 2007. SDX-308, a nonsteroidal anti-inflammatory agent, inhibits NF-kappaB activity, resulting in strong inhibition of osteoclast formation/activity and multiple myeloma cell growth. *Blood* 109(5), tt. 2130-2138.

Fernandes, M. S. et al. 2009. Growth inhibition of human multiple myeloma cells by an oncolytic adenovirus carrying the CD40 ligand transgene. *Clin Cancer Res* 15(15), tt. 4847-4856.

Fernàndez, J. E. et al. 1998. Analysis of the distribution of human CD38 and of its ligand CD31 in normal tissues. *J Biol Regul Homeost Agents* 12(3), tt. 81-91.

Fong, A. a Sun, S. C. 2002. Genetic evidence for the essential role of beta-transducin repeat-containing protein in the inducible processing of NF-kappa B2/p100. *J Biol Chem* 277(25), tt. 22111-22114.

Fuchs, O. 2013. Targeting of NF-kappaB signaling pathway, other signaling pathways and epigenetics in therapy of multiple myeloma. *Cardiovasc Hematol Disord Drug Targets* 13(1), tt. 16-34.

Gardam, S. et al. 2008. TRAF2 and TRAF3 signal adapters act cooperatively to control the maturation and survival signals delivered to B cells by the BAFF receptor. *Immunity* 28(3), tt. 391-401.

Gasparini, C. et al. 2014. NF- κ B pathways in hematological malignancies. *Cell Mol Life Sci* 71(11), tt. 2083-2102.

Gazdar, A. F. et al. 1986. Establishment and characterization of a human plasma cell myeloma culture having a rearranged cellular myc proto-oncogene. *Blood* 67(6), tt. 1542-1549.

Gentleman, R. C. et al. 2004. Bioconductor: open software development for computational biology and bioinformatics. *Genome Biol* 5(10), t. R80.

Gerondakis, S. et al. 2006. Unravelling the complexities of the NF-kappaB signalling pathway using mouse knockout and transgenic models. *Oncogene* 25(51), tt. 6781-6799.

Gertz, M. A. 2013. Pomalidomide and myeloma meningitis. *Leuk Lymphoma* 54(4), tt. 681-682.

Gharbaran, R. 2015. Advances in the molecular functions of syndecan-1 (SDC1/CD138) in the pathogenesis of malignancies. *Crit Rev Oncol Hematol* 94(1), tt. 1-17.

Ghosh, G. et al. 2012. NF- κ B regulation: lessons from structures. *Immunol Rev* 246(1), tt. 36-58.

Ghosh, S. a Karin, M. 2002. Missing pieces in the NF-kappaB puzzle. *Cell* 109 Suppl, tt. S81-96.

Gilmore, T. D. 2007. Multiple myeloma: lusting for NF-kappaB. *Cancer Cell* 12(2), tt. 95-97.

Godwin, P. et al. 2013. Targeting nuclear factor-kappa B to overcome resistance to chemotherapy. *Front Oncol* 3, t. 120.

Gooding, R. P. et al. 1999. Phenotypic and molecular analysis of six human cell lines derived from patients with plasma cell dyscrasia. *Br J Haematol* 106(3), tt. 669-681.

Greipp, P. R. et al. 2005. International staging system for multiple myeloma. *J Clin Oncol* 23(15), tt. 3412-3420.

Greten, F. R. et al. 2007. NF-kappaB is a negative regulator of IL-1beta secretion as revealed by genetic and pharmacological inhibition of IKKbeta. *Cell* 130(5), tt. 918-931.

Grossmann, M. et al. 2000. The anti-apoptotic activities of Rel and RelA required during B-cell maturation involve the regulation of Bcl-2 expression. *EMBO J* 19(23), tt. 6351-6360.

Group, I. M. W. 2003. Criteria for the classification of monoclonal gammopathies, multiple myeloma and related disorders: a report of the International Myeloma Working Group. *Br J Haematol* 121(5), tt. 749-757.

Guttridge, D. C. et al. 1999. NF-kappaB controls cell growth and differentiation through transcriptional regulation of cyclin D1. *Mol Cell Biol* 19(8), tt. 5785-5799.

Hanahan, D. a Weinberg, R. A. 2000. The hallmarks of cancer. *Cell* 100(1), tt. 57-70.

Hanahan, D. a Weinberg, R. A. 2011. Hallmarks of cancer: the next generation. *Cell* 144(5), tt. 646-674.

Hargreaves, D. C. et al. 2001. A coordinated change in chemokine responsiveness guides plasma cell movements. *J Exp Med* 194(1), tt. 45-56.

Hata, H. et al. 1994. Establishment of a monoclonal antibody to plasma cells: a comparison with CD38 and PCA-1. *Clin Exp Immunol* 96(2), tt. 370-375.

Hauer, J. et al. 2005. TNF receptor (TNFR)-associated factor (TRAF) 3 serves as an inhibitor of TRAF2/5-mediated activation of the noncanonical NF-kappaB pathway by TRAF-binding TNFRs. *Proc Natl Acad Sci U S A* 102(8), tt. 2874-2879.

Hauser, A. E. et al. 2002. Chemotactic responsiveness toward ligands for CXCR3 and CXCR4 is regulated on plasma blasts during the time course of a memory immune response. *J Immunol* 169(3), tt. 1277-1282.

Hayden, M. S. a Ghosh, S. 2004. Signaling to NF-kappaB. *Genes Dev* 18(18), tt. 2195-2224.

Hayden, M. S. a Ghosh, S. 2008. Shared principles in NF-kappaB signaling. *Cell* 132(3), tt. 344-362.

Hayden, M. S. a Ghosh, S. 2011. NF- κ B in immunobiology. *Cell Res* 21(2), tt. 223-244.

Hayden, M. S. a Ghosh, S. 2012. NF- κ B, the first quarter-century: remarkable progress and outstanding questions. *Genes Dev* 26(3), tt. 203-234.

He, J. Q. et al. 2006. Rescue of TRAF3-null mice by p100 NF-kappa B deficiency. *J Exp Med* 203(11), tt. 2413-2418.

Hellman, L. et al. 1988. Immunoglobulin synthesis in the human myeloma cell line U-266; expression of two immunoglobulin heavy chain isotypes (epsilon and alpha) after long-term cultivation in vitro. *Eur J Immunol* 18(6), tt. 905-910.

Hengeveld, P. J. a Kersten, M. J. 2015. B-cell activating factor in the pathophysiology of multiple myeloma: a target for therapy? *Blood Cancer J* 5, t. e282.

Henkel, T. et al. 1992. Intramolecular masking of the nuclear location signal and dimerization domain in the precursor for the p50 NF-kappa B subunit. *Cell* 68(6), tt. 1121-1133.

Heusch, M. et al. 1999. The generation of nfkb2 p52: mechanism and efficiency. *Oncogene* 18(46), tt. 6201-6208.

Hideshima, T. et al. 2009. Biologic sequelae of I{kappa}B kinase (IKK) inhibition in multiple myeloma: therapeutic implications. *Blood* 113(21), tt. 5228-5236.

Hideshima, T. et al. 2002. NF-kappa B as a therapeutic target in multiple myeloma. *J Biol Chem* 277(19), tt. 16639-16647.

Hideshima, T. et al. 2007. Understanding multiple myeloma pathogenesis in the bone marrow to identify new therapeutic targets. *Nat Rev Cancer* 7(8), tt. 585-598.

Hideshima, T. et al. 2006. MLN120B, a novel IkappaB kinase beta inhibitor, blocks multiple myeloma cell growth in vitro and in vivo. *Clin Cancer Res* 12(19), tt. 5887-5894.

Hideshima, T. et al. 2001. The proteasome inhibitor PS-341 inhibits growth, induces apoptosis, and overcomes drug resistance in human multiple myeloma cells. *Cancer Res* 61(7), tt. 3071-3076.

Hinz, M. et al. 2012. It takes two to tango: I κ Bs, the multifunctional partners of NF- κ B. *Immunol Rev* 246(1), tt. 59-76.

Hinz, M. et al. 1999. NF-kappaB function in growth control: regulation of cyclin D1 expression and G0/G1-to-S-phase transition. *Mol Cell Biol* 19(4), tt. 2690-2698.

Hinz, M. et al. 2001. Constitutive NF-kappaB maintains high expression of a characteristic gene network, including CD40, CD86, and a set of antiapoptotic genes in Hodgkin/Reed-Sternberg cells. *Blood* 97(9), tt. 2798-2807.

Hinz, M. a Scheidereit, C. 2014. The I κ B kinase complex in NF- κ B regulation and beyond. *EMBO Rep* 15(1), tt. 46-61.

Hirata, T. et al. 2003. Humanized anti-interleukin-6 receptor monoclonal antibody induced apoptosis of fresh and cloned human myeloma cells in vitro. *Leuk Res* 27(4), tt. 343-349.

HMRN. 2014. *Haematological Malignancy Research Network, Myeloma* [Ar-Lein]. Ar gael ar: https://http://www.hmrn.org/statistics/disorders/24 [Cyrchwyd: September].

Horenstein, A. L. et al. 2015. NAD^+-Metabolizing Ectoenzymes in Remodeling Tumor-Host Interactions: The Human Myeloma Model. *Cells* 4(3), tt. 520-537.

Hose, D. et al. 2011. Proliferation is a central independent prognostic factor and target for personalized and risk-adapted treatment in multiple myeloma. *Haematologica* 96(1), tt. 87-95.

Hsu, L. C. et al. 2011. IL-1 β -driven neutrophilia preserves antibacterial defense in the absence of the kinase IKK β . *Nat Immunol* 12(2), tt. 144-150.

Huang, T. T. et al. 2000. A nuclear export signal in the N-terminal regulatory domain of IkappaBalpha controls cytoplasmic localization of inactive NF-kappaB/IkappaBalpha complexes. *Proc Natl Acad Sci U S A* 97(3), tt. 1014-1019.

Hubank, M. 2004. Gene expression profiling and its application in studies of haematological malignancy. *Br J Haematol* 124(5), tt. 577-594.

Hubbard, J. W. 2014. 'A-GEOD-17586_comments.txt' (Affymetrix GeneChip HTA-2_0 - Gene Level - HTA-2_0.r1.Psrs.mps probesets). Affymetrix.

Huxford, T. a Ghosh, G. 2009. A structural guide to proteins of the NF-kappaB signaling module. *Cold Spring Harb Perspect Biol* 1(3), t. a000075.

Ichim, G. a Tait, S. W. 2016. A fate worse than death: apoptosis as an oncogenic process. *Nat Rev Cancer* 16(8), tt. 539-548.

Ikeda, H. et al. 2009. The monoclonal antibody nBT062 conjugated to cytotoxic Maytansinoids has selective cytotoxicity against CD138-positive multiple myeloma cells in vitro and in vivo. *Clin Cancer Res* 15(12), tt. 4028-4037.

Jackson, N. et al. 1989. Two new IgA1-kappa plasma cell leukaemia cell lines (JJN-1 & JJN-2) which proliferate in response to B cell stimulatory factor 2. *Clin Exp Immunol* 75(1), tt. 93-99.

Jayandharan, G. R. et al. 2011. Activation of the NF-kappaB pathway by adeno-associated virus (AAV) vectors and its implications in immune response and gene therapy. *Proc Natl Acad Sci U S A* 108(9), tt. 3743-3748.

Jelinek, D. F. et al. 2003. Identification of a global gene expression signature of B-chronic lymphocytic leukemia. *Mol Cancer Res* 1(5), tt. 346-361.

Johnson, C. et al. 1999. An N-terminal nuclear export signal is required for the nucleocytoplasmic shuttling of IkappaBalpha. *EMBO J* 18(23), tt. 6682-6693.

Jorda, R. et al. 2014. Arylazopyrazole AAP1742 inhibits CDKs and induces apoptosis in multiple myeloma cells via Mcl-1 downregulation. *Chem Biol Drug Des* 84(4), tt. 402-408.

Jost, P. J. a Ruland, J. 2007. Aberrant NF-kappaB signaling in lymphoma: mechanisms, consequences, and therapeutic implications. *Blood* 109(7), tt. 2700-2707.

Jourdan, M. et al. 1998. The myeloma cell antigen syndecan-1 is lost by apoptotic myeloma cells. *Br J Haematol* 100(4), tt. 637-646.

Jourdan, M. et al. 2007. Targeting NF-kappaB pathway with an IKK2 inhibitor induces inhibition of multiple myeloma cell growth. *Br J Haematol* 138(2), tt. 160-168.

Joyce, D. et al. 2001. NF-kappaB and cell-cycle regulation: the cyclin connection. *Cytokine Growth Factor Rev* 12(1), tt. 73-90.

Kaileh, M. a Sen, R. 2012. NF- κ B function in B lymphocytes. *Immunol Rev* 246(1), tt. 254-271.

Kaisho, T. et al. 2001. IkappaB kinase alpha is essential for mature B cell development and function. *J Exp Med* 193(4), tt. 417-426.

Kamińska, J. et al. 2016. Serum soluble CD40L concentration depending on the stage of multiple myeloma and its correlation with selected angiogenic cytokines. *Pol Arch Med Wewn* 126(5), tt. 321-329.

Kanarek, N. a Ben-Neriah, Y. 2012. Regulation of NF- κ B by ubiquitination and degradation of the I κ Bs. *Immunol Rev* 246(1), tt. 77-94.

Kanarek, N. et al. 2010. Ubiquitination and degradation of the inhibitors of NF-kappaB. *Cold Spring Harb Perspect Biol* 2(2), t. a000166.

Kang, B. N. et al. 2006. Transcriptional regulation of CD38 expression by tumor necrosis factor-alpha in human airway smooth muscle cells: role of NF-kappaB and sensitivity to glucocorticoids. *FASEB J* 20(7), tt. 1000-1002.

Karin, M. et al. 2002. NF-kappaB in cancer: from innocent bystander to major culprit. *Nat Rev Cancer* 2(4), tt. 301-310.

Kawano, M. et al. 1988. Autocrine generation and requirement of BSF-2/IL-6 for human multiple myelomas. *Nature* 332(6159), tt. 83-85.

Keats, J. J. et al. 2007. Promiscuous mutations activate the noncanonical NF-kappaB pathway in multiple myeloma. *Cancer Cell* 12(2), tt. 131-144.

Keifer, J. A. et al. 2001. Inhibition of NF-kappa B activity by thalidomide through suppression of IkappaB kinase activity. *J Biol Chem* 276(25), tt. 22382-22387.

Kortuem, K. M. a Stewart, A. K. 2013. Carfilzomib. *Blood* 121(6), tt. 893-897.

Kuehl, W. M. a Bergsagel, P. L. 2012. Molecular pathogenesis of multiple myeloma and its premalignant precursor. *J Clin Invest* 122(10), tt. 3456-3463.

Kuleshov, M. V. et al. 2016. Enrichr: a comprehensive gene set enrichment analysis web server 2016 update. *Nucleic Acids Res* 44(W1), tt. W90-97.

Kumar, S. K. et al. 2008. Improved survival in multiple myeloma and the impact of novel therapies. *Blood* 111(5), tt. 2516-2520.

Kunkel, E. J. a Butcher, E. C. 2003. Plasma-cell homing. *Nat Rev Immunol* 3(10), tt. 822-829.

Kyle, R. A. et al. 2003. Review of 1027 patients with newly diagnosed multiple myeloma. *Mayo Clin Proc* 78(1), tt. 21-33.

Lagging, E. et al. 1996. Distribution of plasma cell markers and intracellular IgE in cell line U266. *Immunol Lett* 49(1-2), tt. 71-77.

Lam, L. T. et al. 2008. Compensatory IKKalpha activation of classical NF-kappaB signaling during IKKbeta inhibition identified by an RNA interference sensitization screen. *Proc Natl Acad Sci U S A* 105(52), tt. 20798-20803.

Landgren, O. et al. 2009. Monoclonal gammopathy of undetermined significance (MGUS) consistently precedes multiple myeloma: a prospective study. *Blood* 113(22), tt. 5412-5417.

Landowski, T. H. et al. 2003. Cell adhesion-mediated drug resistance (CAM-DR) is associated with activation of NF-kappa B (RelB/p50) in myeloma cells. *Oncogene* 22(16), tt. 2417-2421.

Lang, D. T. a the.CRAN.team. 2016. *RCurl: General Network (HTTP/FTP/...) Client Interface for R* [Ar-Lein]. R package version 1.95-4.8: Ar gael ar: http://CRAN.R-project.org/package=RCurl [Cyrchwyd: 15th January].

Lawrence, T. 2009. The nuclear factor NF-kappaB pathway in inflammation. *Cold Spring Harb Perspect Biol* 1(6), t. a001651.

Lee, J. et al. 2012. BAY 11-7082 is a broad-spectrum inhibitor with anti-inflammatory activity against multiple targets. *Mediators Inflamm* 2012, t. 416036.

Leung, T. H. et al. 2004. One nucleotide in a kappaB site can determine cofactor specificity for NF-kappaB dimers. *Cell* 118(4), tt. 453-464.

Li, Q. et al. 1999a. IKK1-deficient mice exhibit abnormal development of skin and skeleton. *Genes Dev* 13(10), tt. 1322-1328.

Li, Q. et al. 1999b. Severe liver degeneration in mice lacking the IkappaB kinase 2 gene. *Science* 284(5412), tt. 321-325.

Li, Z. W. et al. 2008. NF-kappaB in the pathogenesis and treatment of multiple myeloma. *Curr Opin Hematol* 15(4), tt. 391-399.

Liao, G. et al. 2004. Regulation of the NF-kappaB-inducing kinase by tumor necrosis factor receptor-associated factor 3-induced degradation. *J Biol Chem* 279(25), tt. 26243-26250.

Lin, L. a Ghosh, S. 1996. A glycine-rich region in NF-kappaB p105 functions as a processing signal for the generation of the p50 subunit. *Mol Cell Biol* 16(5), tt. 2248-2254.

Lin, P. et al. 2004. Flow cytometric immunophenotypic analysis of 306 cases of multiple myeloma. *Am J Clin Pathol* 121(4), tt. 482-488.

Ling, L. et al. 1998. NF-kappaB-inducing kinase activates IKK-alpha by phosphorylation of Ser-176. *Proc Natl Acad Sci U S A* 95(7), tt. 3792-3797.

Liu, F. et al. 2012. IKK biology. *Immunol Rev* 246(1), tt. 239-253.

Liu, H. et al. 2014. Regulation of Mcl-1 by constitutive activation of NF- κ B contributes to cell viability in human esophageal squamous cell carcinoma cells. *BMC Cancer* 14, t. 98.

Livak, K. J. a Schmittgen, T. D. 2001. Analysis of relative gene expression data using real-time quantitative PCR and the 2(-Delta Delta C(T)) Method. *Methods* 25(4), tt. 402-408.

Mackay, F. a Schneider, P. 2008. TACI, an enigmatic BAFF/APRIL receptor, with new unappreciated biochemical and biological properties. *Cytokine Growth Factor Rev* 19(3-4), tt. 263-276.

Magrangeas, F. et al. 2013. Minor clone provides a reservoir for relapse in multiple myeloma. *Leukemia* 27(2), tt. 473-481.

Mahmoud, M. S. et al. 1998. Induction of CD45 expression and proliferation in U-266 myeloma cell line by interleukin-6. *Blood* 92(10), tt. 3887-3897.

Malek, S. et al. 2001. IkappaBbeta, but not IkappaBalpha, functions as a classical cytoplasmic inhibitor of NF-kappaB dimers by masking both NF-kappaB nuclear localization sequences in resting cells. *J Biol Chem* 276(48), tt. 45225-45235.

Malinin, N. L. et al. 1997. MAP3K-related kinase involved in NF-kappaB induction by TNF, CD95 and IL-1. *Nature* 385(6616), tt. 540-544.

Manohar, S. M. et al. 2011. Cyclin-dependent kinase inhibitor, P276-00 induces apoptosis in multiple myeloma cells by inhibition of Cdk9-T1 and RNA polymerase II-dependent transcription. *Leuk Res* 35(6), tt. 821-830.

Manz, R. A. et al. 1997. Lifetime of plasma cells in the bone marrow. *Nature* 388(6638), tt. 133-134.

Matsuoka, Y. et al. 1967. Production of free light chains of immunoglobulin by a hematopoietic cell line derived from a patient with multiple myeloma. *Proc Soc Exp Biol Med* 125(4), tt. 1246-1250.

Matsuoka, Y. et al. 1968. Synthesis and secretion of immunoglobulins by established cell lines of human hematopoietic origin. *J Immunol* 101(6), tt. 1111-1120.

Matthews, G. M. et al. 2016. NF- κ B dysregulation in multiple myeloma. *Semin Cancer Biol* 39, tt. 68-76.

McCurdy, A. R. a Lacy, M. Q. 2013. Pomalidomide and its clinical potential for relapsed or refractory multiple myeloma: an update for the hematologist. *Ther Adv Hematol* 4(3), tt. 211-216.

McMillin, D. W. et al. 2013. The role of tumour-stromal interactions in modifying drug response: challenges and opportunities. *Nat Rev Drug Discov* 12(3), tt. 217-228.

Meinel, F. G. et al. 2010. The novel, proteasome-independent NF-kappaB inhibitor V1810 induces apoptosis and cell cycle arrest in multiple myeloma and overcomes NF-kappaB-mediated drug resistance. *Mol Cancer Ther* 9(2), tt. 300-310.

Mercurio, F. et al. 1997. IKK-1 and IKK-2: cytokine-activated IkappaB kinases essential for NF-kappaB activation. *Science* 278(5339), tt. 860-866.

Miller, B. S. a Zandi, E. 2001. Complete reconstitution of human IkappaB kinase (IKK) complex in yeast. Assessment of its stoichiometry and the role of IKKgamma on the complex activity in the absence of stimulation. *J Biol Chem* 276(39), tt. 36320-36326.

Millimouno, F. M. et al. 2014. Targeting apoptosis pathways in cancer and perspectives with natural compounds from mother nature. *Cancer Prev Res (Phila)* 7(11), tt. 1081-1107.

Minges Wols, H. A. et al. 2002. The role of bone marrow-derived stromal cells in the maintenance of plasma cell longevity. *J Immunol* 169(8), tt. 4213-4221.

Mitsiades, N. et al. 2002a. Molecular sequelae of proteasome inhibition in human multiple myeloma cells. *Proc Natl Acad Sci U S A* 99(22), tt. 14374-14379.

Mitsiades, N. et al. 2002b. Biologic sequelae of nuclear factor-kappaB blockade in multiple myeloma: therapeutic applications. *Blood* 99(11), tt. 4079-4086.

Mitsiades, N. et al. 2002c. Apoptotic signaling induced by immunomodulatory thalidomide analogs in human multiple myeloma cells: therapeutic implications. *Blood* 99(12), tt. 4525-4530.

Moreau, P. et al. 2015. Frontline therapy of multiple myeloma. *Blood* 125(20), tt. 3076-3084.

Moreaux, J. et al. 2005. The level of TACI gene expression in myeloma cells is associated with a signature of microenvironment dependence versus a plasmablastic signature. *Blood* 106(3), tt. 1021-1030.

Morey, J. S. et al. 2006. Microarray validation: factors influencing correlation between oligonucleotide microarrays and real-time PCR. *Biol Proced Online* 8, tt. 175-193.

Mori, N. et al. 2002. Bay 11-7082 inhibits transcription factor NF-kappaB and induces apoptosis of HTLV-I-infected T-cell lines and primary adult T-cell leukemia cells. *Blood* 100(5), tt. 1828-1834.

Napolitano, G. et al. 2000. Transcriptional activity of positive transcription elongation factor b kinase in vivo requires the C-terminal domain of RNA polymerase II. *Gene* 254(1-2), tt. 139-145.

Naymagon, L. a Abdul-Hay, M. 2016. Novel agents in the treatment of multiple myeloma: a review about the future. *J Hematol Oncol* 9(1), t. 52.

Newton, K. et al. 2008. Ubiquitin chain editing revealed by polyubiquitin linkage-specific antibodies. *Cell* 134(4), tt. 668-678.

Ni, H. et al. 2001. Analysis of expression of nuclear factor kappa B (NF-kappa B) in multiple myeloma: downregulation of NF-kappa B induces apoptosis. *Br J Haematol* 115(2), tt. 279-286.

Nilsson, K. et al. 1970. Established immunoglobulin producing myeloma (IgE) and lymphoblastoid (IgG) cell lines from an IgE myeloma patient. *Clin Exp Immunol* 7(4), tt. 477-489.

Novak, A. J. et al. 2004. Expression of BCMA, TACI, and BAFF-R in multiple myeloma: a mechanism for growth and survival. *Blood* 103(2), tt. 689-694.

O'Connor, B. P. et al. 2003. The rise and fall of long-lived humoral immunity: terminal differentiation of plasma cells in health and disease. *Immunol Rev* 194, tt. 61-76.

O'Connor, B. P. et al. 2004. BCMA is essential for the survival of long-lived bone marrow plasma cells. *J Exp Med* 199(1), tt. 91-98.

Obeng, E. A. et al. 2006. Proteasome inhibitors induce a terminal unfolded protein response in multiple myeloma cells. *Blood* 107(12), tt. 4907-4916.

Odendahl, M. et al. 2005. Generation of migratory antigen-specific plasma blasts and mobilization of resident plasma cells in a secondary immune response. *Blood* 105(4), tt. 1614-1621.

Orian, A. et al. 1999. Structural motifs involved in ubiquitin-mediated processing of the NF-kappaB precursor p105: roles of the glycine-rich region and a downstream ubiquitination domain. *Mol Cell Biol* 19(5), tt. 3664-3673.

Palombella, V. J. et al. 1998. Role of the proteasome and NF-kappaB in streptococcal cell wall-induced polyarthritis. *Proc Natl Acad Sci U S A* 95(26), tt. 15671-15676.

Palumbo, A. et al. 2015. Revised International Staging System for Multiple Myeloma: A Report From International Myeloma Working Group. *J Clin Oncol* 33(26), tt. 2863-2869.

Pasparakis, M. et al. 2002. IkappaB kinase signaling is essential for maintenance of mature B cells. *J Exp Med* 196(6), tt. 743-752.

Patten, P. E. et al. 2008. CD38 expression in chronic lymphocytic leukemia is regulated by the tumor microenvironment. *Blood* 111(10), tt. 5173-5181.

Paíno, T. et al. 2015. Phenotypic identification of subclones in multiple myeloma with different chemoresistant, cytogenetic and clonogenic potential. *Leukemia* 29(5), tt. 1186-1194.

Perel, G. et al. 2016. Carfilzomib (Kyprolis): A Novel Proteasome Inhibitor for Relapsed And/or Refractory Multiple Myeloma. *P T* 41(5), tt. 303-307.

Perez-Andres, M. et al. 2009. Soluble and membrane levels of molecules involved in the interaction between clonal plasma cells and the immunological microenvironment in multiple myeloma and their association with the characteristics of the disease. *Int J Cancer* 124(2), tt. 367-375.

Perkins, N. D. 2006. Post-translational modifications regulating the activity and function of the nuclear factor kappa B pathway. *Oncogene* 25(51), tt. 6717-6730.

Pierce, J. W. et al. 1997. Novel inhibitors of cytokine-induced IkappaBalpha phosphorylation and endothelial cell adhesion molecule expression show anti-inflammatory effects in vivo. *J Biol Chem* 272(34), tt. 21096-21103.

Podar, K. et al. 2007. The malignant clone and the bone-marrow environment. *Best Pract Res Clin Haematol* 20(4), tt. 597-612.

R-Core-Team. 2014. *R: A Language and Environment for Statistical Computing* [Ar-Lein]. R Foundation for Statistical Computing, Vienna, Austria. Ar gael ar: http://www.R-project.org/ [Cyrchwyd.

Rajkumar, S. V. et al. 2014. International Myeloma Working Group updated criteria for the diagnosis of multiple myeloma. *Lancet Oncol* 15(12), tt. e538-548.

Rauert-Wunderlich, H. et al. 2013. The IKK inhibitor Bay 11-7082 induces cell death independent from inhibition of activation of NF κ B transcription factors. *PLoS One* 8(3), t. e59292.

Reddy, N. a Czuczman, M. S. 2010. Enhancing activity and overcoming chemoresistance in hematologic malignancies with bortezomib: preclinical mechanistic studies. *Ann Oncol* 21(9), tt. 1756-1764.

Richardson, P. G. et al. 2012. Management of treatment-emergent peripheral neuropathy in multiple myeloma. *Leukemia* 26(4), tt. 595-608.

Richardson, P. G. et al. 2004. Proteasome inhibition in hematologic malignancies. *Ann Med* 36(4), tt. 304-314.

Ritchie, M. E. et al. 2015. limma powers differential expression analyses for RNA-sequencing and microarray studies. *Nucleic Acids Res* 43(7), t. e47.

Rothwarf, D. M. a Karin, M. 1999. The NF-kappa B activation pathway: a paradigm in information transfer from membrane to nucleus. *Sci STKE* 1999(5), t. RE1.

Ruiz-Argüelles, G. J. a San Miguel, J. F. 1994. Cell surface markers in multiple myeloma. *Mayo Clin Proc* 69(7), tt. 684-690.

Ryseck, R. P. et al. 1992. RelB, a new Rel family transcription activator that can interact with p50-NF-kappa B. *Mol Cell Biol* 12(2), tt. 674-684.

Régnier, C. H. et al. 1997. Identification and characterization of an IkappaB kinase. *Cell* 90(2), tt. 373-383.

San Miguel, J. F. et al. 2002. Immunophenotypic evaluation of the plasma cell compartment in multiple myeloma: a tool for comparing the efficacy of different treatment strategies and predicting outcome. *Blood* 99(5), tt. 1853-1856.

Sasaki, Y. et al. 2008. NIK overexpression amplifies, whereas ablation of its TRAF3-binding domain replaces BAFF:BAFF-R-mediated survival signals in B cells. *Proc Natl Acad Sci U S A* 105(31), tt. 10883-10888.

Sasaki, Y. a Iwai, K. 2016. Roles of the NF- κ B Pathway in B-Lymphocyte Biology. *Curr Top Microbiol Immunol* 393, tt. 177-209.

Sen, R. a Baltimore, D. 1986. Multiple nuclear factors interact with the immunoglobulin enhancer sequences. *Cell* 46(5), tt. 705-716.

Senftleben, U. et al. 2001. Activation by IKKalpha of a second, evolutionary conserved, NF-kappa B signaling pathway. *Science* 293(5534), tt. 1495-1499.

Sezer, O. et al. 2002. Immunocytochemistry reveals RANKL expression of myeloma cells. *Blood* 99(12), tt. 4646-4647; author reply 4647.

Shaughnessy, J. et al. 2005. Gene expression profiling and multiple myeloma. *Best Pract Res Clin Haematol* 18(4), tt. 537-552.

Siebenlist, U. et al. 2005. Control of lymphocyte development by nuclear factor-kappaB. *Nat Rev Immunol* 5(6), tt. 435-445.

Siegel, D. S. et al. 2012. A phase 2 study of single-agent carfilzomib (PX-171-003-A1) in patients with relapsed and refractory multiple myeloma. *Blood* 120(14), tt. 2817-2825.

Sigurdardottir, E. E. et al. 2015. The Role of Diagnosis and Clinical Follow-up of Monoclonal Gammopathy of Undetermined Significance on Survival in Multiple Myeloma. *JAMA Oncol* 1(2), tt. 168-174.

Slifka, M. K. et al. 1995. Bone marrow is a major site of long-term antibody production after acute viral infection. *J Virol* 69(3), tt. 1895-1902.

Slonim, D. K. a Yanai, I. 2009. Getting started in gene expression microarray analysis. *PLoS Comput Biol* 5(10), t. e1000543.

Solan, N. J. et al. 2002. RelB cellular regulation and transcriptional activity are regulated by p100. *J Biol Chem* 277(2), tt. 1405-1418.

Staudt, L. M. a Dave, S. 2005. The biology of human lymphoid malignancies revealed by gene expression profiling. *Adv Immunol* 87, tt. 163-208.

Stewart, A. K. et al. 2009. How I treat multiple myeloma in younger patients. *Blood* 114(27), tt. 5436-5443.

Strickson, S. et al. 2013. The anti-inflammatory drug BAY 11-7082 suppresses the MyD88-dependent signalling network by targeting the ubiquitin system. *Biochem J* 451(3), tt. 427-437.

Tai, Y. T. et al. 2003. CD40 induces human multiple myeloma cell migration via phosphatidylinositol 3-kinase/AKT/NF-kappa B signaling. *Blood* 101(7), tt. 2762-2769.

Takeda, T. et al. 2016. Mangiferin induces apoptosis in multiple myeloma cell lines by suppressing the activation of nuclear factor kappa B-inducing kinase. *Chem Biol Interact* 251, tt. 26-33.

Tanaka, M. et al. 1999. Embryonic lethality, liver degeneration, and impaired NF-kappa B activation in IKK-beta-deficient mice. *Immunity* 10(4), tt. 421-429.

Tarte, K. et al. 2002. Generation of polyclonal plasmablasts from peripheral blood B cells: a normal counterpart of malignant plasmablasts. *Blood* 100(4), tt. 1113-1122.

Terpos, E. et al. 2010. High serum lactate dehydrogenase adds prognostic value to the international myeloma staging system even in the era of novel agents. *Eur J Haematol* 85(2), tt. 114-119.

The UniProt Consortium. 2017. UniProt: the universal protein knowledgebase. *Nucleic Acids Res* 45(D1), tt. D158-D169.

Tirumurugaan, K. G. et al. 2008. Regulation of the cd38 promoter in human airway smooth muscle cells by TNF-alpha and dexamethasone. *Respir Res* 9, t. 26.

Tong, A. W. et al. 2000. CD40 ligand-induced apoptosis is Fas-independent in human multiple myeloma cells. *Leuk Lymphoma* 36(5-6), tt. 543-558.

Tong, A. W. et al. 1994. Anti-CD40 antibody binding modulates human multiple myeloma clonogenicity in vitro. *Blood* 84(9), tt. 3026-3033.

Torti, D. a Trusolino, L. 2011. Oncogene addiction as a foundational rationale for targeted anti-cancer therapy: promises and perils. *EMBO Mol Med* 3(11), tt. 623-636.

Vallabhapurapu, S. a Karin, M. 2009. Regulation and function of NF-kappaB transcription factors in the immune system. *Annu Rev Immunol* 27, tt. 693-733.

Vallabhapurapu, S. et al. 2008. Nonredundant and complementary functions of TRAF2 and TRAF3 in a ubiquitination cascade that activates NIK-dependent alternative NF-kappaB signaling. *Nat Immunol* 9(12), tt. 1364-1370.

Vermes, I. et al. 1995. A novel assay for apoptosis. Flow cytometric detection of phosphatidylserine expression on early apoptotic cells using fluorescein labelled Annexin V. *J Immunol Methods* 184(1), tt. 39-51.

Villunger, A. et al. 1998. Functional granulocyte/macrophage colony stimulating factor receptor is constitutively expressed on neoplastic plasma cells and mediates tumour cell longevity. *Br J Haematol* 102(4), tt. 1069-1080.

Walczak, H. et al. 2012. Generation and physiological roles of linear ubiquitin chains. *BMC Biol* 10, t. 23.

Walker, B. A. et al. 2014. Intraclonal heterogeneity is a critical early event in the development of myeloma and precedes the development of clinical symptoms. *Leukemia* 28(2), tt. 384-390.

Wang, C. et al. 2001. TAK1 is a ubiquitin-dependent kinase of MKK and IKK. *Nature* 412(6844), tt. 346-351.

Wang, C. Y. et al. 1998. NF-kappaB antiapoptosis: induction of TRAF1 and TRAF2 and c-IAP1 and c-IAP2 to suppress caspase-8 activation. *Science* 281(5383), tt. 1680-1683.

Wang, V. Y. et al. 2012. The transcriptional specificity of NF-κB dimers is coded within the κB DNA response elements. *Cell Rep* 2(4), tt. 824-839.

Warnes, G. R. et al. 2016. *gplots: Various R Programming Tools for Plotting Data* [Ar-Lein]. R package version 3.0.1. . Ar gael ar: http://CRAN.R-project.org/package=gplots [Cyrchwyd: 4th September].

Wei, T. a Simko, V. 2016. *corrplot: Visualization of a Correlation Matrix* [Ar-Lein]. Ar gael ar: http://CRAN.R-project.org/package=corrplot [Cyrchwyd: 12th October].

Weiss, B. M. et al. 2009. A monoclonal gammopathy precedes multiple myeloma in most patients. *Blood* 113(22), tt. 5418-5422.

Wijdenes, J. et al. 1996. A plasmocyte selective monoclonal antibody (B-B4) recognizes syndecan-1. *Br J Haematol* 94(2), tt. 318-323.

Willimott, S. et al. 2007. Regulation of CD38 in proliferating chronic lymphocytic leukemia cells stimulated with CD154 and interleukin-4. *Haematologica* 92(10), tt. 1359-1366.

Wu, C. J. et al. 2006. Sensing of Lys 63-linked polyubiquitination by NEMO is a key event in NF-kappaB activation [corrected]. *Nat Cell Biol* 8(4), tt. 398-406.

Xi, H. et al. 2016. Myeloma bone disease: Progress in pathogenesis. *Prog Biophys Mol Biol* 122(2), tt. 149-155.

Xia, Z. P. et al. 2009. Direct activation of protein kinases by unanchored polyubiquitin chains. *Nature* 461(7260), tt. 114-119.

Xiao, G. et al. 2001. NF-kappaB-inducing kinase regulates the processing of NF-kappaB2 p100. *Mol Cell* 7(2), tt. 401-409.

Xie, P. et al. 2007. Tumor necrosis factor receptor-associated factor 3 is a critical regulator of B cell homeostasis in secondary lymphoid organs. *Immunity* 27(2), tt. 253-267.

Yamaoka, S. et al. 1998. Complementation cloning of NEMO, a component of the IkappaB kinase complex essential for NF-kappaB activation. *Cell* 93(7), tt. 1231-1240.

Yang, Y. et al. 2002. Soluble syndecan-1 promotes growth of myeloma tumors in vivo. *Blood* 100(2), tt. 610-617.

Yaron, A. et al. 1998. Identification of the receptor component of the IkappaBalpha-ubiquitin ligase. *Nature* 396(6711), tt. 590-594.

Ye, J. et al. 2012. Primer-BLAST: a tool to design target-specific primers for polymerase chain reaction. *BMC Bioinformatics* 13, t. 134.

Yin, L. et al. 2000. NF-kappa B regulates transcription of the mouse telomerase catalytic subunit. *J Biol Chem* 275(47), tt. 36671-36675.

Zangari, M. et al. 2012. Impact of bortezomib on bone health in myeloma: a review of current evidence. *Cancer Treat Rev* 38(8), tt. 968-980.

Zarnegar, B. et al. 2008. Control of canonical NF-kappaB activation through the NIK-IKK complex pathway. *Proc Natl Acad Sci U S A* 105(9), tt. 3503-3508.

Zhan, F. et al. 2002. Global gene expression profiling of multiple myeloma, monoclonal gammopathy of undetermined significance, and normal bone marrow plasma cells. *Blood* 99(5), tt. 1745-1757.

Zhang, B. et al. 2002. Myeloid cell factor-1 is a critical survival factor for multiple myeloma. *Blood* 99(6), tt. 1885-1893.

Zhang, X. G. et al. 1990. Granulocyte-macrophage colony-stimulating factor synergizes with interleukin-6 in supporting the proliferation of human myeloma cells. *Blood* 76(12), tt. 2599-2605.

Zheng, C. et al. 2011. Structural studies of NF- κ B signaling. *Cell Res* 21(1), tt. 183-195.

Appendix

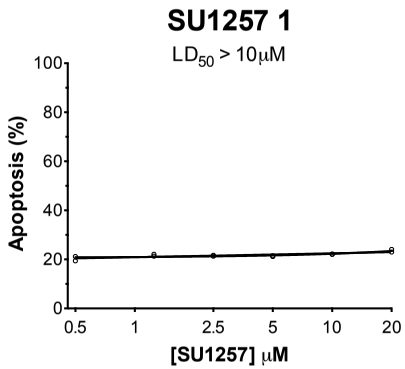
SU1257 1
LD50 > 10μM
Apoptosis (%)
[SU1257] μM

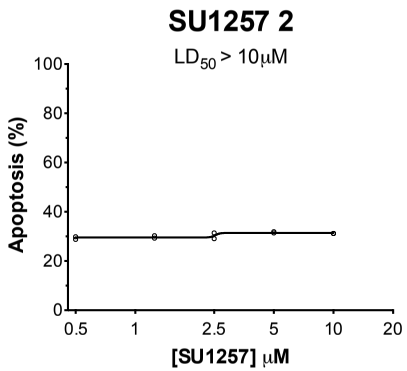
SU1257 2
LD50 > 10μM
Apoptosis (%)
[SU1257] μM

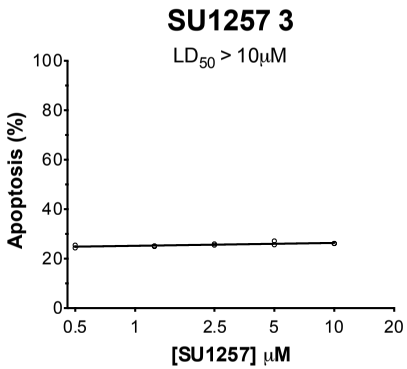
SU1257 3
LD50 > 10μM
Apoptosis (%)
[SU1257] μM

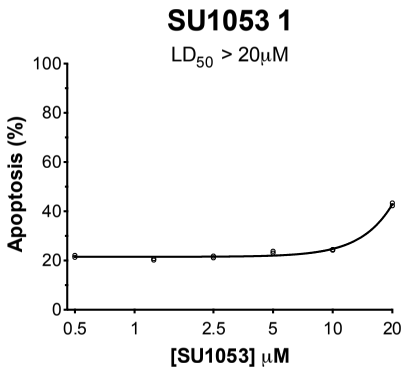
SU1053 1
LD50 > 20μM
Apoptosis (%)
[SU1053] μM

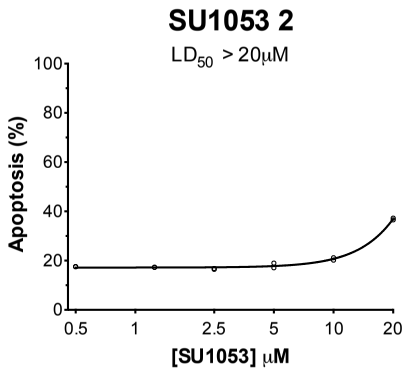
SU1053 2
LD50 > 20μM
Apoptosis (%)
[SU1053] μM

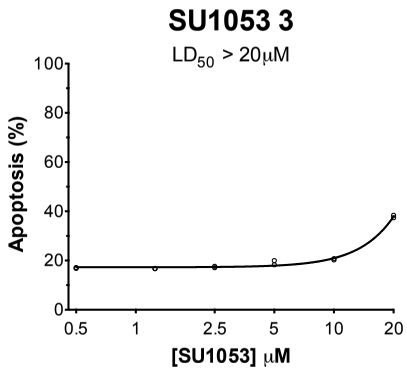
SU1053 3
LD50 > 20μM
Apoptosis (%)
[SU1053] μM

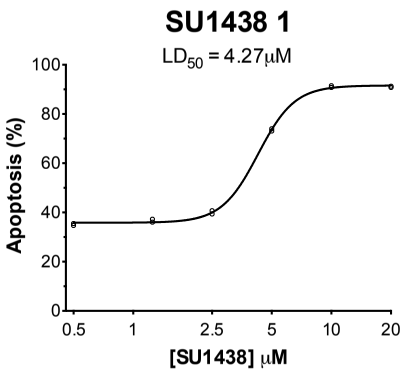
SU1438 1
LD50 = 4.27μM
Apoptosis (%)
[SU1438] μM

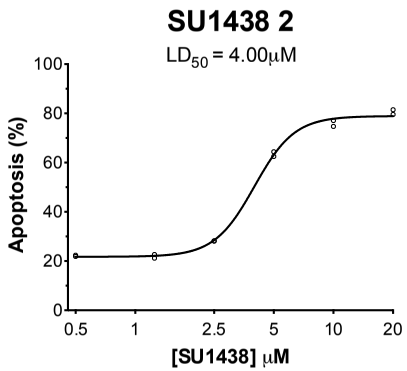
SU1438 2
LD50 = 4.00μM
Apoptosis (%)
[SU1438] μM

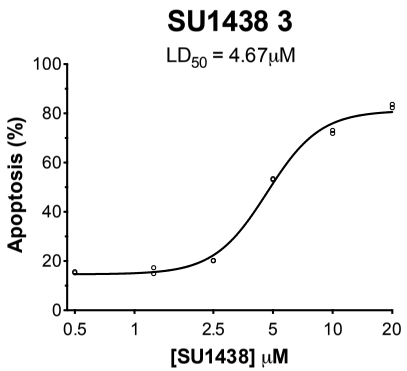
SU1438 3
LD50 = 4.67μM
Apoptosis (%)
[SU1438] μM

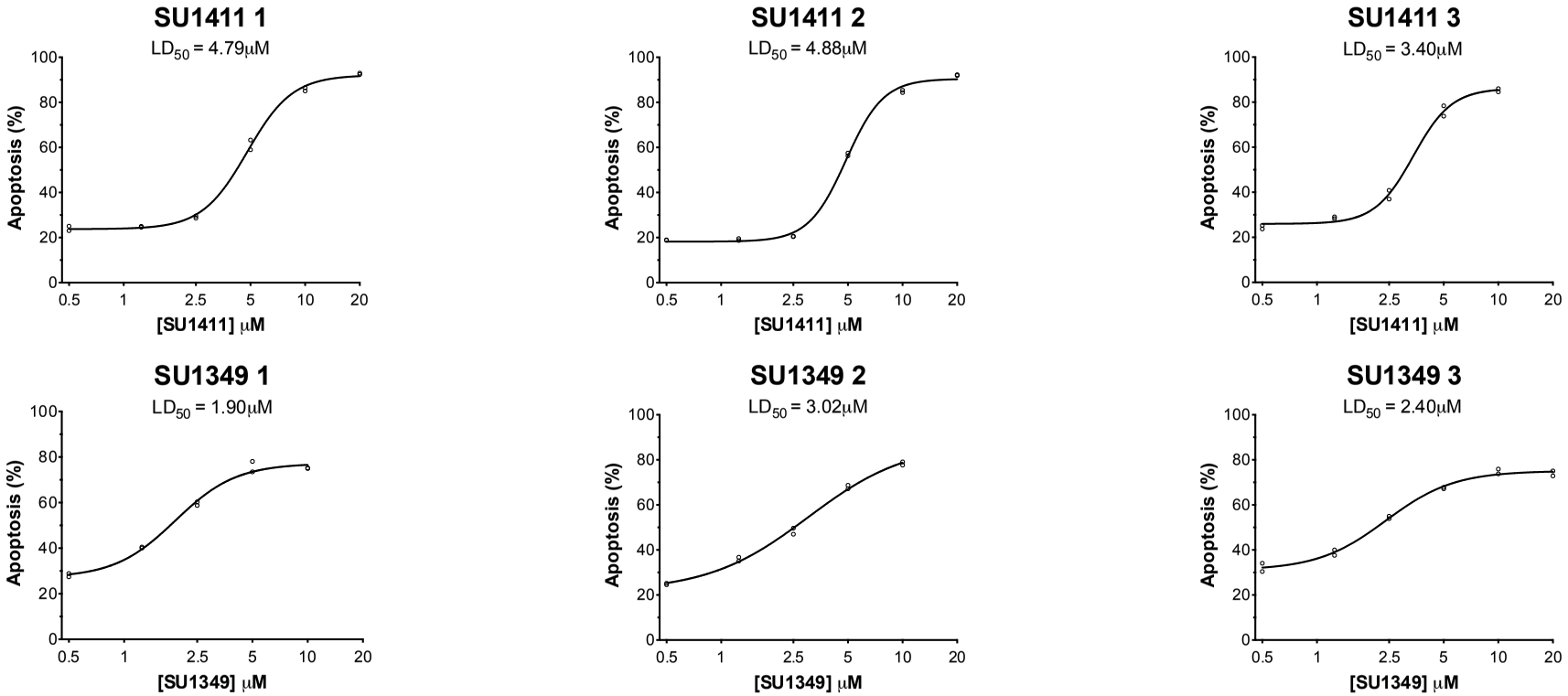

Figure I The does-dependent cytotoxicity profiles at 48h in the MM cell line RPMI8226 that corresponds to the experiment in which the 4h microarray samples for the respective SU compound was collected.

RPMI8226 cells were incubated with increasing concentrations of SU1257, SU1053, SU1438, SU1411 and SU1349. At 4h, cells were harvested from untreated and 2.5μM SU compound treated conditions to generate TRIzol® lysates that were subsequently processed to RNA extracts. Prior to RNA extraction, the collected samples were first validated by measuring the dose-dependent cytotoxicity at 48h using Annexin V/PI positivity an Accuri C6 flow cytometer. The data was input into GraphPad Prism 6.0 and dose-response curves were constructed. LD_{50} values were interpolated and are reported for each SU compound above the respective dose-response curve. The data shown represents $n = 1$, duplicate for each SU compound in the RPMI8226 cell line and corresponds to the 15 sets of microarray samples used in the microarray experiment and subsequent analysis.

Table I Down-regulated DE genes unique to the UT vs. SU1349 contrast.
The genes represented in this list correspond to the 419 DE genes referred to in Figure 5.7.

ADSS	CASP2	DHX57	GNL2
AHCTF1	CASP3	DIMT1	GOLPH3L
AIMP2	CCDC101	DNAJA1	GPAM
AKAP9	CCDC117	DNAJB1	GPATCH1
AKTIP	CCDC138	DOLK	GPR135
ALAS1	CCNE2	DOLPP1	GRWD1
AMD1	CCNF	DPH2	GTF2A1
ANKRD10-IT1	CCP110	DYNC1LI1	GTPBP8
ANKRD13C	CCR2	E2F6	GXYLT1
ANKRD32	CDC23	E2F7	H3F3B
ANLN	CDC25A	E2F8	HCFC2
APEX2	CDC40	EEA1	HCP5
ARHGAP11A	CDC5L	EFNA4	HEATR6
ARHGAP11B	CDC6	EIF2AK3	HELB
ARL13B	CDC7	EPC2	HEXIM1
ASNSD1	CDCA7	ERRFI1	HMGCR
ASTE1	CDK12	ESF1	HMGCS1
ASXL2	CDK17	ETAA1	HSF2
ASXL3	CDS1	EXO1	HSPA1A
ATG14	CEBPZ	F8A2	HSPA1B
ATMIN	CENPC1	FAM111B	HSPA8
ATP6V1B2	CEP152	FAM116A	ICT1
AURKA	CEP350	FAM122A	ID2
B4GALT5	CEP85	FAM54A	ID2B
BAG2	CHD1	FAM59A	IKZF5
BCAS2	CHKA	FAM72A	IMP3
BIRC3	CHML	FAM72B	INTS6
BLZF1	CKAP2L	FAM72C	INTS7
BORA	CKS2	FAM72D	ISCA1P1
BRCA2	CLSPN	FANCL	IVNS1ABP
BRWD1	CNTRL	FANCM	JMY
C11orf82	COIL	FASTKD1	KAT7
C12orf29	COMMD2	FASTKD2	KBTBD8
C12orf35	CREB1	FBXL3	KCNQ5-IT1
C12orf4	CRNKL1	FBXO21	KCTD12
C14orf135	CRY1	FBXO32	KDM4A
C15orf23	CRYBG3	FERMT1	KIAA1731
C15orf42	CXCR4	FIGNL1	KIF11
C16orf70	DBR1	FLJ27352	KIF18A
C18orf54	DCLRE1A	FTSJ3	KIF20B
C1orf135	DDX10	GCLC	KIF21A
C21orf91	DDX20	GDPGP1	KIF23
C2orf44	DDX3X	GEN1	KIF2C
C2orf69	DDX52	GLMN	KIF5B
C7orf26	DENND4C	GMNN	KLHL11
CAMSAP2	DHX36	GMPS	KLHL12

KLHL20	MTERFD1	PRDM4	SMEK1
KRIT1	MTF2	PRIM1	SMG8
LDLR	MTIF2	PRPF39	SMURF2
LEO1	MYB	PRRG4	SMYD5
LMTK2	MYNN	PTCD2	SNORA81
LOC100190986	NABP1	RAD17	SNORD1B
LOC100288842	NBN	RBBP5	SNORD75
LOC100506294	NBPF1	RBL1	SPAST
LOC643837	NBPF16	RBM25	SPOPL
LONRF1	NBPF24	RBM28	SPTLC3
LRIF1	NBPF8	RBM34	SRSF7
LRIG2	NBPF9	RFWD3	STAG3L4
LRIG3	NDUFAF4	RIOK1	STAM2
LSG1	NKAP	RIPK1	STIL
MADD	NLK	RIPK2	SUCNR1
MALT1	NOC3L	RN5S82	SYNJ1
MAP3K1	NOL11	RND3	SYNRG
MARS2	NPAT	RNF122	TACO1
MAT2A	NR1D1	RNU7-40P	TADA1
MB21D1	NRARP	ROCK2	TAF1A
MED19	NT5DC3	RPAP3	TAF4B
MED21	NUAK2	RPF1	TAF5
MED8	NUFIP1	RPF2	TAGAP
MEPCE	NUP153	RPP40	TDG
METTL1	ORC5	RRP15	TFB2M
METTL13	OSBPL11	RSBN1L	TFRC
METTL14	PANX1	RUNX1-IT1	TGFBR2
METTL18	PAPOLG	RYBP	THOC1
MGA	PDP2	SAP130	THUMPD2
MGC27345	PELI1	SASS6	TIMM22
MGC57346	PGBD4	SELRC1	TIPIN
MIER3	PHAX	SETDB2	TLR4
MINA	PHLPP2	SGOL1	TMCO7
MIR1184-1	PI4K2A	SH2D4A	TMEM138
MIR1184-2	PIGA	SHQ1	TMEM184C
MIR1281	PIK3CB	SIRT1	TMEM185B
MIR186	PIK3R1	SKIL	TMEM39A
MIR4427	PLEKHA3	SLC19A2	TMEM60
MIR4659A	PLK4	SLC20A1	TMTC3
MIR4737	PNRC2	SLC25A19	TNFRSF1B
MIS18BP1	POC5	SLC25A33	TRAF6
MLLT10	POGK	SLC29A3	TRAFD1
MORC3	POLA2	SLC35A1	TRIM59
MOSPD1	POLR1B	SLC35A5	TSC22D2
MPV17L2	POLR1E	SLC38A2	TTF1
MRPL39	POLR3B	SLC4A1AP	TTK
MSANTD4	POLR3C	SLK	TTPAL
MSH6	PPIF	SMARCAD1	TUBB4B
MSMO1	PPWD1	PTCD2	SNORA81

MT1X	PRAMEF2	RAD17	SNORD1B
TUBD1	VANGL1	ZBTB41	ZNF518A
TULP3	VEZF1	ZCCHC10	ZNF556
UPF3B	WDR47	ZCCHC8	ZNF600
URB2	WDR76	ZFP36L2	ZNF614
USP1	WDR89	ZNF10	ZNF770
USP12	WEE1	ZNF184	ZNF776
USP31	WSB1	ZNF280C	ZNF93
UTP11L	YARS2	ZNF322	ZNHIT6
UTP15	YEATS4	ZNF322P1	ZRANB1
UTP18	ZBTB40	ZNF468	ZNF518A

Table II Up-regulated DE genes unique to the UT vs. SU1349 contrast.
The genes represented in this list correspond to the 83 DE genes referred to in Figure 5.7.

ACOT12	CSAD	LAMB2P1	NEXN-AS1
ACRC	CTLA4	LAMB4	NPR3
ADAM20P1	DDR2	LHFPL3-AS2	OMG
ARL9	DIO2	LOC100128288	OOEP
AVIL	EFCAB8	LOC100506606	OR11H12
BAAT	EPHX3	LOC100506855	OR2AE1
BCAR4	ERP27	LOC200726	OR2K2
BCL2L10	FGF7	LOC339894	OR9A1P
BTLA	FNDC7	LOC348120	OR9A3P
C12orf5	GOLGA6C	LOC93432	PLAC8L1
C14orf178	HMP19	LRGUK	PLCL2-AS1
C1orf138	HTR1D	LRRTM2	PNLDC1
C1orf162	ICOS	LY6G5B	PYGM
C1orf189	IDI2	MGAM	RFPL3-AS1
C5orf47	IDI2-AS1	MGARP	SERPINC1
CASS4	IGKV4-1	MICALCL	SLC22A1
CCDC62	IGKV5-2	MIR4514	SLC23A1
CDKL2	ITGA1	MSH4	SLC9C2
COL14A1	ITGB1BP2	MSTN	TMED6
CPB2	KIAA0825	MYO5C	VHLL
CPLX4	KLRAP1	NEB	

Table III Alternate DE genes for the UT vs. SU1349 contrast where Log_2 (FC) ≥ 1.5 in both directions, and $p \leq 0.05$.

The genes represented in this list correspond to the 92 DE genes used in the Enrichr analysis for the UT vs. SU1349 contrast. The 58 down regulated DE genes (Log_2 (FC) ≤ -1.5 and $p \leq 0.05$) are shown on the left and the 34 up regulated DE genes (Log_2 (FC) ≥ 1.5 and $p \leq 0.05$) are shown on the right.

Log_2 (FC) ≤ -1.5		Log_2 (FC) ≥ 1.5	
BLZF1	MED21	ACOT12	PLCL2-AS1
C15orf42	MIER3	ACRC	PNLDC1
C2orf44	MIR4500	ADAM20P1	SLC10A5
CCNE2	MIR4737	ARL9	TMED6
CEP85	MTF2	BAAT	VHLL
CHKA	MYNN	C12orf5	
CKAP2L	PAPOLG	C1orf162	
CLSPN	PIK3R1	C1orf189	
DIMT1	POC5	C5orf47	
DNAJB1	POLA2	CASS4	
EFNA4	POLR3B	CPB2	
EPC2	RFXAP	CPLX4	
EXO1	RIOK1	CTLA4	
FAM111B	RIPK1	ERP27	
FAM72D	RND3	ICOS	
GDPGP1	RPF2	IDI2-AS1	
HEATR3	RPP40	ITGA1	
HEATR6	SAP130	LHFPL3-AS2	
HELB	SIRT1	LOC100128288	
HMGCR	SLC25A19	LOC100506606	
HMGCS1	SLC38A2	LOC100506855	
HSPA1B	SRSF7	LOC339894	
INTS7	TAF5	LRRTM2	
KCNQ5-IT1	TMEM185B	MGAM	
KDM4A	TRAF6	MSH4	
KIF20B	VEZF1	MSTN	
KIF23	ZNF280C	OMG	
LDLR	ZNF322	OR11H1	
MB21D1	ZNF322P1	OR9A3P	

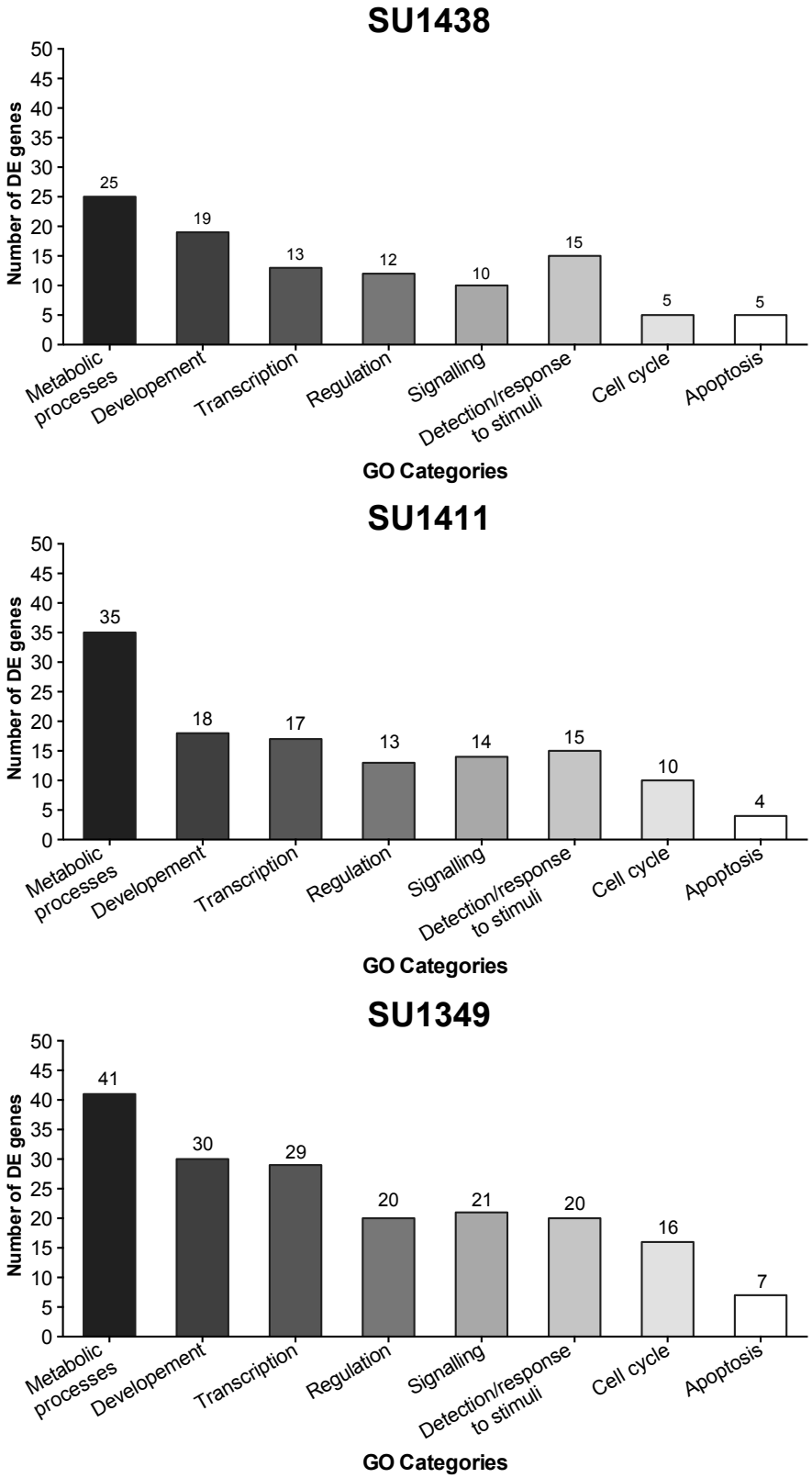

Figure II The number of DE genes associated with each GO category for the comparisons UT vs. SU1438, UT vs. SU1411 and UT vs. SU1349.
The DE gene lists for UT vs. SU1438 and UT vs. SU1411 (Log_2 (FC) ≥ 1 and $p \leq 0.05$.) and UT vs. SU1349 (Log_2 (FC) ≥ 1.5 and $p \leq 0.05$.) were inserted into Enrichr separately to retrieve a list of GO terms associated with each list of DE genes. The GO terms were sorted into GO categories using R Studio and the number of DE genes appearing in each GO category is shown for each SU compound in the bar graphs.

Table IV The identity of the 35 DE genes that are involved in the biological GO's regulated by UT v.s. SU1438 ($p \leq 0.05$, Log2 (fold change) ≥ 1).

	1 GO category											
	ARL17A	LEAP2	METTL4	MN1	OR11H1	PUS7L	SLC10A5	STAG1	TAS2R3	TAS2R4	TAS2R5	UTP6
Metabolic processes						✓	✓					✓
Development				✓								
Detection/response to stimuli		✓			✓				✓	✓	✓	
Regulation												
Cell cycle								✓				
Transcription			✓									
Signalling	✓											
Apoptosis												

	2 GO categories						3 GO categories				4 GO categories	
	BCO2	DENND4A	RBBP6	SLC20A1	SLC7A6	UBA2	DAAM1	CTNND1	NOL8	OVGP1	BCL9	BCLAF1
Metabolic processes	✓	✓	✓	✓	✓	✓	✓	✓	✓	✓		✓
Development			✓		✓		✓	✓	✓	✓	✓	
Detection/response to stimuli										✓	✓	✓
Regulation	✓	✓									✓	
Cell cycle									✓			
Transcription						✓						✓
Signalling				✓			✓	✓			✓	
Apoptosis												✓

Table IV continued

	4 GO categories			5 GO categories				7 GO categories			8 GO categories
	CLPX	POLR2A	SOX30	CMYA5	GCNT4	OFD1	SRSF6	ATP7A	PRKCI	RASA1	ANXA1
Metabolic processes	✓	✓	✓	✓	✓	✓	✓	✓	✓	✓	✓
Development	✓	✓	✓	✓	✓	✓	✓	✓	✓	✓	✓
Detection/response to stimuli			✓		✓	✓	✓	✓	✓		✓
Regulation	✓	✓		✓	✓		✓	✓	✓	✓	✓
Cell cycle						✓				✓	✓
Transcription	✓	✓	✓	✓	✓		✓	✓	✓	✓	✓
Signalling				✓		✓		✓	✓	✓	✓
Apoptosis								✓	✓	✓	✓

Table V The identity of the 42 DE genes that are involved in the biological GO's regulated by UT v.s. SU1411 ($p \leq 0.05$, Log_2 (fold change) ≥ 1).

	1 GO category									
	ARL17A	LEAP2	ME2	NUF2	PDS5B	PUS7L	SLC10A5	SNX4	TAS2R3	TAS2R4
Metabolic processes			✓			✓	✓	✓		
Development										
Detection/response to stimuli		✓							✓	✓
Regulation										
Cell cycle				✓	✓					
Transcription										
Signalling	✓									
Apoptosis										

	1 GO category			2 GO categories						
	TAS2R5	UTP20	UTP6	AOC2	BCO2	CSE1L	DENND4A	IGF2BP3	PRG2	RBBP6
Metabolic processes		✓	✓	✓	✓	✓	✓	✓	✓	✓
Development										✓
Detection/response to stimuli	✓			✓					✓	
Regulation					✓		✓			
Cell cycle										
Transcription						✓		✓		
Signalling										
Apoptosis										

Table V continued

	2 GO categories			3 GO categories					4 GO categories		
	SLC7A6	UBA2	SMEK2	AKAP5	CTNND1	NOL8	NSUN2	OVGP1	BCLAF1	CLPX	SOX30
Metabolic processes	✓	✓	✓	✓	✓	✓	✓	✓	✓	✓	✓
Development	✓				✓	✓		✓		✓	✓
Detection/response to stimuli								✓	✓		✓
Regulation				✓						✓	
Cell cycle						✓	✓				
Transcription		✓	✓				✓		✓	✓	✓
Signalling				✓	✓						
Apoptosis									✓		

	5 GO categories					6 GO categories			7 GO categories		
	CMYA5	IQGAP2	OFD1	PDE5A	ATP7A	RGS2	UBR2	ATRX	PRKCI	RASA1	UBR5
Metabolic processes	✓	✓	✓	✓	✓	✓	✓	✓	✓	✓	✓
Development	✓	✓	✓	✓	✓	✓	✓	✓	✓	✓	✓
Detection/response to stimuli			✓		✓		✓	✓	✓		✓
Regulation	✓	✓		✓	✓	✓		✓	✓	✓	✓
Cell cycle			✓			✓	✓	✓		✓	✓
Transcription	✓	✓		✓		✓	✓	✓	✓	✓	✓
Signalling	✓	✓	✓	✓	✓	✓	✓	✓	✓	✓	✓
Apoptosis					✓				✓	✓	

Table VI The identity of the 53 DE genes that are involved in the biological GO's regulated by UT v.s. SU1349 ($p \leq 0.05$, Log_2 (fold change) ≥ 1.5).

	1 GO category									2 GO categories		
	ACOT12	ARL9	CHKA	MGAM	OR11H1	PAPOLG	RPP40	SLC10A5	SLC25A19	BAAT	CASS4	CCNE2
Metabolic processes	✓		✓	✓		✓	✓	✓	✓	✓		
Development										✓		
Detection/ response to stimuli					✓							
Regulation												
Cell cycle												✓
Transcription											✓	✓
Signalling		✓									✓	
Apoptosis												

	2 GO categories									3 GO categories		
	CPLX4	DIMT1	EFNA4	ERP27	GDPGP1	ICOS	MED21	SLC38A2	SRSF7	BLZF1	HELB	MB21D1
Metabolic processes	✓	✓			✓			✓	✓	✓		✓
Development			✓			✓	✓			✓	✓	
Detection/ response to stimuli				✓								✓
Regulation					✓	✓	✓					
Cell cycle										✓	✓	
Transcription		✓		✓					✓		✓	
Signalling	✓		✓					✓				✓
Apoptosis												

Table VI continued

	3 GO categories				4 GO categories							
	SAP130	RND3	TAF5	VEZF1	CTLA4	EPC2	HMGCS1	INTS7	KIF20B	LRRTM2	MSTN	POLR3B
Metabolic processes	✓	✓	✓		✓	✓	✓	✓	✓	✓	✓	✓
Development		✓		✓	✓	✓	✓		✓	✓	✓	
Detection/ response to stimuli				✓			✓	✓			✓	✓
Regulation					✓				✓	✓		
Cell cycle	✓		✓			✓		✓	✓			
Transcription	✓		✓	✓		✓	✓	✓				✓
Signalling		✓			✓					✓	✓	✓
Apoptosis												

	4 GO categories		5 GO categories			6 GO categories					
	POLA2	OMG	CPB2	DNAJB1	MTF2	EXO1	KDMA4A	KIF23	LDLR	MSH4	CLSPN
Metabolic processes			✓	✓	✓	✓	✓	✓	✓	✓	✓
Development	✓	✓	✓	✓	✓	✓	✓	✓	✓	✓	✓
Detection/ response to stimuli		✓	✓	✓			✓		✓	✓	
Regulation	✓	✓	✓	✓	✓	✓			✓		✓
Cell cycle	✓				✓	✓	✓	✓		✓	✓
Transcription	✓		✓	✓	✓	✓	✓	✓	✓	✓	✓
Signalling		✓				✓		✓	✓		
Apoptosis											✓

Table VI continued

	7 GO categories					8 GO categories
	HMGCR	ITGA1	PIK3R1	RIPK1	TRAF6	SIRT1
Metabolic processes	✓	✓	✓	✓	✓	✓
Development	✓	✓	✓	✓	✓	✓
Detection/ response to stimuli	✓	✓	✓	✓	✓	✓
Regulation	✓	✓	✓	✓	✓	✓
Cell cycle						✓
Transcription	✓	✓	✓	✓	✓	✓
Signalling	✓	✓	✓	✓	✓	✓
Apoptosis	✓	✓	✓	✓	✓	✓

Table VII The resulting DE gene lists for SU1438, SU1411 and SU1349 contrasts based on their GO category relevance.

The 21, 25 and 41 selected DE genes selected based on their enrichment analysis result for GO category for SU1438, SU1411 and SU1349. A DE gene for SU1438 and SU1411 is Log_2 (FC) ≥ 1 and $p \leq 0.05$, whereas for SU1349 it is Log_2 (FC) ≥ 1.5 and $p \leq 0.05$.

UT vs. SU1438	UT vs. SU1411	UT vs. SU1349
ANXA1	UBR5	SIRT1
ATP7A	RASA1	ITGA1
PRKCI	PRKCI	HMGCR
RASA1	ATRX	PIK3R1
CMYA5	UBR2	RIPK1
GCNT4	RGS2	TRAF6
OFD1	ATP7A	CLSPN
SRSF6	PDE5A	EXO1
BCL9	OFD1	KDM4A
BCLAF1	IQGAP2	KIF23
CLPX	CMYA5	LDLR
POLR2A	SOX30	MSH4
SOX30	CLPX	MTF2
DAAM1	BCLAF1	CPB2
CTNND1	SMEK2	DNAJB1
NOL8	NOL8	POLA2
SLC20A1	NSUN2	POLR3B
UBA2	CTNND1	CTLA4
ARL17A	AKAP5	EPC2
METTL4	UBA2	HMGCS1
STAG1	IGF2BP3	INTS7
	CSE1L	KIF20B
	PDS5B	LRRTM2
	NUF2	MSTN
	ARL17A	OMG
		HELB
		SAP130
		SRSF7
		TAF5
		VEZF1
		BLZF1
		MB21D1
		RND3
		CPLX4
		DIMT1
		EFNA4
		ERP27
		SLC38A2
		CCNE2
		CASS4
		ARL9

Table VIII The results of the pathway enrichment analysis by the 21 DE genes selected for the UT vs. SU1438 contrast.
DE genes that were selected for further analysis based on relevant signalling pathways have been highlighted.

	WikiPathways 2015		BioCarta 2015		Reactome 2015	
Genes	**No.**	**Terms**	**No.**	**Terms**	**No.**	**Terms**
ANXA1	4	Prostaglandin synthesis and regulation, spinal cord injury, breast/pancreatic cancer pathways	1	Corticosteroids and cardioprotection	6	$G\alpha_i$ and $G\alpha_q$ signalling, formyl peptide receptor binding, peptide ligand-binding receptors, Gastrin-CREB signalling via PKC and MAPK
ATP7A	1	Iron uptake and transport	0	-	4	Detoxification of ROS, ion transport by P-type ATPases, ion channel transport, cellular response to stress
PRKCI	9	Wnt, EGF/EGFR, G protein and insulin signalling, miRs in muscle cell differentiation, miR-targeted genes in epithelium, CRH, signalling in Glioblastoma	1	Insulin signalling	8	Cell-cell junction organisation and communication, tight junction interaction, p75NTR signals via NF-κB p75NTR and NGF signalling
RASA1	6	EGF/ EGFR, EPO receptor, HGFR, TCR, MAPK and PDGF signalling	7	TPO, EGF, IGF-1 and PDGF signalling, regulation of splicing by sam68, sprouty regulation of TK signals, HIV-1 negative effector of FAS and TNF	8	VEGFA signalling to result in VEGFR2 mediated cell proliferation, PDGF and EPHB-mediated signalling, signal transduction, axon guidance
CMYA5	0	-	0	-	0	-
GCNT4	0	-	0	-	3	Post-translational protein modification, O-linked glycosylation of mucins
OFD1	0	-	0	-	12	Protein loss for interphase, mitotic centrosome protein recruitment, PLK1 regulated G2/M phase transition, Hedgehog signalling, organelle biogenesis and maintenance

Table VIII continued

SRSF6	1	mRNA processing	0	-	13	mRNA splicing, RNA polymerase II transcription termination, post-elongation processing of transcript, transport of mature transcript to cytoplasm
BCL9	1	Wnt signalling	0	-	8	Formation and deactivation of β-catenin transactivating complex, Wnt signalling
BCLAF1	0	-	0	-	0	-
CLPX	0	-	0	-	0	-
POLR2A	2	mRNA processing, transcription initiation	6	Pain repression by the transcription regulator DREAM, estrogen receptor regulation, chromatin remodeling and transcription initiation in carcinoma cells, telomerase regulation, IFN-β pathway	48	mRNA splicing and RNA polymerase II transcription initation/ elongation, miRNA biogenesis, mRNA capping, DNA NER, regulation of RNA pathways, HIV life cycle and transcription
SOX30	0	-	0		0	-
CTNND1	1	Wnt signalling and pluripotency	0		7	Cell-cell junction organisation and communication, VEGF signalling and VEGFR2 mediated vascular permeability, adherens junction interactions
NOL8	0	-	0		0	-
SLC20A1	0	-	0		3	SLC-mediated transmembrane transport of inorganic cations, anions and amino acids, sodium-coupled phosphate co-transporters

Table VIII continued

UBA2	0	-	1	Basic mechanisms of SUMOylation	5	SUMOylation, processing and activation of SUMO, post-translational protein modification
ARL17A	0	-	0		0	-
METTL4	0	-	0		0	-
STAG1	0	-	0		12	Mitotic prometaphase, metaphase, anaphase, telophase/cytokinesis, S and M phase, establishment of sister chromatin cohesion and separation
DAAM1	0					

EGFR- epidermal growth factor receptor, **CRH**- corticotropin-releasing hormone, **EPO**- erythropoietin, **HGFR**- hepatocyte growth factor receptor, **TCR**- T-cell receptor, **MAPK**- mitogen-activated protein kinase, **PDGF**- platelet-derived growth factor, **TPO**- thyroid peroxidase, **IGF-1**- insulin-like growth factor 1, **TK**- tyrosine kinase, **HIV**- human immunodeficiency virus, **TNF**- tumour necrosis factor, **IFN-β**- interferon-β, **PKC**- protein kinase C, **ROS**- reactive oxygen species, **ATP**- adenosine triphosphate, **SUMO**- small ubiquitin-like modifier, **p75NTR**- p75 neurotrophin receptor, **NGF**- nerve growth factor, **VEGFA**- vascular endothelial growth factor A, **VEGFR2**- vascular endothelial growth factor receptor 2, **EPHB**- ephrin receptor B, **SLC**- solute carrier, **NER**- nucleotide excision repair.

Table IX The results of the pathway enrichment analysis by the 25 DE genes selected for the UT vs. SU1411 contrast.
DE genes that were selected for further analysis based on relevant signalling pathways have been highlighted.

	WikiPathways 2015		BioCarta 2015		Reactome 2015	
Genes	**No.**	**Terms**	**No.**	**Terms**	**No.**	**Terms**
UBR5	1	Tryptophan metabolism	0	-	0	-
RASA1	6	EGF/ EGFR, EPO receptor, HGFR, TCR, MAPK and PDGF signalling	7	TPO, EGF, IGF-1 and PDGF signalling, regulation of splicing by sam68, sprouty regulation of TK signals, HIV-1 negative effector of FAS and TNF	8	VEGFA signalling resulting in VEGFR2 mediated cell proliferation, PDGF- and EPHB-mediated signalling, signal transduction, axon guidance
PRKCI	9	Wnt, EGF/EGFR, G protein and insulin signalling, muscle cell differentiation, miR-targeted genes in epithelium, CRH, Glioblastoma signalling	1	Insulin signalling	8	Cell-cell junction organisation and communication, tight junction interaction, p75NTR signals via NF-κB p75NTR and NGF signalling
ATRX	2	miR-targeted genes in epithelium and squamous cell	0	-	0	-
UBR2	0	-	0	-	2	Antigen processing (ubiquitination and proteasome degradation), class I MHC antigen processing and presentation
RGS2	2	Calcium regulation in cardiac cells, myometrial relaxation and contraction	0	-	2	$G\alpha_q$ signalling, gastrin-CREB signalling
ATP7A	1	Iron uptake and transport	0	-	4	Detoxification of ROS, P-type ATPase ion transport, ion channel transport, cellular response to stress
PDE5A	0	-	0	-	3	Nitric oxide stimulates guanylate cyclase, cGMP effects, platelet homeostasis

Table IX continued

OFD1	0	-	0	-	12	Protein loss for interphase, mitotic centrosome protein recruitment, PLK1 regulated G2/M phase transition, Hedgehog signalling, organelle biogenesis and maintenance
IQGAP2	1	G13 signalling pathway	0	-	0	-
CMYA5	0	-	0	-	0	-
SOX30	0	-	0		0	-
CLPX	0	-	0	-	0	-
BCLAF1	0	-	0	-	0	-
SMEK2	1	Integrated breast cancer pathway	0	-	0	-
NOL8	0	-	0		0	-
CTNND1	1	Wnt signalling and pluripotency	0		7	Cell-cell junction organisation, VEGF signalling for vascular permeability, adherens junction interactions
AKAP5	1	G protein signalling	0	-	8	AMPA receptor trafficking, glutamate binding, AMPA receptor activation, insulin secretion, energy metabolism, neurotransmitter receptor binding, transmission across chemical synapses
UBA2	0	-	1	Basic mechanisms of SUMOylation	5	SUMOylation, processing and activation of SUMO, post-translational protein modification,
IGF2BP3	0	-	0	-	2	IGF-2 mRNA binding proteins, gene expression
CSE1L	0	-	0	-	0	-

Table IX continued

PDS5B	0	-	0	-	10	Establishment and resolution of sister chromatid cohesion, mitotic prometaphase, metaphase, anaphase, telophase/cytokinesis, M phase and S phase
NUF2	0	-	0	-	6	Establishment and separation of sister chromatid cohesion, mitotic prometaphase, metaphase, anaphase and M phase
ARL17A	0	-	0	-	0	-
NSUN2	0	-	0	-	3	tRNA processing and modification, gene expression

EGFR- epidermal growth factor receptor, **CRH**- corticotropin-releasing hormone, **EPO**- erythropoietin, **HGFR**- hepatocyte growth factor receptor, **TCR**- T-cell receptor, **MAPK**- mitogen-activated protein kinase, **PDGF**- platelet-derived growth factor, **TPO**- thyroid peroxidase, **IGF**- insulin-like growth factor, **TK**- tyrosine kinase, **HIV**- human immunodeficiency virus, **TNF**- tumour necrosis factor, **ROS**- reactive oxygen species, **SUMO**- small ubiquitin-like modifier, **p75NTR**- p75 neurotrophin receptor, **NGF**- nerve growth factor, **VEGFA**- vascular endothelial growth factor A, **VEGFR2**- vascular endothelial growth factor receptor 2, **MHC**- major histocompatibility complex, **CREB**- cAMP response element-binding protein, **cGMP**- cyclic guanosine monophosphate, **PLK**- polo-like kinase.

Table X The results of the pathway enrichment analysis by the 41 DE genes selected for the UT vs. SU1349 contrast.
DE genes that were selected for further analysis based on relevant signalling pathways have been highlighted.

	WikiPathways 2015		BioCarta 2015		Reactome 2015	
Genes	**No.**	**Terms**	**No.**	**Terms**	**No.**	**Terms**
SIRT1	5	SREBF, androgen and breast/prostate cancer signalling	1	Regulation of transcriptional activity by promyelocytic leukemia protein	6	Negative regulation of rRNA expression, stress response and HSF1-mediated heat shock response
ITGA1	6	Cellular organisation and cell surface interactions	6	B cell survival and cell surface interactions	11	Cellular organisation and cell surface interactions
HMGCR	6	SREBF and breast cancer signalling, statin and cholesterol synthesis	0	-	5	Lipid and fatty acid metabolism, SREBP activated gene expression and SREBP-mediated cholesterol biosynthesis
PIK3R1	33	B and T cell signalling, growth factor (PDGF, EGF) signalling, TLR, notch, RANK-RANKL, IL-1/2/3/4/5/6/7/9/11 and AMPK signalling, apoptosis modulation	48	B cell survival, TCR, IL-2/7, RAS, EGF, PDGF, PI3K/AKT, VEGF signalling. Anti-apoptotic pathways, PTEN cell cycle arrest and apoptosis	74	IL, TCR, PI3K/AKT, $G\alpha_q$ protein, MAPK, BCR, VEGF, EGFR, FGFR, SCF-KIT, insulin, GM-CSF and PDGF signalling, CD28 co-stimulation and signalling
RIPK1	8	Apoptosis modulation, TNF, TLR and MAPK signalling	9	NF-κB (with TRAF6), TNFR1, TNFR2 signalling, induction of apoptosis through death receptors 3, 4 and 5	18	IKK complex recruitment, NF-κB activation via ZBP1 and RIP-1, TLR signalling, caspase-8 activation, programmed cell death and apoptosis
TRAF6	11	TCR, TLR, MAPK, IL-1/17 and RANK-RANKL signalling, apoptosis modulation	6	NF-κB (with RIPK1), CD40L, BCMA and TLR, IL-1R signalling	49	IKK complex recruitment by RIPK1, NF-κB and MAPK induction, NF-κB activation and signals survival, TLR, TCR, IL-1 and MAPK signalling, cell death

Table X continued

CLSPN	0	-	0	-	7	Cell cycle progression (G2/M), cell cycle checkpoints, apoptosis modulation, stress response
EXO1	1	DNA mismatch repair	0	-	4	DNA mismatch repair
KDM4A	0	-	0	-	3	Histone demethylation and chromatin organisation
KIF23	0	-	0	-	5	Megakaryocyte development, platelet production, cell cycle progression (M phase, telophase and cytokinesis), MHC II antigen presentation
LDLR	10	Cholesterol and lipid homeostasis, SREBP signalling, Statin pathway, Wnt signalling pathway, Vitamin B12 and folate metabolism, DNA damage response	1	SREBP control of lipid synthesis	7	Visual perception, lipoprotein and lipid metabolism, lipid transport
MSH4	0	-	0	-	2	Meiosis
MTF2	0	-	0	-	2	DNA and histone methylation, epigenetic gene regulation
CPB2	1	Complement and coagulation cascade	1	Fibrinolysis pathway	2	Hormone metabolism, angiotensinogen metabolism
DNAJB1	3	miR-targeted genes in squamous cell, leukocytes and epithelium	0	-	6	Stress response, HSF1-mediated heat shock response.
POLA2	2	Cell cycle progression and DNA replication	0	-	23	Cell cycle progression (M/G_1 and G_1/S), telomere synthesis and maintenance, DNA replication
POLR3B	1	Transcription initiation	0	-	11	RNA polymerase I and III transcription,
CTLA4	2	TCR signalling, allograft rejection	2	TCR signalling, T cell activation	2	Co-stimulation with CD28, CTLA4 inhibitory signal

Table X continued

EPC2	0	-	0	-	0	-
HMGCS1	4	Cholesterol and lipid homeostasis, SREBP signalling, cholesterol biosynthesis, endochondral ossification	1	SREBP control of lipid synthesis	5	SREBP control of lipid synthesis, lipid, fatty acid and ketone metabolism
INTS7	0	-	0	-	0	-
KIF20B	1	Gastric cancer network	0	-	0	-
LRRTM2	0	-	0	-	0	-
MSTN	1	Hypertrophy model	0	-	0	-
OMG	1	Spinal cord injury	0	-	4	P75NTR and NGF signalling, axongenesis
HELB	0	-	0	-	0	-
SAP130	0	-	0	-	6	Epigenetic regulation of rRNA expression, histone acetylation, chromatin organisation
SRSF7	1	mRNA processing	0	-	13	RNA polymerase II transcription, mRNA transcript transport, mRNA splicing
TAF5	1	Transcription initiation	0	-	13	RNA polymerase II transcription
VEZF1	0	-	0	-	0	-
BLZF1	0	-	0	-	3	Cell cycle progression (S phase, prophase)
MB21D1	0	-	0	-	2	Pathogen detection and immune response
RND3	0	-	0	-	0	-
CPLX4	0	-	0	-	0	-

Table X continued

DIMT1	0	-	0	-	0	-
EFNA4	0	-	0	-	4	EPH-Ephrin signalling, axon guidance
ERP27	0	-	0	-	0	-
SLC38A2	4	Endochondral ossification, miR-targeted genes in squamous cell and epithelium, neurotransmitter release	0	-	8	Neurotransmitter release, SLC-mediated transmembrane transport
CCNE2	6	Cell cycle progression (G1 to S phase), DNA damage response	1	p53 signalling pathways	14	Cell cycle progression (G_1/S phase), cell cycle checkpoints, DNA damage response
CASS4	0	-	0	-	0	-
ARL9	0	-	0	-	0	-

PDGF- platelet-derived growth factor, **EGFR**-epidermal growth factor receptor, **TLR**- toll-like receptor, **RANKL**- receptor activator of NF-κB ligand, **SREBP**-sterol regulatory element–binding protein, **IL**- interleukin, **AMPK**- AMP-activated protein kinase, **TNFR**- tumour necrosis factor receptor, **MAPK**- mitogen-activated protein kinase, **TCR**- T-cell receptor, **PI3K/AKT**- phosphatidylinositol-3-kinase and protein kinase B, **VEGF**- vascular endothelial growth factor, **PTEN**- phosphatase and tensin homolog, **BCMA**- B-cell maturation antigen, **BCR**- B-cell receptor, **FGFR**-fibroblast growth factor receptor, **SCF-KIT**- stem cell factor ligated to KIT, **GM-CSF**- granulocyte macrophage colony-stimulating factor, **ZBP1**- Z-DNA-binding protein 1, **HSF1**- Heat shock factor protein 1 **p75NTR**- p75 neurotrophin receptor, **NGF**- nerve growth factor, **EPH**- erythropoietin-producing human hepatocellular receptor **Ephrin**- EPH ligand, **SLC**- solute carrier.

Table XI The quantitative expression data UT vs. SU1438 ($p \leq 0.05$, $Log_2FC \geq 1$) selected DE genes based on the pathway enrichment analysis results.
The table presents the Log_2 expression (mean ± SEM), Log_2 (FC) and the adjusted p value where $n = 3$ of the 8 DE genes selected based on pathway enrichment analysis results for UT vs. SU1438. Down regulated DE genes are shown in red and up regulated are in green.

		RMA normalised Log_2 expression	Log_2 (FC)	Adjusted p value
PRKCI	**UT**	7.98 ± 0.14	-1.332	4.79×10^{-4}
	SU1438	6.65 ± 0.01		
OFD1	**UT**	7.32 ± 0.18	-1.151	1.02×10^{-3}
	SU1438	6.17 ± 0.25		
SRSF6	**UT**	8.92 ± 0.12	-1.006	5.40×10^{-4}
	SU1438	7.91 ± 0.05		
BCL9	**UT**	6.94 ± 0.25	-1.005	1.05×10^{-2}
	SU1438	5.94 ± 0.12		
POLR2A	**UT**	8.79 ± 0.04	-1.137	1.61×10^{-3}
	SU1438	7.65 ± 0.05		
UBA2	**UT**	8.34 ± 0.11	-1.057	9.87×10^{-4}
	SU1438	7.28 ± 0.08		
STAG1	**UT**	7.17 ± 0.16	-1.018	5.28×10^{-3}
	SU1438	6.15 ± 0.07		
DAAM1	**UT**	5.15 ± 0.23	-1.156	8.19×10^{-4}
	SU1438	4.00 ± 0.07		

Table XII The quantitative expression data UT v.s. SU1411 ($p \leq 0.05$, Log2FC ≥ 1) selected DE genes based on the pathway enrichment analysis results.

The table presents the Log2 expression (mean ± SEM), Log2 (FC) and the adjusted p value where $n = 3$ of the 6 DE genes selected based on pathway enrichment analysis results for UT vs. SU1411. Down regulated DE genes are shown in red and up regulated are in green.

		RMA normalised Log_2 expression	Log_2 (FC)	Adjusted *p* value
PRKCI	**UT**	7.98 ± 0.11	-1.797	3.58×10^{-5}
	SU1411	6.18 ± 0.17		
OFD1	**UT**	7.32 ± 0.15	-1.096	1.58×10^{-3}
	SU1411	6.23 ± 0.13		
UBA2	**UT**	8.34 ± 0.11	-1.201	3.71×10^{-4}
	SU1411	7.14 ± 0.12		
PDS5B	**UT**	6.88 ± 0.17	-1.170	6.01×10^{-3}
	SU1411	5.71 ± 0.14		
NUF2	**UT**	6.63 ± 0.34	-1.227	4.88×10^{-2}
	SU1411	5.40 ± 0.16		
NSUN2	**UT**	7.64 ± 0.03	-1.124	1.54×10^{-4}
	SU1411	6.52 ± 0.13		

Table XIII The quantitative expression data UT v.s. SU1349 ($p \leq 0.05$, $Log_2FC \geq 1.5$) selected DE genes based on the pathway enrichment analysis results.
The table presents the Log_2 expression (mean ± SEM), Log_2 (FC) and the adjusted p value where $n = 3$ of the 9 DE genes selected based on pathway enrichment analysis results for UT vs. SU1349. Down regulated DE genes are shown in red and up regulated are in green.

		RMA normalised Log_2 expression	Log_2 (FC)	Adjusted p value
PIK3R1	**UT**	6.11 ± 0.16	-1.556	1.73×10^{-6}
	SU1349	4.56 ± 0.19		
TRAF6	**UT**	6.53 ± 0.08	-1.537	1.06×10^{-7}
	SU1349	5.00 ± 0.23		
RIPK1	**UT**	7.27 ± 0.06	-1.568	1.80×10^{-8}
	SU1349	5.70 ± 0.13		
CLSPN	**UT**	7.25 ± 0.10	-1.771	2.87×10^{-5}
	SU1349	5.48 ± 0.36		
POLA2	**UT**	8.33 ± 0.10	-1.629	8.35×10^{-5}
	SU1349	6.70 ± 0.37		
POLR3B	**UT**	6.74 ± 0.05	-1.567	2.46×10^{-7}
	SU1349	5.17 ± 0.14		
SRSF7	**UT**	7.53 ± 0.07	-1.707	3.18×10^{-6}
	SU1349	5.82 ± 0.18		
TAF5	**UT**	6.05 ± 0.16	-1.876	2.12×10^{-7}
	SU1349	4.17 ± 0.11		
CCNE2	**UT**	5.86 ± 0.06	-1.817	4.72×10^{-7}
	SU1349	4.04 ± 0.03		

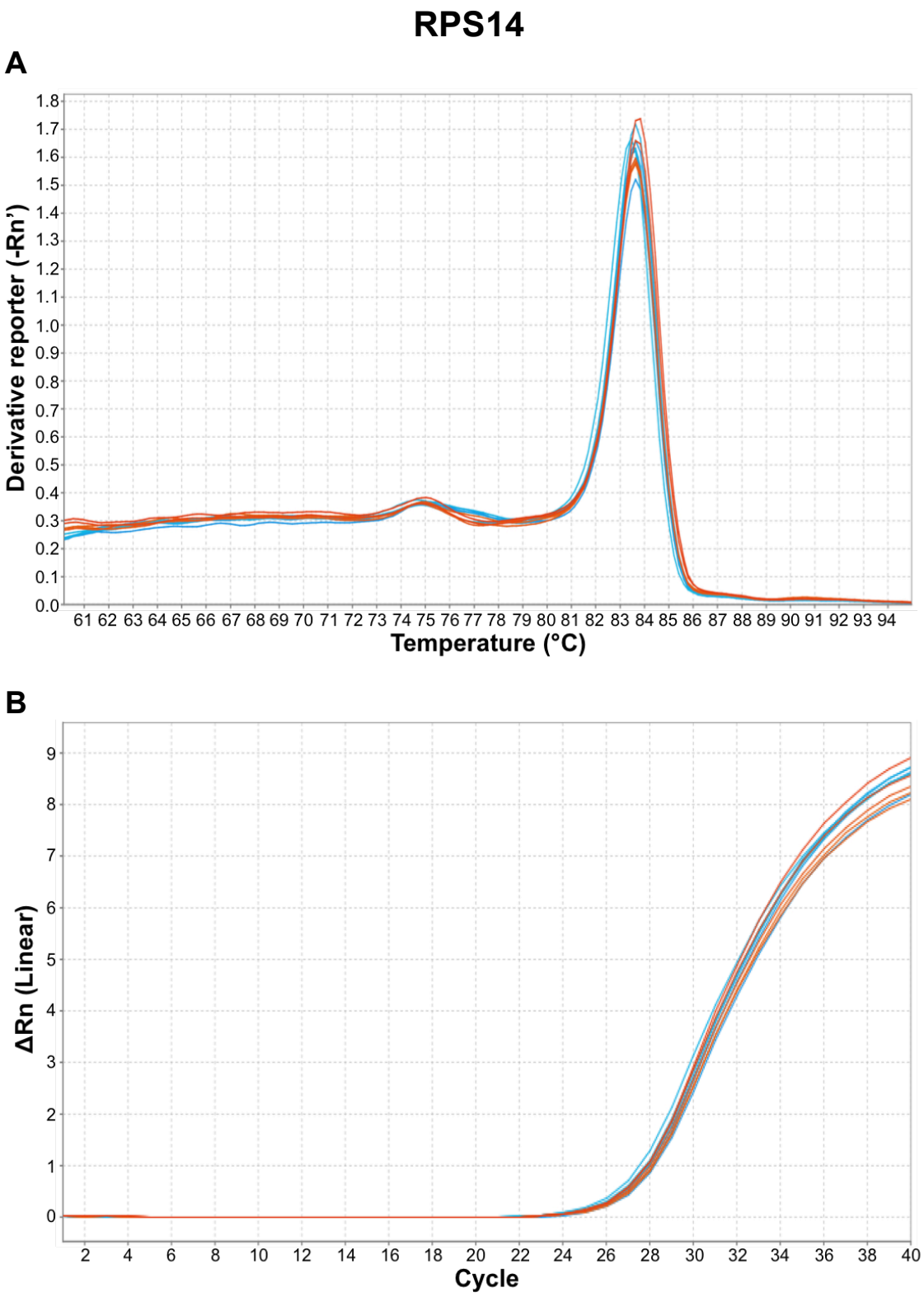

Figure III Representative examples of a melting curve and an amplification plot produced when the RPS14 primer pair is used in qRT-PCR as an endogenous control.

qRT-PCR was used to validate the DE genes identified through microarray analysis. RPS14 was used as an endogenous control gene in all qRT-PCR experiments. Representative examples of a RPS14 melting curve (**A**) and amplification plot (**B**) are shown for untreated RPMI8226 cells (■) and RPMI8226 cells treated for 4h with SU1411 (■). The data shown represents n = 3, duplicate.

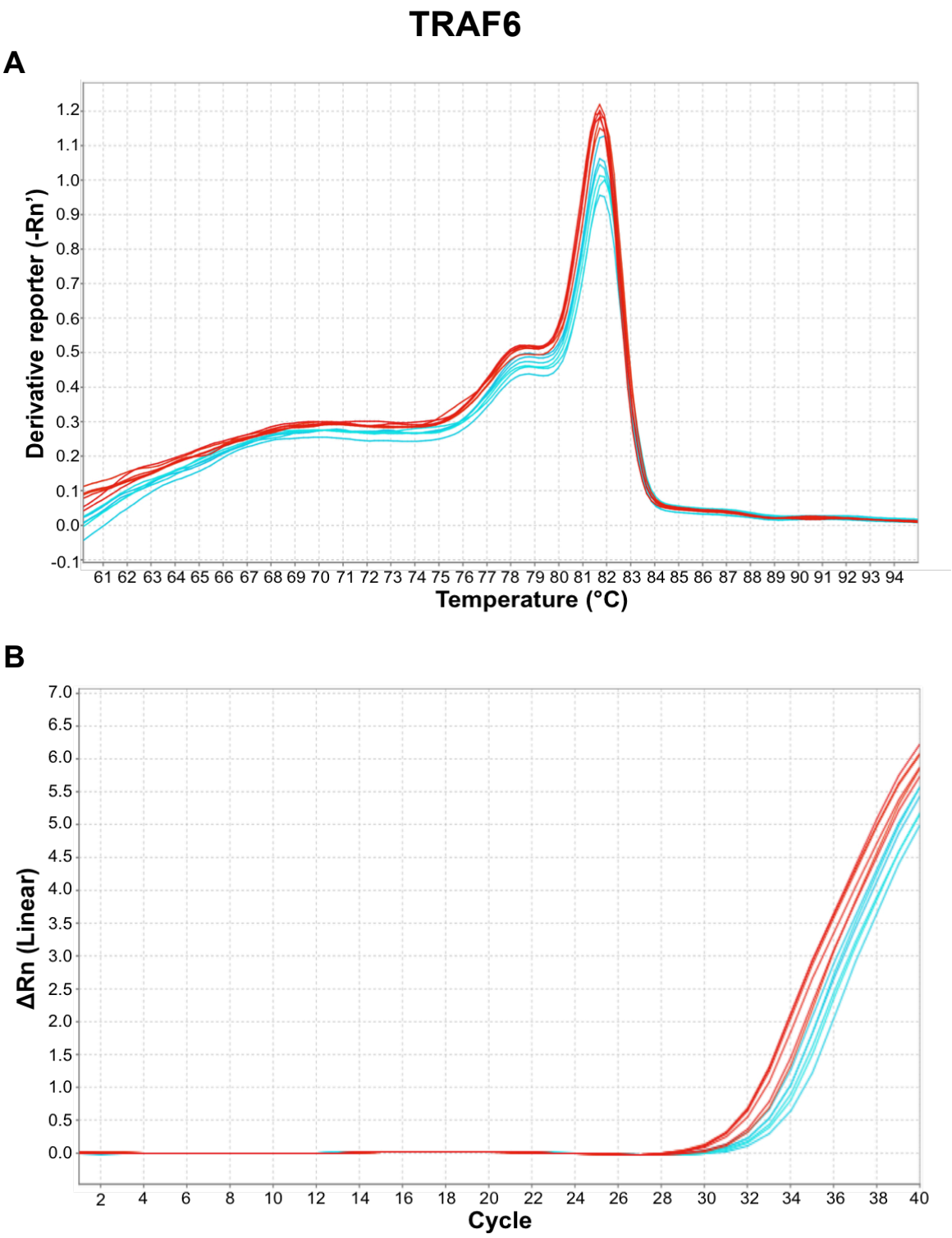

Figure IV Representative examples of a melting curve and an amplification plot produced when the TRAF6 primer pair was used in qRT-PCR.
qRT-PCR was used to validate the DE genes identified through microarray analysis. TRAF6 was one of those DE genes validated using qRT-QPCR experiments. Representative examples of a TRAF6 melting curve (**A**) and amplification plot (**B**) are shown for untreated RPMI8226 cells (■) and RPMI8226 cells treated for 4h with SU1411 (■). The data shown represents n = 3, duplicate.

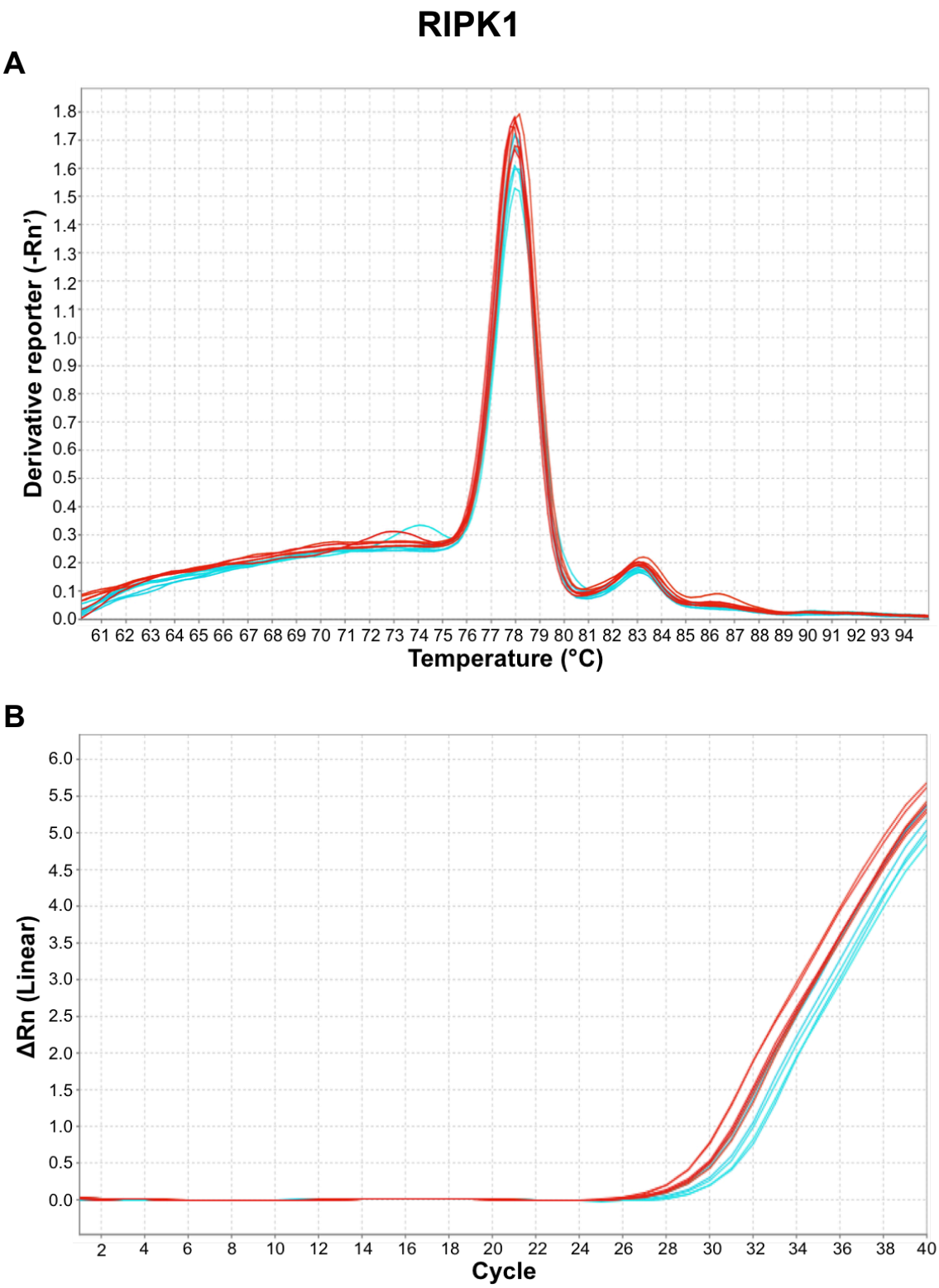

Figure V Representative examples of a melting curve and an amplification plot produced when the RIPK1 primer pair was used in qRT-PCR.
qRT-PCR was used to validate the DE genes identified through microarray analysis. RIPK1 was one of those DE genes validated using qRT-QPCR experiments. Representative examples of a RIPK1 melting curve (**A**) and amplification plot (**B**) are shown for untreated RPMI8226 cells (■) and RPMI8226 cells treated for 4h with SU1411 (■). The data shown represents n = 3, duplicate.

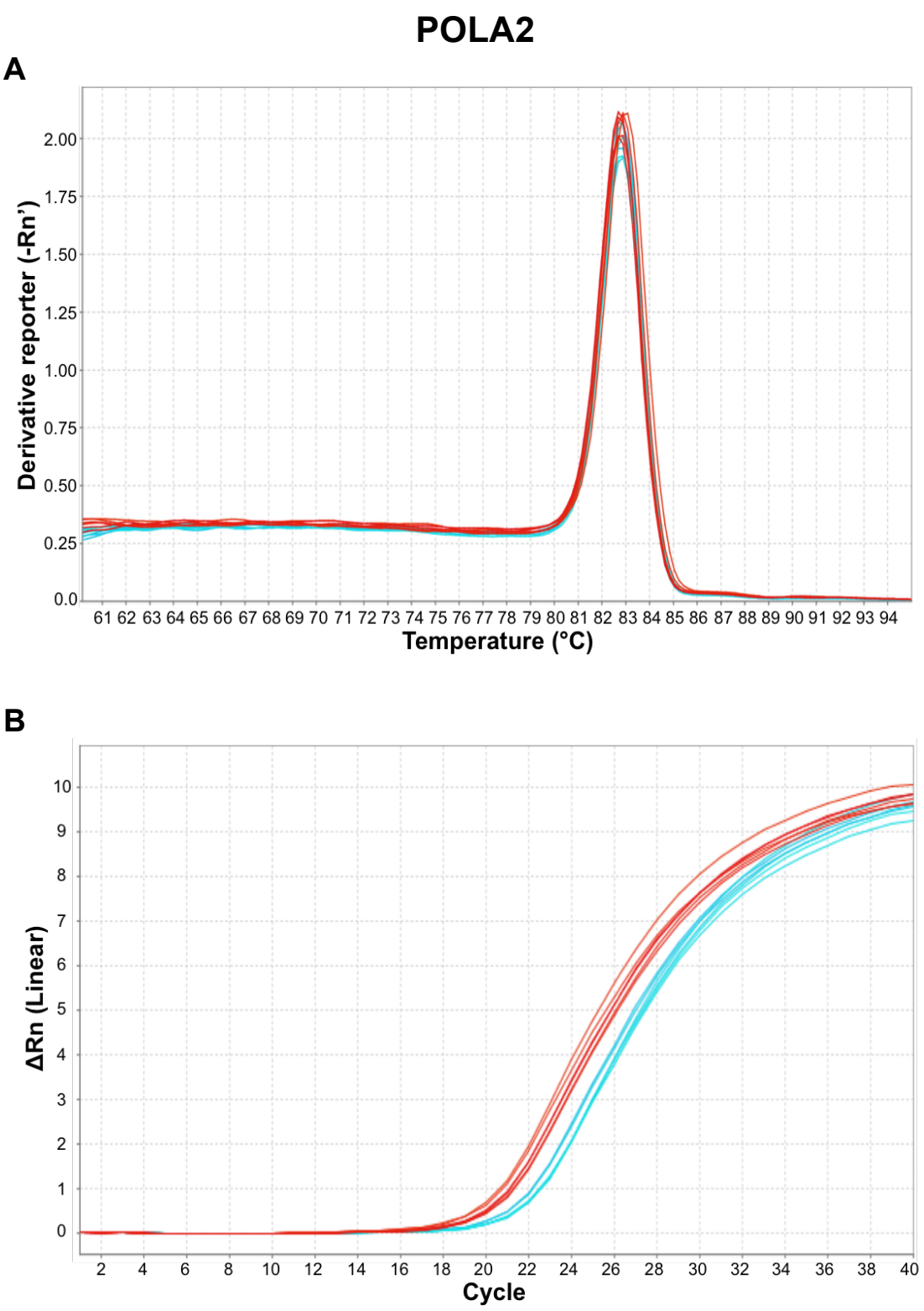

Figure VI Representative examples of a melting curve and an amplification plot produced when the POLA2 primer was used in qRT-PCR.
qRT-PCR was used to validate the DE genes identified through microarray analysis. POLA2 was one of those DE genes validated using qRT-QPCR experiments. Representative examples of a POLA2 melting curve (**A**) and amplification plot (**B**) are shown for untreated RPMI8226 cells (■) and RPMI8226 cells treated for 4h with SU1411 (■).The data shown represents n = 3, duplicate.

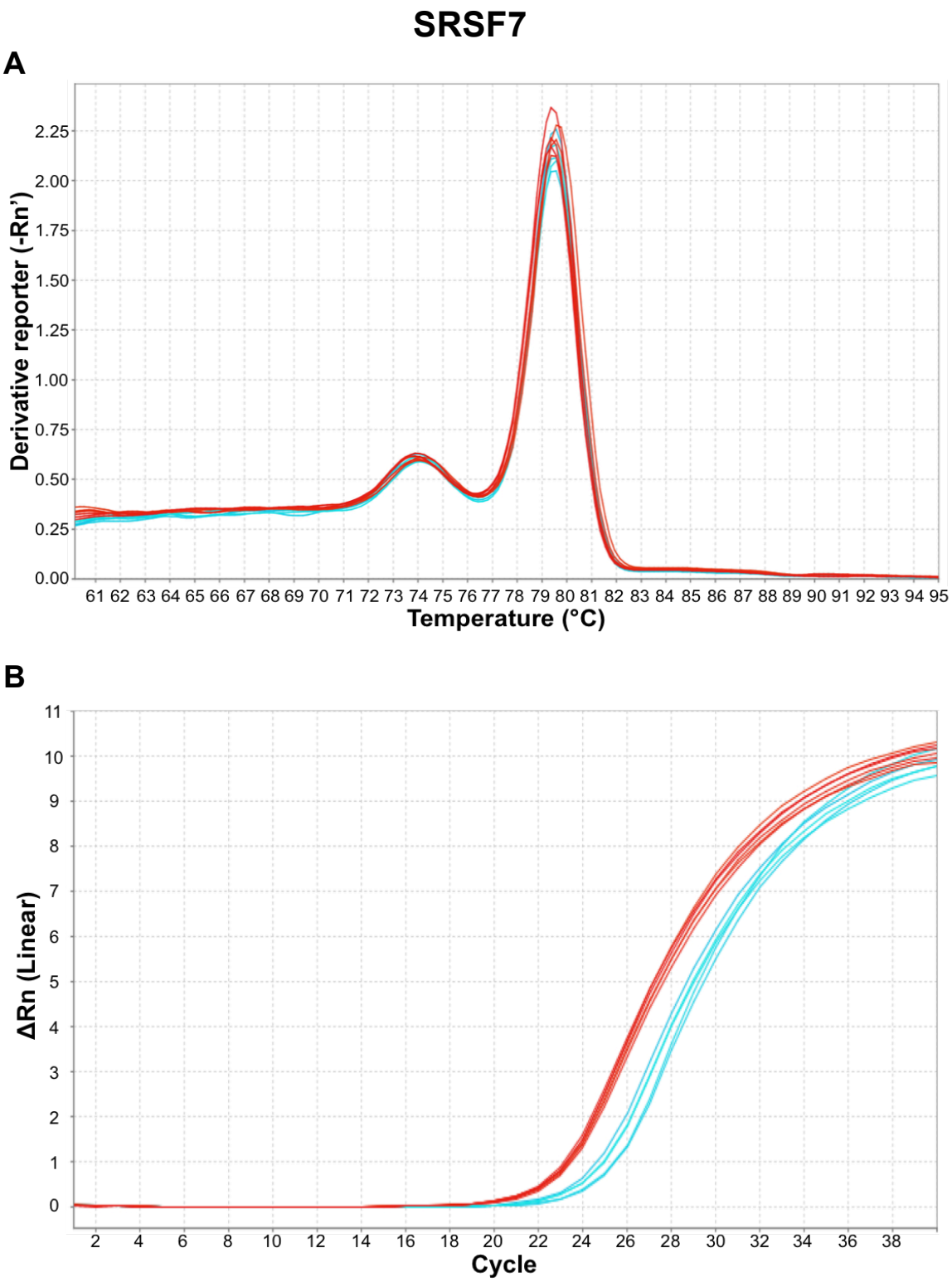

Figure VII Representative examples of a melting curve and an amplification plot produced when the SRSF7 primer was used in qRT-PCR.
qRT-PCR was used to validate the DE genes identified through microarray analysis. SRSF7 was one of those DE genes validated using qRT-QPCR experiments. Representative examples of a SRSF7 melting curve (**A**) and amplification plot (**B**) are shown for untreated RPMI8226 cells (■) and RPMI8226 cells treated for 4h with SU1411 (■). The data shown represents n = 3, duplicate.

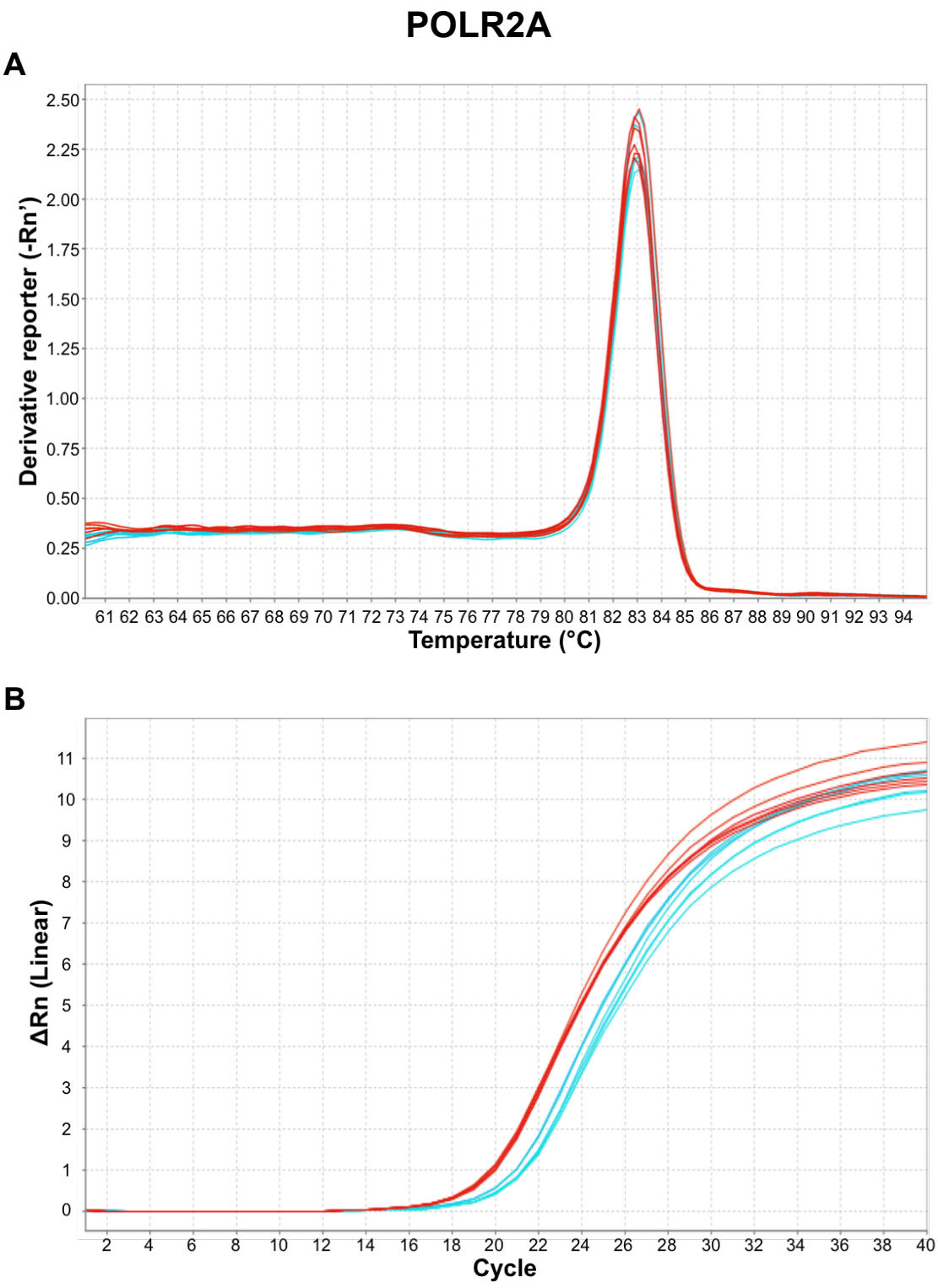

Figure VIII Representative examples of a melting curve and an amplification plot produced when the POLR2A primer was used in qRT-PCR.
qRT-PCR was used to validate the DE genes identified through microarray analysis. POLR2A was one of those DE genes validated using qRT-QPCR experiments. Representative examples of a POLR2A melting curve (**A**) and amplification plot (**B**) are shown for untreated RPMI8226 cells (■) and RPMI8226 cells treated for 4h with SU1411 (■). The data shown represents n = 3, duplicate.

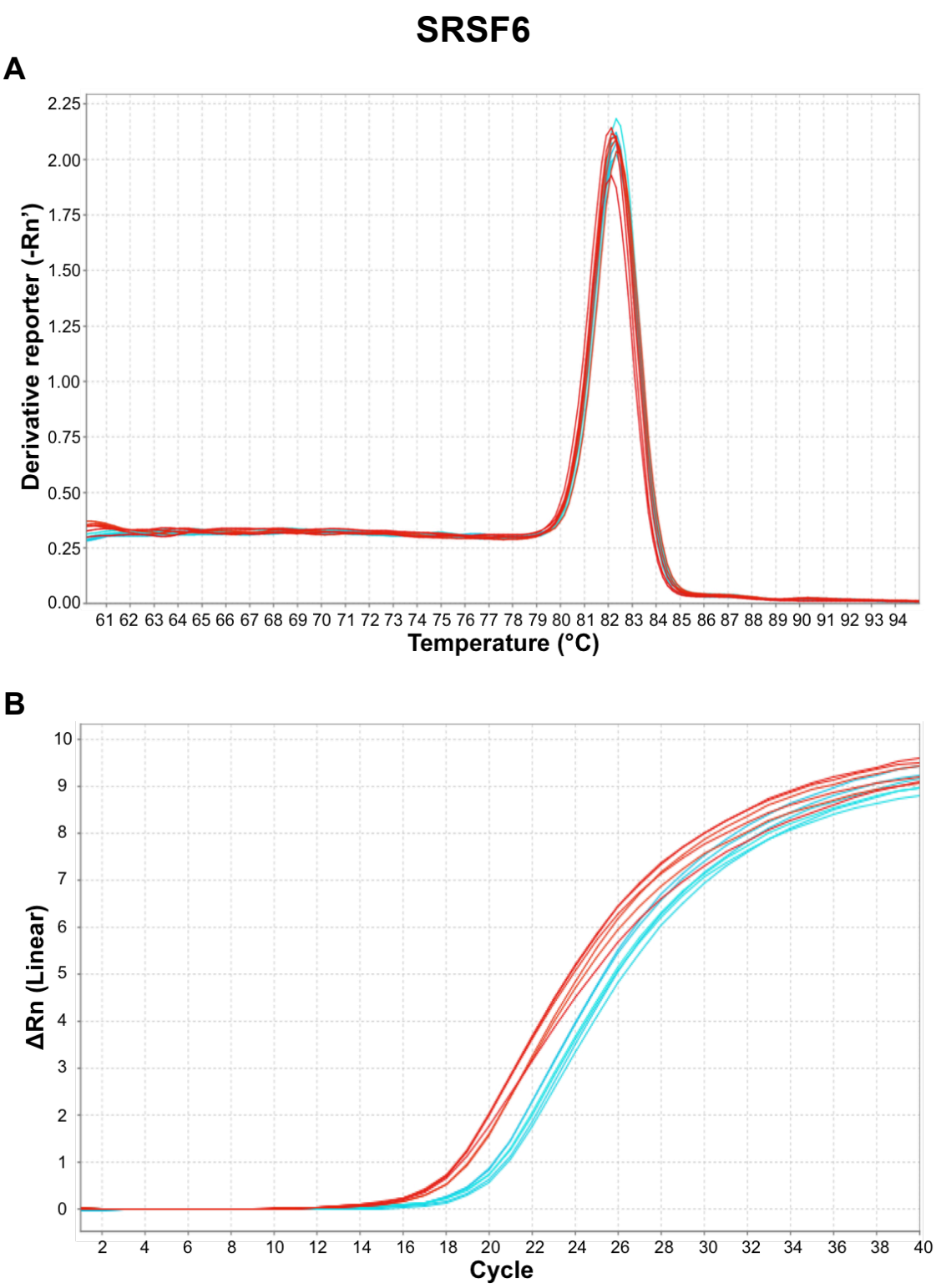

Figure IX Representative examples of a melting curve and an amplification plot produced when the SRSF6 primer was used in qRT-PCR.
qRT-PCR was used to validate the DE genes identified through microarray analysis. SRSF6 was one of those DE genes validated using qRT-QPCR experiments. Representative examples of a SRSF6 melting curve (**A**) and amplification plot (**B**) are shown for untreated RPMI8226 cells (■) and RPMI8226 cells treated for 4h with SU1411 (■). The data shown represents n = 3, duplicate.

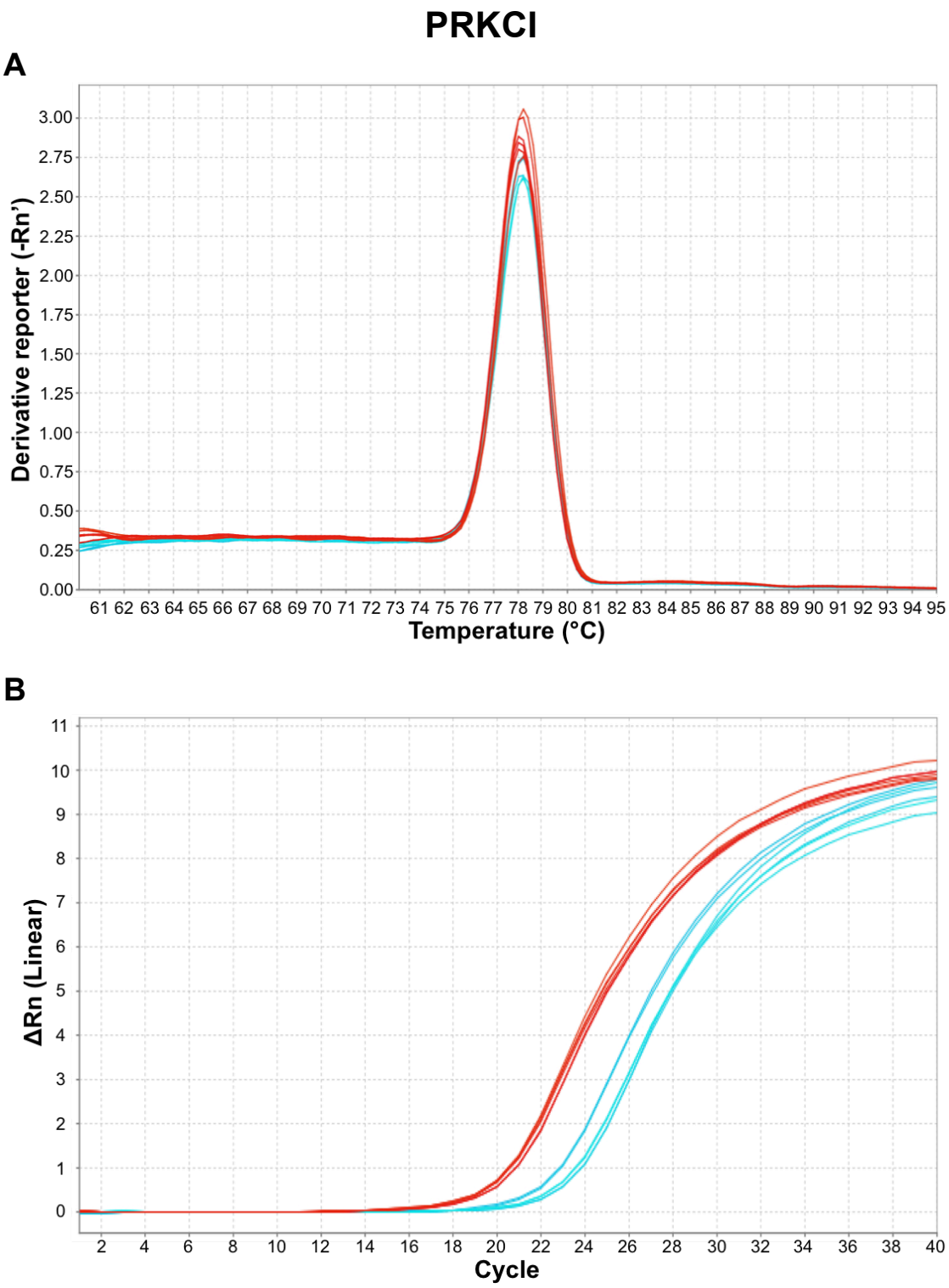

Figure X Representative examples of a melting curve and an amplification plot produced when the PRKCI primer was used in qRT-PCR.
qRT-PCR was used to validate the DE genes identified through microarray analysis. PRKCI was one of those DE genes validated using qRT-QPCR experiments. Representative examples of a PRKCI melting curve (**A**) and amplification plot (**B**) are shown for untreated RPMI8226 cells (■) and RPMI8226 cells treated for 4h with SU1411 (■). The data shown represents n = 3, duplicate.

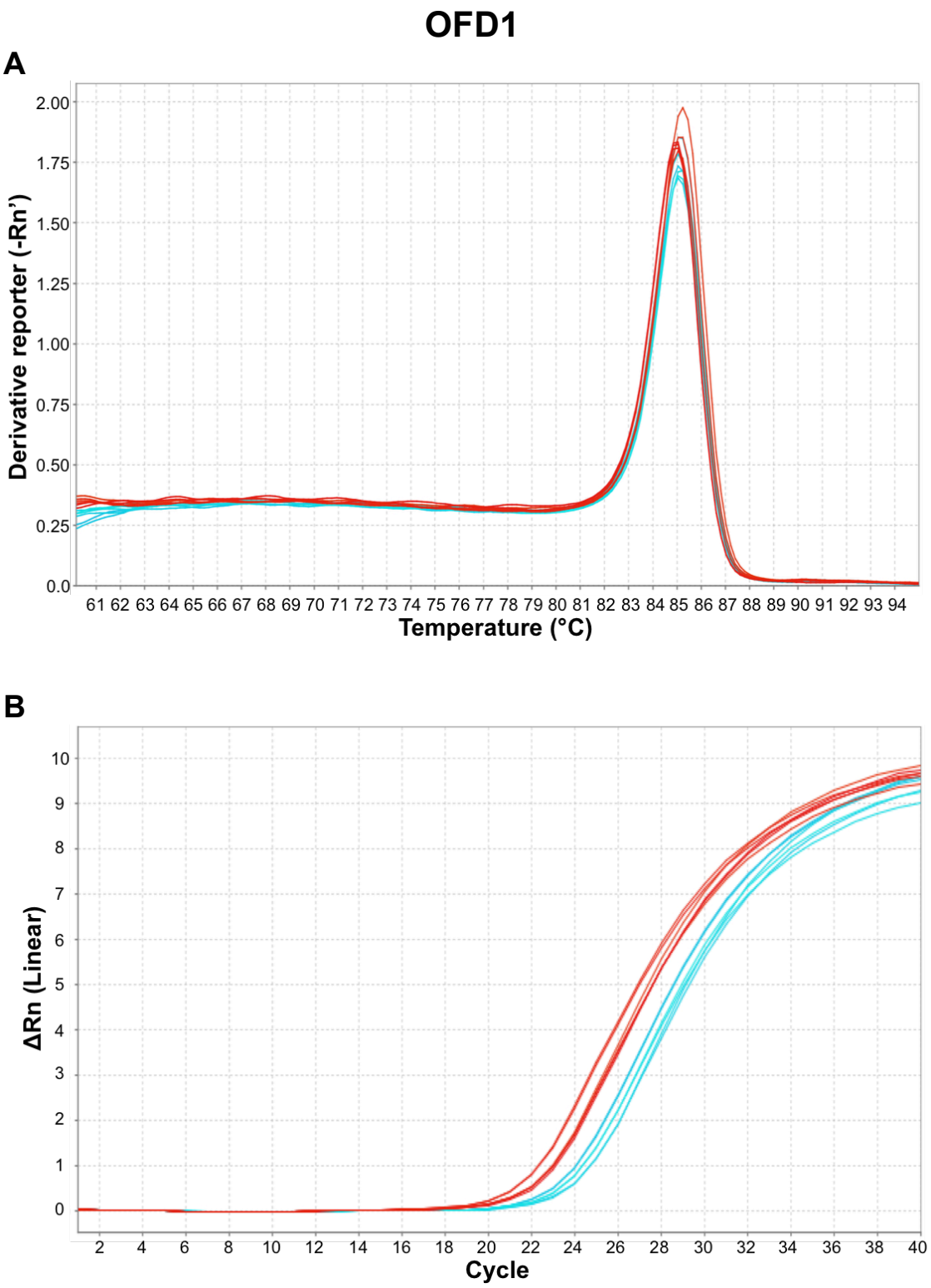

Figure XI Representative examples of a melting curve and an amplification plot produced when the OFD1 primer was used in qRT-PCR.
qRT-PCR was used to validate the DE genes identified through microarray analysis. OFD1 was one of those DE genes validated using qRT-QPCR experiments. Representative examples of a OFD1 melting curve (**A**) and amplification plot (**B**) are shown for untreated RPMI8226 cells (■) and RPMI8226 cells treated for 4h with SU1411 (■). The data shown represents n = 3, duplicate.

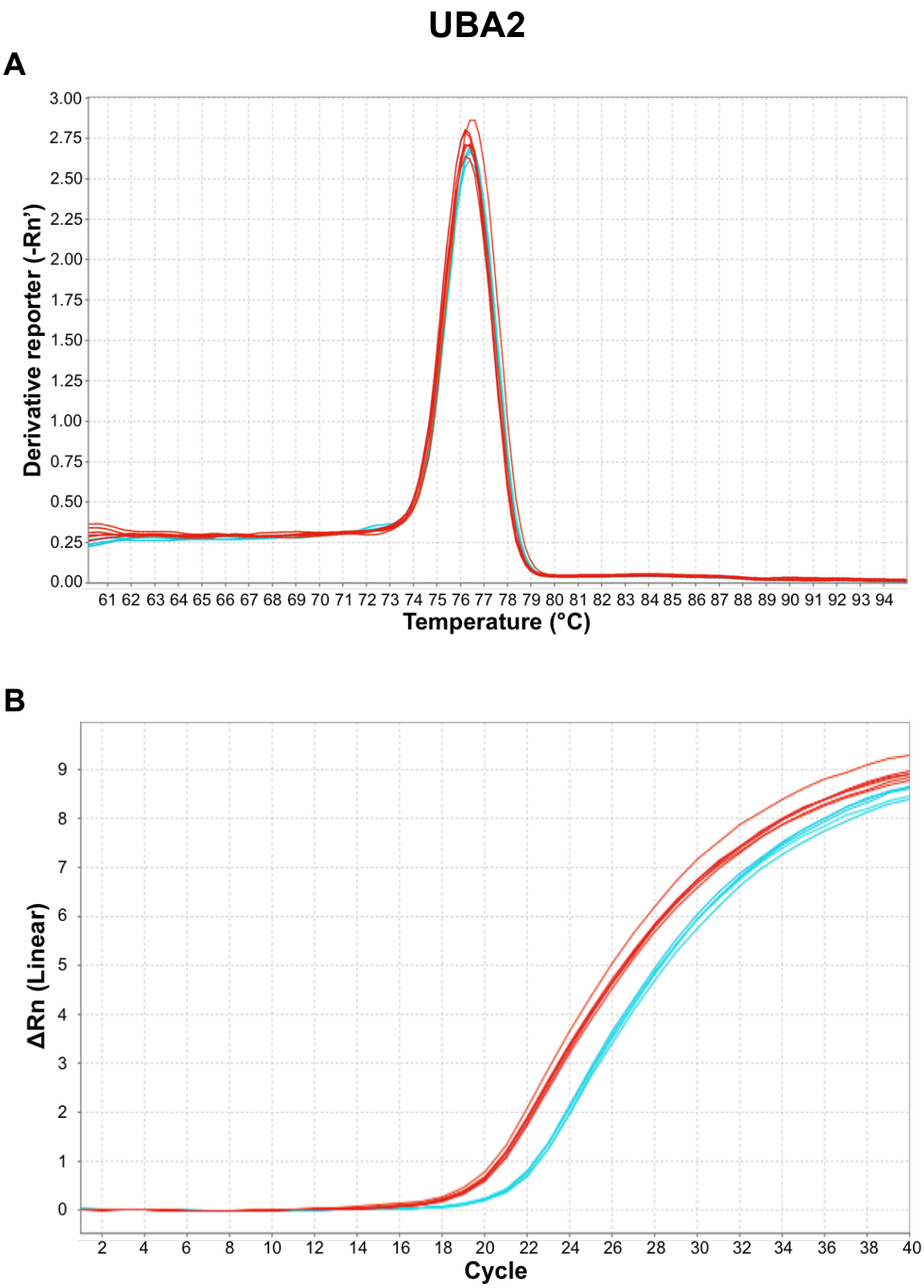

Figure XII Representative examples of a melting curve and an amplification plot produced when the UBA2 primer was used in qRT-PCR.
qRT-PCR was used to validate the DE genes identified through microarray analysis. UBA2 was one of those DE genes validated using qRT-QPCR experiments. Representative examples of a UBA2 melting curve (**A**) and amplification plot (**B**) are shown for untreated RPMI8226 cells (■) and RPMI8226 cells treated for 4h with SU1411 (■). The data shown represents n = 3, duplicate.

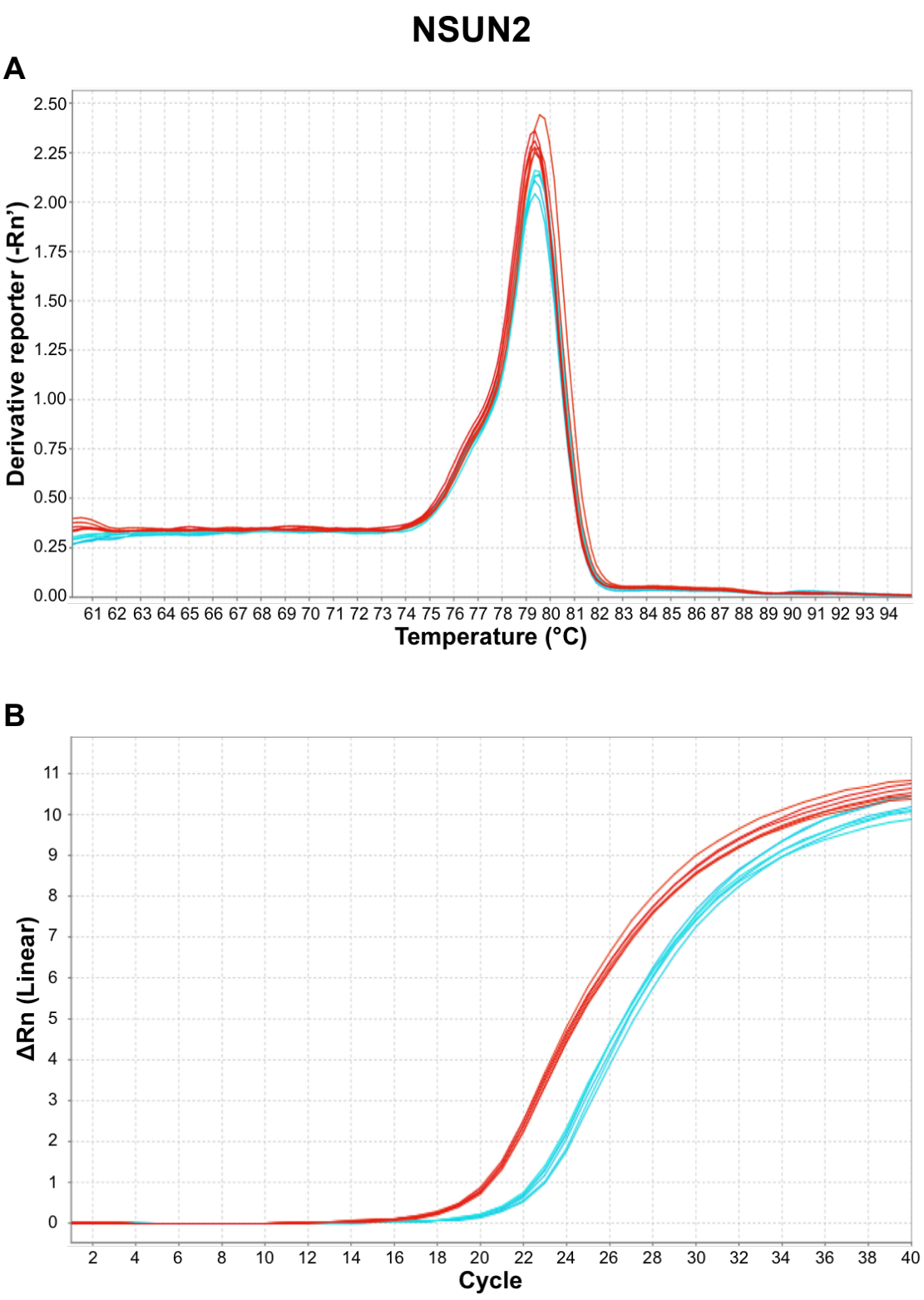

Figure XIII Representative examples of a melting curve and an amplification plot produced when the NSUN2 primer was used in qRT-PCR.
qRT-PCR was used to validate the DE genes identified through microarray analysis. NSUN2 was one of those DE genes validated using qRT-QPCR experiments. Representative examples of a NSUN2 melting curve (**A**) and amplification plot (**B**) are shown for untreated RPMI8226 cells (■) and RPMI8226 cells treated for 4h with SU1411 (■). The data shown represents n = 3, duplicate.

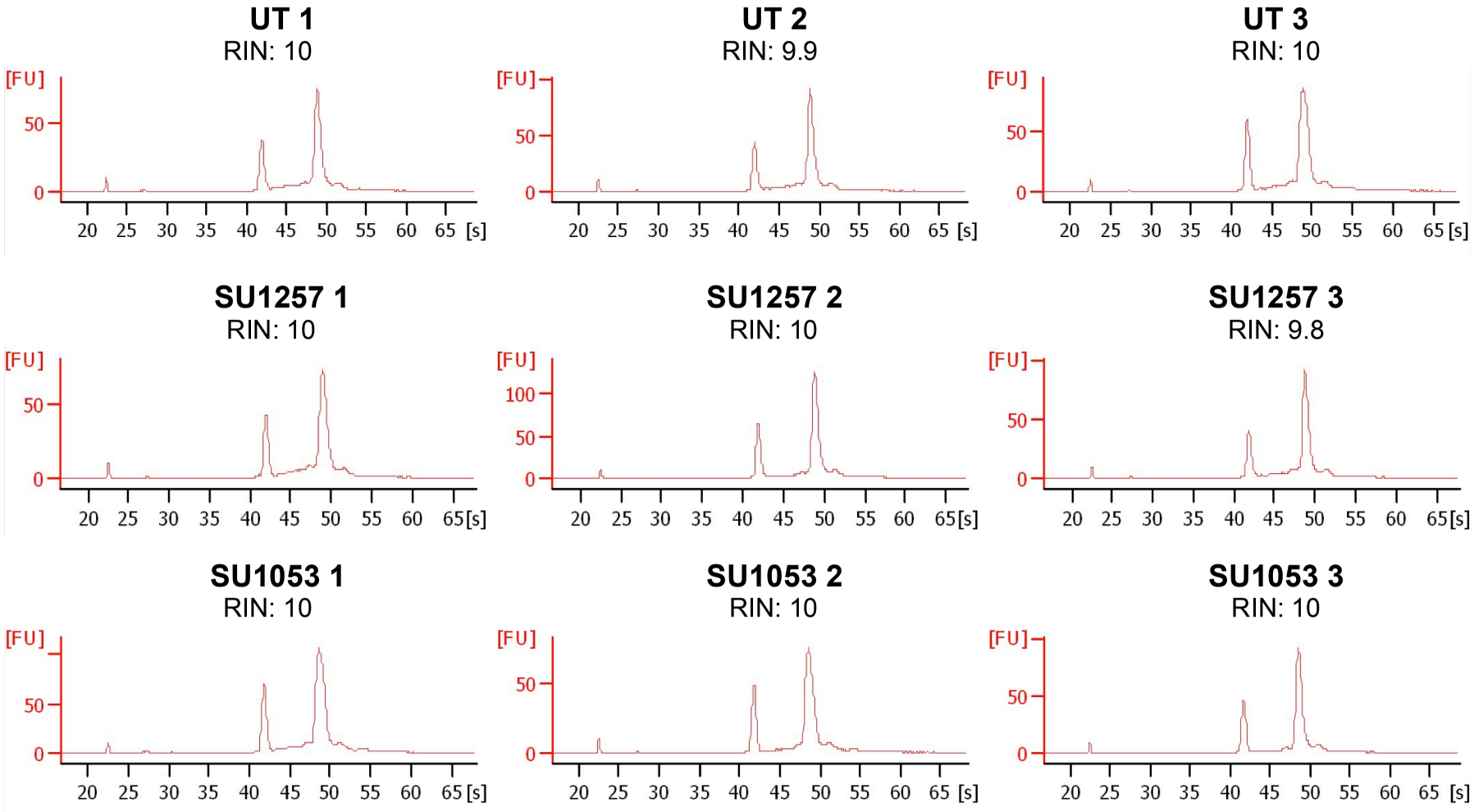
UT 1
RIN: 10
UT 2
RIN: 9.9
UT 3
RIN: 10
SU1257 1
RIN: 10
SU1257 2
RIN: 10
SU1257 3
RIN: 9.8
SU1053 1
RIN: 10
SU1053 2
RIN: 10
SU1053 3
RIN: 10
[FU]
[s]

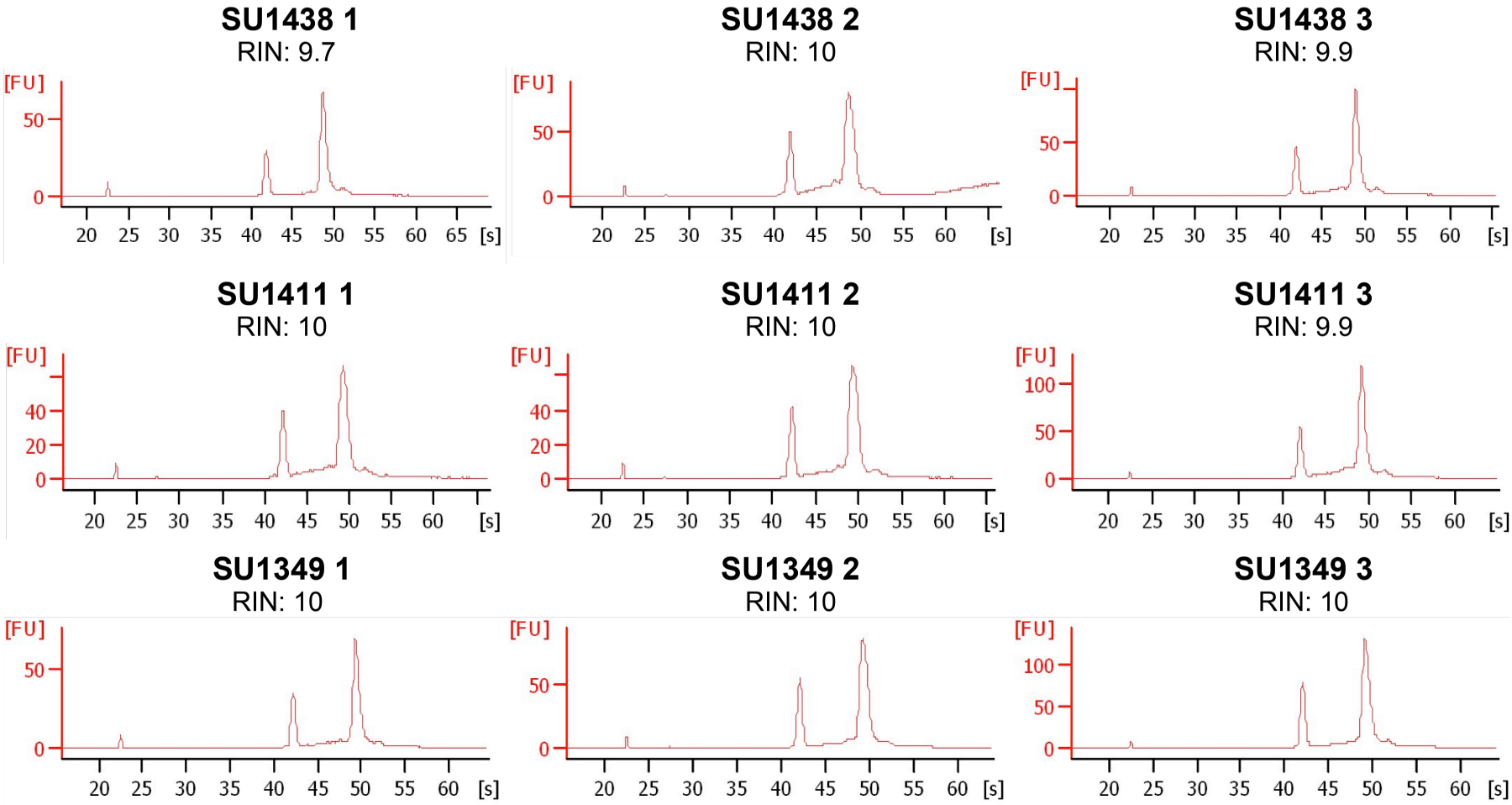

Figure XIV The RNA integrity number of the qRT-PCR RNA extracts used for validation of the microarray.
The quality of the RNA generated for the qRT-PCR to validate the microarray data was tested by measuring the RNA integrity number (RIN) using an Agilent 2100 Bioanalyzer System. The electropherograms for each sample were used to calculate RIN and clearly show the two main peaks corresponding to 18S and 28S ribosomal RNA, respectively. An RIN threshold of 6 was set and samples were only processed to cDNA if RIN > 6.

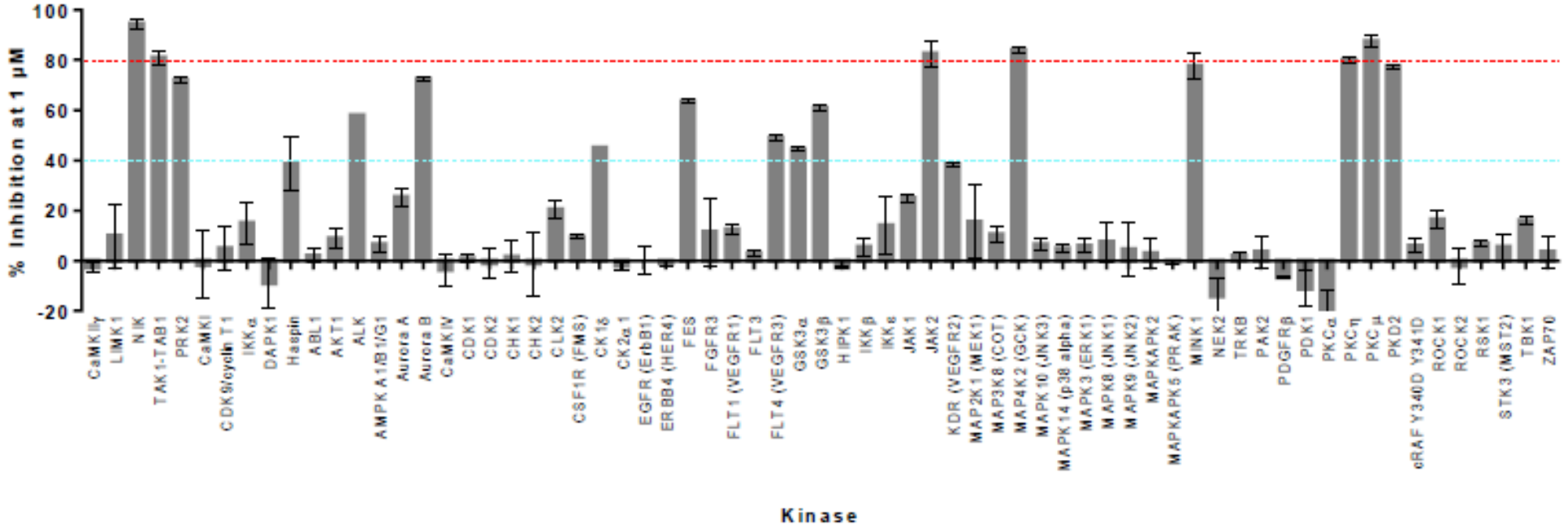

Figure XV The kinome screening data for CW15337 at a concentration of 1µM.
This figure was provided by Prof. Simon MacKay at the University of Strathclyde. The percentage of inhibition is shown for each kinase when CW15337 is used at a concentration of 1µM.